frontiers | Research Topics

Natural and synthetic microbiology for the production of novel biomolecules for applications in the areas of food, fuel, farming, pharma and environment

Edited by
Monika Prakash Rai and Guneet Kaur

Coordinated by
Sujata Sinha

Published in
Frontiers in Microbiology

ISSN 1664-8714
ISBN 978-2-8325-5245-2
DOI 10.3389/978-2-8325-5245-2

About Frontiers

Frontiers is more than just an open access publisher of scholarly articles: it is a pioneering approach to the world of academia, radically improving the way scholarly research is managed. The grand vision of Frontiers is a world where all people have an equal opportunity to seek, share and generate knowledge. Frontiers provides immediate and permanent online open access to all its publications, but this alone is not enough to realize our grand goals.

Frontiers journal series

The Frontiers journal series is a multi-tier and interdisciplinary set of open-access, online journals, promising a paradigm shift from the current review, selection and dissemination processes in academic publishing. All Frontiers journals are driven by researchers for researchers; therefore, they constitute a service to the scholarly community. At the same time, the *Frontiers journal series* operates on a revolutionary invention, the tiered publishing system, initially addressing specific communities of scholars, and gradually climbing up to broader public understanding, thus serving the interests of the lay society, too.

Dedication to quality

Each Frontiers article is a landmark of the highest quality, thanks to genuinely collaborative interactions between authors and review editors, who include some of the world's best academicians. Research must be certified by peers before entering a stream of knowledge that may eventually reach the public - and shape society; therefore, Frontiers only applies the most rigorous and unbiased reviews. Frontiers revolutionizes research publishing by freely delivering the most outstanding research, evaluated with no bias from both the academic and social point of view. By applying the most advanced information technologies, Frontiers is catapulting scholarly publishing into a new generation.

What are Frontiers Research Topics?

Frontiers Research Topics are very popular trademarks of the *Frontiers journals series*: they are collections of at least ten articles, all centered on a particular subject. With their unique mix of varied contributions from Original Research to Review Articles, Frontiers Research Topics unify the most influential researchers, the latest key findings and historical advances in a hot research area.

Find out more on how to host your own Frontiers Research Topic or contribute to one as an author by contacting the Frontiers editorial office: frontiersin.org/about/contact

Natural and synthetic microbiology for the production of novel biomolecules for applications in the areas of food, fuel, farming, pharma and environment

Topic editors
Monika Prakash Rai — Motilal Nehru National Institute of Technology Allahabad, India
Guneet Kaur — University of Guelph, Canada

Topic coordinator
Sujata Sinha — Indian Council of Medical Research (ICMR), India

Citation
Prakash Rai, M., Kaur, G., Sinha, S., eds. (2024). *Natural and synthetic microbiology for the production of novel biomolecules for applications in the areas of food, fuel, farming, pharma and environment*. Lausanne: Frontiers Media SA.
doi: 10.3389/978-2-8325-5245-2

Table of contents

frontiers | Frontiers in Microbiology

TYPE Editorial
PUBLISHED 19 July 2024
DOI 10.3389/fmicb.2024.1458803

OPEN ACCESS

EDITED AND REVIEWED BY
William James Hickey,
University of Wisconsin-Madison,
United States

*CORRESPONDENCE
Sujata Sinha
✉ sinha738@gmail.com

RECEIVED 03 July 2024
ACCEPTED 09 July 2024
PUBLISHED 19 July 2024

CITATION
Sinha S, Kaur G and Prakash Rai M (2024) Editorial: Natural and synthetic microbiology for the production of novel biomolecules for applications in the areas of food, fuel, farming, pharma and environment.
Front. Microbiol. 15:1458803.
doi: 10.3389/fmicb.2024.1458803

Editorial: Natural and synthetic microbiology for the production of novel biomolecules for applications in the areas of food, fuel, farming, pharma and environment

Sujata Sinha[1]*, Guneet Kaur[2] and Monika Prakash Rai[3]

[1]Department of Health Research, Indian Council of Medical Research, New Delhi, India, [2]School of Engineering, University of Guelph, Guelph, ON, Canada, [3]Department of Biotechnology, Motilal Nehru National Institute of Technology Allahabad, Prayagraj, India

KEYWORDS

bioactives, novel biocatalysts, novel microbes, engineered enzymes, bioprocessing, biosensing methods

Editorial on the Research Topic
Natural and synthetic microbiology for the production of novel biomolecules for applications in the areas of food, fuel, farming, pharma and environment

This Research Topic aimed at getting the latest insight into the production of biomolecules using microbial sources and the development of novel and sensitive microbial detection strategies. Various screening methods for isolation of high-performance strains, yield/productivity enhancement of microbial metabolites such as bioprocess optimization by statistical methods, genetic engineering, and advanced purification methods have been reported. New techniques for identifying improved strains have also been developed and reported to support this. Some of the remarkable microbial research related to the industrial production of metabolites, health, and medicine was published in this Research Topic and is summarized in this editorial.

The production of microbial derived molecules such as exosomes and L-asparaginase and their applications in biomedicine and health such as immunomodulation, gut health, drug delivery, and cancer treatment was reviewed (Tsegaye et al.; Liu). The reviews emphasized on the design of efficient isolation and purification strategies as well as engineering methods for enhanced functionalities of these molecules for biomedical applications. Development and use of *in-silico* methods for rapid screening of effective variants, techniques to assess *in-vivo* distribution and long-term safety was also highlighted considering their applications for human health.

Bacillus licheniformis ALSZ2 has been reported (Amin et al.) for lactase production having commercial potential for having lactose intolerant people. Statistical design of media optimization was performed to choose out of 100 strains in the soil polluted with dairy products for isolation of most potent microbial lactase producer with unique lactase capacities. Two level Plackett-Burman design was used for weighing fifteen variables using three factors, lactase activity was enhanced 4 times and 13 U/ml enzyme was achieved.

Genetic engineering strategies for enhanced and tailored production of prodniginines and rhamnolipids has been reported (Kossmann et al.) as biocontrol agents effective against plant nematodes. Bacterial secondary metabolites from genetically engineered *Pseudomonas putida* are of particular interest due to good plant compatibility and low toxicity. These are not as readily accessible so a new hybrid synthetic route was established in the same strain for enhancing the production of bipyrrole precursor and mutasynthesis optimization. Chemically synthesized and supplemented monopyrroles conversion to tripyrrolic compounds and subsequent semisynthesis provided the hydroxylated prodiginine which showed reduced infectiousness in *Arabidopsis thaliana* plants from *Heterodera schachtii*. 50% nematode control was achieved with combined application with rhamnolipids due to the impaired motility and style thrusting of parasites.

Modified yeasts producing proginsenediol-dammarane type ginsenosides, such as G-Rh2, G-Rg3, and G-Rd have been shown to enhance production in *Saccharomyces cerevisiae* (Lin et al.). It was developed by previously reported PnUGT33 as the necessary enzyme for the synthesis and manufacturing of G-Rg3. Two gene modules, LKG and EGH, were built for high level production of desired metabolites. In LKG31 (254.07 mg/L ± 56.49 mg/L) in the optimized YPD (yeast extract, peptone, and dextrose) medium with yeasts overexpressing the ScPGM1, ScPGM2, and ScUGP1 genes, 51 mg/L G-Rg3 production increased threefold. However, this work was unable to be successfully incorporated into the the EGH module (EGH-31 and EGH-53) and efforts to raise the strain titer (56.68 mg/L) after 96 h failed.

Lactic acid bacteria (LAB) (Vasundaradevi et al.) was reported as biocontrol agent to be effective against phytopathogenic fungus. Seven isolates were shown to inhibit its growth, out of which only two obtained from fruits *Ficus* and *Tinospora* exhibited promising antifungal properties against *Alternaria alternata*. Molecular identification technique was used for identifying strains showing higher adaptability to a wide temperature range and salt tolerance of up to 7%. Cell free supernatant (CFS) inhibition was quite high as even 5% crude CFS reduced the fungal growth by >70% while a complete inhibition was reported at 10%. Inhibition was against mycelial growth and conidial germination and it was effective even after long periods of cold storage of CFS.

Human health promoting bioactive compounds were reported from various parts of the medicinal mushroom *Ganoderma lucidum* (Tajik et al.) which include peptides, fatty acids, polysaccharides and triterpenoids. Extracts of isolated compounds from *G lucidum* has been found to be have carcinostatic effects on cancer cell lines like lung, pancreas, breast, skin etc., and triterpenoids have been reported to be the most important bioactive compounds with such effects. Glucose as carbon and corn steep liquor (CSL) as nitrogen source was found to be the best for stimulating the production of a triterpenoid called ganoderic acid based on optimization studies. This was secreted from stem and shell of mushroom and showed substantial anti-microbial and anti-cancer activity in *in-vitro* conditions.

Industrial uses of microbes and ultra-sensitive detection has been revolutionized in the recent times. This is of great importance in the case of anti-microbial resistance. *Pseudomonas aeruginosa*, a principal pathogen responsible for urinary tract infections has been known as difficult to eradicate and has evolved as the main candidate for drug resistance due to the indiscriminate uses of antibiotics. Rapid and efficient detection of microbes as well as their drug resistance genes is desirable for early clinical diagnosis and proper treatment. Recombinant polymerase amplification clustered regularly interspaced short palindromic repeats associated with protein 13a to establish one tube and two step reaction systems for detecting the mexX drug resistance gene in *Pseudomonas* was developed (Zhu et al.). This method outperformed the traditional PCR and qRT-PCR (quantitative Real-time polymerase chain reaction) and limit of detection was as low as 10 aM and 1 aM respectively Primer was specifically designed for drug resistance mexX gene. Method was verified with industrial samples and commercial lateral flow dipstick with LoD of 10 Fm and showed great accuracy.

Design of robust microbial systems as a source of metabolites having commercial value and/or catering to low volume high value products using novel strategies has attracted attention under the sustainable circular economy concept. Ultrasensitive microbial detection in clinical/environmental samples in the areas of health and medicine are of special importance. This Research Topic intends to motivate upcoming researchers to work in these areas which will lead to new innovations and applications in the areas of health, medicine, and industrial (bio)production.

Author contributions

SS: Conceptualization, Formal analysis, Project administration, Resources, Writing–original draft, Writing–review & editing. GK: Conceptualization, Formal analysis, Writing–original draft, Writing–review & editing, Visualization, Resources. MP: Formal analysis, Conceptualization, Project administration, Writing–original draft, Resources.

Funding

The author(s) declare that no financial support was received for the research, authorship, and/or publication of this article.

Conflict of interest

The authors declare that the research was conducted in the absence of any commercial or financial relationships that could be construed as a potential conflict of interest.

Publisher's note

frontiers | Frontiers in Microbiology

TYPE Original Research
PUBLISHED 02 May 2023
DOI 10.3389/fmicb.2023.1151882

OPEN ACCESS

EDITED BY
Monika Prakash Rai,
Amity University, India

REVIEWED BY
Pramod B. Shinde,
Central Salt and Marine Chemicals Research Institute (CSIR), India
Finian Leeper,
University of Cambridge, United Kingdom

*CORRESPONDENCE
J. Pietruszka
✉ j.pietruszka@fz-juelich.de
A. S. S. Schleker
✉ sylvia.schleker@uni-bonn.de
A. Loeschcke
✉ a.loeschcke@fz-juelich.de

†These authors have contributed equally to this work and share first authorship

‡These authors have contributed equally to this work and share last authorship

RECEIVED 26 January 2023
ACCEPTED 03 April 2023
PUBLISHED 02 May 2023

CITATION
Kossmann DF, Huang M, Weihmann R, Xiao X, Gätgens F, Weber TM, Brass HUC, Bitzenhofer NL, Ibrahim S, Bangert K, Rehling L, Mueller C, Tiso T, Blank LM, Drepper T, Jaeger K-E, Grundler FMW, Pietruszka J, Schleker ASS and Loeschcke A (2023) Production of tailored hydroxylated prodiginine showing combinatorial activity with rhamnolipids against plant-parasitic nematodes.
Front. Microbiol. 14:1151882.
doi: 10.3389/fmicb.2023.1151882

Production of tailored hydroxylated prodiginine showing combinatorial activity with rhamnolipids against plant-parasitic nematodes

D. F. Kossmann[1,2†], M. Huang[3†], R. Weihmann[4†], X. Xiao[3], F. Gätgens[4], T. M. Weber[2], H. U. C. Brass[2], N. L. Bitzenhofer[4], S. Ibrahim[4], K. Bangert[4], L. Rehling[3], C. Mueller[5], T. Tiso[5], L. M. Blank[5], T. Drepper[4], K.-E. Jaeger[1,4], F. M. W. Grundler[3], J. Pietruszka[1,2*‡], A. S. S. Schleker[3*‡] and A. Loeschcke[4*‡]

[1]Institute of Bio- and Geosciences (IBG-1): Biotechnology, Forschungszentrum Jülich GmbH, Jülich, Germany, [2]Institute of Bioorganic Chemistry, Forschungszentrum Jülich, Heinrich Heine University Düsseldorf, Jülich, Germany, [3]INRES, Molecular Phytomedicine, University of Bonn, Bonn, Germany, [4]Institute of Molecular Enzyme Technology, Forschungszentrum Jülich, Heinrich Heine University Düsseldorf, Jülich, Germany, [5]iAMB—Institute of Applied Microbiology, ABBt—Aachen Biology and Biotechnology, RWTH Aachen University, Aachen, Germany

Bacterial secondary metabolites exhibit diverse remarkable bioactivities and are thus the subject of study for different applications. Recently, the individual effectiveness of tripyrrolic prodiginines and rhamnolipids against the plant-parasitic nematode *Heterodera schachtii*, which causes tremendous losses in crop plants, was described. Notably, rhamnolipid production in engineered *Pseudomonas putida* strains has already reached industrial implementation. However, the non-natural hydroxyl-decorated prodiginines, which are of particular interest in this study due to a previously described particularly good plant compatibility and low toxicity, are not as readily accessible. In the present study, a new effective hybrid synthetic route was established. This included the engineering of a novel *P. putida* strain to provide enhanced levels of a bipyrrole precursor and an optimization of mutasynthesis, i.e., the conversion of chemically synthesized and supplemented monopyrroles to tripyrrolic compounds. Subsequent semisynthesis provided the hydroxylated prodiginine. The prodiginines caused reduced infectiousness of *H. schachtii* for *Arabidopsis thaliana* plants resulting from impaired motility and stylet thrusting, providing the first insights on the mode of action in this context. Furthermore, the combined application with rhamnolipids was assessed for the first time and found to be more effective against nematode parasitism than the individual compounds. To obtain, for instance, 50% nematode control, it was sufficient to apply 7.8 μM hydroxylated prodiginine together with 0.7 μg/ml (~1.1 μM) di-rhamnolipids, which corresponded to *ca.* ¼ of the individual EC_{50} values. In summary, a hybrid synthetic route toward a hydroxylated prodiginine was established and its effects and combinatorial activity with rhamnolipids on plant-parasitic nematode *H. schachtii* are presented, demonstrating potential application as antinematodal agents.

KEYWORDS

Prodiginines, plant-parasitic nematodes, plant protection, mutasynthesis and semisynthesis, *Pseudomonas putida*, combinatorial activity, rhamnolipids

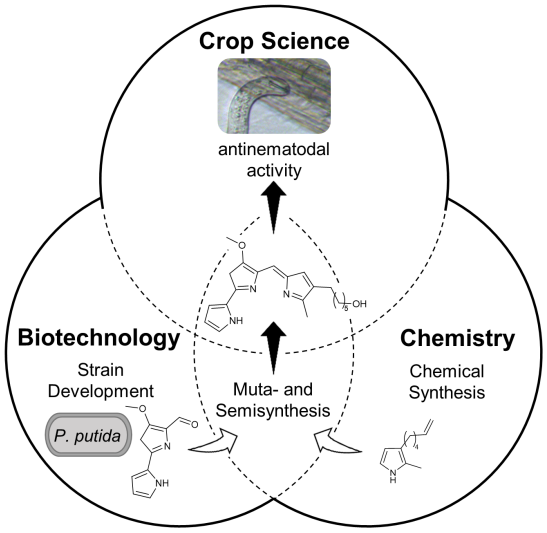

GRAPHICAL ABSTRACT

1. Introduction

Prodiginines are a group of bacterial secondary metabolites with diverse remarkable bioactivities, among which anticancer and antimicrobial effects have perhaps been described in most detail thus far (Fürstner, 2003; Stankovic et al., 2014; Hu et al., 2016; Sakai-Kawada et al., 2019; Yip et al., 2019; Berning et al., 2021; Li et al., 2022). Notably, prodiginine-producing bacteria such as *Streptomyces* and *Serratia* species also dwell in the rhizosphere, the dynamic micro-biosphere around the plant roots and site of manifold chemical interactions between the bacteria and plants (Berg, 2009; Lugtenberg and Kamilova, 2009; Meschke et al., 2012). Here, direct interactions can result in hormonal stimulation, increased stress tolerance and improved nutrient availability and uptake by plant roots. In addition, indirect beneficial effects for the plant can result from the suppression of pathogens. Although the ecophysiological role of prodiginines is still poorly understood, various bioactivities of prodigiosin (**1**) and related tripyrrolic analogs against several plant pathogens have already been reported (Someya et al., 2001; Meschke et al., 2012; Rahul et al., 2014; Roberts et al., 2021). Recently, their effectiveness against the plant-parasitic nematode (PPN) *Heterodera schachtii*, the causative agent of tremendous losses in crop plants, was described (Habash et al., 2020). Moreover, naturally-occurring bacterial secondary metabolites with surfactant properties, namely rhamnolipids, were recently reported to act against *H. schachtii* (Bredenbruch et al., 2023). It has further been shown that prodigiosin (**1**) possesses combinatorial antibacterial activities when applied together with biosurfactants, such as the lipopeptide serrawettin W1 and rhamnolipids (Hage-Hülsmann et al., 2018). It has been postulated that the pigment can only exert its full antimicrobial activity in combination with biosurfactants (Williamson et al., 2008; Roberts et al., 2021).

The aim of the present interdisciplinary study was to facilitate access to the relevant compounds and to investigate their combinatorial activities against *H. schachtii*. *Pseudomonas putida* has become a widely established biotechnological host for natural product biosynthesis (Nikel et al., 2016; Loeschcke and Thies, 2020; Weimer et al., 2020) including heterologous prodigiosin and rhamnolipid production (Domröse et al., 2015; Tiso et al., 2020; Cook et al., 2021). The rhamnolipid bioprocess has already been industrially implemented by Evonik Industries AG while research to improve accessing prodiginine derivatives is ongoing: recent studies showed heterologous expression of the *pig* gene cluster of *Serratia marcescens* via chromosomal integration, which established the biosynthesis of prodigiosin (**1**) (Domröse et al., 2015, 2019; Cook et al., 2021). Further, a mutasynthesis approach enabled the generation of new prodiginines (Klein et al., 2017, 2018). This procedure was based on the partial disruption of the native biosynthesis pathway and feeding of monopyrrole precursor analogs, which were incorporated into new tripyrrolic compounds. A limitation of this mutasynthesis approach was a relatively low product yield of 2–12% (Klein et al., 2017). Therefore, the development of a novel mutasynthesis *chassis* with enhanced bipyrrole production capacity and an optimization of mutasynthesis were identified as promising strategies to obtain target prodiginines more efficiently.

In previous work, a prodiginine bearing a terminal allylalcohol group (**2**) was reported to show remarkable plant growth promoting properties. In addition, it was not toxic for *Caenorhabditis elegans* at concentrations where prodigiosin (**1**) was lethal for this non-target organism (Habash et al., 2020). Based on these findings, the focus of the present study is the development of a feasible synthetic approach to hydroxylated prodiginines for investigations of anti-nematode activity. This study thus reports a mutasynthesis approach in a novel, efficient bipyrrole-producing *P. putida* strain and subsequent chemical conversion, i.e., semisynthesis, toward hydroxylated prodiginine **3** (Figure 1). The mode of action against *H. schachtii* as well as combinatorial activity with di-rhamnolipids (**4**) were investigated for the first time, demonstrating potential application as antinematodal agents.

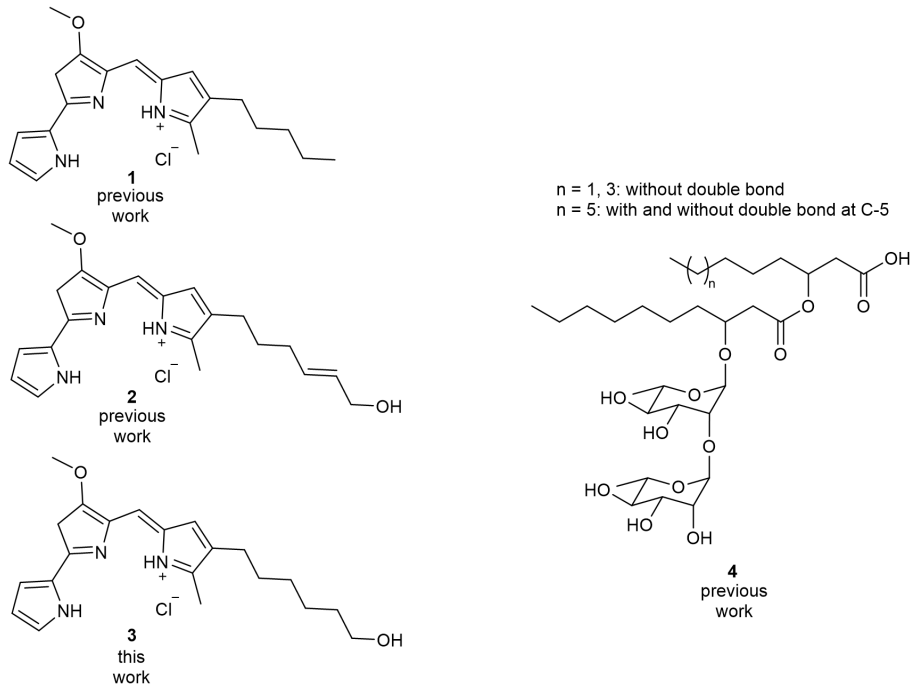

FIGURE 1
Bioactive compounds assessed in this study. The synthesis of prodigiosin **(1)** and hydroxylated derivative **(2)** has been established in previous studies. A synthesis route to hydroxylated prodiginine **(3)** is presented in this study, enabling the compound's application together with di-rhamnolipids **(4)**, which can be obtained via microbial biosynthesis as a mixture of congeners as indicated.

2. Results

2.1. Development of an enhanced *Pseudomonas putida chassis* for optimized mutasynthesis

In natural prodigiosin (**1**) biosynthesis, the monopyrrole MAP (2-methyl-3-amylpyrrole, **5**) and the bipyrrole MBC (4-methoxy-2,2′-bipyrrole-5-carbaldehyde, **6**) are condensed by a ligase (PigC in *S. marcescens*) to a tripyrrolic scaffold. The mutasynthesis approach has previously been established successfully in *P. putida* pig-r2 Δ*pigD* (Klein et al., 2017, 2018). The strain harbored the entire *S. marcescens pig* gene cluster—with the exception of the first MAP biosynthetic gene *pigD*, which was replaced by an antibiotic resistance gene. By feeding chemically synthesized monopyrroles to this MAP-deficient *P. putida* pig-r2 Δ*pigD* strain, the PigC-catalyzed condensation with MBC (**6**) led to novel tripyrrolic compounds in these previous studies.

Since mutasynthesis might be limited by biosynthetic provision of the bipyrrole precursor MBC (**6**), we aimed to establish a streamlined MBC-producing *chassis* preferentially lacking genetic and metabolic burdens. As a new strategy, a truncated *pig* gene cluster specifically designed to facilitate the biosynthesis of the bipyrrole **6** was integrated in the host. To this end, the artificial *pigAFGHIJKLMN* gene cluster (excluding the MAP (**5**) biosynthesis-encoding genes *pigBDE* and the ligase-encoding *pigC*, see Supplementary Figure S1) was assembled by PCR and yeast recombinational cloning into the yTREX vector following established protocols (Domröse et al., 2017; Weihmann et al., 2020). In this process, the promotor-less *lacZ* gene was inserted downstream of *pigN* (Figure 2A). The resulting vector was used for random transposon Tn5-based integration of the recombinant operon in the *P. putida* bacterial chromosome and LacZ was utilized as transcription reporter. Based on that, clones with strong gene expression were indicated by blue coloration as a result of X-gal conversion. Of these clones, 19 were selected and subjected to small scale cultivation, metabolite extraction and LC–MS analysis to verify bipyrrole product accumulation. Results were comparatively evaluated in relation to the previously established mutasynthesis *chassis P. putida* pig-r2 Δ*pigD* (Figure 2B). While four strains did not produce any detectable amounts of MBC (**6**), one clone (MBC17) produced a lower amount of MBC (**6**) than *P. putida* pig-r2 Δ*pigD*, and 14 accumulated the bipyrrole at higher levels (up to 8-fold increased). The best producer (MBC18) showed likewise elevated transcript levels (approx. 4-fold), indicating that a higher expression level could be reached in the new strain, which in turn contributed to higher bipyrrole synthesis. The enhanced MBC (**6**) level was verified for MBC18 in larger scale as applied in preparative mutasynthesis: Both strains, *P. putida* pig-r2 Δ*pigD* and MBC18, were cultivated in TB medium and polyurethane (PU) foam cubes were added as adsorbent for the hydrophobic compound, as previously established for prodigiosin (**1**) recovery (Domröse et al., 2015). Extracts from PU of the cultures with the newly constructed strain MBC18 contained about 12-fold more MBC (**6**) than those of the previously reported strain *P. putida* pig-r2 Δ*pigD* — a promising precondition for mutasynthesis.

The next step was to evaluate the capacity of the new strains for mutasynthesis with MBC17, MBC13, and MBC18 representing a low, an intermediate, and a high MBC level producer, respectively. The ligase PigC was thus introduced into these strains by plasmid-based expression from the IPTG-inducible P_{tac} promoter in pVLT33-pigC

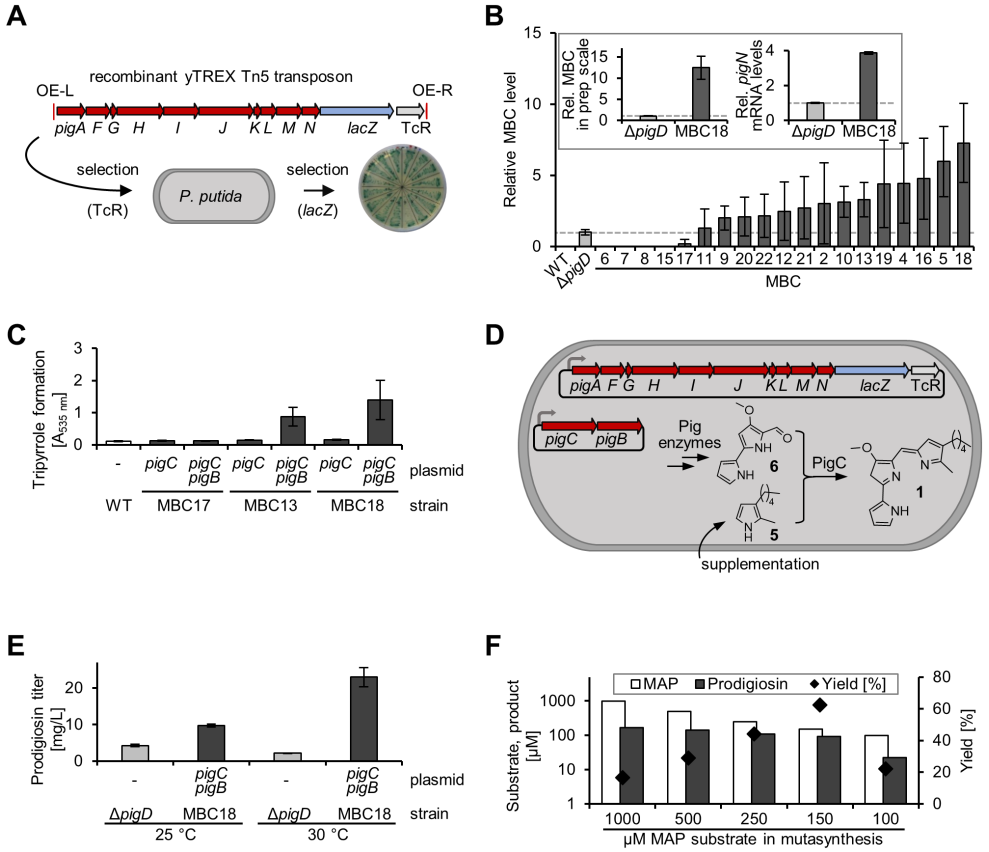

FIGURE 2
Construction of a *Pseudomonas putida* mutasynthesis *chassis*. **(A)** The artificial 4-methoxy-2,2′-bipyrrole-5-carbaldehyde (MBC) biosynthesis-encoding gene cluster was assembled by yeast-cloning and integrated in the bacterial chromosome via Tn5 transposition. After that, expressing clones were selected based on LacZ reporter activity. **(B)** Relative MBC production in small scale cultivation of engineered *P. putida* shown as x-fold increase relative to the signal of *P. putida* pig-r2 Δ*pigD*. Left Inset: Evaluation in preparative mutasynthesis setup (100 ml scale, MBC18 with pVLT33-pigC-pigB). Right inset: Relative *pigN* mRNA levels. **(C)** Dependence of the condensation of biosynthesized MBC (**6**) with supplemented MAP (**5**) on co-expression of PigB in *P. putida* stains MBC17, –13, –18 with plasmids pVLT33-pigC or pVLT33-pigC-pigB, respectively, in small scale cultivation. **(D)** Genetic setup of the new mutasynthesis *chassis* carrying the MBC (**6**) biosynthetic genes in the chromosome and expressing *pigC* and *pigB* from a plasmid. **(E)** Mutasynthesis performance of the newly established *chassis P. putida* MBC18/pVLT33-pigC-pigB in comparison with hitherto used *P. putida* pig-r2 Δ*pigD* in small scale cultivation at 25 or 30°C. The product was detected in extracts via spectrophotometry. Shown are mean values of independently replicated measurements (min. triplicates) with the respective standard deviation. **(F)** Optimization of preparative mutasynthesis in 5×100 ml scale with *P. putida* MBC18/pVLT33-pigC-pigB. The amount of substrate MAP (**5**) was varied from 1,000 µM to 100 µM to optimize conditions with respect to isolated prodigiosin (**1**) and corresponding yields (% mol of product relative to the substance amount of substrate).

(Brands et al., 2020). After small scale cultivation with supplementation of MAP (**5**, 1 mM), cells were extracted and prodigiosin-specific absorption was measured at 535 nm (Figure 2C). However, no noteworthy conversion of the fed monopyrrole to prodigiosin could be detected with either strain (MBC17, MBC13, MBC18/*pigC*).

Since it is known that in *in vitro* assays PigC does not require any additional proteins for functioning (Brass et al., 2019; Brands et al., 2020) it could be excluded that a generally necessary component was missing in the new strains. However, the previous *pigD* deletion mutant *P. putida* pig-r2 Δ*pigD* could facilitate conversion and it additionally contained functional PigB and PigE-encoding genes. This suggested an important role of either one or both of these proteins in the mutasynthesis setup (see Supplementary Figure S1). Based on their localization at the membrane and the proven importance of their membrane-anchoring domains, it may further be speculated that the last precursor-delivering enzymes PigN/F and PigB, as well as PigC could form a membrane-associated protein complex (Williamson et al., 2005; Chawrai et al., 2012; Couturier et al., 2019). This suggested that this complex consisting of PigC and PigN/F, but devoid of PigB might not be functional (see also Supplementary Figures S2, S3). PigB co-expression was therefore tested next by using plasmid pVLT33-pigC-pigB in the new strains (Figures 2C,D). While in the low-level precursor providing strain MBC17, co-expression of PigB did not lead to prodigiosin (**1**) formation, an increased signal was observed with MBC13 and highest levels were found in the high-level MBC-providing strain MBC18 (MBC17, MBC13, MBC18/*pigC-pigB*).

As a next step, mutasynthetic prodigiosin (**1**) production of the newly established *chassis P. putida* MBC18/pVLT33-pigC-pigB was assessed in comparison with hitherto used *P. putida* pig-r2 Δ*pigD*. To this end, small scale cultivation was used to test performance at 25°C as previously established (Klein et al., 2017, 2018) and at the optimal *P. putida* growth temperature 30°C (Figure 2E). At 25°C, 4.2 and 10 mg/L prodigiosin were obtained, while at 30°C, 2.3 and 21 mg/L were produced with *P. putida* pig-r2 Δ*pigD* and MBC18/pVLT33-pigC-pigB, respectively. These results therefore verified enhanced

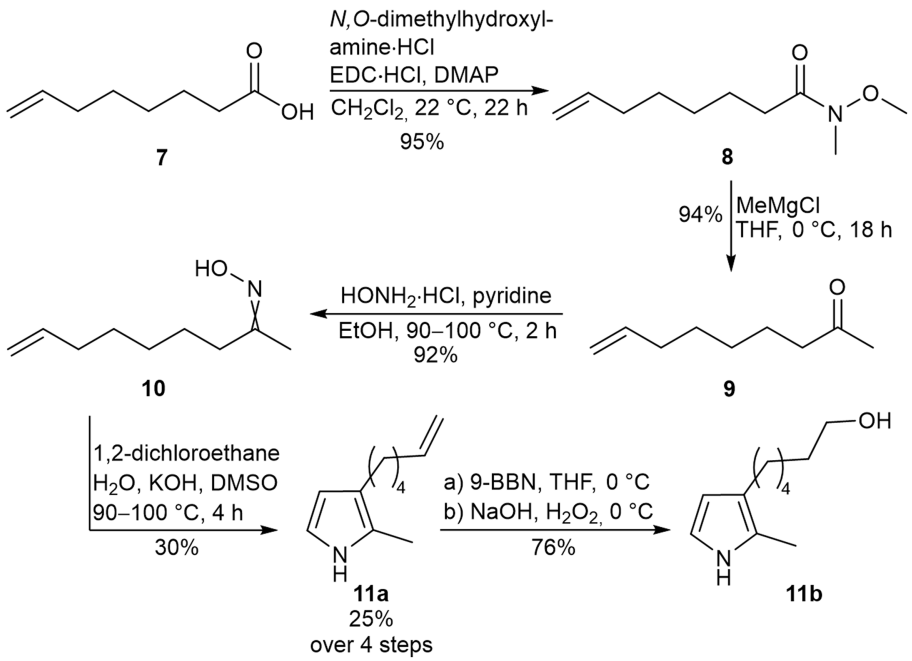

FIGURE 3
Synthesis route toward the 2,3-disubstituted pyrrole precursors **11a** and **11b**.

performance of the newly constructed *chassis*, especially at 30°C, so all following experiments were conducted at this temperature.

Since during small scale cultivation under the applied conditions with excess of MAP (1 mM, **5**), MBC (**6**) was consumed to below limits of quantification, an adjustment of MAP concentrations was tested next. Hence, different MAP (**5**) concentrations were supplemented to *P. putida* MBC18/pVLT33-pigC-pigB in order to potentially match the levels of both precursors in preparative scale experiments and optimize yields (Figure 2F). The best yield of 62% purified product was obtained with 150 µM MAP (**5**). Isolation by soxhlet extraction of PU and column chromatography on silica yielded 17 mg prodigiosin (**1**) from 500 ml mutasynthesis cultures. This outcome corresponding to 34 mg/l represented an improvement to previously reported 17 mg/l, obtained with the same pyrrole via comparable procedures (Klein et al., 2017). Remaining MBC (**6**) was below 2 µM in this experiment (Supplementary Figure S4). This procedure was therefore deemed as suitable for further steps toward accessing the hydroxylated target compound **3**.

2.2. Chemical synthesis of pyrroles, muta- and semisynthesis of hydroxylated prodiginine 3

In order to establish a synthesis route to a hydroxylated prodiginine tripyrrole, a pyrrole with terminal double bond was aimed as precursor to allow a late-stage semisynthetic functionalization. Previously reported prodiginine **2** was synthesized chemically in a condensation reaction of *Boc*-**6** and a pyrrole with allylalcohol function (Habash et al., 2020). With this approach, the functional group is already applied, but further modification and derivatization are less feasible. The here presented mutasynthesis approach is more flexible in terms of late-stage functionalization and allows to functionalize the obtained mutasynthesis product in a variety of ways, such as with a bromination or oxidation. In order to yield the hydroxylated prodiginine **3**, we applied a hydroboration as semisynthetic step.

Starting from carboxylic acid **7**, Weinreb-amide **8** and ketone **9** were obtained in two steps, consecutively. Afterwards, oxime **10** was synthesized to be used as starting material in the Trofimov pyrrole synthesis toward pyrrole **11a**, as previously described (Mikhaleva et al., 1981; Trofimov et al., 2015; Klein et al., 2018). The Trofimov pyrrole synthesis represents the yield-limiting step in this synthesis sequence (Figure 3). This could be explained by the strongly basic reaction conditions, which favor side-product formations as described previously (Ivanov et al., 2014). Observed side-products were a ketoxime diether and an *N*-alkylated pyrrole, which could be removed by flash column chromatography on silica. In a subsequent hydroboration with the organoborane 9-BBN (9-Borabicyclo[3.3.1]nonane), a hydroxylated pyrrole **11b** was obtained as precursor.

Both pyrroles were tested as mutasynthons, but only pyrrole **11a** was converted in *P. putida* MBC18/pVLT33-pigC-pigB (Figure 4A). The hydroxylated group likely prevents the pyrrole **11b** from crossing the cell membrane, since PigC-mediated condensation was observed in experiments with lysate (Figure 4B). Therefore, 150 µM **11a** was applied in a preparative mutasynthesis, yielding 30 mg/L of the corresponding tripyrrole **12** which corresponds to 54% yield.

The hydroxylated prodiginine **3** was synthesized in a final semisynthetic step by hydroboration of the obtained mutasynthesis product **12**, yielding targeted compound **3** in 65% yield (Figure 4C). Notably, for the hydroboration to be successful, the mutasynthesis product had to be purified via reversed phase column chromatography in advance. Overall, a hybrid synthesis route for a

10.3389/fmicb.2023.1151882

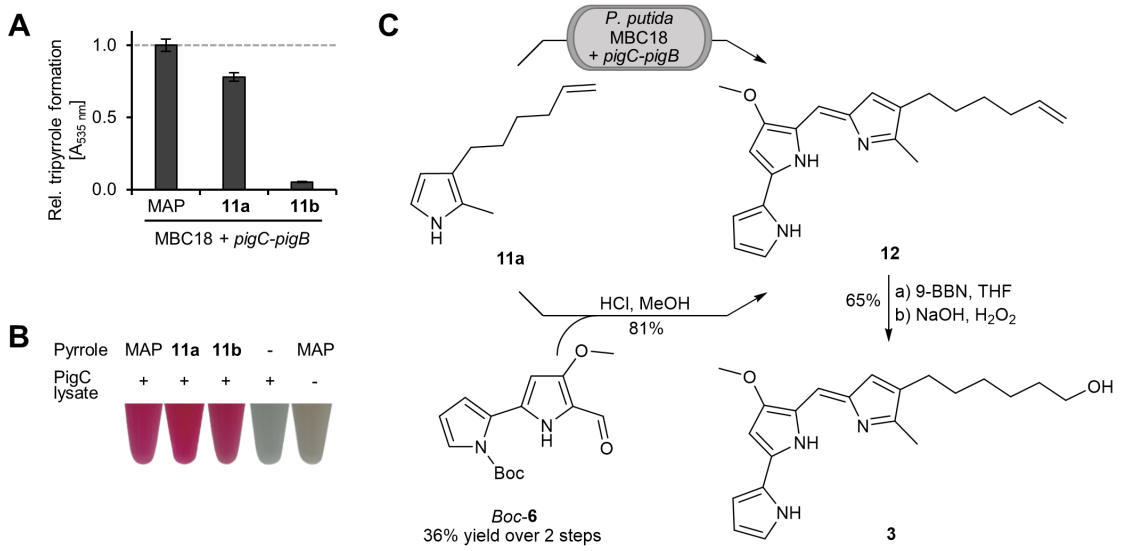

FIGURE 4
Synthetic route toward hydroxylated prodiginine 3. **(A)** Mutasynthetic tripyrrole formation upon feeding of **11a** and **11b**, respectively, in small scale cultivation of *P. putida* MBC18/pVLT33-pigC–pigB. The products were detected spectrophotometrically and quantified relative to the signal upon MAP (**5**) supplementation. Mean values of triplicate measurements with the respective standard deviation are shown. **(B)** Assessment *in vitro* of PigC substrate acceptance, shown as tripyrrole-typical coloration of reaction mixtures after incubation of lysate from PigC-expressing *E. coli* cells with MBC (**6**) and monopyrroles. **(C)** Synthesis scheme of hydroxylated prodiginine **3**. Pyrrole **11a** was supplemented to the MBC producing strain *P. putida* MBC18/pVLT33-pigC–pigB in preparative mutasynthesis to obtain the product **12**. As reference, the compound was also synthesized chemically in a condensation reaction with *Boc*-protected MBC (**6**). By the following semisynthetic hydroboration step, the final hydroxylated prodiginine **3** could be obtained.

hydroxylated prodiginine involving advantageous biosynthesis of the bipyrrole precursor **6** instead of laborious organic synthesis could be established.

2.3. Impact of prodiginines on the plant-parasitic nematode *Heterodera schachtii*

The main focus in this study was on hydroxylated prodiginine **3** for the above mentioned reasons. Additionally, the natural product prodigiosin (**1**) was used as reference in all subsequent assays. The individual effects of the hydroxylated prodiginine **3** and prodigiosin (**1**) against the PPN *H. schachtii* were determined first. To this end, the half maximal effective concentration (EC_{50}) for the reduction of nematode numbers on the model plant *Arabidopsis thaliana* was assessed. Prodiginines were found to inhibit nematode infestation by up to 80%. The EC_{50} (nematode infection) was 31.2 µM for hydroxylated prodiginine **3** and 15.1 µM for prodigiosin (**1**) (Figure 5). Although the synthesis of the previously presented prodiginine **2** is relatively laborious it appeared still interesting to validate its impact on *H. schachtii*. Prodiginine **2** and an alternative prodiginine with a side chain one carbon longer than prodiginine **3** (compound **13**, see Supplementary Information) did not exhibit stronger effects compared to prodiginine **3** (see Supplementary Figure S6) thus justifying our focus on hydroxylated prodiginine **3**.

A next aim was to pinpoint the nematode's life stage(s) and the time during host-pathogen interaction when the effect of prodiginines on the nematode becomes obvious. Therefore a time-resolved analysis of the nematodes' reaction to application of prodigiosin (**1**) and the hydroxylated prodiginine **3** was performed. To this end, fitness parameters of second-stage juveniles of *H. schachtii* (J2), nematode infection of *A. thaliana* and nematode development at the plant were investigated. These parameters were evaluated at different time points during exposure of the parasite to the above determined EC_{50} (nematode infection).

The motility of *H. schachtii* J2, which were exposed to prodigiosin (**1**) and the hydroxylated prodiginine **3** at their EC_{50} concentrations for 1 h, was significantly reduced by 32 and 39%, respectively, compared to the control (Figure 6A). An investigation of *H. schachtii* J2 stylet movement revealed a significant reduction in the frequency of thrusting at *A. thaliana* roots by 19 and 16% upon prodigiosin (**1**) and hydroxylated prodiginine **3** application, respectively (Figure 6B). This could be the reason that the number of nematodes that successfully penetrated the root epidermis (Figure 6C) and established a sedentary interaction with the plant was significantly reduced by prodiginines by 28 to 41% compared to the control (Figure 6D). Finally, the growth of *H. schachtii* females and males developing from J2 that successfully infected the plant despite prodiginine exposure was slightly reduced but not significantly impaired by prodiginines (Figure 6E).

The presented data provides for the first time specific hints to the mode of action of prodiginines and substantiates that prodiginines exert a direct antagonistic effect on *H. schachtii*. In contrast, the antinematodal effect of rhamnolipids has recently been shown to be indirect, i.e., triggering plant defense mechanisms (Bredenbruch et al., 2023). Based on these findings,

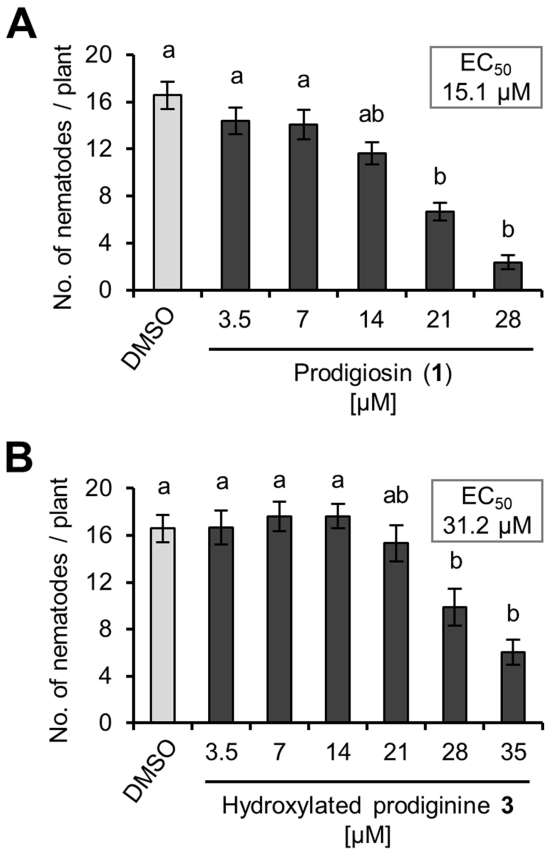

FIGURE 5
EC_{50} determination of prodiginines on the plant-parasitic nematode *Heterodera schachtii*. **(A)** Impact of prodigiosin (**1**) on nematodal plant infestation. **(B)** Impact of hydroxylated prodiginine **3** on nematodal plant infestation. The impact on *H. schachtii* was assessed as reduction of nematode numbers on *Arabidopsis thaliana*. EC_{50} values (effective concentration that causes a reduction of nematode infestation of *A. thaliana* by 50%) were calculated by using 'CompuSyn'. Results are expressed as the mean±standard error of three independent biological replicates ($n \geq 18$). Different letters indicate statistically significant differences among treatments according to Dunn's Method ($p<0.05$).

it is intriguing to assess the combined effects of prodiginines and rhamnolipids as a synergistic activity against nematodes may be hypothesized. For these investigations the previously evaluated and described mixture of di-rhamnolipid congeners (Bredenbruch et al., 2023) was chosen, which revealed an EC_{50} (nematode infection) of 2.8 µg/mL (corresponding to approximately ~ 4.3 µM; Supplementary Figure S7).

Investigations of the combined activities of prodiginines (**1** and **3**) and di-rhamnolipids (**4**) revealed that the combination of the two compounds was more effective against nematode parasitism than the individual compounds, i.e., the combined application reduced the required concentrations for the same effect (Figures 6F,G). To obtain, for instance, 50% nematode control, it was sufficient to apply ¼ the concentration of hydroxylated prodiginine **3** and di-rhamnolipids (**4**) together or prodigiosin (**1**) and di-rhamnolipids (**4**) together instead of the full dose of each compound individually (see Supplementary Figure S8 for dose response curves and combination index plots).

3. Discussion

3.1. Development of hybrid synthesis toward tailored hydroxylated prodiginine

The concept of mutasynthesis is highly attractive for synthetic chemists as a method for structural diversification of natural products by using genetically engineered microorganisms (Kirschning et al., 2007). By using nature's enzymatic biosynthetic machinery for the synthesis of precursor MBC (**6**) this study presents an environmentally friendly way by avoiding heavy metal catalyzed synthesis of *Boc*-**6** (Dairi et al., 2006; Domröse et al., 2015). Furthermore, this approach allows the incorporation of non-native building blocks into new derivatives due to enzyme promiscuity (Sun et al., 2015).

While in our previous studies, prodigiosin (**1**) biosynthesis resulted in titers, e.g., ranging from 60 to 150 mg/L (Domröse et al., 2015, 2017, 2019) depending on the applied conditions, mutasynthetic derivatives were only obtained with 0.6–3.1 mg/L (Klein et al., 2018) or maximally 19.8 mg/L (Klein et al., 2017). In general, this may reflect poor substrate entry into the cells, a low activity of PigC toward unnatural substrates, an insufficient MBC (**6**) supply, or a combination of these factors. In the present study, the MBC (**6**) supply was addressed by implementing expression of MBC (**6**) biosynthetic genes, which successfully led to reaching enhanced titers of 30–34 mg/L. Further improvements are conceivable with alternative ligase enzymes. The new strain setup of *P. putida* MBC18 allows their exchange more easily by use of alternative plasmids, whereas strain *P. putida* pig-r2 Δ*pigD* carried all *pig* genes in the chromosome. In this context, our studies uncovered, that coexpression of *pigB* is essential in this setup. It might be speculated that the enzymes PigN/F and PigB, that naturally deliver the pyrrole precursors, as well as PigC assemble to form a membrane-associated complex (Williamson et al., 2005; Chawrai et al., 2012; Couturier et al., 2019). This may hypothetically ensure fast product release via the membrane. Our findings suggest that an only partial assembly of this putative complex consisting of PigC and PigN/F, but devoid of PigB is not functional. Notably in this context, *Janthinobacterium lividum* appears to contain a *pigCB* fusion in its *pig* gene cluster (Schloss et al., 2010). However, further studies are required to elucidate these interactions.

Previous studies investigated the versatile substrate range of the condensing enzyme PigC (Klein et al., 2017, 2018; Brass et al., 2019). According to these findings, the present study focused on a mutasynthesis approach toward tailored hydroxylated prodiginines by feeding modified pyrroles to the new strain *P. putida* MBC18. In advance, the mutasynthesis experiment was optimized concerning the yields (Figure 2F). Notably, feeding a high amount of MAP (**5**) did not lead to a likewise high amount of prodigiosin (**1**) and thus resulted in relatively low yields up to 17%. Interestingly, by varying the MAP (**5**) concentration in a range of 100–1,000 µM, the prodigiosin (**1**) concentrations obtained (93–167 µM) were relatively constant and did not reflect the magnitude of the fed pyrrole concentration (Figure 2F). This observation could be explained by a substrate inhibition of involved enzymes. A PigC substrate inhibition by MAP (**5**) has been demonstrated in a previous study: conversion assays using different concentrations of MAP (**5**) at a fixed MBC (**6**) concentration suggested an ordered kinetic mechanism in which MBC (**6**) has to bind before MAP (**5**) (Chawrai et al., 2012). In the present study, 62% prodigiosin (**1**), obtained with an adjusted MAP (**5**) concentration, is the highest

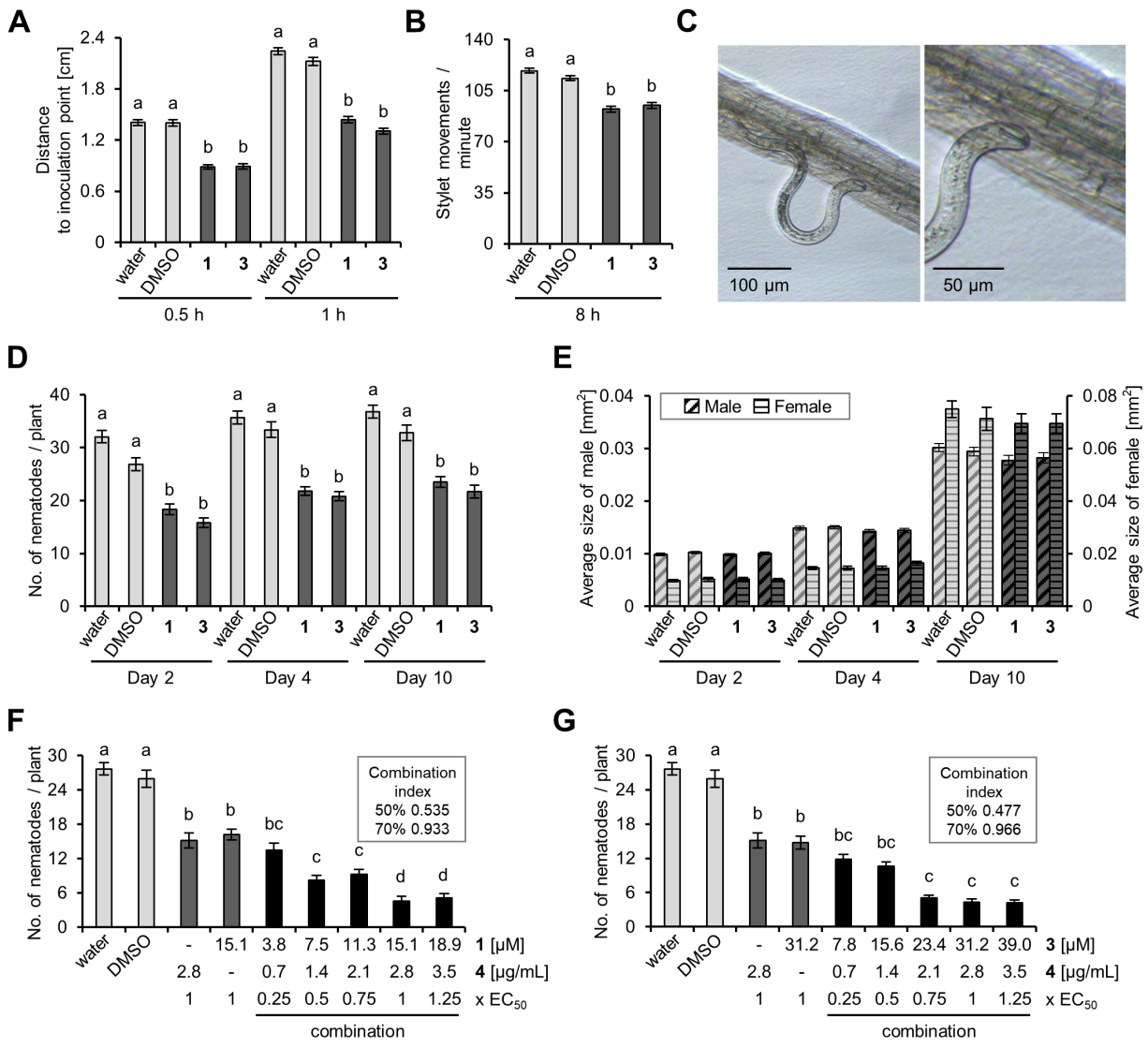

FIGURE 6
Prodiginine impact on *Heterodera schachtii* fitness parameters, plant parasitism, and combined activity with di-rhamnolipids. **(A)** *H. schachtii* J2 motility, assessed as distance to an inoculation point after incubation. **(B)** Stylet thrusting at *Arabidopsis thaliana* roots, assessed as movements/min. **(C)** *A. thaliana* root with an invading J2. **(D)** Nematode infection rate at *A. thaliana*, investigated at different time points after inoculation. **(E)** Nematode size development, evaluated during 10days after inoculation. **(F,G)** The combined effect of prodigiosin (**1**) and di-rhamnolipids (**4**) as well as hydroxylated prodiginine **3** and di-rhamnolipids (**4**), respectively, was assessed at 10days after inoculation. Combination indices were calculated using 'CompuSyn'. Results are expressed as the mean±standard error of at least three biological replicates [n≥614 **(A)**; *n*=40 **(B)**; *n*=56 (D); *n*≥70 **(E)**; *n*≥20 **(F)**; *n*≥22 **(G)**]. Different letters indicate statistically significant differences among treatments according to Dunn's Method ($p<0.05$). EC_{50} is the effective concentration that causes a reduction of nematode infestation of *A. thaliana* by 50%. Prodigiosin (**1**) and hydroxylated prodiginine **3** were used at their EC_{50} concentration in **A**, **B**, **D**.

yield achieved in a preparative scale. However, further investigation and optimization of the mutasynthesis approach may lead to even higher yields, for example by feeding the pyrrole over a period of time to overcome PigC substrate inhibition.

As mentioned above, a strength of mutasynthesis is the substrate promiscuity of the enzymes used. Results of an *in vitro* PigC assay showed acceptance for both pyrroles **11a** and **11b** (Figure 4B). However, using **11b** as mutasynthon in an *in vivo* approach did not result in formation of the targeted hydroxylated prodiginine **3**, rendering an alternative approach necessary. We assume that the hydroxyl group prevents the pyrrole **11b** from crossing the cell membrane. To overcome this issue, pyrrole **11a** was supplemented as mutasynthon to produce prodiginine **12** in a yield of 54%. The hydroxyl group was introduced in a semisynthetic step toward the targeted prodiginine **3**. Notably, the mutasynthesis product **12** had to be purified via reversed-phase column chromatography for the final hydroboration step to succeed. Alternative purification methods, such as aqueous washing steps (sat. NH_4Cl, sat. $NaHCO_3$, sat. Na_2SO_4, sat. NaCl or sat. LiCl) or normal phase column chromatography (silica or alox) led to an apparently inactivated prodiginine, which did not show any conversion to the hydroxylated prodiginine **3**, not even under high excess of the hydroboration agent 9-BBN. Quantitative ^{1}H-NMR spectroscopy showed, that the purity of the mutasynthesis product, which was isolated by normal phase column chromatography

increased from 60 ± 3% to 92 ± 5% after an additional reversed-phase column chromatography. This finding was crucial for the success of the hybrid synthesis toward hydroxylated prodiginine **3**, even if the impurities that led to an inactivation of isolated mutasynthesis products could not be identified and further investigations are necessary.

3.2. Prodiginine-induced reduction of the fitness and infectiousness of the plant-parasitic nematode *Heterodera schachtii*

Since PPN mostly inhabit the soil and primarily attack below-surface parts of plants, it is often challenging to control PPN. Microscopic life in the rhizosphere is particularly robust and naturally occurring microbial compounds have been studied and commercialized as potent bioactive ingredients against a diversity of soil-borne pathogens over the past decades (Handelsman and Stabb, 1996; Haas and Défago, 2005; Köhl et al., 2019). Our previous work revealed that prodiginines and rhamnolipids possess activity against the PPN *H. schachtii* (Habash et al., 2020; Bredenbruch et al., 2023). Rhamnolipids exert their activity by triggering plant defense responses effective against nematodes. Unlike that, this current study demonstrated that prodigiosin (**1**) and hydroxylated prodiginine **3** directly antagonize *H. schachtii* J2 by inhibiting motility and stylet thrusting (Figures 6A,B). The J2 is the infective larval stage of *H. schachtii*, which migrates within the soil towards the root. In the natural habitat, *H. schachtii* J2 migrate at the maximum speed when there is no lateral movement and each body part usually follows the movement of its front part (Wallace, 1958). The presence of the investigated prodiginines appears to hinder nematode forward movement.

Stylet thrusting of *H. schachtii* J2 is a prerequisite for destructively invading the host's root tissue and later—after reaching the vascular cylinder—carefully probing plant cells until a suitable cell is found, which becomes the initial syncytial cell (ISC). The frequency of this stylet movement is significantly reduced by prodiginines, as demonstrated in this study. The continuous vigorous stylet thrusting of J2 is an energy consuming process (Wyss and Zunke, 1986; Grundler et al., 1991; Wyss, 1992; Wyss and Grundler, 1992). Since it has been described that prodiginines can uncouple mitochondrial F-ATPases due to their H^+/Cl-symport activity (Konno et al., 1998), their direct effect on the cellular energy metabolism might be one explanation for the lower frequency of J2 stylet movements.

Once *H. schachtii* J2 accomplish the formation of permanent feeding sites, they become immobile and change from a migratory into a sedentary form (Wyss, 1992). Prodiginines were observed to interfere with nematode invasion and infection of *A. thaliana*. However, female and male development at the host plant is not influenced by prodiginines at 2 and 4 days after the inoculation, while it is slightly impaired after 10 days (Figures 6D,E). As stated in our previous study, a significant reduction of female size due to prodigiosin application can be observed after 13 days (Habash et al., 2020). Probably, the impact of prodiginines on the pathogen's development at the root becomes obvious only at later time points after infection. Future studies should investigate this aspect further and additionally determine whether prodiginine exposure interferes with reproduction.

While investigations on the molecular mode of action for the interaction of prodiginines with nematodes are missing, studies of their effects on bacteria document a disturbing impact on biological membranes and reactive oxygen species (ROS) generation (Darshan and Manonmani, 2015, 2016; Suryawanshi et al., 2017; Ravindran et al., 2020; Choi et al., 2021). Whether prodiginines cause disruption of PPN membranes and whether this contributes to the observed effects still needs to be elucidated.

Unlike "single compound - single target" approaches, multicomponent therapeutics enable interactions with multiple targets (Keith et al., 2005; Hopkins, 2007; Yildirim et al., 2007). The discovery of drug–drug combinations offers promising strategies for (1) the improvement of drug treatment efficacy, (2) the reduction of drug dosage to avoid toxicity, and (3) the minimization of drug resistance evolution (Jia et al., 2009; Cheng et al., 2019). Our results demonstrate that, when applying prodiginines and di-rhamnolipids combined, only ¼ of the concentration rather than the full dose of each single agent is required to achieve the same nematode control efficacy (50% reduction of nematode infestation; Figures 6F,G). This validates the two compounds to exert synergistic effects. Intriguingly, by increasing the doses for combinations, the combined effect is diminished and even appears antagonistic. Similar results were reported previously in the analyses of antibacterial effects, which were dependent on the ratio of prodigiosin and rhamnolipids (Hage-Hülsmann et al., 2018).

Synergistic effects between biosurfactants including rhamnolipids and various antibiotics have been described multiple times before (Boonlarppradab et al., 2008; Williamson et al., 2008; Sotirova et al., 2012; Magalhães and Nitschke, 2013; Das et al., 2014; Rossi et al., 2016). On the one hand, rhamnolipids, which exhibit surface-active properties, can increase the solubility of the drug and facilitate its access to target cells (Beal and Betts, 2000; Abdel-Mawgoud et al., 2010). On the other hand, rhamnolipids can perturb the packing of the cell membrane phospholipids by intercalating into the bilayer, which leads to increased permeability of the cell membrane (Dowhan, 1997; Ortiz et al., 2006). As a consequence, the interaction of combined applications facilitates more effective penetration through biological interfaces to better reach the site of action (Bhadoriya et al., 2013; Bnyan et al., 2018; Hage-Hülsmann et al., 2018).

However, the role of rhamnolipids in combined antinematodal activity goes far beyond that. Plants have developed sophisticated defense mechanisms that enhance resistance to their enemies. After perception of rhamnolipids, early events of cell signaling, including calcium influx, MAP kinase activation, ROS accumulation, and defense-related gene stimulation were detected in plants (Garcia-Brugger et al., 2006; Varnier et al., 2009). Besides, rhamnolipids also trigger the activation of a phytohormone-regulated immune signaling network and thus modulate late defense responses to a diversity of phytopathogens (Pieterse et al., 2012; Sanchez et al., 2012). A recent study confirmed that di-rhamnolipids put *A. thaliana* on alert so that the plant responds stronger to *H. schachtii* attack (Bredenbruch et al., 2023). The combined application of rhamnolipids and prodiginines may therefore effectuate molecular structures and processes on multiple levels in both, the plant and the pathogen, and may pose a promising starting point for the development of multicomponent antinematodal agents.

4. Materials and methods

4.1. Engineering and characterization of *Pseudomonas putida* strains, PigC activity assay

4.1.1. Bacterial strains and standard cultivation conditions

Cultivation of *P. putida* KT2440 (Nelson et al., 2002; Belda et al., 2016) was conducted at 30°C, if not stated otherwise, shaking (130 rpm) in Erlenmeyer shake flasks in LB medium (Carl Roth, Karlsruhe, Germany), or on LB agar plates (LB medium completed with 15 g/L Agar). Small scale production tests were conducted in TB medium (Carl Roth, Karlsruhe, Germany) in Flowerplates (m2p-labs GmbH, Baesweiler, Germany). Cultures of *P. putida* pig-r2 Δ*pigD* (Klein et al., 2017) were supplemented with 80 µg/mL streptomycin, MBC strains created in the present study with 50 µg/mL tetracycline, and MBC strains carrying pVLT33 derived plasmids with 25 µg/mL kanamycin. *Escherichia coli* strains S17-1 (Simon et al., 1983; used for conjugation), and DH5α (Hanahan, 1983; used for cloning) were cultivated at 37°C under constant agitation (120 rpm) in shake flasks in liquid LB medium or on LB agar plates.

4.1.2. Cloning of integrative yTREX vector with MBC biosynthetic genes and ligase expression plasmids

The synthetic MBC biosynthesis-encoding *pig* gene cluster was PCR-amplified in three parts for assembly into the yTREX vector (Domröse et al., 2017; Weihmann et al., 2020) which was linearized with endonuclease I-*Sce*I: *pigA* (primers AD142 + 171, 1,239 bp), *pigFGHI* (primers AD172 + 162, 4,867 bp) and *pigJKLMN* (primers AD163 + 164, 5,033 bp) using vector pPIG (Loeschcke et al., 2013) as template. In addition, *lacZ* was amplified as promotorless gene (primers AD124 + 125, 3,127 bp) using vector pRcExpII2-YF1-FixJ-PFixK2-LacZ (Weihmann et al., 2020) as template. All genes were amplified with the respective 5′-UTR sequences including the ribosome binding sites; primers added homology arms to each of the fragments. Assembly of the vector yTREX-MBC-lacZ, carrying the gene cassette *pigA-pigFGHIJKLMN-lacZ*, in *Saccharomyces cerevisiae* VL6-48 was conducted as previously described (Domröse et al., 2017; Weihmann et al., 2020). Plasmid pVLT33-pigC, carrying the *pigC* gene with an adapted codon usage for *P. putida* (Brands et al., 2020), was used for PigC expression. The *pigB* gene was amplified (primers RW144 + 145, 2090 bp) using yTREX-pig (Domröse et al., 2017) as template. The vector and PCR product were hydrolyzed with endonucleases *Hind*III und *Xba*I and ligated to obtain pVLT33-pigC-pigB. All plasmids and oligonucleotides are listed in Supplementary Table S1.

4.1.3. Generation of MBC producing *Pseudomonas putida* strains

To generate *P. putida* production strains, the plasmid yTREX-MBC-lacZ was transformed into *E. coli* S17-1 and further transferred to *P. putida* KT2440 via conjugation as previously described (Weihmann et al., 2020). Since yTREX constructs do not replicate in *P. putida*, positive selection for strains in which Tn5 transposition of the recombinant yTREX transposon occurred, could be conducted by using LB medium supplemented with tetracycline. In addition, 25 µg/mL irgasan was added to prevent *E. coli* growth. Among exconjugants, production strains were identified visually after 16 h of cultivation on agar plates (Weihmann et al., 2020): The selection medium after conjugation was additionally supplemented with 0.3 mM X-gal (stock solution: 50 mM in DMF), and expression strains were identified by blue color due to β-galactosidase activity.

4.1.4. Analysis of MBC biosynthesis in *Pseudomonas putida*

For verification of MBC biosynthesis in small scale cultivation, expression cultures of *P. putida* pig-r2 Δ*pigD* and MBC strains (denoted with 2, 4, 5, 6, 7, 8, 9, 10, 11, 12, 13, 15, 16, 17, 18, 20, 21 or 22) (n = 4, independent biological replicates) were cultivated in Flowerplates. To this end, 1 mL precultures in LB medium were used for inoculation of 1,1 mL main cultures in TB medium to an OD (650 nm) of 0.05. Flowerplates were covered with breathable air sheets (139.7 µm sterile Rayon films, VWR North America Cat.No. 60941-086) and incubated for 24 h (30°C, 1,400 rpm). After that, 700 µL samples were used for cell harvesting (15,000 rpm, 5 min). The pellet was resuspended in 300 µL methanol and subjected to sonication in a water bath (Sonorex RH 100 H) for 10 min. After centrifugation (15,000 rpm, 5 min), the supernatant was dried at 45°C under reduced pressure (in a Concentrator 5,301). For 2-phase extraction, 300 µL DCM und 300 µL MilliQ-water were added and mixed well, before centrifugation (15,000 rpm, 3 min). The organic lower layer was transferred in a fresh reaction tube and the extraction repeated. The resulting pooled DCM was again dried (45°C, Eppendorf Concentrator 5,301). Samples were resuspended in 200 µL methanol, centrifuged (15,000 rpm, 1 min) and finally subjected to LC–MS analysis or stored until that at 4°C. LC–MS analysis was conducted using an HP 1100 Series LC/MSD (Agilent Analytical Instruments) with an Atlantis T3 column (3 µm, 3*100 mm) from Waters. The eluents water (A) and methanol (B), both supplemented with 0.1% formic acid, were used for gradient chromatography at 0.6 mL/min flow rate: Starting at 90% A and 10% B, increasing to 60% B in 4 min, then in further 2 min to 100% B, which was maintained for 4 min. After that, starting conditions were implemented again (10% B) and held for 1 min. Sample volumes of 10 were injected and detection was accomplished with a G1315A DAD-detector and an G1946A mass spectrometer (API-ES, positive ion mode, single quadrupole detector, m/z-range 100–2000). After verification of specific signals corresponding to the ion $[M+H]^+$ of MBC (191 m/z), the UV/Vis signal (364 nm) of the corresponding peaks detected at 6.7 min were evaluated for relative quantification with reference to the values obtained with strain *P. putida* pig-r2 Δ*pigD*. For subsequent routine MBC analysis, HPLC-PDA analysis using an LC-10Ai (Shimadzu Deutschland GmbH, Duisburg, Germany) was also applied with an SPDM10Avp photodiode array detector (PDA), and an Accucore™ C18 HPLC column (2.6 µm, 4.6*50 mm) from Thermo Fisher Scientific (Walkham, United States). At a column oven temperature of 30°C, 10 µL samples were analyzed at 1 mL/min flow rate in a gradient elution using water (A) and acetonitrile (B), both with 0.1% formic acid: Starting at 95%A and 5% B for 0.5 min, increasing to 25% B at 0.9 min, to 55% at 9.5 min, and to 98% at 10 min, which was held for 1 min, before returning to 5% B at 11.5 min, which was maintained for 2 min. Chromatograms were recorded at 360 nm and detected MBC at 4.5 min (λ_{max} 363 nm). To analyze MBC in 100 mL cultures, 1 g polyurethane (PU) foam

cubes were added as described for mutasynthesis conditions, and extracted with 15 mL ethanol.

4.1.5. Quantification of *pig* gene transcript by RT-qPCR

Reverse transcription (RT) followed by quantitative PCR (qPCR) was employed to quantify mRNA levels of *pigN*. Precultures, grown in LB medium, were used to inoculate 1 mL TB main cultures of *P. putida* pig-r2 Δ*pigD* and MBC18 with pVLT33-pigC-pigB to an OD (650 nm) of 0.05 ($n = 3$, independent biological replicates). These were incubated shaking (1,200 rpm) at 30°C for 4 h, before induction of the latter with 0.5 mM IPTG (10 µL of a 50 mM stock solution in water). After additional 4 h incubation, 500 µL of each culture were harvested to extract total RNA with the NucleoSpin® RNA-Kit (Macherey-Nagel, Düren, Germany). DNAse treatment was conducted in three steps with DNase from Macherey-Nagel, Qiagen (Hilden, Germany) and Ambion (Thermo Fisher Scientific). The Maxima Reverse Transcriptase (Thermo Fisher Scientific) was used for reverse transcription of 2000 ng RNA in 20 µL volumes. The qPCR reaction mix contained 9.2 µL of the cDNA solution (diluted to correspond to 50 ng RNA), 0.4 µL containing 4 pmol of each primer (stocks: 10 pmol/µL), and 10 µL Maxima SYBR Green/ROX qPCR Master Mix (2x; Thermo Fisher Scientific). All qPCR reactions were carried out as technical quadruplicates in addition to the biological triplicates. Controls without reverse transcriptase and without template as well as monitoring of PCR product melting curves ensured signal specificity. Calibration with the pPIG plasmid allowed determination of *pigN* copy numbers in *P. putida* pig-r2 Δ*pigD* and MBC18, which were 177×10^4 ($\pm 4 \times 10^4$) and 683×10^4 ($\pm 12 \times 10^4$) per 100 ng total RNA, respectively. For direct comparison, the data was evaluated as expression levels relative to the signal of *P. putida* pig-r2 Δ*pigD*. To corroborate comparability, the transcript levels of *rpoD* were analyzed as internal control, which yielded similar results in both strains as expected [571×10^4 ($\pm 16 \times 10^4$) and 750×10^4 ($\pm 30 \times 10^4$) per 100 ng total RNA].

4.1.6. Mutasynthesis in small scale cultivation

Expression cultures of *P. putida* pig-r2 Δ*pigD* and strains MBC13, −17, −18 with plasmids pVLT33-pigC or pVLT33-pigC-pigB ($n = 3$, independent biological replicates) were cultivated in Flowerplates. Precultures in 1 mL LB medium were used for inoculation of 1 mL main cultures in TB medium to an OD (650 nm) of 0.05. Flowerplates were covered with breathable air sheets and incubated for 4 h (30°C, 1,200 rpm), before 1 mM MAP was supplemented to the cultures (20 µL of a 50 mM stock solution in DMSO) and gene expression in strains with plasmids was induced by addition of 0.5 mM IPTG (10 µL of a 50 mM stock solution in water). Cultivation was subsequently continued for 20 h at 30°C or 25°C. After that, cultures were harvested (12,000 rpm, 2 min). The pellets were pre-resolved with 20 µL milliQ-water and extracted with 500 µL acidified ethanol [4% (*v*/*v*) 1 N HCl in ethanol]. After centrifugation (2 min, 14,000 rpm), 150 µL samples were either diluted by a factor of 10 or directly subjected to spectrophotometric analysis in a microplate reader "Infinite M1000 pro" (Tecan Group LTD., Maennedorf, Switzerland) to measure characteristic absorption spectra from 400 to 700 nm. Plotting the absorption at 535 nm facilitated comparative evaluation. For quantification of prodigiosin formation via the previously published molar extinction coefficient (Domröse et al., 2015), the signal of the Tecan plate reader was calibrated with solutions of known concentration based on ε (535 nm) [$M^{-1}\ cm^{-1}$] = 139,800 (Domröse et al., 2015). Prodigiosin titers (expressed in mg/L) were determined by considering the molecular weight of the compound (323.432 g/mol) and the extracted culture volume.

4.1.7. PigC substrate acceptance assay

The *in vitro* assay with cell lysate of *E. coli* BL21 (DE3) pET28a(+)-*pigC* was performed as described previously (Klein et al., 2017; Brass et al., 2019). Accordingly, the heterologous expression of PigC was carried out using *E. coli* BL21 (DE3) pET28a(+)-*pigC* cells, which were stored at −20°C after cultivation and harvesting. Frozen cells (1 g) were thawed and resuspended in potassium phosphate buffer (KP_i buffer, 50 mM, pH 7.0; 5 mL). The cell suspension was disrupted using a SONOPULS Ultrasonic homogenizer (Bandelin, Berlin, Germany) for 2 × 5 min (five cycles, 40% power), to obtain lysed cells which were used for the PigC substrate acceptance assay. The assay solution contained 440 µL of cell lysate in KP_i buffer (50 mM, pH 7.0), 25 µL of a pyrrole **5**, **11a**, **11b** solution in DMSO (20 mM, end concentration: 1 mM), 25 µL of an MBC (**6**) solution in DMSO (20 mM, end concentration: 1 mM) and 10 µL of an ATP•Na_2 solution in water (62.5 mM, end concentration: 1.25 mM). The reaction mixture was shaken in a 1.5 mL tube at 300 rpm and 30°C for 4 h. The supernatant was removed after centrifugation (5 min, 21,100 rcf, 23°C) and the prodiginine pellet was resuspended in 300 µL acidic ethanol [4% (*v*/*v*) 1 N HCl in ethanol]. After centrifugation (5 min, 21,100 rcf, 23°C), the supernatant was transferred in a new 1.5 mL reaction tube and documented photographically.

4.2. Chemical precursor syntheses

4.2.1. General experimental procedures for chemical syntheses

All reactions were carried out under nitrogen atmosphere and magnetic stirring. Used glassware and magnetic stirring bars were dried previously at 110°C. All starting materials were purchased from commercial sources without further purification unless stated otherwise. Dichloromethane, diethyl ether, ethyl acetate (EtOAc) and petroleum ether (PE) were distilled prior to use. Tetrahydrofuran (THF) was used directly. Reactions were monitored by GC–MS, ^{1}H-NMR and thin layer chromatography (TLC; Polygram SIL G/UV254, Macherey-Nagel) using an acidic solution of *p*-anisaldehyde for staining or UV light at 245 nm for visualization. Purification of reaction products was carried out by flash chromatography on silica gel 60 (particle size 0.040–0.063 mm, 230–240 mesh, Macherey-Nagel). Analytics were carried out as described in the Supplementary Information, including Supplementary Tables S2, S3, and Supplementary Figure S5. The precursors 2-methyl-3-*N*-amylpyrrole (MAP, **5**), *tert*-butyloxycarbonyl-5′-formyl-4′-methoxy-1*H*,1′*H*-2,2′-bipyrrole (*boc*-MBC, *Boc*-**6**) and prodigiosin (**1**) as chemical references were synthesized as previously described (Dairi et al., 2006; Domröse et al., 2015).

4.2.2. *N*-methoxy-*N*-methyloct-7-enamide (8)

To a solution of 7-octenoic acid (2 mL, 13.0 mmol, 1.0 eq.) in dichloromethane (70 mL) was added *N*,O-dimethylhydroxylamine hydrochloride (1.19 g, 19.5 mmol, 1.50 eq.),

N-(3-dimethylaminopropyl)-*N*′ethylcarbodiimid hydrochloride (3.03 g, 19.5 mmol, 1.5 eq.) and 4-(dimethylamino)pyridine (2.38 g, 19.5 mmol, 1.5 eq.). After stirring for 22 h at 22°C, the reaction mixture was quenched with a saturated solution of NaCl and extracted with dichloromethane (3 × 50 mL). The combined organic layers were first washed with 1 N HCl, afterwards with saturated $NaHCO_3$ solution and dried over $MgSO_4$. After removal of the solvent under reduced pressure *N*-methoxy-*N*-methyloct-7-enamide (**8**, 2.29 g, 12.4 mmol, 95%) was obtained as a yellow oil and was used for the following experiment without further purification. R_f = 0.15 (PE/EtOAc 85:15); **^{1}H-NMR** (600 MHz, $CDCl_3$): δ [ppm] = 1.36 (m_c, 2H, 4-H), 1.41 (m_c, 2H, 5-H), 1.64 (m_c, 2H, 3-H), 2.05 (m_c, 2H, 6-H), 2.41 (t, $^3J_{2,3}$ = 7.7 Hz, 2H, 2-H), 3.18 (s, 3H, 1″-H), 3.68 (s, 3H, 1′-H), 4.93 (dd, $^{cis,3}J_{8a,7}$ = 10.2 Hz, $^2J_{8a,8b}$ = 1.2 Hz, 1H, 8-H_a), 4.99 (ddd, $^{trans,3}J_{8b,7}$ = 17.1 Hz, $^2J_{8b,8a}$ = 1.8 Hz, $^4J_{8b,6}$ = 1.8 Hz, 1H, 8-H_b), 5.80 (ddt, $^{trans,3}J_{7,8b}$ = 17.0 Hz, $^{cis,3}J_{7,8a}$ = 10.2 Hz, $^3J_{7,6}$ = 6.7 Hz, 1H, 7-H); **^{13}C-NMR** (151 MHz, $CDCl_3$): δ [ppm] = 24.6 (C-3), 28.8 (C-4), 29.1 (C-5), 32.0 (C-2), 32.3 (C-1″) 33.8 (C-6) 61.3 (C-1′), 114.5 (C-8), 139.1 (C-7); **IR** (ATR-film): $\tilde{\nu}$ [1/cm] = 3,074, 2,931, 2,855, 1,667, 1,463, 1,415, 1,384, 1,178, 998, 910, 732; **MS** (APCI, positive ion): *m*/*z* = 186 [$(M)^+$], 97, 83, 55.

4.2.3. Non-8-en-2-one (9)

N-methoxy-*N*-methyloct-7-enamide (**8**, 2.29 g, 12.4 mmol, 1.0 eq.) was dissolved in dry THF (100 mL) and methylmagnesium chloride (3 M in diethyl ether, 12.4 mL, 37.1 mmol, 3.0 eq.) was added within 15 min at 0°C. The reaction mixture was stirred for 1.5 h at 0°C and afterwards quenched by the addition of a saturated solution of NH_4Cl at 0°C and extracted with dichloromethane (3 × 60 mL). The combined organic layers were dried over $MgSO_4$ and the solvent was evaporated under reduced pressure to yield non-8-en-2-one (**9**, 1.63 g, 11.6 mmol, 94%) as a yellowish oil without further purification. R_f = 0.40 (PE/EtOAc 85:15); **^{1}H-NMR** (600 MHz, $CDCl_3$): δ [ppm] = 1.25–1.34 (m, 2H, 5-H), 1.35–1.43 (m, 2H, 6-H), 1.58 (tt, $^3J_{4,3}$ = 7.5 Hz, $^3J_{4,5}$ = 7.5 Hz, 2H, 4-H), 2.05 (m, 2H, 7-H), 2.13 (s, 3H, 1-H), 2.42 (t, $^3J_{3,4}$ = 7.5 Hz, 2H, 3-H), 4.93 (ddt, $^{cis,3}J_{9a,8}$ = 10.2 Hz, $^4J_{9a,7}$ = 2.3 Hz, $^2J_{9a,9b}$ = 1.2 Hz, 1H, 9-H_a), 4.99 (dd, $^{trans,3}J_{9b,8}$ = 17.1 Hz, $^2J_{9b,9a}$ = 1.7 Hz, 1H, 9-H_b), 5.79 (ddt, $^{trans,3}J_{8,9b}$ = 17.0 Hz, $^{cis,3}J_{8,9a}$ = 10.2 Hz, $^3J_{8,7}$ = 6.7 Hz, 1H, 8-H); **^{13}C-NMR** (151 MHz, $CDCl_3$): δ [ppm] = 23.8 (C-4), 28.7 (C-5), 28.8 (C-6), 30.0 (C-1), 33.7 (C-7), 43.9 (C-3), 114.6 (C-9), 139.0 (C-8), 209.4 (C-2); **IR** (ATR-film): $\tilde{\nu}$ [1/cm] = 2,928, 2,855, 1738, 1721, 1,443, 1,363, 1,217, 907; **MS** (APCI, positive ion): *m*/*z* = 123.

4.2.4. Dec-9-en-2-one oxime (10)

To a solution of the non-8-en-2-one (**9**, 1.73 g, 12.4 mmol, 1.0 eq.) in ethanol (6.2 mL) was added pyridine (0.78 g, 0.8 mL, 9.89 mmol, 0.8 eq.) and grounded hydroxylamine hydrochloride (1.5 eq.). The reaction mixture was refluxed for 2 h and afterwards extracted with dichloromethane (3 × 25 mL). The combined organic layers were washed with 1 N HCl (3 × 20 mL) and dried over $MgSO_4$. After removal of the solvent under reduced pressure, dec-9-en-2-one oxime (**10**, 1.76 g, 11.3 mmol, 92%) was obtained in a diastereomeric mixture of *E*:*Z* (1:3) without further purification. R_f = 0.34 (PE/EtOAc 80:20); **^{1}H-NMR** (600 MHz, $CDCl_3$): δ [ppm] = 1.28–1.36 (m, 2H, 5-H), 1.37–1.44 (m, 2H, 6-H), 1.51 (tt, $^3J_{4,3}$ = 7.5 Hz, $^3J_{4,5}$ = 7.5 Hz, 2H, 4-H), 1.87 (s, 3H, 1-H), 2.05 (dt, $^3J_{7,6}$ = 6.4 Hz, $^3J_{7,8}$ = 6.4 Hz, 2H, 7-H), 2.18 (t, $^3J_{3,4}$ = 7.5 Hz, 2H, 3-H), 4.94 (ddt, $^{cis,3}J_{9a,8}$ = 10.2 Hz, $^4J_{9a,7}$ = 2.4 Hz, $^2J_{9a,9b}$ = 1.3 Hz, 1H, 9-H_a), 5.00 (dd, $^{trans,3}J_{9b,8}$ = 17.1 Hz, $^2J_{9b,9a}$ = 1.5 Hz, 1H, 9-H_b), 5.80 (ddt, $^{trans,3}J_{8,9b}$ = 17.0 Hz, $^{cis,3}J_{8,9a}$ = 10.4 Hz, $^3J_{8,7}$ = 6.6 Hz, 1H, 8-H); **^{13}C-NMR** (151 MHz, $CDCl_3$): δ [ppm] = 13.4 (C-1), 26.2 (C-4), 28.7 (C-5), 28.8 (C-6), 33.7 (C-7), 35.8 (C-3), 114.4 (C-9), 139.1 (C-8), 159.1 (C-2); **IR** (ATR-film): $\tilde{\nu}$ [1/cm] = 3,074, 2,929, 2,855, 1,637, 1,461, 1,369, 910; **MS** (APCI, positive ion): *m*/*z* = 156 [$(M)^+$], 83; **HRMS** (ESI, positive ion): calculated for $C_9H_{18}NO$ $[(M+H)]^+$ = 156.1383, found = 156.1384.

4.2.5. 3-(hex-5-en-1-yl)-2-methyl-1*H*-pyrrole (11a)

A reaction mixture of dec-9-en-2-one oxime (**10**, 0.72 g, 4.64 mmol, 1.0 eq.), potassium hydroxide (1.30 g, 46.4 mmol, 5.0 eq.), water (62.7 mg, 62.3 µL, 3.48 mmol, 0.75 eq.) and DMSO (8.9 mL) was heated at 90–100°C (using previously degassed DMSO on molecular sieves (3.5 Å) could increase the yield). Over a period of 2 h, a solution of 1,2-dichloroethane (1.38 g, 1.10 mL, 13.9 mmol, 3.5 eq.) in DMSO (1 mL) was added dropwise. After 1 h of 1,2-dichloroethane addition a secondary amount of potassium hydroxide (5.0 eq.) was added. After an overall reaction time of 4 h at 90–100°C the reaction mixture was allowed to reach room temperature and subsequently ice water (20 mL) was added. The mixture was extracted with diethyl ether (3 × 20 mL) and the combined organic layers were dried over $MgSO_4$. After the solvent was evaporated under reduced pressure the crude product was purified by column chromatography on silica gel [PE:dichloromethane (60:40) + 1% trimethylamine (*v*/*v*)] to obtain 3-(hex-5-en-1-yl)-2-methyl-1*H*-pyrrole (**11a**, 228 mg, 1.40 mmol, 30%) as yellowish oil. R_f = 0.37 (PE/dichloromethane 60:40); **^{1}H-NMR** (600 MHz, $CDCl_3$): δ [ppm] = 1.44 (tt, $^3J_{3'',2''}$ = 7.5 Hz, $^3J_{3'',4''}$ = 7.5 Hz, 2H, 3″-H), 1.51–1.59 (m, 2H, 2″-H), 2.02–2.14 (m, 2H, 4″-H), 2.18 (s, 3H, 1′-H), 2.39 (t, $^3J_{1'',2''}$ = 7.6 Hz, 2H, 1″-H), 4.93 (dd, $^{cis,3}J_{6a'',5''}$ = 10.2 Hz, $^2J_{6a'',6b''}$ = 1.2 Hz, 1H, 6″-H_a), 5.00 (dd, $^{trans,3}J_{6b'',5''}$ = 17.1 Hz, $^2J_{6b'',6a''}$ = 1.7 Hz, 1H, 6″-H_b), 5.82 (ddt, $^{trans,3}J_{5'',6b''}$ = 16.9 Hz, $^{cis,3}J_{5'',6a''}$ = 10.2 Hz, $^3J_{5'',4''}$ = 6.7 Hz, 1H, 5″-H), 6.01 (dd, $^4J_{4,1}$ = 2.8 Hz, $^3J_{4,5}$ = 2.8 Hz, 1H, 4-H), 6.59 (dd, $^3J_{5,1}$ = 2.7 Hz, $^3J_{5,4}$ = 2.7 Hz, 1H, 5-H), 7.70 (brs, 1H, 1-NH); **^{13}C-NMR** (151 MHz, $CDCl_3$): δ [ppm] = 11.2 (C-1′), 25.9 (C-1″), 28.9 (C-3″), 31.0 (C-2″), 33.9 (C-4″), 109.0 (C-4), 114.3 (C-6″), 115.0 (C-5), 119.7 (C-3), 123.4 (C-2), 139.4 (C-5″); **IR** (ATR-film): $\tilde{\nu}$ [1/cm] = 3,385, 2,928, 2,855, 1741, 1,467, 1,363, 1,217, 907, 712; **MS** (APCI, positive ion): *m*/*z* = 164 [$(M)^+$]; 121, 108; **HRMS** (ESI, positive ion): calculated for $C_{11}H_{18}N$ $[(M+H)]^+$ = 164.1434, found = 164.1433.

4.2.6. 6-(2-methyl-1*H*-pyrrol-3-yl)hexan-1-ol (11b)

9-BBN (0.5 N in THF, 5.54 g, 3.10 mmol, 2.2 eq.) was added to a solution of 3-(hex-5-en-1-yl)-2-methyl-1*H*-pyrrole (**11a**, 230 mg, 1.41 mmol, 1.0 eq.) in dry THF (11.6 mL) over a period of 15 min at 0°C. After stirring for 1 h at 0°C, the reaction mixture was heated up at 70°C under reflux for 3 h. Subsequently an aqueous solution of 3 N NaOH (2.35 g, 2.35 mL, 7.05 mmol, 5.0 eq.) and 30% H_2O_2 (2.24 g, 2.00 mL, 19.7 mmol, 14.0 eq.) was added at 0°C. After 1 h at 0°C the reaction mixture was allowed to reach room temperature and was stirred for further 15 h at 22°C. Ice water (40 mL) was added and the mixture was extracted with dichloromethane (3 × 50 mL). The combined organic layer was dried over $MgSO_4$, the solvent was evaporated under reduced pressure and the crude product was purified by column chromatography on silica gel [PE:ethyl acetate (70:30 to 50:50) + 1% trimethylamine (*v*/*v*)] to isolate 6-(2-methyl-1*H*-pyrrol-3-yl)hexan-1-ol (**11b**, 193 mg, 1.06 mmol, 76%) as orange oil. R_f = 0.20 (PE/EtOAc 70:30); **^{1}H-NMR** (600 MHz, $CDCl_3$): δ [ppm] = 1.20 (brs, 1H, 1-OH), 1.34–1.42 (m, 4H, 3-H, 4-H), 1.51–1.61 (m, 4H, 2-H, 5-H), 2.18 (s, 3H, 1″-H), 2.39 (t, $^3J_{6,5}$ = 7.7 Hz, 2H, 6-H),

3.64 (t, $^{3}J_{1,2}$ = 7.1 Hz, 2H, 1-H), 6.00 (dd, $^{4}J_{4',1'}$ = 2.8 Hz, $^{3}J_{4',5'}$ = 2.8 Hz, 1H, 4′-H), 6.59 (dd, $^{3}J_{5',1'}$ = 2.7 Hz, $^{3}J_{5',4'}$ = 2.7 Hz, 1H, 5′-H), 7.72 (brs, 1H, 1′-NH); **^{13}C-NMR** (151 MHz, $CDCl_3$): δ [ppm] = 11.2 (C-1″), 25.8 (C-4), 26.0 (C-6), 29.4 (C-3), 31.4 (C-5), 33.0 (C-2), 62.7 (C-1), 109.0 (C-4′), 115.0 (C-5′), 119.7 (C-3′), 123.4 (C-2′); **IR** (ATR-film): $\tilde{\nu}$ [1/cm] = 3,373, 2,928, 2,855, 1735, 1,436, 1,363, 1,223, 1,059, 748; **MS** (APCI, positive ion): *m*/*z* = 182 [$(M)^+$], 164, 108; **HRMS** (ESI, positive ion): calculated for $C_{11}H_{20}NO$ [$(M+H)]^+$ = 182.1539, found = 182.1539.

4.3. Muta- and semisynthetic hydroxylated prodiginine production

4.3.1. General procedure for preparative scale mutasynthesis

A preculture of *P. putida* MBC18 with pVLT33-pigC-pigB in LB medium (25 µg/mL kanamycin) was incubated in a shake flask at 30°C and 130 rpm overnight. Five main cultures of 100 mL each in TB medium (25 µg/mL kanamycin) were inoculated to an OD_{650} of 0.05 and incubated in 1 l baffled flask with air-sheet seals for 4 h at 30°C and 130 rpm. The pyrrole precursor was dissolved in DMSO (5–50 mM stock, 10 mL). To each culture 2 mL of pyrrole stock solution was added (final concentration 0.1–1.0 mM). Induction was performed with 0.5 mM IPTG (50 mM stock in dH2O; 1 mL). After an additional hour at 30°C and 130 rpm, 1 g of polyurethane (PU) foam cubes (Softpur, Göllheim, Germany: Softpur foam, 25 kgm^{-3} density, 4 kPa compression hardness, each cube approximately 1 cm^3) were added to each culture and the cultures were incubated for further 23 h at 30°C and 130 rpm. After a total of 28 h of cultivation, the foam cubes were wrung out, washed with dH_2O, and then extracted with diethyl ether (250–500 mL) in a soxhlet extractor. After evaporation of the solvent, the crude product was dissolved in diethyl ether (20 mL), washed with water, and the aqueous layer was extracted with dichloromethane (3 × 15 mL). The combined organic layers were washed with saturated NaCl (20 mL) and dried over $MgSO_4$. After evaporation of the solvent, the crude product was purified by flash column chromatography on silica gel (CH_2Cl_2 + 1.0–1.5% NH_3 in MeOH). For subsequent hydroboration, the product was further purified by reversed-phase chromatography (column: ISAspher 100–5 C18 AQ, 5 µm, 150*20 mm from ISERA GmbH, Düren, Germany; column oven: 35°C; eluent: 60:40 acetonitrile:water + 0.1% formiate; flow rate 15 mL/min; injection of samples in 1 mL ethanol) to obtain the mutasynthesis product as red solid.

4.3.2. 4-Methoxy-5-[(5-methyl-4-hex-5-en-1-yl-2*H*-pyrrol-2-yliden)methyl]-1*H*,1′*H*-2,2′-bipyrrol (3)

According to the general procedure for preparative mutasynthesis and the use of pyrrole **11a** (12.2 mg, 75.0 µmol, 7.5 mM in DMSO, end concentration in 500 mL culture: 0.15 mm) as precursor prodiginine **12** (15.0 mg, 40.3 µmol, 54%) was obtained as red solid. R_f = 0.15 (dichloromethane); **^{1}H-NMR** (600 MHz, $CDCl_3$): δ [ppm] = 1.43 (tt, $^{3}J_{8'',7''}$ = 7.5 Hz, $^{3}J_{8'',9''}$ = 7.5 Hz, 2H, 8″-H), 1.53–1.59 (m, 2H, 7″-H), 2.08 (dt, $^{3}J_{9'',8''}$ = 7.2 Hz, $^{3}J_{9'',10''}$ = 7.2 Hz, 2H, 9″-H), 2.41 (t, $^{3}J_{6'',7''}$ = 7.6 Hz, 2H, 6″-H), 2.54 (s, 3H, 12″-H), 4.01 (s, 3H, 7-H), 4.95 (dd, $^{cis,3}J_{11a'',10''}$ = 10.2 Hz, $^{2}J_{11a'',11b''}$ = 2.2 Hz, 1H, 11″-H_a), 5.01 (dd, $^{trans,3}J_{11b'',10''}$ = 17.1 Hz, $^{2}J_{11b'',11a''}$ = 1.7 Hz, 1H, 11″-H_b), 5.80 (ddt, $^{trans,3}J_{10'',11b''}$ = 16.9 Hz, $^{cis,3}J_{10'',11a''}$ = 10.2 Hz, $^{3}J_{10'',9''}$ = 6.7 Hz, 1H, 10″-H), 6.08 (d, $^{4}J_{3,1}$ = 2.0 Hz, 1H, 3-H), 6.36 (dd, $^{3}J_{4',5'}$ = 3.7 Hz, $^{4}J_{4',1'}$ = 2.3 Hz, 4′-H), 6.68 (d, ^{3}J = 2.6 Hz), 6.92 (ddd, ^{3}J = 3.9 Hz, ^{3}J = 2.5 Hz, ^{3}J = 1.3 Hz), 6.96 (s, 1H), 7.24 (d, $^{4}J_{3'',1''}$ = 2.7 Hz, 1H, 3″-H), 12.58 (brs, 1H, 1′-NH), 12.75 (brs, 2H, 1-NH, 1″-NH); **^{13}C-NMR** (151 MHz, $CDCl_3$): δ [ppm] = 12.6 (C-12″), 25.3 (C-6″), 28.6 (C-8″), 29.7 (C-7″), 33.7 (C-9″), 58.9 (C-7), 93.0 (C-3), 111.9 (C-4′), 114.7 (C-10″), 116.1 (C-8), 117.2 (C-3′), 120.9 (C-5), 122.4 (C-2′), 125.3 (C-2″), 127.1 (C-5′), 128.3 (C-4″), 128.4 (C-3″), 138.8 (C-9″), 146.9 (C-5″), 147.9 (C-2), 165.9 (C-4); **IR** (ATR-Film): $\tilde{\nu}$ [1/cm] = 3,163, 3,099, 2,974, 2,928, 2,857, 1,630, 1,604, 1,544, 1,512, 1,414, 1,356, 1,261, 1,158, 1,137, 1,044, 993, 960, 838, 756; **MS** (APCI, positive-Ion): *m*/*z* = 336 [$(M)^+$], 266, 163; **HRMS** (ESI, positive ion): calculated for $C_{21}H_{26}N_3O$ [$(M+H)]^+$ = 336.2070, found = 336.2076.

4.3.3. Semisynthesis toward 6-(2-((4-methoxy-1*H*,1′*H*-(2,2′-bipyrrole)-5-yl) methylene)-5-methyl-2*H*-pyrrole-4-yl)hexan-1-ol (3)

9-BBN (0.5 n in THF, 94.2 mg, 0.05 mmol, 2.2 eq.) was added to a solution of 4-Methoxy-5-((5-methyl-4-hex-5-en-1-yl-2H-pyrrole-2-yliden)methyl)-1*H*,1′*H*-2,2′-bipyrrole (**12**, 9 mg, 0.02 mmol, 1.0 eq.) in dry THF (2 mL) over a period of 15 min at 0°C. After stirring for 1 h at 0°C, the reaction mixture was heated up at 70°C under reflux for 3 h. Subsequently an aqueous solution of 3 N NaOH (39.9 mg, 105 µL, 0.12 mmol, 5.0 eq.) and 30% H_2O_2 (38.0 mg, 34.1 µL, 0.34 mmol, 14.0 eq.) was added at 0°C. After 1 h at 0°C the reaction mixture was allowed to reach room temperature and was stirred for further 15 h at 22°C. Ice water (10 mL) was added and the mixture was extracted with dichloromethane (3 × 15 mL). The combined organic layer was dried over $MgSO_4$, the solvent was evaporated under reduced pressure and the crude product was purified by column chromatography on silica gel [dichloromethane + 0.5–4.0% trimethylamine (*v*/*v*)] to isolate 6-(2-((4-methoxy-1*H*,1′*H*-(2,2′-bipyrrole)-5-yl)methylene)-5-methyl-2*H*-pyrrole-4-yl)hexan-1-ol (**3**, 6.10 mg, 0.02 mmol, 65%) as red solid. R_f = 0.16 (PE/EtOAc 50:50); **^{1}H-NMR** (600 MHz, $CDCl_3$): δ [ppm] = 1.28 (brs, 1H, 12″-OH), 1.37 (m_c, 4H, 8″-H, 9″-H), 1.50–1.63 (m, 4H, 7″-H, 10″-H), 2.40 (t, $^{3}J_{6'',7''}$ = 7.6 Hz, 2H, 6″-H), 2.54 (s, 3 H, 13″-H), 3.64 (t, $^{3}J_{11'',10''}$ = 6.6 Hz, 2H, 11″-H), 4.00 (s, 3H, 7-H), 6.08 (d, $^{4}J_{3,1}$ = 1.9 Hz, 1H, 3-H), 6.35 (dd, $^{3}J_{4',5'}$ = 4.3 Hz, $^{4}J_{4',1'}$ = 2.0 Hz, 1H, 4′-H), 6.67 (d, $^{4}J_{3'',1''}$ = 2.6 Hz, 1H, 3″-H), 6.92 (ddd, $^{3}J_{3',4'}$ = 3.9 Hz, $^{4}J_{3',5'}$ = 2.5 Hz, $^{4}J_{3',1'}$ = 1.4 Hz, 1H, 3′-H), 6.94 (s, 1H, 8-H), 7.23 (dd, $^{3}J_{5',4'}$ = 2.7 Hz, $^{3}J_{5',1'}$ = 1.3 Hz, 1-H, 5′-H), 12.56 (brs, 1H, 1′-NH), 12.72 (brs, 2H, 1-NH, 1″-NH); **^{13}C-NMR** (151 MHz, $CDCl_3$): δ [ppm] = 12.6 (C-13″), 25.0 (C-6″), 25.7 (C-8″), 29.1 (C-9″), 30.2 (C-7″), 32.9 (C-10″), 58.9 (C-7), 63.1 (C-11″), 93.0 (C-3), 111.9 (C-4′), 116.3 (C-8), 117.3 (C-3′), 120.9 (C-5), 122.4 (C-2′), 125.3 (C-2″), 127.2 (C-5′), 128.3 (C-4″), 128.4 (C-3″), 147.0 (C-5″), 148.0 (C-2), 166.0 (C-4); **IR** (ATR-film): $\tilde{\nu}$ [1/cm] = 3,422, 3,172, 2,930, 2,861, 1,630, 1,602, 1,543, 1,511, 1,363, 1,261, 1,137, 960, 748; **MS** (APCI, positive ion): *m*/*z* = 354 [$(M)^+$], 279, 157; **HRMS** (ESI, positive ion): calculated for $C_{21}H_{28}N_3O_2$ [$(M+H)]^+$ = 354.2176, found = 354.2179.

4.4. Assessment of effects on the plant-parasitic nematode *Heterodera schachtii*

4.4.1. Plant material and nematode culture

Arabidopsis thaliana Columbia (Col-0) seeds were surface-sterilized by soaking in 0.7% sodium hypochlorite for 5 min and

submerging them in 70% (*v*/*v*) ethanol for 1 min. Subsequently, the seeds were rinsed with sterile distilled water 5 times, dried at room temperature for 4 h and stored at 4°C for further experiments. *H. schachtii* cysts were harvested from the roots of mustard (*Sinapsis alba*), which was grown aseptically on modified Knop agar medium, and submerged with sterile 3 mM $ZnCl_2$ in the Baermann funnel (Grundler et al., 1991). After 7 days, the freshly hatched second-stage juveniles (J2s) were collected for subsequent analysis. All preparation procedures were performed under aseptic conditions.

4.4.2. EC_{50} (nematode infection) determination of di-rhamnolipids and prodiginines

EC_{50} determination of selected compounds was performed in an *in vitro* agar system: Petri dishes (90 mm diameter) were filled with modified Knop medium (Sijmons et al., 1991; Matera et al., 2021) supplemented with prodiginines or di-rhamnolipids at different concentrations (Supplementary Table S4). Stock solutions of prodiginines in DMSO were applied to implement a final concentration of 0.5% DMSO. The di-rhamnolipids, which were obtained by microbial production as a congener mixture as previously described (Bredenbruch et al., 2023), were solved in water. Accordingly, modified Knop medium alone or supplemented with 0.5% (v/v) DMSO served as control. On the medium, 2 surface-sterilized *A. thaliana* seeds were germinated aseptically and incubated in a climate chamber under a red/blue light with a 16-h/8-h light/dark photoperiod at 24°C (Sijmons et al., 1991). At 12 days post seeding, each plant was inoculated with approximately 60 *H. schachtii* J2s. At 10 days post inoculation, the total number of males and females on each plant was counted under a Stereo Microscope (Leica, Germany). EC_{50} was determined by using software 'CompuSyn' (Chou and Martin, 2005). Three independent biological replicates of the experiment were performed. Each biological replicate included at least 6 technical replicates (plants) per variant.

4.4.3. Determination of the combinatorial effect of compounds on nematode infection

Assays to measure combinatorial effects were carried out in an analogous experimental set-up as the EC_{50} determination described above. The concentration of compounds alone or in combination is detailed in Supplementary Table S5. The compound combination effects (antagonistic, additive or synergistic) were evaluated according to the Combination Index Plot obtained by the software 'CompuSyn' (Chou and Martin, 2005). The experiments were performed independently in triplicate.

4.4.4. Time-resolved analyses of the compounds' impact on nematodes

The time-resolved analysis consisted of four assays investigating nematode motility, stylet thrusting, infection, and development. Petri dishes (90 mm diameter) were filled with modified Knop medium supplemented with prodigiosin (**1**) or hydroxylated prodiginine **3** at the determined EC_{50}, which is 15.1 and 31.2 µM, respectively. Modified Knop medium alone or supplemented with 0.5% (*v*/*v*) DMSO served as controls.

4.4.4.1. Nematode motility

Approximately 30 *H. schachtii* J2 were inoculated in the center of a Petri dish containing the test compound. The location of J2s was documented after 30 and 60 min and the distance to the inoculation point was measured by Image J (Schneider et al., 2012). The experiment was performed independently in quadruplicate.

4.4.4.2. Nematode stylet thrusting

Two surface-sterilized *A. thaliana* seeds were germinated aseptically on the medium containing the test compound. At 12 days post seeding, approximately 60 *H. schachtii* J2 were inoculated to each plant. At 6 h post inoculation, 10 J2, which successfully penetrated the root epidermis, were tracked under a Stereo Microscope (Leica, Germany) in order to count the number of stylet movements for 5 min. The experiment was performed independently in quadruplicate.

4.4.4.3. Nematode infection and development

Two surface-sterilized *A. thaliana* seeds were germinated aseptically on the medium containing the test compound. At 12 days post seeding, approximately 60 *H. schachtii* J2 were inoculated to each plant. At 2, 4 and 10 days post inoculation, the number of males and females was counted, and the size of male and female nematodes was measured under a LeicaS4E Stereo Microscope (Leica, Germany) equipped with Leica Application Suite (LAS) software. Four independent biological replicates with 14 plants per variant and biological replicate ($n = 56$) were conducted for the nematode infection assay. Three independent biological replicates with in total $n = 70$ technical replicates (nematodes) were performed for the development experiment.

4.4.5. Statistical analysis of bioactivity evaluating data

All data are expressed as mean ± standard error (SE). Statistical analysis was performed by using one-way analysis of variance (ANOVA; $p < 0.05$; SIGMAPLOT 12.5, Systat Software, Inc., San Jose, CA, United States).

Data availability statement

The original contributions presented in the study are included in the article/Supplementary material, further inquiries can be directed to the corresponding authors.

Author contributions

AL, AS, JP, FG, K-EJ, and TD conceived the research concept and designed the experiments. RW, FG, SI, NB, KB, DK, TW, and HB performed microbiological work as well as chemical syntheses and production of prodiginines. CM, TT, and LB provided rhamnolipids. MH, XX, and LR conducted investigations of antinematode activities. DK, RW, and MH drafted the manuscript with input from all the authors. All authors contributed to the article and approved the submitted version.

Funding

The work was supported by grants from the German Bioeconomy Science Center. The scientific activities of the Bioeconomy Science Center were financially supported by the Ministry of Culture and Science within the framework of the NRW Strategieprojekt BioSC (no. 313/323-400-00213). Parts of this work were funded by the state of NRW in the project RhamnoLizer. This

work was supported by the Open Access Publication Fund of the University of Bonn.

Acknowledgments

The authors thank Birgit Henßen for analytical support. We further gratefully acknowledge excellent technical support by Ute Schlee and Stefan Neumann.

Conflict of interest

The authors declare that the research was conducted in the absence of any commercial or financial relationships that could be construed as a potential conflict of interest.

Publisher's note

Supplementary material

The Supplementary material for this article can be found online at: https://www.frontiersin.org/articles/10.3389/fmicb.2023.1151882/full#supplementary-material

References

Abdel-Mawgoud, A. M., Lépine, F., and Déziel, E. (2010). Rhamnolipids: diversity of structures, microbial origins and roles. *Appl. Microbiol. Biotechnol.* 86, 1323–1336. doi: 10.1007/s00253-010-2498-2

Beal, R., and Betts, W. B. (2000). Role of rhamnolipid biosurfactants in the uptake and mineralization of hexadecane in *Pseudomonas aeruginosa*. *J. Appl. Microbiol.* 89, 158–168. doi: 10.1046/j.1365-2672.2000.01104.x

Belda, E., Van Heck, R. G. A., Lopez-sanchez, M. J., Cruveiller, S., Barbe, V., Fraser, C., et al. (2016). The revisited genome of *Pseudomonas putida* KT2440 enlightens its value as a robust metabolic chassis. *Environ. Microbiol.* 18, 3403–3424. doi: 10.1111/1462-2920.13230

Berg, G. (2009). Plant-microbe interactions promoting plant growth and health: perspectives for controlled use of microorganisms in agriculture. *Appl. Microbiol. Biotechnol.* 84, 11–18. doi: 10.1007/s00253-009-2092-7

Berning, L., Schlütermann, D., Friedrich, A., Berleth, N., Sun, Y., Wu, W., et al. (2021). Prodigiosin sensitizes sensitive and resistant urothelial carcinoma cells to cisplatin treatment. *Molecules* 26:1294. doi: 10.3390/molecules26051294

Bhadoriya, S. S., Madoriya, N., Shukla, K., and Parihar, M. (2013). Biosurfactants: a new pharmaceutical additive for solubility enhancement and pharmaceutical development. *Biochem. Pharmacol. Open Access* 2:113. doi: 10.4172/2167-0501.1000113

Bnyan, R., Khan, I., Ehtezazi, T., Saleem, I., Gordon, S., O'Neill, F., et al. (2018). Surfactant effects on lipid-based vesicle properties. *J. Pharm. Sci.* 107, 1237–1246. doi: 10.1016/j.xphs.2018.01.005

Boonlarppradab, C., Kauffman, C. A., Jensen, P. R., and Fenical, W. (2008). Marineosins a and B, cytotoxic spiroaminals from a marine- derived actinomycete. *Org. Biomol. Chem.* 10, 5505–5508. doi: 10.1021/ol8020644

Brands, S., Brass, H. U. C., Klein, A. S., Pietruszka, J., Ruff, A. J., and Schwaneberg, U. (2020). A colourimetric high-throughput screening system for directed evolution of prodigiosin ligase PigC. *Chem. Commun.* 56, 8631–8634. doi: 10.1039/d0cc02181d

Brass, H. U. C., Klein, A. S., Nyholt, S., Classen, T., and Pietruszka, J. (2019). Condensing enzymes from Pseudoalteromonadaceae for prodiginine synthesis. *Adv. Synth. Catal.* 361, 2659–2667. doi: 10.1002/adsc.201900183

Bredenbruch, S., Mueller, C., Atemnkeng, H., Schroeder, L., Tiso, T., Blank, L. M., et al. (2023). The biological activity of bacterial rhamnolipids is linked to their molecular structure. *bioRxiv* [Epub ahead of preprint], doi: 10.1101/2023.01.23.525263

Chawrai, S. R., Williamson, N. R., Mahendiran, T., Salmond, G. P. C., and Leeper, F. J. (2012). Characterisation of PigC and HapC, the prodigiosin synthetases from *Serratia* sp. and *Hahella chejuensis* with potential for biocatalytic production of anticancer agents. *Chem. Sci.* 3, 447–454. doi: 10.1039/c1sc00588j

Cheng, F., Kovács, I. A., and Barabási, A.-L. (2019). Network-based prediction of drug combinations. *Nat. Commun.* 10:1197. doi: 10.1038/s41467-019-09186-x

Choi, S. Y., Lim, S., Yoon, K., Lee, J. I., and Mitchell, R. J. (2021). Biotechnological activities and applications of bacterial pigments violacein and prodigiosin. *J. Biol. Eng.* 15:10. doi: 10.1186/s13036-021-00262-9

Chou, T., and Martin, N. (2005). *CompuSyn for Drug Combinations: PC Software and User's Guide: A Computer Program for Quantitation of Synergism and Antagonism in Drug Combinations, and the Determination of IC50 and ED50 and LD50 Values*. ComboSyn Inc., Paramus.

Cook, T. B., Jacobson, T. B., Venkataraman, M. V., Hofstetter, H., Amador-Noguez, D., Thomas, M. G., et al. (2021). Stepwise genetic engineering of pseudomonas putida enables robust heterologous production of prodigiosin and glidobactin a. *Metab. Eng.* 67, 112–124. doi: 10.1016/j.ymben.2021.06.004

Couturier, M., Bhalara, H. D., Chawrai, S. R., Monson, R., Williamson, N. R., Salmond, G. P. C., et al. (2019). Substrate flexibility of the flavin-dependent dihydropyrrole oxidases PigB and HapB involved in antibiotic prodigiosin biosynthesis. *Chembiochem* 21, 523–530. doi: 10.1002/cbic.201900424

Dairi, K., Tripathy, S., Attardo, G., and Lavallée, J.-F. (2006). Two-step synthesis of the bipyrrole precursor of prodigiosins. *Tetrahedron Lett.* 47, 2605–2606. doi: 10.1016/j.tetlet.2006.02.035

Darshan, N., and Manonmani, H. K. (2015). Prodigiosin and its potential applications. *J. Food Sci. Technol.* 52, 5393–5407. doi: 10.1007/s13197-015-1740-4

Darshan, N., and Manonmani, H. K. (2016). Prodigiosin inhibits motility and activates bacterial cell death revealing molecular biomarkers of programmed cell death. *AMB Express* 6:50. doi: 10.1186/s13568-016-0222-z

Das, P., Yang, X.-P., and Ma, L. Z. (2014). Analysis of biosurfactants from industrially viable pseudomonas strain isolated from crude oil suggests how rhamnolipids congeners affect emulsification property and antimicrobial activity. *Front. Microbiol.* 5:696. doi: 10.3389/fmicb.2014.00696

Domröse, A., Hage-Hülsmann, J., Thies, S., Weihmann, R., Kruse, L., Otto, M., et al. (2019). Pseudomonas putida rDNA is a favored site for the expression of biosynthetic genes. *Sci. Rep.* 9:7028. doi: 10.1038/s41598-019-43405-1

Domröse, A., Klein, A. S., Hage-Hülsmann, J., Thies, S., Svensson, V., Classen, T., et al. (2015). Efficient recombinant production of prodigiosin in pseudomonas putida. *Front. Microbiol.* 6:972. doi: 10.3389/fmicb.2015.00972

Domröse, A., Weihmann, R., Thies, S., Jaeger, K. E., Drepper, T., and Loeschcke, A. (2017). Rapid generation of recombinant pseudomonas putida secondary metabolite producers using yTREX. *Synth. Syst. Biotechnol.* 2, 310–319. doi: 10.1016/j.synbio.2017.11.001

Dowhan, W. (1997). "The role of phospholipids in cell function" in *Advances in Lipobiology*. ed. R. W. Gross (Amsterdam Niederlande: Elsevier), 79–107.

Fürstner, A. (2003). Chemistry and biology of roseophilin and the prodigiosin alkaloids: a survey of the last 2500 years. *Angew. Chemie - Int. Ed.* 42, 3582–3603. doi: 10.1002/anie.200300582

Garcia-Brugger, A., Lamotte, O., Vandelle, E., Bourque, S., Lecourieux, D., Poinssot, B., et al. (2006). Early signaling events induced by elicitors of plant defenses. *Mol. Plant-Microbe Interact.* 19, 711–724. doi: 10.1094/MPMI-19-0711

Grundler, F. M. W., Schnibbe, L., and Wyss, U. (1991). *In vitro* studies on the behaviour of second-stage juveniles of *Heterodera schachtii* (Nematoda: Heteroderidae) in response to host plant root exudates. *Parasitology* 103, 149–155. doi: 10.1017/S0031182000059394

Haas, D., and Défago, G. (2005). Biological control of soil-borne pathogens by fluorescent pseudomonads. *Nat. Rev. Microbiol.* 3, 307–319. doi: 10.1038/nrmicro1129

Habash, S. S., Brass, H. U. C., Klein, A. S., Klebl, D. P., Weber, T. M., Classen, T., et al. (2020). Novel prodiginine derivatives demonstrate bioactivities on plants, nematodes, and fungi. *Front. Plant Sci.* 11:579807. doi: 10.3389/fpls.2020.579807

Hage-Hülsmann, J., Grünberger, A., Thies, S., Santiago-Schübel, B., Klein, A. S., Pietruszka, J., et al. (2018). Natural biocide cocktails: combinatorial antibiotic effects of prodigiosin and biosurfactants. *PLoS One* 13:e0200940. doi: 10.1371/journal.pone.0200940

Hanahan, D. (1983). Studies on transformation of Escherichia coli with plasmids. *J. Mol. Biol.* 166, 557–580. doi: 10.1016/S0022-2836(83)80284-8

Handelsman, J., and Stabb, E. V. (1996). Biocontrol of soilborne plant pathogens. *Plant Cell* 8, 1855–1869. doi: 10.1105/tpc.8.10.1855

Hopkins, A. L. (2007). Network pharmacology. *Nat. Biotechnol.* 25, 1110–1111. doi: 10.1038/nbt1007-1110

Hu, D. X., Withall, D. M., Challis, G. L., and Thomson, R. J. (2016). Structure, chemical synthesis, and biosynthesis of Prodiginine natural products. *Chem. Rev.* 116, 7818–7853. doi: 10.1021/acs.chemrev.6b00024

Ivanov, A. V., Shcherbakova, V. S., Mikhaleva, A. I., and Trofimov, B. A. (2014). One-pot synthesis of pyrroles from ketones, hydroxylamine, and 1,2-dibromoethane in the system KOH-DMSO. *Russ. J. Org. Chem.* 50, 1775–1778. doi: 10.1134/S1070428014120100

Jia, J., Zhu, F., Ma, X., Cao, Z. W., Li, Y. X., and Chen, Y. Z. (2009). Mechanisms of drug combinations: interaction and network perspectives. *Nat. Rev. Drug Discov.* 8, 111–128. doi: 10.1038/nrd2683

Keith, C. T., Borisy, A. A., and Stockwell, B. R. (2005). Multicomponent therapeutics for networked systems. *Nat. Rev. Drug Discov.* 4, 71–78. doi: 10.1038/nrd1609

Kirschning, A., Taft, F., and Knobloch, T. (2007). Total synthesis approaches to natural product derivatives based on the combination of chemical synthesis and metabolic engineering. *Org. Biomol. Chem.* 5, 3245–3259. doi: 10.1039/b709549j

Klein, A. S., Brass, H. U. C., Klebl, D. P., Classen, T., Loeschcke, A., Drepper, T., et al. (2018). Preparation of cyclic Prodiginines by Mutasynthesis in pseudomonas putida KT2440. *Chembiochem* 19, 1545–1552. doi: 10.1002/cbic.201800154

Klein, A. S., Domröse, A., Bongen, P., Brass, H. U. C., Classen, T., Loeschcke, A., et al. (2017). New Prodigiosin derivatives obtained by Mutasynthesis in pseudomonas putida. *ACS Synth. Biol.* 6, 1757–1765. doi: 10.1021/acssynbio.7b00099

Köhl, J., Kolnaar, R., and Ravensberg, W. J. (2019). Mode of action of microbial biological control agents against plant diseases: relevance beyond efficacy. *Front. Plant Sci.* 10:845. doi: 10.3389/fpls.2019.00845

Konno, H., Matsuya, H., Okamoto, M., Sato, T., Tanaka, Y., Yokoyama, K., et al. (1998). Prodigiosins uncouple mitochondrial and bacterial F-ATPases: evidence for their H^+/cl^- symport activity. *J. Biochem.* 124, 547–556. doi: 10.1093/oxfordjournals.jbchem.a022147

Li, P., He, S., Zhang, X., Gao, Q., Liu, Y., and Liu, L. (2022). Structures, biosynthesis, and bioactivities of prodiginine natural products. *Appl. Microbiol. Biotechnol.* 106, 7721–7735. doi: 10.1007/s00253-022-12245-x

Loeschcke, A., Markert, A., Wilhelm, S., Wirtz, A., Rosenau, F., Jaeger, K.-E., et al. (2013). TREX: a universal tool for the transfer and expression of biosynthetic pathways in bacteria. *ACS Synth. Biol.* 2, 22–33. doi: 10.1021/sb3000657

Loeschcke, A., and Thies, S. (2020). Engineering of natural product biosynthesis in *Pseudomonas putida*. *Curr. Opin. Biotechnol.* 65, 213–224. doi: 10.1016/j.copbio.2020.03.007

Lugtenberg, B., and Kamilova, F. (2009). Plant-growth-promoting Rhizobacteria. *Annu. Rev. Microbiol.* 63, 541–556. doi: 10.1146/annurev.micro.62.081307.162918

Magalhães, L., and Nitschke, M. (2013). Antimicrobial activity of rhamnolipids against listeria monocytogenes and their synergistic interaction with nisin. *Food Control* 29, 138–142. doi: 10.1016/j.foodcont.2012.06.009

Matera, C., Grundler, F. M. W., and Schleker, A. S. S. (2021). Sublethal fluazaindolizine doses inhibit development of the cyst nematode *Heterodera schachtii* during sedentary parasitism. *Pest Manag. Sci.* 77, 3571–3580. doi: 10.1002/ps.6411

Meschke, H., Walter, S., and Schrempf, H. (2012). Characterization and localization of prodiginines from Streptomyces lividans suppressing *Verticillium dahliae* in the absence or presence of *Arabidopsis thaliana*. *Environ. Microbiol.* 14, 940–952. doi: 10.1111/j.1462-2920.2011.02665.x

Mikhaleva, A. I., Trofimov, B. A., Vasilev, A. N., Komarova, G. A., and Skorobogatova, V. I. (1981). Pyrroles from ketoximes and acetylene. Dihaloethanes in place of acetylene in reactions with cyclohexanone oxime. *Acad. Sci. USSR* 9, 1202–1204.

Nelson, K. E., Weinel, C., Paulsen, I. T., Dodson, R. J., Hilbert, H., Santos, V. A. P. M., et al. (2002). Complete genome sequence and comparative analysis of the metabolically versatile *Pseudomonas putida* KT2440. *Environ. Microbiol.* 4, 799–808. doi: 10.1046/j.1462-2920.2002.00366.x

Nikel, P. I., Chavarría, M., Danchin, A., and de Lorenzo, V. (2016). From dirt to industrial applications: pseudomonas putida as a synthetic biology chassis for hosting harsh biochemical reactions. *Curr. Opin. Chem. Biol.* 34, 20–29. doi: 10.1016/j.cbpa.2016.05.0111367-5931/#

Ortiz, A., Teruel, J. A., Espuny, M. J., Marqués, A., Manresa, Á., and Aranda, F. J. (2006). Effects of dirhamnolipid on the structural properties of phosphatidylcholine membranes. *Int. J. Pharm.* 325, 99–107. doi: 10.1016/j.ijpharm.2006.06.028

Pieterse, C. M. J., Van Der Does, D., Zamioudis, C., Leon-Reyes, A., and Van Wees, S. C. M. (2012). Hormonal modulation of plant immunity. *Annu. Rev. Cell Dev. Biol.* 28, 489–521. doi: 10.1146/annurev-cellbio-092910-154055

Rahul, S., Chandrashekhar, P., Hemant, B., Chandrakant, N., Laxmikant, S., and Satish, P. (2014). Nematicidal activity of microbial pigment from *Serratia marcescens*. *Nat. Prod. Res.* 28, 1399–1404. doi: 10.1080/14786419.2014.904310

Ravindran, A., Anishetty, S., and Pennathur, G. (2020). Molecular dynamics of the membrane interation and localisation of prodigiosin. *J. Mol. Graph. Model.* 98:107614. doi: 10.1016/j.jmgm.2020.107614

Roberts, D. P., Selmer, K., Lupitskyy, R., Rice, C., Buyer, J. S., Maul, J. E., et al. (2021). Seed treatment with prodigiosin controls damping-off of cucumber caused by Pythium ultimum. *AMB Express* 11:10. doi: 10.1186/s13568-020-01169-2

Rossi, C. C., Santos-Gandelman, J. F., Barros, E. M., Alvarez, V. M., Laport, M. S., and Giambiagi-deMarval, M. (2016). Staphylococcus haemolyticus as a potential producer of biosurfactants with antimicrobial, anti-adhesive and synergistic properties. *Lett. Appl. Microbiol.* 63, 215–221. doi: 10.1111/lam.12611

Sakai-Kawada, F. E., Ip, C. G., Hagiwara, K. A., and Awaya, J. D. (2019). Biosynthesis and bioactivity of prodiginine analogs in marine bacteria, Pseudoalteromonas: a mini review. *Front. Microbiol.* 10:1715. doi: 10.3389/fmicb.2019.01715

Sanchez, L., Courteaux, B., Hubert, J., Kauffmann, S., Renault, J. H., Clément, C., et al. (2012). Rhamnolipids elicit defense responses and induce disease resistance against biotrophic, hemibiotrophic, and necrotrophic pathogens that require different signaling pathways in Arabidopsis and highlight a central role for salicylic acid. *Plant Physiol.* 160, 1630–1641. doi: 10.1104/pp.112.201913

Schloss, P. D., Allen, H. K., Klimowicz, A. K., Mlot, C., Gross, J. A., Savengsuksa, S., et al. (2010). Psychrotrophic strain of *Janthinobacterium lividum* from a cold Alaskan soil produces prodigiosin. *DNA Cell Biol.* 29, 533–541. doi: 10.1089/dna.2010.1020

Schneider, C. A., Rasband, W. S., and Eliceiri, K. W. (2012). NIH image to ImageJ: 25 years of image analysis. *Nat. Methods* 9, 671–675. doi: 10.1038/nmeth.2089

Sijmons, P., Grundler, F., von Mende, N., Burrows, P. R., and Wyss, U. (1991). Arabidopsis thaliana as a new model host for plant-parasitic nematodes. *Plant J.* 1, 245–254. doi: 10.1111/j.1365-313X.1991.00245.x

Simon, R., Priefer, U., and Pühler, A. (1983). A broad host range mobilization system for *in vivo* genetic engineering: transposon mutagenesis in Gram negative bacteria. *Nat. Biotechnol.* 1, 784–791. doi: 10.1038/nbt1183-784

Someya, N., Nakajima, M., Hirayae, K., Hibi, T., and Akutsu, K. (2001). Synergistic antifungal activity of chitinolytic enzymes and prodigiosin produced by biocontrol bacterium, Serratia marcescens strain B2 against gray mold pathogen. *Botrytis cinerea. J. Gen. Plant Pathol.* 67, 312–317. doi: 10.1007/pl00013038

Sotirova, A., Avramova, T., Stoitsova, S., Lazarkevich, I., Lubenets, V., Karpenko, E., et al. (2012). The importance of rhamnolipid-biosurfactant-induced changes in bacterial membrane lipids of Bacillus subtilis for the antimicrobial activity of thiosulfonates. *Curr. Microbiol.* 65, 534–541. doi: 10.1007/s00284-012-0191-7

Stankovic, N., Senerovic, L., Ilic-Tomic, T., Vasiljevic, B., and Nikodinovic-Runic, J. (2014). Properties and applications of undecylprodigiosin and other bacterial prodigiosins. *Appl. Microbiol. Biotechnol.* 98, 3841–3858. doi: 10.1007/s00253-014-5590-1

Sun, H., Liu, Z., Zhao, H., and Ang, E. L. (2015). Recent advances in combinatorial biosynthesis for drug discovery. *Drug Des. Devel. Ther.* 9, 823–833. doi: 10.2147/DDDT.S63023

Suryawanshi, R. K., Patil, C. D., Koli, S. H., Hallsworth, J. E., and Patil, S. V. (2017). Antimicrobial activity of prodigiosin is attributable to plasma-membrane damage. *Nat. Prod. Res.* 31, 572–577. doi: 10.1080/14786419.2016.1195380

Tiso, T., Ihling, N., Kubicki, S., Biselli, A., Schonhoff, A., Bator, I., et al. (2020). Integration of genetic and process engineering for optimized rhamnolipid production using pseudomonas putida. *Front. Bioeng. Biotechnol.* 8:976. doi: 10.3389/fbioe.2020.00976

Trofimov, B. A., Mikhaleva, A. I., Ivanov, A. V., Shcherbakova, V. S., and Ushakov, I. A. (2015). Expedient one-pot synthesis of pyrroles from ketones, hydroxylamine, and 1,2-dichloroethane. *Tetrahedron* 71, 124–128. doi: 10.1016/j.tet.2014.11.031

Varnier, A. L., Sanchez, L., Vatsa, P., Boudesocque, L., Garcia-Brugger, A., Rabenoelina, F., et al. (2009). Bacterial rhamnolipids are novel MAMPs conferring resistance to *Botrytis cinerea* in grapevine. *Plant Cell Environ.* 32, 178–193. doi: 10.1111/j.1365-3040.2008.01911.x

Wallace, H. R. (1958). Movement of eelworms. The influence of pore size and moisture content of the soil on the migration of larvae of the beet eelworm. *Heterodera schachtii Schmidt. Ann. Appl. Biol.* 46, 74–85. doi: 10.1111/j.1744-7348.1958.tb02179.x

Weihmann, R., Domröse, A., Drepper, T., Jaeger, K. E., and Loeschcke, A. (2020). Protocols for yTREX/Tn5-based gene cluster expression in pseudomonas putida. *Microb. Biotechnol.* 13, 250–262. doi: 10.1111/1751-7915.13402

Weimer, A., Kohlstedt, M., Volke, D. C., Nikel, P. I., and Wittmann, C. (2020). Industrial biotechnology of *Pseudomonas putida*: advances and prospects. *Appl. Microbiol. Biotechnol.* 104, 7745–7766. doi: 10.1007/s00253-020-10811-9

Williamson, N. R., Fineran, P. C., Ogawa, W., Woodley, L. R., and Salmond, G. P. C. (2008). Integrated regulation involving quorum sensing, a two-component system, a GGDEF/EAL domain protein and a post-transcriptional regulator controls swarming and RhlA-dependent surfactant biosynthesis in Serratia. *Environ. Microbiol.* 10, 1202–1217. doi: 10.1111/j.1462-2920.2007.01536.x

Williamson, N. R., Simonsen, H. T., Ahmed, R. A. A., Goldet, G., Slater, H., Woodley, L., et al. (2005). Biosynthesis of the red antibiotic, prodigiosin, in Serratia: identification of a novel 2-methyl-3-n-amyl-pyrrole (MAP) assembly pathway, definition of the terminal condensing enzyme, and implications for undecylprodigiosin biosynthesis in Streptomyces. *Mol. Microbiol.* 56, 971–989. doi: 10.1111/j.1365-2958.2005.04602.x

Wyss, U. (1992). Observations on the feeding behavior of Heterodera schachtii throughout development, including events during moulting. *Fundam. Appl. Nematol.* 15, 75–89.

Wyss, U., and Grundler, F. M. W. (1992). Feeding behavior of sedentary plant parasitic nematodes. *Netherlands J. Plant Pathol.* 98, 165–173. doi: 10.1007/BF01974483

Wyss, U., and Zunke, U. (1986). Observations on the behaviour of second stage juveniles of Heterodera schachtii inside host roots. *Rev. Nématologie* 9, 153–165.

Yildirim, M. A., Goh, K.-I., Cusick, M. E., Barabási, A.-L., and Vidal, M. (2007). Drug-target network. *Nat. Biotechnol.* 25, 1119–1126. doi: 10.1038/nbt1338

Yip, C. H., Yarkoni, O., Ajioka, J., Wan, K. L., and Nathan, S. (2019). Recent advancements in high-level synthesis of the promising clinical drug, prodigiosin. *Appl. Microbiol. Biotechnol.* 103, 1667–1680. doi: 10.1007/s00253-018-09611-z

frontiers | Frontiers in Microbiology

TYPE Original Research
PUBLISHED 19 June 2023
DOI 10.3389/fmicb.2023.1191102

OPEN ACCESS

EDITED BY
Monika Prakash Rai,
Amity University, India

REVIEWED BY
Jifeng Yuan,
Xiamen University, China
Zhihua Zhou,
Shanghai Institutes for Biological Sciences (CAS), China

*CORRESPONDENCE
Bing Hao
✉ bing.hao@hotmail.com
Sheng Chao Yang
✉ shengchaoyang@163.com

RECEIVED 21 March 2023
ACCEPTED 31 May 2023
PUBLISHED 19 June 2023

CITATION
Lin Y, Wang YN, Zhang GH, Chen G, Yang QH, Hao B and Yang SC (2023) Reconstruction of engineered yeast factory for high yield production of ginsenosides Rg3 and Rd. *Front. Microbiol.* 14:1191102. doi: 10.3389/fmicb.2023.1191102

Reconstruction of engineered yeast factory for high yield production of ginsenosides Rg3 and Rd

Yuan Lin[1,2,3], Yi Na Wang[1,2,3], Guang Hui Zhang[1,2,3], Geng Chen[1,2,3], Qing Hui Yang[3], Bing Hao[1,2,4]* and Sheng Chao Yang[1,2,4]*

[1]State Key Laboratory of Conservation and Utilization of Bio-Resources in Yunnan, The Key Laboratory of Medicinal Plant Biology of Yunnan Province, National and Local Joint Engineering Research Center on Germplasms Innovation and Utilization of Chinese Medicinal Materials in Southwest China, Yunnan Agricultural University, Kunming, Yunnan, China, [2]Key Laboratory of Medicinal Plant Biology, Yunnan Agricultural University, Kunming, Yunnan, China, [3]College of Agronomy and Biotechnology, Yunnan Agricultural University, Kunming, Yunnan, China, [4]Yunnan Characteristic Plant Extraction Laboratory, Kunming, Yunnan, China

Panax notoginseng is one of the most valuable traditional Chinese herbs. The main active ingredients, dammarane-type ginsenosides, show multiple pharmacological activities. Recently, the key UDP-dependent glycosyltransferases (UGTs) involved in the biosynthesis of common ginsenosides have been widely studied. However, only a few UGTs that catalyze ginsenoside formation have been reported. This study further investigated the new catalytic function of 10 characterized *UGTs* from the public database. *PnUGT31*(*PnUGT94B2*) and *PnUGT53* (*PnUGT71B8*)exhibited promiscuous sugar-donor specificity of UDP-glucose and UDP-xylose, which could catalyze the glycosylation of C20-OH sites and elongation of the sugar chain at the C3 and/or C20 sites. We further analyzed the expression patterns in *P. notoginseng* and predicted the catalytic mechanisms of *PnUGT31* and *PnUGT53* using molecular docking simulations. Moreover, different gene modules were built to increase the yield of ginsenosides in engineered yeast. The metabolic flow of the proginsenediol (PPD) synthetic pathway was enhanced by LPPDS gene modules based on the engineered strain. The resulting yeast was constructed to produce 1.72g/L PPD in a shaking flask, but cell growth was significantly inhibited. EGH and LKG gene modules were constructed to achieve high-level production of dammarane-type ginsenosides. The production of G-Rg3 controlled by LKG modules increased 3.84 times (254.07mg/ L), whereas the G-Rd titer reached 56.68mg/L after 96h in shaking flask culture under the control of all modules, both of which yielded the highest values for known microbes.

KEYWORDS

***Panax notoginseng*, ginsenosides, glycosyltransferase, biosynthesis, engineered yeast**

Introduction

The underground part of *Panax notoginseng* has been widely used for treating cancer and cardiovascular and cerebrovascular diseases (Zhang et al., 2018). Damarane-type saponin is considered to be the main active agent responsible for various pharmacological activities. At present, more than 200 ginsenosides have been found in *P. notoginseng*, and dammarane-type saponins account for 98%. More specifically, dammarane-type ginsenoside Rb1 (G-Rb1), Rb2

(G-Rb2), Rg1 (G-Rg1), Re (G-Re), Rc (G-Rc) and notoginoside R1 (N-R1) account for more than 90% of the total saponins (Wan et al., 2006; Wei et al., 2018). Depending on the position of the hydroxyl group, dammarane-type saponins can be divided into proginsendiol-type (PPD-type) and proginsentriol-type (PPT-type) saponins. More than 20 dammarane-type saponins have been tested in animal experiments and preclinical studies, and the proginsenodiol-type ginsenosides, G-CK, G-Rh2, G-F2, and G-Rg3, have shown significant anticarcinogenic activity (Chen et al., 2013; Wang et al., 2018; Chen et al., 2019; Liu et al., 2020). It is worth noting that G-Rg3 has entered the stage of clinical studies as an efficient antitumor agent (Sun et al., 2017).

Dammarane-type ginsenosides are tetracyclic triterpenes. The hydroxyl groups at the C3, C6, and C20 sites of the skeleton can be glycosylated by different sugar donors to form ginsenosides. During the biosynthesis of ginsenosides, the final step of glycosylation is normally catalyzed by UDP-dependent glycosyltransferase (UGT) with the supplementation of UDP-sugar donors such as UDP-glucose (UDP-Glu), UDP-xylose (UDP-Xyl), UDP-rhamnose, and UDP-arabinose, and substituting sites can form sugar chains that combine multiple sugar groups. Glycosyltransferases are a group of multi-gene superfamilies which can transfer sugar from the substrate to specific receptor molecules. All UGTs involved in ginsenoside biosynthesis belong to family 1 glycosyltransferases (GT1 family), which uses 5 ‘-uridine diphosphate - sugar as glycosyl donors. Based on the similarity of amino acid sequences, *UGTs* from plants can be divided into 94 subfamilies and clades that have not yet been classified (Ross et al., 2001). Previous reports have shown that the *UGTs* involved in the biosynthesis of dammarane-type saponins are mainly distributed in the UGT71, UGT74, and UGT94 subfamilies of plants.

Currently, the acquisition of dammarane-type saponins depends heavily on the raw plant materials, and their content is easily affected by various environmental factors. In fact, more than 200 types of dammarane-type ginsenosides only account for approximately 2% of the dry weight of 3-year-old *P. notoginseng*, that is hard to meet the market demand for rare ginsenosides. Synthetic biology offers a new strategy for producing valuable compounds via heterologous organisms. To overcome this yield limit, more than 10 *UGT* genes have been engineered in yeast to produce ginsenosides. Although some achievements have been made in the microbial production of dammarane-type ginsenosides, the highest yield of proginsenodiol-type ginsenosides, such as Rg3 is still less than 100 mg/L (Jiang et al., 2022).

To date, five versions of the genome and abundant transcriptomes of *P. notoginseng* have been published, and nearly 100 *UGTs* have been identified in *P. notoginseng* (Wang et al., 2020; Yang et al., 2021). These rich data from the genome, transcriptome, and metabolome provide a solid foundation for exploring the functions of UGTs. Here, based on the *UGTs* obtained from previous studies, we further identified two UDP-xylose-dependent glycosyltransferases capable of biosynthesizing vinaginsenosides R16 and R18, as well as UDP-Glu for glycosylation at the C20 site and sugar chain extension. Based on the reconstructed PPD-producing *Saccharomyces cerevisiae*, we used these two *UGTs* to establish a cell factory to produce part of the PPD-type ginsenosides as an alternative source for expanding the industrial production of ginsenosides to protect wild populations of *Panax* plants, such as *P. notoginseng*.

Abbreviations: qRT-PCR, real-time reverse transcriptase polymerase chain reaction; PPD, protopanaxadriol; PPT, proginsentriol-type; UGT, UDP-dependent glycosyltransferase; HPLC, high performance liquid chromatography; LC–MS, liquid chromatography-mass spectrometry; NMR, nuclear magnetic resonance spectroscopy; LC–MS/MS, chromatography-tandem mass spectrometry; G-, ginsenside; V-, vinaginsenosides; GT, glycosyltransferases; UDP-Glu, UDP-glucose; UDP-Xyl, UDP-xylose.

Materials and methods

Strains and materials

Saccharomyces cerevisiae strain BY4742 (Wuhan Miaoling Biotechnology Co., LTD, China) was used as the initial strain for engineering. *Escherichia coli* strain BL21 (DE3; TransGen Biotech, China) and *S. cerevisiae* strain W303-1B were used for heterologous expression. *E. coli* DH5α and Trans-T1 chemically competent cells (TransGen Biotech) were used for the cloning of UGTs. The codon-optimized gene was synthesized by Tsingke Biotechnology (Beijing, China). All primers and strains used in this study are listed in Supplementary Tables S1, S2. The standards and substrate compounds PPD, PPT, and ginsenosides (>98%) were purchased from DeSiTe Biotechnology (Chengdu, China) and PuRuiFa Technology (Chengdu, China).

Cloning and heterologous expression of recombinant *Pn*UGT proteins

The coding sequence of UDP-glycosyltransferase was determined by PCR-amplified from *P. notoginseng* and cloned into the pEASY vector (TransGen Biotech, Beijing, China). Briefly, *UGT* genes were ligated into the pET28a vector with a 6×His-tag using the Golden Gate Assembly Kit (NEB, USA) and transformed into *E. coli* BL21 (DE3). *UGT* genes with a C-terminal 6×His-tag were ligated into the YCplac22 vector using the ClonExpress II One Step Cloning Kit (Vazyme Biotech Co., Ltd., Nanjing, China).

After the sequence was correctly constructed into *E. coli*, positive clones were selected and cultured in 4 mL LB medium containing 100 mg/L kanamycin (Kan) at 37°C for 12–16 h, and the bacteria solution was transferred into 400 mL LB + Kan^+ medium for further culture until the OD_{600} value reached 0.5–0.8. The medium was induced with 0.1 mM isopropyl-β-D-thiogalacto-pyranoside (IPTG) at 15°C for 16 h. The cells were collected and resuspended in 100 mM lysis buffer (pH 7.4). The cell suspension was lysed at 4°C and 2000 bar with a high pressure cell fragmentation instrument (Constant Systems, Britain). The supernatant obtained by centrifugation was concentrated and used for enzymatic reactions.

The recombinant yeast strains were cultivated in 2 mL YPD medium at 30°C for 16–18 h, and then transferred to 50 mL YPD medium for further culture for 2 days. The cells were collected and suspended in 15 mL of PBS (pH 7.4). The yeast cells were broken at 4°C and high pressure of 3,000 bar. The supernatant obtained by centrifugation was concentrated and used for enzymatic reactions.

Enzyme assays

Enzymatic assays of UGTs were performed in random combinations, consisting of UDP-glucose, UDP-arabinose, UDP-rhamnose, and UDP-xylose as sugar donors with 11 ginsenoside substrates. The 100 μL reaction system included 100 mM phosphate buffer (pH = 7.4), 2 mM UDP-sugar donors, 1 mM ginsenoside, 50 μL crude UGT enzyme, incubated at 35°C for 12 h and terminated by adding 100 μL of methanol. The lysates of *E. coli* harboring the pET28a vector and *S. cerevisiae* harboring the YCplac22 vector were used as negative controls. After centrifugation at 14,000 ×*g* for 10 min, the supernatant was filtered through a 0.22 mm nylon syringe filter and prepared for HPLC and LC–MS analysis. After the enzymatic assays system was expanded ten times, the reactants were incubated in a thermostatic oscillator with a revolution of 800 rpm/min, and n-butanol was used at a ratio of 1:1 to terminate the reaction. The supernatant obtained after centrifugation was subjected to NMR analysis.

Real-time reverse transcriptase polymerase chain reaction quantification

Omega Plant RNA Kit (Omega Bio-Tek, China) was used to isolate the total RNA of *P. notoginseng*, and the HiScript II One Step RT-PCR Kit (Vazyme, China) was used to obtain cDNA. *PnUGT53* and *Pn3-29* were amplified by real-time PCR (RT-qPCR) using SYBR Green Realtime PCR Master Mix (Vazyme, China). The primers are listed in Supplementary Table S1.

Construction, cultivation, and metabolite extraction of yeast strains

The establishment of the gene expression cassette required two rounds of PCR cloning. Q5 High-Fidelity DNA Polymerase Cloning Kit (NEB, United States) was used to amplify basic fragments containing promoters, genes, terminators, selective markers, and homologous fragments of the yeast genome in the first round. Each basic fragment has a special homologous sequence of 40–75 bp on either side for recombination or fusion PCR. In the second round, gene expression cassettes were obtained by fusion of basic fragments. All fusion fragments were purified, quantified, and co-transformed into yeast cells using the standard lithium acetate method for assembly and integration. Correct clones were first inoculated into 2 mL synthetic dropout medium and grown at 30°C until the OD_{600} value reached 0.8–1.0, and the bacteria solution was subsequently transferred into 30 mL YPD medium and grown at 30°C for 5–6 days. To extract ginsenosides from the fermentation culture cells, the cells were collected and suspended in 6 mL methanol. After ultrasonication for 30 min, the separated supernatants were used for HPLC analysis.

Chemical analysis

The HPLC analysis was performed using an Agilent 1200 series preparative HPLC system (Santa Clara, CA, United States). Chromatographic separation of ginsenosides from enzyme assay products was carried out at 25°C on a Phenomenex 00D-4,627-E0 Kinetex 5 μm Biphenyl 100 Å, LC Column (100 mm × 4.6 mm, 5 μm, United States). The detection wavelength for the ginsenosides was 203 nm. The gradient elution system comprised water (A) and acetonitrile (B). There are two gradient programs for separation, the first gradient program: 0 ~ 4 min (15–30% B), 9 ~ 15 min (40–42% B), 18 ~ 25 min (60–100% B); the second gradient program: 0 ~ 6 min (20–30% B), 8 ~ 12 min (40–42% B), 25 ~ 30 min (90–100% B), and the flow rate was kept at 1.0 mL/min.

LC–MS and LC–MS/MS was performed using a Micro ToF MS instrument (Bruker Daltonics) equipped with an Agilent HP1100 series LC system. The chromatographic column and gradient elution programs are the same as in HPLC analysis. The products were identified in negative mode. All spectra were recorded in negative ion mode over 50–1,000 m/z under 6.01 L/min dry gas flow, 203 nm detection wavelength, 180°C dry temperature, 1 bar nebulizer pressure, and 14.5 kV probe voltage.

To isolate of new glycosylated products from enzyme assays, the glycosylated products were collected from the n-butanol phase of the enzyme assay suspension and dried using a Termovap Sample Concentrator to yield a dry residue. The dry residue was dissolved in methanol and further purified with an Agilent Agilent ZORBAX SB-C18 column (9.4 × 250 mm 5 μm, 2.2 μm, Shimadzu, CA, United States) (solvent A: water; solvent B: acetonitrile; the gradient: 0 ~ 7 min (40–50% B), 16 ~ 20 min (60–70%); flow rate 2 mL/min). The resulting methanol phase was collected and completely evaporated to yield the crystallized product, which was weighed and dissolved in deuterium pyridine-d5 for NMR analysis. ^{1}H and ^{13}C NMR spectra were obtained using an 800 MHz Bruker Avance III spectrometer.

For the separation of ginsenosides from yeast fermentation products, an Agilent Poroshell 120 EC-C18 column (100 mm × 3.0 mm, 2.7 μm) was used for gradient elution at 35°C. The gradient elution system comprised water (A) and acetonitrile (B). There are two gradient programs for separation, the first gradient program: 0 ~ 6 min (15–30% B), 11 ~ 17 min (40–42% B), 25 ~ 27 min (100–100% B); the second gradient program: 0 ~ 7 min (30–40% B), 7 ~ 12 min (40–42% B), 13 ~ 19 min (60–90% B), 21 ~ 25 min (100–100% B), and the flow rate was kept at 0.8 mL/min. The calibration curves of the standard samples were generated based on the integrated peak of HPLC, which was used to quantify of G-CK, G-Rg3, G-Rh2, G-Rd and PPD.

Results

Functional characterization of *PnUGT31* from *Panax notoginseng*

A total of 116 *UGT*s from *P. notoginseng* were obtained from the PanaxGDB database[1] (Lin et al., 2022). According to previous studies, UGTs that catalyze dammarane-type ginsenoside belong mainly to the UGT 74, 94, and 71 families. Therefore, we screened 19 candidate *UGTs* from these families as candidate genes which closely related to other UGTs that catalyze dammarane-type ginsenosides in the phylogenetic tree (Supplementary Figure S1). Information regarding

1 http://panaxGDB.ynau.edu.cn

these 19 candidate *UGT* genes is provided in Supplementary Table S3. We found that *UGT*s involved in the biosynthesis of dammarane-type ginsenosides were mainly highly expressed in the rhizomes or roots of *P. notoginseng* (Supplementary Figure S2). Finally, ten candidate *UGT*s with high-level expression in roots or rhizomes were selected from these 19 *UGTs* for functional verification (Supplementary Figure S2). The UDP-xylose-dependent catalytic activity of the 10 *PnUGTs* was screened by heterologous expression of recombinant *Pn*UGT proteins in *E. coli* or *S. cerevisiae*. Eleven dammarane-type ginsenosides were selected as substrates for enzyme assays. HPLC and LC-MC results showed that *Pn*UGT31 (*PnUGT94B2*) could catalyze xylosylation of G-F2 to produce an unknown product 1 with a fragment feature of 915.5 (m/z, $[M-H]^-$) mass (Figure 1). NMR analysis revealed that product 1 was vinaginsenoside R16 (V-R16). The results showed *Pn*UGT31 catalyzes the elongation of the second sugar chain at the C20 site of G-F2 with xylose to produce V-R16 (Figures 1, 2A,B; Supplementary Figures S3A–C).

The sequence characteristics of *Pn*UGT31 were consistent with those previously reported *Pn*3-31, which catalyzes G-Rh2 to produce G-Rg3 (Wang et al., 2020). In our study, *Pn*UGT31 showed catalytic activity to produce G-Rg3, G-F2, G-Rd, V-R16,G-Rb1 and G-F1 starting from G-Rh2 with UDP-glycose and UDP-xylose as the substrates (Figure 1; Supplementary Figure S4). Moreover, *Pn*UGT31 showed the capability of glycosylating the C20-OH and elongating the sugar chain at the C3 or/and C20 sites. These new catalytic functions of *Pn*UGT31 have not been reported yet. When the molar mass ratio of the sugar donor to the substrate is 5:1, *Pn*UGT31 can catalyze the formation of G-F2 and G-Rg3 from G-Rh2 in an enzyme system simultaneously (Supplementary Figure S4). Although parts of G-Rg3 were consumed by continuous glycosylation, the peak area of G-Rg3 was still higher than that of G-F2, indicating that *Pn*UGT31 preferred elongation of the sugar chain at the C3 and/or C20 sites over glycosylation of the C20-OH site (Supplementary Figure S4). Interestingly, we found that *Pn*UGT31 could not catalyze C20-OH glycosylation in the presence of an extra group at the C6-position of the saponin skeleton.

The three-dimensional protein structure of *Pn*UGT31 was predicted and molecular blind docking prediction was conducted with 11 PPD-type ginsenosides and four UDP-sugar donors. There were seven UDP-xylose and 11 UDP-glucose hydrogen-bonding residues between these two sugar-donor ligands and *Pn*UGT31, mainly distributed in the Ser261-Glu262, Trp317-Gln320, His335-Trp338, and Asp359-Gln360 regions (Figures 2C,D). The key residues responsible for the hydrogen-bonding activity between *Pn*UGT31 and the four dammarane-type ginsenosides (G-Rh2, G-Rg3, G-F2, and G-Rd) were Trp317-Gln320, Gln228-Arg229, and His20-Ser22 (Supplementary Figure S5). Trp317-Gln320 are the conserved residues in the PSPG region, where is the overlapping region that sugar donor ligands interact with the protein (Supplementary Figure S5).

Functional characterization of *PnUGT53* from *Panax notoginseng*

In vitro enzyme assays, we found that *Pn*UGT53 (*Pn*UGT71B8) could catalyze the xylosylation of G-Rg3 to form the known product 2 with 915.5 (m/z, [M-H]-) mass, which was identified as vinaginsenoside R18 (V-18) by NMR analysis (Supplementary Figures S3D–F; Figures 3A,B). This is the first demonstration of a key UGT enzyme in the biosynthesis of V-18. *Pn*UGT53 could catalyze the C20-OH site of PPD, PPT, and G-Rg3 to produce G-CK, G-F1, and G-Rd with the supplementation of UDP-glucose, respectively (Supplementary Figure S4;

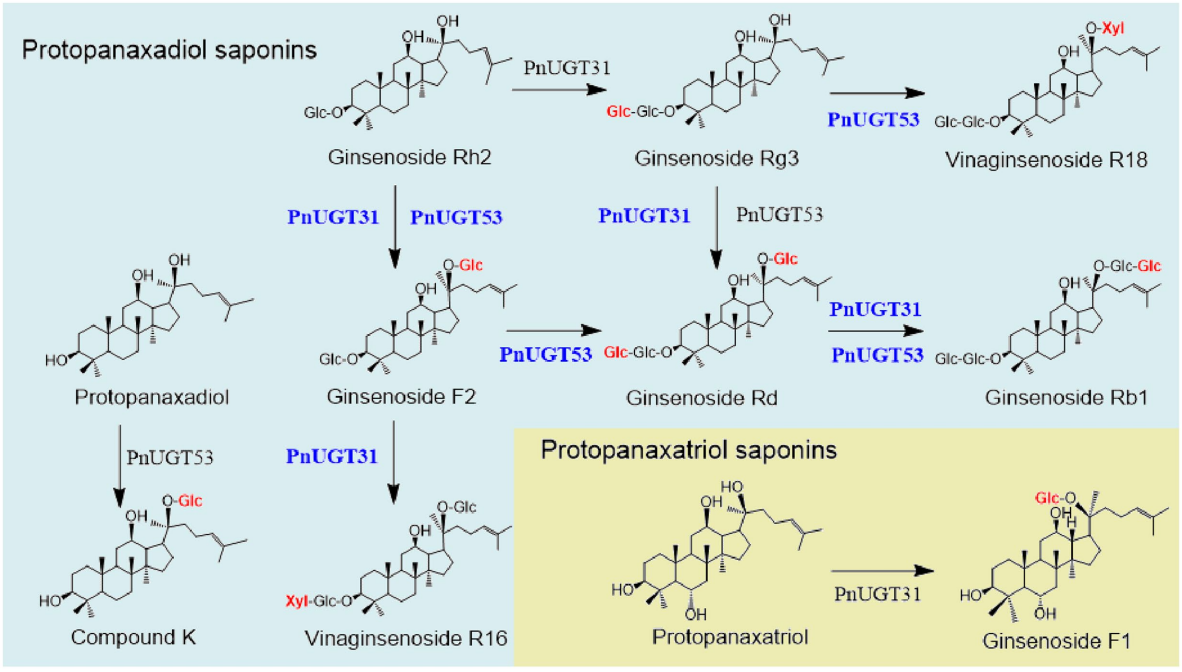

FIGURE 1
Role of glycosyltransferase (*Pn*UGT31 and *Pn*UGT53) from *P. notoginseng* in ginsenosides biosynthesis pathway.

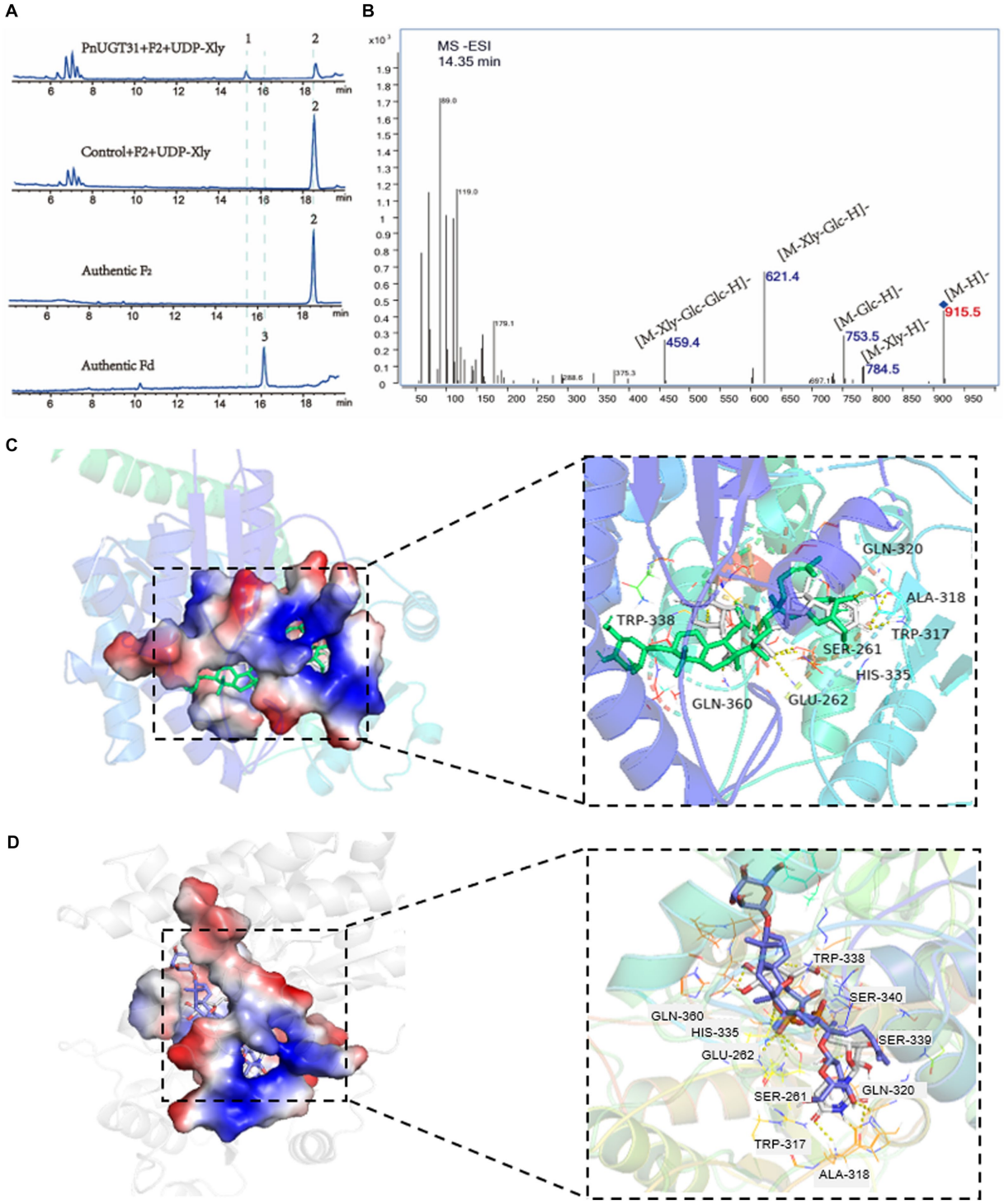

FIGURE 2
Function and enzymatic reaction mechanism study of *Pn*UGT31. The blue fonts represent the first reported functions in this study. **(A)** HPLC results of enzyme assays including PnUGT31, G-F2 and UDP-xylose, peak 1 presents new products 1, peak 2 presents G-F2, peak 3 presents G-Fd. **(B)** MS/MS results of product 1. **(C,D)** shows a simulation of molecular docking between protein *Pn*UGT31 with ligands. The ligands in **(C)** are UDP-xylose and G-F2; The ligands in **(D)** are UDP-glucose and G-F2.

Figure 1). It also catalyzed the continuous glycosylation of G-Rh2 via the G-F2 and G-Rd pathways to generate G-Rb1 (Supplementary Figure S4; Figure 1). *Pn*UGT53 catalyzed the glycosylation of C20-OH and elongation of the sugar chain at the C3 and/or C20 sites but favored the glycosylation of the C20-OH site under these two conditions. G-Rg3, the product of the extension of the sugar chain, was not found, even though the ratio of sugar donors was higher *in vitro* assays (Supplementary Figure S4; Figure 1). After glycosylation at C6-OH, *Pn*UGT53 could not further catalyze the glycosylation of C20-OH in the saponin skeleton.

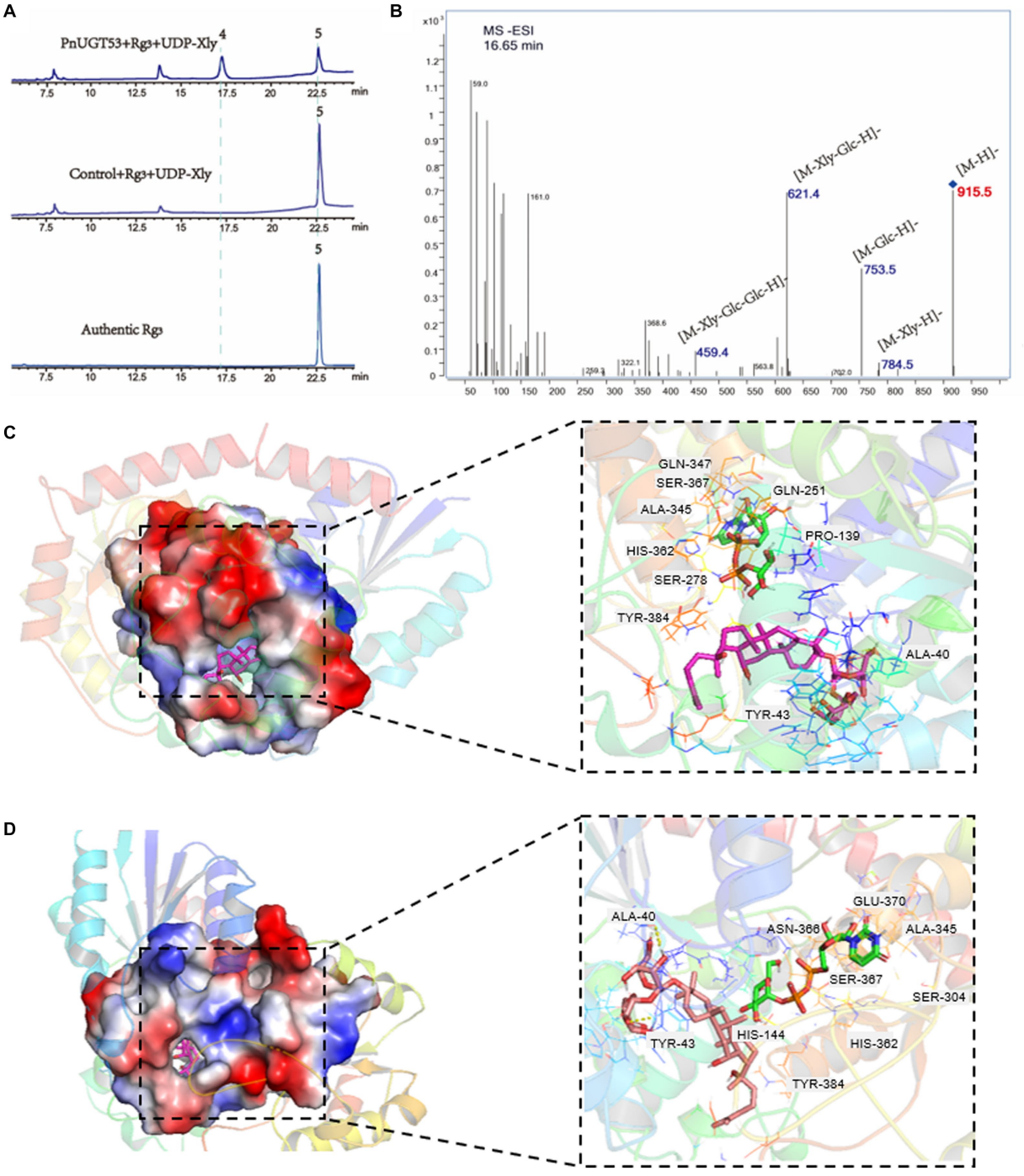

FIGURE 3
Function and enzymatic reaction mechanism of *Pn*UGT53. **(A)** HPLC results of enzyme assays including *Pn*UGT53, G-Rg3 and UDP-xylose, peak 4 was new products 2, peak 2 was G-Rg3. **(B)** MS/MS results of new product 2. **(C,D)** Shows a simulation of molecular docking between protein *Pn*UGT53 with ligands. The ligands in **(C)** are UDP-xylose and G-Rg3; The ligands in **(D)** are UDP-glucose and G-Rg3.

PnUGT53 is highly homologous to the previously reported *Pn3-29* (99.79%). *Pn*3-29 can catalyze G-Rg3, PPD, and PPT to generate G-Rd, G-CK, and G-F1, respectively. However, the catalytic capacity of *Pn*UGT53 differs from that of the reported *Pn*3-29, the sequences of these two genes were compared. The results showed that there were only differences in one amino acid and three nucleobases. Alphafold2 predicted that the spatial folding structure of the two proteins was completely consistent, and the different amino acids were not located in the key region of the substrate-bonding site (Supplementary Figure S6). Eleven ginsenosides and four UDP-sugar donors were selected as ligands for molecular docking (Supplementary Figure S6; Figures 3C,D). The results showed that their differential loci were not key sites for substrate selection. Therefore, it remains to be seen whether these two genes have similar catalytic functions. Molecular blind docking prediction showed two to six hydrogen bonds were observed between different receptor sites

and *Pn*UGT53 in the Ala40-Asp45 and Arg81-Ile84 regions (Figures 3C,D; Supplementary Figure S6). *Pn*UGT53 forms eight and seven hydrogen bonds with UDP-xylose and UDP-glucose ligands, respectively, and these two sugar ligands exhibit a hydrogen-bonding reaction with residues Ala345, Ser367, Typ384, and His362 (Figures 3C,D; Supplementary Figure S6). These four residues may be active sites for UDP sugar binding.

To further verify whether *Pn3-29* and *PnUGT53* have the same expression pattern in *P. notoginseng*, we designed primers for their differential nucleobases for RT-qPCR. The gene expression trends of *Pn3-29* and *PnUGT53* in the different tissues of 1-year-old and 2-year-old *P. notoginseng* plants were similar (Figures 4A,B,D,E). Interestingly, The expression levels of *PnUGT53* and *Pn3-29* significantly differented in the 3-year-old *P. notoginseng*. The relative expression level of *PnUGT53* has significantly increased in flower buds and rhizomes of 3-years old *P. notoginseng*, whereas the relative expression level of *Pn3-29* in 3-years old *P. notoginseng* was significantly increased in the flower buds (Figures 4C,F). Moreover, the relative expression levels of *Pn3-29* in different tissues of 1–3 years old plants were higher than those of *PnUGT53* (Figure 4). Single SNPs within the gene may directly affect the expression levels of *PnUGT53* and *Pn3-29* in *P. notoginseng*.

Design and construction of engineered yeast for PPD production

PPD is a direct precursor of G-Rh2. The yeast strain BY4742 was employed as the starting strain according to a previous study to construct a PPD-producing yeast strain ZW04BY (Wang et al., 2019). Strain ZW04BY produced 652 mg/L and 851 mg/L PPD after 96 h and 120 h in a shake flasks (Figure 5D; Supplementary Figure S7). Our results show that the PPD yield of strain ZW03BY in a shake flasks was higher than in a previous study (529.0 mg/L). There was still a possibility of converting more accumulated dammarenediol (DM) into PPD. To increase the metabolic flow of PPD biosynthesis, codon-optimized *PgPPDS* controlled by the $TDH3 + UAS_{TEF1\text{-}CIT1\text{-}CLB2}$ promoter was inserted into the strain ZW04BY. Previous studies have shown that the selection of combinatorial promoters enhances gene expression (Blazeck et al., 2012). To increase the copy number of the *PgPPDS* in yeast, the δ sequence was selected as inserted locus, while G418 (geneticin) was selected as resistance selection tags (Parekh et al., 1996; Wang et al., 1996). This engineered strain was constructed based on LPPDS gene modules named LPPDS (Figure 5A). Compared with the control strain ZW04BY, the PPD yield of strain LPPDS reached 1.72 g/L, double the control yield (Figure 5D; Table 1). Although the engineered strain LPPDS could show significantly improved PPD production, the OD_{600} value showed that the cell growth of the strain LPPDS was significantly inhibited compared to the control, which might be due to the metabolic inhibition (Figure 5E).

High-level production of proginsenodiol-type ginsenosides

Both *Pn*UGT31 and *Pn*UGT53 catalyze continuous glycosylation of G-Rh2 to G-Rb1. In this study, *PnUGT31* and *PnUGT53* were

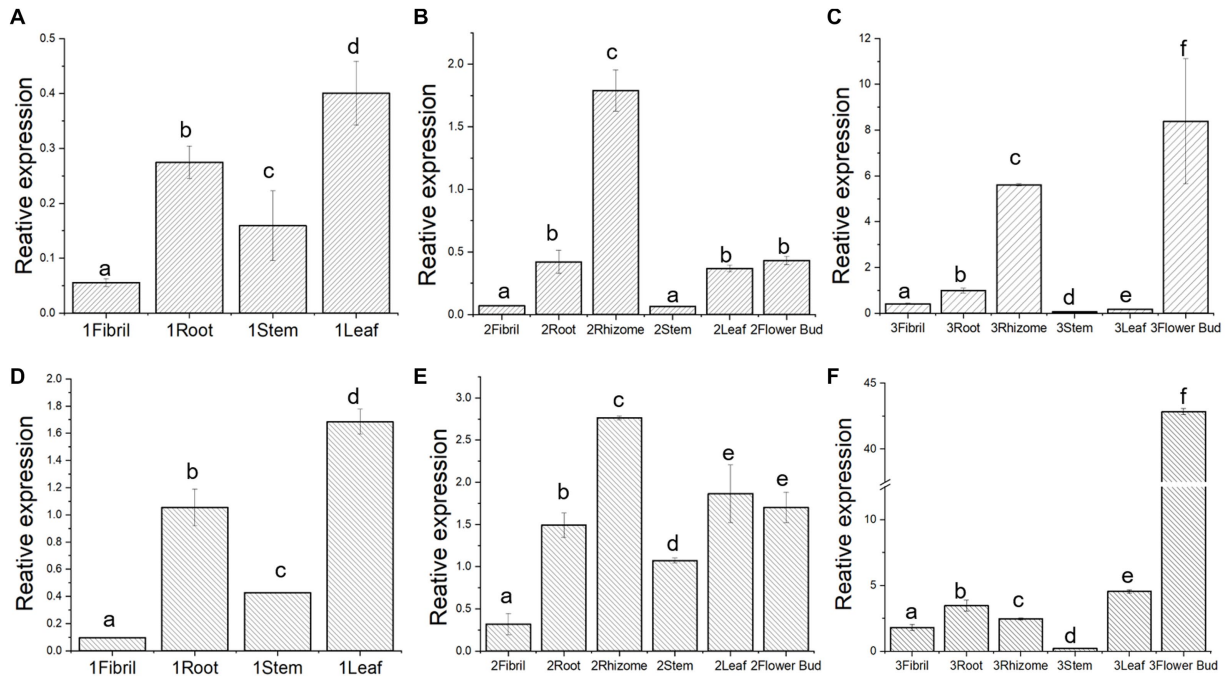

FIGURE 4
Expression pattern and enzymatic reaction mechanism study of *Pn*UGT53 and *Pn*3-29. **(A–C)** Relative expression of *Pn*UGT53 in different tissues of 1-, 2- and 3-year-old *P. notoginseng*; **(D–F)** Relative expression of *Pn*3-29 in different tissues of 1-, 2- and 3-year-old *P. notoginseng*. p <0.05, different letters represent significant differences between different parts.

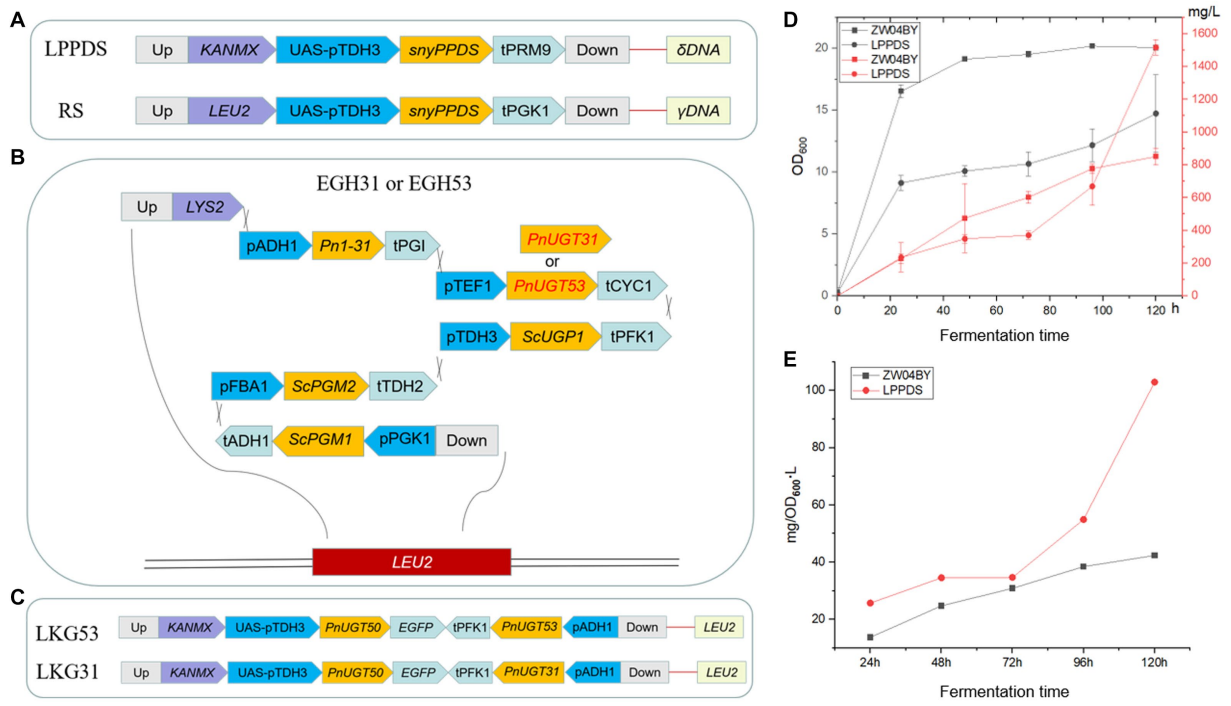

FIGURE 5
Schematic representation of the gene modular construction and PPD yield of strain LPPDS. **(A)** Construction of LPPDS and RS module. **(B)** Construction of EGH31 and EGH53 module. **(C)** Construction of LKG31 and LKG53 module. **(D)** The yield of PPD produced by strain LPPDS and ZW04BY. **(E)** Ratio of PPD yield to OD_{600} of strain LPPDS and ZW04BY.

TABLE 1 The yield of ginsenosides produced by engineering yeast.

	Yield (mg/L)				
Strains	PPD	G-CK	G-Rh2	G-Rg3	G-Rd
ZW04BY	851 ± 51.87	–	–	–	–
LPPDS	1722.10 ± 80.72	–	–	–	–
EGH31	947.32 ± 78.95	–	–	52.48 ± 21.02	–
EGH53	1027.66 ± 60.22	20.48 ± 0.20	4.40 ± 0.13	–	–
LKG31	721.36 ± 71.37	–	12.80 ± 9.59	254.06 ± 56.49	–
LKG53	745.75 ± 147.29	–	35.42 ± 5.37	–	–
LKG31RS	795.41 ± 83.54	–	0.72 ± 0.14	164.58 ± 24.54	26.21 ± 12.86
LKG53RS	908.46 ± 64.58	–	54.57 ± 6.36	–	–
LKG53EGHLPPDS	1313.75 ± 87.33	–	55.70 ± 1.44	–	56.68 ± 16.21

placed under the control of the TEF1 promoter and CYC1 terminator and inserted into the *EGH1* (*Yir007w*) locus of *S. cerevisiae* strain ZW04BY. The effect of glucosidase on the desugarization and degradation of ginsenosides can be reduced by knocking out EGH1, which can hydrolyze various *β*-glucosides (Dai et al., 2014; Zhuang et al., 2017; Figure 5B; Supplementary Table S2). The fragment contained the *Pn*1-31 gene was inserted to increase the production of G-Rh2 precursor in yeast (Supplementary Figure S2). To increase the UDP-glucose stock, phosphoglucomutase 1 (*Sc*PGM1), phosphoglucomutase 2 (*Sc*PGM2), and UDP-glucose-phosphorylase (*Sc*UGP1) genes were controlled by the *PGK1*, *FBA1*, and *TDH3* promoters and *ADH1*, *TDH2* and *PFK1* terminators, respectively (Figure 5B; Supplementary Table S2). All the above genes constituted the EGH-31 and EGH-53 gene modules, and the corresponding engineered strains were named EGH31 or EGH53, respectively (Figure 5B; Supplementary Table S2).

The HPLC results of the yeast fermentation extracts showed that strain EGH31 produced peaks of DM, PPD, and G-Rg3, but intermediate G-Rh2, suggesting that G-Rh2 was completely consumed in the biosynthesis of saponins in the downstream pathway (Figures 6A,B). There was also evidence of G-Rg3 formation, but no G-F2 peak was observed, which further confirmed that *Pn*UGT31 preferentially catalyzes sugar chain extension (Figure 6A). The products of strain EGH53 showed

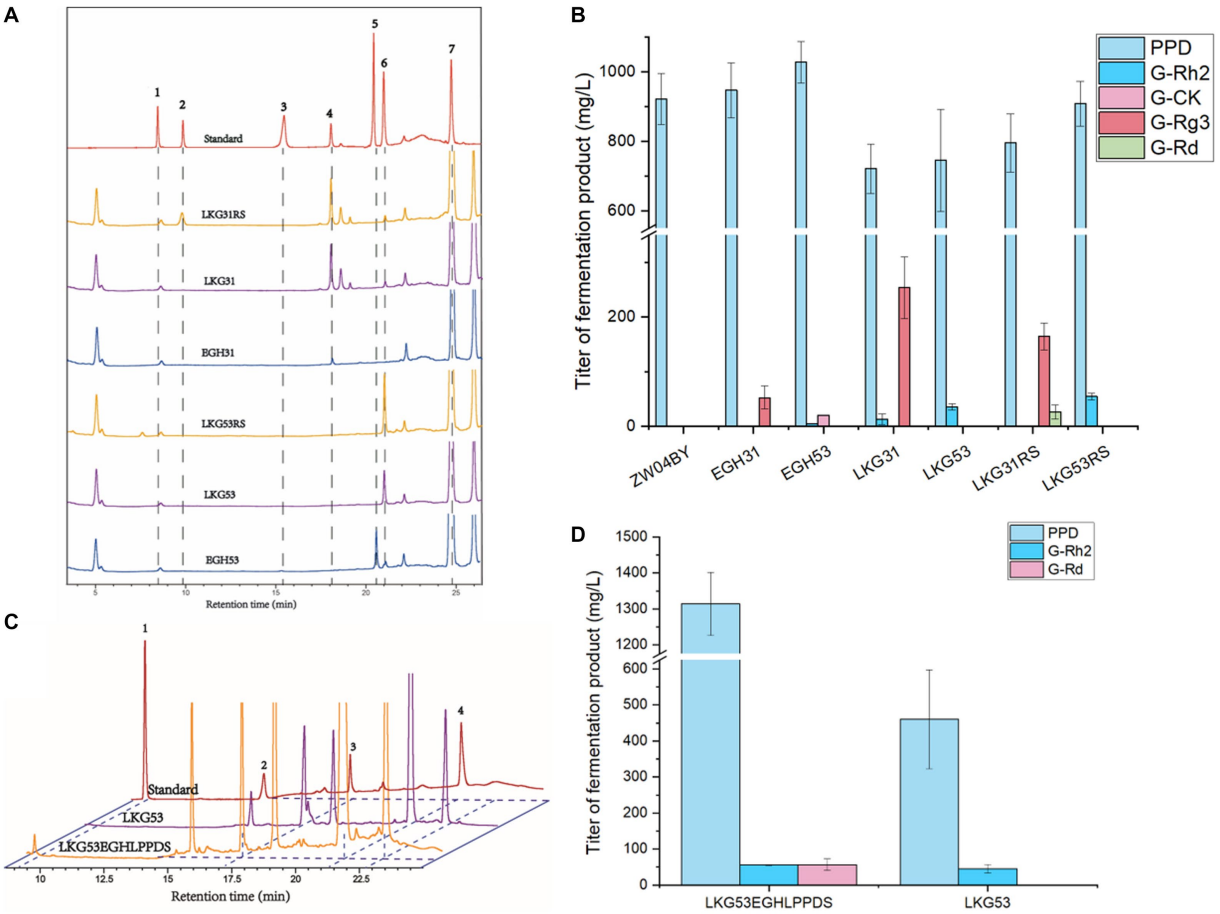

FIGURE 6
Ginsenoside products from engineered yeast. **(A)** HPLC results of engineered yeast after 120h in shaking flask. The gradient elution system 1 for separation of ginsenosides from yeast products. Peak 1 represents ginsenoside Rb1; Peak 2 represents ginsenoside Rd.; Peak 3 represents ginsenoside F2; Peak 4 represents ginsenoside Rg3; Peak 5 represents ginsenoside CK; Peak 6 represents ginsenoside Rh2; Peak 7 represents PPD. **(B)** The yield of ginsenosides produced by engineered yeast after 120h in shaking flask. **(C)** HPLC results of ginsenoside Rd. produced by engineered strain LKG53EGHLPPDS. Peak 1 represents ginsenoside Rd., peak 2 represents ginsenoside Rg3, peak 3 represents ginsenoside Rh2 and peak 4 represents PPD. The gradient elution system 2 for separation of ginsenosides from yeast products. **(D)** The yield of ginsenosides produced by strain LKG53EGHLPPDS in shaking flask after 96h.

peaks for DM, PPD, G-Rh2, and G-CK, and the titer of G-CK was significantly higher than that of G-Rh2, further verifying that *Pn*UGT53 prefers the glycosylation of C20-OH rather than catalyzing the extension of the sugar chain (Figure 6A). No peaks for G-Rd and G-Rb1 were detected in the fermentation extracts of strains EGH31 and EGH53, indicating that *Pn*UGT53 and *Pn*UGT31 have weak catalytic synthesis abilities for G-Rd and G-Rb1 or generate fewer precursor substances (Figure 6B). The results showed strain EGH31 could produce 0.95 ± 0.08 g/L PPD and 52.48 ± 21.02 mg/L G-Rg3, whereas strain EGH53 could produce 1.03 ± 0.06 g/L PPD, 20.48 ± 0.20 mg/L G-CK and 4.40 ± 0.13 mg/L G-Rh2 (Figure 6B; Table 1).

Accumulation of key precursors

The precursor G-Rh2 produced by the engineered yeasts EGH31 and EGH53 was consumed, resulting in low production of ginsenosides in the downstream pathway. Insufficient precursor G-Rh2 did not generate sufficient G-Rb1. To improve the titer of G-Rh2, SnyPnUGT50, the expression controlled by the *TDH3* + $UAS_{TEF1\text{-}CIT1\text{-}CLB2}$ promoter, was selected to catalyze PPD to generate G-Rh2. Sny*Pn*UGT50 significantly increased the titer of G-Rh2 from PPD in yeast (Wang et al., 2019). The insertion of *PnUGT53* and *PnUGT31* fragments promoted ginsenosides biosynthesis in the downstream pathway. *LEU2* was selected as the insertion locus to recover leucine selection labels. The gene modules mentioned above were named LKG-31 or LKG-53, and the corresponding engineered strains were designated LKG31 and LKG53, respectively (Figure 5C; Supplementary Table S2). After shaking for 120 h, strain LKG53 consumed more PPD than EGH53. The absence of G-CK indicated that UGT53 was consumed to catalyze PPD to produce G-Rh2, which increased 8-fold the titer of G-Rh2, from 4.40 ± 0.13 mg/ L to 35.42 ± 5.37 mg/ L. In addition, the G-Rg3 yield of strain LKG31 (254.07 ± 56.49 mg/ L) was 3.84 times higher than that of strain EGH31 (52.48 ± 21.02 mg/L; Figure 6B; Table 1). These results show that the LKG module significantly increased the titer of G-Rg3 in *S. cerevisiae*.

To increase the PPD precursor yield, two methods were employed to increase the conversion rate of DM to PPD. The insertion of the LPPDS module at the δ sequence site may inhibit of cell growth. To exclude cell growth inhibition caused by the insertion site, the engineered yeast strains LKG31RS or LKG53RS were constructed based on the LKG31 and LKG53 strains by replacing with γ sequence as the insertion site. The engineered yeast strains LKG31RS and LKG53RS, and their control strain LKG, were cultured in a shake flask for 120 h. These results revealed the presence of G-Rd in the strain LKG31RS (Figure 6A). Meanwhile, the PPD titers of strains LKG31RS and LKG53RS increased by 10.27 and 21.76%, respectively. Compared to the control group, the total saponin production in the downstream pathway also increased (Figure 6B; Table 1). In addition, the OD_{600} of these strains was not significantly difference compared to the control strain LKG31 or LKG53 (data not shown). HPLC results showed that the peak area of DM decreased by 80.03%, whereas the total saponin production increased by 23.3%. The peak area of DM from strain LPPDS decreased by 85.02% compared to the control strain ZW04BY, and total saponin (PPD) production increased by 132.3%. Therefore, the introducting of the RS module alleviated cell-growth inhibition to a certain extent and increased the PPD conversion rate, which was slightly lower than that of the LPPDS module. Quantitative analysis showed that strain LKG31RS produced 795.41 ± 83.54 mg/L PPD, 0.72 ± 0.14 mg/L G-Rh2, 164.58 ± 24.54 mg/L G-Rg3 and 26.21 ± 12.86 mg/L G-Rd. Strain LKG53RS produced 908.46 ± 64.58 mg/L PPD and 54.57 ± 6.36 mg/L G-Rh2 (Figure 6B; Table 1).

Owing to the restriction of the enzyme activity of *Pn*UGT31 and *Pn*UGT53, appropriately increasing the accumulation of the precursors PPD and G-Rh2 is helps improve the biosynthesis of downstream saponins. The resulting strain was named LKG53EGHLPPDS after stacking the above three modules. The G-Rh2 titer of strain LKG53EGHLPPDS (55.67 ± 1.44 mg/L) increased by 23.86% compared with that of strain LKG53 (44.97 ± 12.01 mg/L) following incubation in a shake flask for 96 h (Figures 6C,D; Table 1). The PPD yield of strain LKG53EGHLPPDS was 1313.75 ± 87.33 mg/L, and that of strain LKG53 was 460.15 ± 137.48 mg/L, Which is a 185% increase (Figures 6C,D; Table 1). Strain LKG53EGHLPPDS also produced 56.68 ± 16.21 mg/L G-Rd, twice higher than that of strain LKG31RS (Figures 6C,D; Table 1).

Discussion

P. notoginseng has the highest agricultural output value in traditional Chinese medicine, owing to various bioactive ginsenosides. The biosynthetic pathways and heterologous biosynthesis of ginsenosides and saponins have recently attracted significant attention. In this study, known *UGTs* from previous studies on ginsenoside biosynthesis were screened from the PDB (panaxGDB) to discover new catalytic functions of *Pn*UGT53 and *Pn*UGT31. Moreover, the key UGT (*Pn*UGT53) of V-18 biosynthesis was identified for the first time.

A previous study reported that UGTs involved in dammarane-type ginsenoside biosynthesis might catalyze different substrates even with high sequence homology (98.11–99.37%; Zhao et al., 2020). We found that the sequence homology between *PnUGT53* and *PnGT95* was 98.74%. *Pn*GT95 was reported to catalyze the glycosylation of hydroxyl groups at C20 and C6 sites of dammarane-type saponins (Yu et al., 2019). However, *Pn*UGT53 catalyzed the glycosylation of C20-OH, extended the sugar chain of dammarane-type saponins, and accepted UDP-xylose as a sugar donor in our study. *Pn*UGT53 and *Pn*UGT95 exhibited similar but different catalytic functions. Their expression patterns in different tissues of 3-year-old *P. notoginseng* plants were also distinct. *Pn*UGT53 was highly expressed in the flowers, whereas *Pn*UGT95 was highly expressed in the rhizomes of 3-year-old *P. notoginseng*. Other studies showed that more than 40 UGTs catalyze ginsenosides in the UGT94 family of *P. ginseng*, and the amino acid identity between *UGTs* is higher than 98%, but the catalytic activities or functions are quite different (Yang et al., 2020).

To further investigate the catalytic mechanisms of *Pn*UGT31 and *Pn*UGT53, we performed molecular docking simulations. Previous studies have shown that ten conserved residues in the PSPG region are directly linked to sugar donors (Li et al., 2007). Correspondingly, in the predicted model, *Pn*UGT53 and *Pn*UGT31 had four and six amino acid residues connected to sugar ligands, respectively, which also corresponded to the conserved residues in the PSPG region. Among the 44 amino acids in the PSPG region, tryptophan, aspartic acid/glutamic acid, and glutamine at positions 22, 43, and 44 are easily hydrogen-bonded to sugar ligands (Osmani et al., 2009). However, *Pn*UGT31 and *Pn*UGT53 lacked the corresponding hydrogen bonds at positions 43 and 44. The overlap of the donor and acceptor pockets in *Pn*UGT31 may increase the probability of an interaction between the two. When a protein performs a catalytic function, its structure is not invariable, and interdomain interactions between the C-terminal- and N-terminal domains are often found (Li et al., 2007). Protein structure prediction and molecular docking technology can be used to predict the interactions between proteins and ligand molecules, but their accuracy still needs to be verified by further experiments.

To increase the production of ginsenosides, the engineered ZW04BY was reconstructed to produce two times higher PPD than the reported yield. This may be due to differences in the number of gene copies obtained by yeast transformation in single cells, which causes biological differences among strains, or the selection of G418-resistant transformants. In this study, G418 resistance screening was performed twice for the LPPDS and LKG modules of strain LKG53EGHLPPDS. A higher concentration of G418 (400 mg/L) was selected for the second screening, which was applied to strain LKG53 as a chassis cell. After replacing strain LKG31 as the chassis cell, transformants could not be obtained through G418 resistance screening, which the copy number and expression level of the *KANMX* gene in strains LKG53 and LKG31 might have caused. In addition, the insertion of the LPPDS module resulted in the inhibition of the cell growth of the strain LPPDS and strain LKG53EGHLPPDS. We hypothesized that because 2, 3-oxsqualene is a common precursor of the synthesis of steroidal saponins and PPD, the production of PPD was greatly increased and the precursor 2,3-oxsqualene was consumed in large quantities, which might restrict the biosynthesis of steroidal saponins necessary for cell growth in plastids eventually causing cell growth inhibition (Parks and Casey, 1995). It could also

be that δ sequences are involved in the reverse transcription process in yeast cells, and excessive consumption δ sequences may impose a metabolic burden on cells. Therefore, we designed the RS module to change the insertion site into γ sequences. The results showed that cell growth inhibition was alleviated, but the transformation efficiency of DM was lower than that of the LPPDS module.

Both *Pn*UGT31 and *Pn*UGT53 continuously catalyzed G-Rh2 to produce G-Rb1. However, *PnUGT31* and *PnUGT53* were constructed into engineered yeast, and G-Rb1 was not detected in the fermentation products of all engineered yeasts. The same situation was observed in the engineered yeast platforms *Pn*3-31 and *Pn*3-29 in a previous study (Wang et al., 2020). We suspect that this may be due to the lower accumulation of the G-Rd precursor or the weak activity of the enzyme that catalyzes G-Rd to produce Rb1. Moreover, results showed that codon optimized *PnUGT31* in strains was able to produce more downstream ginsenosides than *PnUGT53*. Enzymatic activity is the main limiting factor in the production of PPD-type saponins by engineered yeast. However, the adaptability of genes to the yeast expression systems must also be considered. The gene expression level of *SynCYP2* from *P. notoginseng,* which catalyzes PPD to generate protopanaxatriol (PPT), was lower than that from *P. ginseng* in engineered yeast, even though the abundance of PPT-type ginsenosides in *P. notoginseng* was higher than that in *P. ginseng* (Li et al., 2021).

In this study, engineered yeasts producing PPD, G-Rh2, G-Rg3, G-Rd, and other ginsenosides were successfully constructed, but there is still much work to be done to improve the production of dammarane-type ginsenosides by *S. cerevisiae*. The previously reported *Pn*UGT33 was selected as the key enzyme for G-Rg3 production to construct engineered yeast. Yeasts overexpressing *ScPGM1*, *ScPGM2*, and *ScUGP1* genes produced 51 mg/L G-Rg3 in the optimized YPD medium, which was lower than that of LKG31 (254.07 mg/ L). In this study, the EGH module was not successfully constructed into the LKG31RS genome for unknown reasons, and we failed to increase the G-Rd titer of strain LKG53EGHLPPDS (56.68 mg/L), yet it was the highest yield from a known engineered yeast.

Conclusion

In this study, new catalytic activity of PnUGT31 and PnUGT53 was identified and utilized in yeast cell factory producing damarane-type ginsenosides using metabolic engineering. We constructed appropriate gene modules, and finally increased the titer of G-Rg3 and G-Rd in yeast. This study established an efficient method for the production of G-Rg3 and G-Rd. Meanwhile, the synthetic biology strategy of this study can also be used for heterologous synthesis of other natural products in yeast.

Data availability statement

The datasets presented in this study can be found in online repositories. The names of the repository/repositories and accession number(s) can be found in the article/ Supplementary material.

Author contributions

BH, YL, and SY conceived the study. YL, GC, and YW performed the experiments. GZ, YL, and SY the designed experiments. YL and QY analyzed the data. BH and YL drafted the manuscript. YL, BH, and SY reviewed and edited the manuscript. All authors contributed to the article and approved the submitted version.

Funding

This work was supported by Major Science and Technology Projects in Yunnan Province (2019ZF011-1), Fundamental Research Project of Yunnan (202101AS070037), Science and Technology Innovation team of Yunnan (202105AE160011), The Major Science and Technique Programs in Yunnan Province (202102AE090042), Yunnan Characteristic Plant Extraction Laboratory (2022YKZY001), the First Projects of Science and Technology Plan in the Biomedical field in 2021 (202102AA310048), and National Natural Science Foundation of China (grant nos. 81960691 and 82160727).

Acknowledgments

We are thankful to the co-authors for their contributions to this project, the Key Laboratory of Medicinal Plant Biology for essential research facilities support. Many thanks to Yun Hengji (Kunming Institute of Botany) for identifying plant materials, Hui feng Jiang (Tianjin Institute of Industrial Biotechnology) for kindly offering yeast strain W303 and plasmid YCplac22, PET-28a.

Conflict of interest

The authors declare that the research was conducted in the absence of any commercial or financial relationships that could be construed as a potential conflict of interest.

Publisher's note

Supplementary material

The Supplementary material for this article can be found online at: https://www.frontiersin.org/articles/10.3389/fmicb.2023.1191102/full#supplementary-material

References

Blazeck, J., Garg, R., Reed, B., and Alper, H. S. (2012). Controlling promoter strength and regulation in *Saccharomyces cerevisiae* using synthetic hybrid promoters. *Biotechnol. Bioeng.* 109, 2884–2895. doi: 10.1002/bit.24552

Chen, Z., Wei, X., Shen, L., Zhu, H., and Zheng, X. (2019). 20 (S)-ginsenoside-Rg3 reverses temozolomide resistance and restrains epithelial-mesenchymal transition progression in glioblastoma. *Cancer Sci.* 110, 389–400. doi: 10.1111/cas.13881

Chen, Y., Xu, Y., Zhu, Y., and Li, X. (2013). Anti-cancer effects of ginsenoside compound k on pediatric acute myeloid leukemia cells. *Cancer Cell Int.* 13, 24–26. doi: 10.1186/1475-2867-13-24

Dai, Z., Wang, B., Liu, Y., Shi, M., Wang, D., Zhang, X., et al. (2014). Producing aglycons of ginsenosides in bakers' yeast. *Sci. Rep.* 4:3698. doi: 10.1038/srep03698

Jiang, Z., Gao, H., Liu, R., Xia, M., Lu, Y., Wang, J., et al. (2022). Key glycosyltransferase genes of Panax notoginseng: identification and engineering yeast construction of rare ginsenosides. *ACS Synth. Biol.* 11, 2394–2404. doi: 10.1021/acssynbio.2c00094

Li, L., Modolo, L. V., Escamilla-Trevino, L. L., Achnine, L., Dixon, R. A., and Wang, X. (2007). Crystal structure of *Medicago truncatula* UGT85H2--insights into the structural basis of a multifunctional (iso)flavonoid glycosyltransferase. *J. Mol. Biol.* 370, 951–963. doi: 10.1016/j.jmb.2007.05.036

Li, X., Wang, Y., Fan, Z., Wang, Y., Wang, P., Yan, X., et al. (2021). High-level sustainable production of the characteristic protopanaxatriol-type saponins from Panax species in engineered *Saccharomyces cerevisiae*. *Metab. Eng.* 66, 87–97. doi: 10.1016/j.ymben.2021.04.006

Lin, Y., Hao, B., Lu, Y. C., Lin, Y., Hao, B., Lu, Y. C., et al. (2022). PanaxGDB: a comprehensive platform for Panax. *Front. Plant Sci.* 13:883818. doi: 10.3389/fpls.2022.883818

Liu, Y., Wang, J., Qiao, J., Liu, S., Wang, S., Zhao, D., et al. (2020). Ginsenoside Rh2 inhibits HeLa cell energy metabolism and induces apoptosis by upregulating voltage-dependent anion channel 1. *Int. J. Mol. Med.* 46, 1695–1706. doi: 10.3892/ijmm.2020.4725

Osmani, S. A., Bak, S., and Møller, B. L. (2009). Substrate specificity of plant UDP-dependent glycosyltransferases predicted from crystal structures and homology modeling. *Phytochemistry* 70, 325–347. doi: 10.1016/j.phytochem.2008.12.009

Parekh, R. N., Shaw, M. R., and Wittrup, K. D. (1996). An integrating vector for tunable, high copy, stable integration into the dispersed ty delta sites of *Saccharomyces cerevisiae*. *Biotechnol. Prog.* 12, 16–21. doi: 10.1021/bp9500627

Parks, L. W., and Casey, W. M. (1995). Physiological implications of sterol biosynthesis in yeast. *Annu. Rev. Microbiol.* 49, 95–116. doi: 10.1146/annurev.mi.49.100195.000523

Ross, J., Li, Y., Lim, E., and Bowles, D. J. (2001). Higher plant glycosyltransferases. *Genome Biol.* 2, REVIEWS3004–REVIEWS3009. doi: 10.1186/gb-2001-2-2-reviews3004

Sun, M., Ye, Y., Xiao, L., Duan, X., Zhang, Y., and Zhang, H. (2017). Anticancer effects of ginsenoside Rg3 (review). *Int. J. Mol. Med.* 39, 507–518. doi: 10.3892/ijmm.2017.2857

Wan, J. B., Yang, F. Q., Li, S. P., Wang, T. Y., and Cui, M. X. (2006). Chemical characteristics for different parts of Panax notoginseng using pressurized liquid extraction and HPLC-ELSD. *J Pharmaceut Biomed.* 41, 1596–1601. doi: 10.1016/j.jpba.2006.01.058

Wang, J., Tian, L., Khan, M. N., Zhang, L., Chen, Q., Zhao, Y., et al. (2018). Ginsenoside Rg3 sensitizes hypoxic lung cancer cells to cisplatin via blocking of NF-κB mediated epithelial–mesenchymal transition and stemness. *Cancer Lett.* 415, 73–85. doi: 10.1016/j.canlet.2017.11.037

Wang, X., Wang, Z., and Da Silva, N. A. (1996). G418 selection and stability of cloned genes integrated at chromosomal delta sequences of *Saccharomyces cerevisiae*. *Biotechnol. Bioeng.* 49, 45–51. doi: 10.1002/(SICI)1097-0290(19960105)49:1<45::AID-BIT6>3.0.CO;2-T

Wang, D., Wang, J., Shi, Y., Li, R., Fan, F., Huang, Y., et al. (2020). Elucidation of the complete biosynthetic pathway of the main triterpene glycosylation products of Panax notoginseng using a synthetic biology platform. *Metab. Eng.* 61, 131–140. doi: 10.1016/j.ymben.2020.05.007

Wang, P., Wei, W., Ye, W., Li, X., Zhao, W., Yang, C., et al. (2019). Synthesizing ginsenoside Rh2 in *Saccharomyces cerevisiae* cell factory at high-efficiency. *Cell Discov.* 5, 1–14. doi: 10.1038/s41421-018-0075-5

Wei, G., Dong, L., Yang, J., Zhang, L., Xu, J., Yang, F., et al. (2018). Integrated metabolomic and transcriptomic analyses revealed the distribution of saponins in *Panax notoginseng*. *Acta Pharm. Sin. B* 8, 458–465. doi: 10.1016/j.apsb.2017.12.010

Yang, C., Li, C., Wei, W., Wei, Y., Liu, Q., Zhao, G., et al. (2020). The unprecedented diversity of UGT94-family UDP-glycosyltransferases in Panax plants and their contribution to ginsenoside biosynthesis. *Sci. Rep.* 10:15394. doi: 10.1038/s41598-020-72278-y

Yang, Z., Liu, G., Zhang, G., Yan, J., Dong, Y., Lu, Y., et al. (2021). The chromosome-scale high-quality genome assembly of Panax notoginseng provides insight into dencichine biosynthesis. *Plant Biotechnol. J.* 19, 869–871. doi: 10.1111/pbi.13558

Yu, L., Chen, Y., Shi, J., Wang, R., Yang, Y., Yang, L., et al. (2019). Biosynthesis of rare 20(R)-protopanaxadiol/protopanaxatriol type ginsenosides through *Escherichia coli* engineered with uridine diphosphate glycosyltransferase genes. *J. Ginseng Res.* 43, 116–124. doi: 10.1016/j.jgr.2017.09.005

Zhang, S., Chen, C., Lu, W., and Wei, L. (2018). Phytochemistry, pharmacology, and clinical use of Panax notoginseng flowers buds. *Phytother. Res.* 32, 2155–2163. doi: 10.1002/ptr.6167

Zhao, J., Wang, R. F., Zhao, S., and Wang, Z. T. (2020). Advance in glycosyltransferases, the important bioparts for production of diversified ginsenosides. *Chin J Nat Medicines.* 18, 643–658. doi: 10.1016/S1875-5364(20)60003-6

Zhuang, Y., Yang, G. Y., Chen, X., Liu, Q., Zhang, X., Deng, Z., et al. (2017). Biosynthesis of plant-derived ginsenoside Rh2 in yeast via repurposing a keypromiscuous microbial enzyme. *Metab. Eng.* 42, 25–32. doi: 10.1016/j.ymben.2017.04.009

frontiers | Frontiers in Microbiology

TYPE Original Research
PUBLISHED 13 September 2023
DOI 10.3389/fmicb.2023.1180463

OPEN ACCESS

EDITED BY
Monika Prakash Rai,
Amity University, India

REVIEWED BY
Atte Johannes Von Wright,
University of Eastern Finland, Finland
Sowmyalakshmi Subramanian,
McGill University, Canada

*CORRESPONDENCE
Safaa M. Ali
✉ Safaa.mohamedali@yahoo.com;
✉ Sali@srtacity.sci.eg

RECEIVED 06 March 2023
ACCEPTED 12 June 2023
PUBLISHED 13 September 2023

CITATION
Amin AA, Olama ZA and Ali SM (2023) Characterization of an isolated lactase enzyme produced by *Bacillus licheniformis* ALSZ2 as a potential pharmaceutical supplement for lactose intolerance.
Front. Microbiol. 14:1180463.
doi: 10.3389/fmicb.2023.1180463

Characterization of an isolated lactase enzyme produced by *Bacillus licheniformis* ALSZ2 as a potential pharmaceutical supplement for lactose intolerance

Alaa A. Amin[1], Zakia A. Olama[1] and Safaa M. Ali[2]*

[1]Botany and Microbiology Department, Faculty of Science, Alexandria University, Alexandria, Egypt, [2]Nucleic Acid Research Department, Genetic Engineering and Biotechnology Research Institute, the City of Scientific Research and Technological Applications, Alexandria, Egypt

Introduction: Lactose intolerance is a widespread problem that affects people of many different races all over the world. The following pharmacological supplements can improve the lives of those who suffer from this issue.

Methods: This work focused on lactase producer isolation and statistical design (Plackett–Burman, and BOX–Behnken) to maximize the effectiveness of environmental factors. A lactase-producing bacterium was chosen from a discovery of 100 strains in soil that had previously been polluted with dairy products. Plackett-Burman investigated fifteen variables.

Results: The most critical variables that lead to increased lactase synthesis are glucose, peptone, and magnesium sulfate ($MgSO_4$). The ideal process conditions for the creation of lactase yield among the stated variables were then determined using a BOX-Benken design. To establish a polynomial quadratic relationship between the three variables and lactase activity, the Box–Behnken design level was used. The EXCEL-solver nonlinear optimization technique was used to predict the best form for lactase production. The ideal temperature and pH levels have been determined, both before and after the lactase purification process, to achieve the highest performance of isolated lactase.

Conclusion: According to this study, *Bacillus licheniformis* is a perfect supply of the lactase enzyme (β -Galactosidase), It can be used as a product to assist people who have health issues due to lactose intolerance.

KEYWORDS

lactase, Plackett-Burman, Box-Benken, characterization, purification

1. Introduction

Enzymes are active proteins that function as biochemical catalysts (Piumetti and Illanes, 2022). These are biomolecules that are required for both the synthesis and breakdown reactions of living organisms (Aggarwal et al., 2021). The enzymes known as β-galactosidases (EC 3.2.1.23), sometimes known as lactases, hydrolyze lactose (the most prevalent milk sugar) into

glucose and galactose (Liburdi and Marco, 2022). Although these enzymes are accessible in a range of biological systems, such as plants or microorganisms, they are currently only available commercially from yeasts, molds, and bacteria (Saqib et al., 2017; Martarello et al., 2019). Although these enzymes from various bacteria have varied features, their specificity is fundamentally the same (Ramos and Malcata, 2011; Kocabaş et al., 2021). Each chain of the four polypeptides in the tetramer of β-galactosidase has 1,023 amino acids, and together they form five different structural domains (Sedzro et al., 2018; Swentowsky, 2021). One of these domains is the jellyroll barrel, while the others are fibronectin, b-sandwich, and a central domain with a TIM-type barrel that also serves as the active site. Tetramer subunits make up the core domain, which is catalytically active (Wang et al., 2021). The catalytic site is disabled when a tetramer is broken up into dimers. Those enzymes are active proteins and their function as biocatalysts were discovered by Cao et al. (2021). Similarly, the β-galactosidase amino acid sequence was done by Poch et al. (1992) and the structure was determined by Jacobson et al. (1994). This enzyme's amino-terminal sequence contains a-peptide that engages in a-complementation and aids in the formation of the subunit interaction (Aydin and Coin, 2021; Xu et al., 2021). Numerous organisms, including fungi, plants, yeast, and bacteria, may produce lactase (Shaima'a and Rashid, 2017). In the industrial sector, bacterial strains offer a lot of promise for large-scale manufacturing. Lactase generated by bacteria was frequently used to hydrolyze lactose because of its ease of fermentation, high activity, and good stability (Movahedpour et al., 2022). β-Galactosidase is used in a variety of industries (Ureta et al., 2021). β-galactosidase is utilized to handle whey disposal concerns on a commercial scale in addition to manufacturing lactose-free goods for lactose-intolerant patients (Paulo, 2018). To avoid the problem of hygroscopic lactose crystallizing in food, β -galactosidase is employed to hydrolyze the lactose in frozen, concentrated sweets (Portnoy and Barbano, 2021). This treatment lowers the lactose level of milk so that lactose-intolerant people can drink it. Lack of lactase, a digestive enzyme that prevents the body from hydrolyzing lactose in meals, is the primary cause of lactose intolerance. About 75% of people worldwide have lactose intolerance, which significantly lowers their quality of life (Venkateswarulu et al., 2017; Peele et al., 2018). Probiotic supplements may be beneficial for those with lactase deficiency. The dairy industry used lactase-producing bacterial strains to cure milk-based products (Venkateswarulu et al., 2017). Stomach pain and abdominal distension, abdominal colic, diarrhea, and nausea are all signs of lactose intolerance (Shrestha et al., 2021). Lactase deficiency can be classified as primary, congenital, or secondary. Primary lactase insufficiency affects adults aged 2 to 20. A more prevalent variety is primary lactase deficiency, which is caused by a decrease in β-galactosidase production along the small intestine's brush boundaries (lactase). The second kind of lactase deficit is a birth defect in lactase production, which is brought on by a genetic defect and is defined by patients having either little or nonexistent lactase enzyme at all. The third kind, sometimes referred to as secondary lactase deficit, is when there are inadequate levels of this enzyme as a result of a GI tract issue (Paulo, 2018; Szilagyi et al., 2019; Muzaffar et al., 2021).

The current study's major purpose is to develop exploitation tactics for the eventual advantage of extracellular bacterial lactase production. The goal of this study was to uncover a novel approach to lactase manufacturing in a newly discovered lactase producer. Furthermore, the utilization of mathematical models was the main emphasis of the current investigation to optimize the growth conditions that result in the best lactase productivity from a newly discovered *Bacillus licheniformis ALSZ2*. To our knowledge, lag phase bacterial lactase production has not yet been documented in the literature; the current study's findings are the first report of Egyptian lactase manufacturing that is significantly cost-effective.

2. Materials and method

2.1. Isolation and screening of lactase producers

Samples of diverse dairy products (12) (milk, Romy cheese, and karish cheese) were collected in a sterile dry container. For bacterial isolation and colony purification, an LB medium that was diluted to one-tenth of medium strength was used. For lactase production, 100 purified bacterial isolates were screened. Isolation of lactase-producing bacteria was achieved using an LB broth medium fortified with lactose substrate (5%) and 1% X-gal. Blue color after growth refers to lactase production.

2.1.1. Rapid plate assay method

Qualitative identification of lactase producers was achieved using an LB agar medium containing 1 mM of IPTG (substrate of lactase) and X-gal (1%). The solidified agar plates were incubated in an inverted position at 37°C for 24 h. Isolated colonies that are blue (positive lactase producer) were subcultured in nutrient broth and incubated at 37°C and preserved for further studies (Petassi et al., 2020).

2.2. Molecular identification of the most potent producer

Fresh bacterial cells are used for DNA extraction using GeneJET Genomic DNA Purification Kit. Using standard primers (F: AGA GTTTGATCMTGGCTCAG and R: TACGGYACCTTGTTACGACTT) (Alkhafaje et al., 2019) intended to magnify a 1,500 base pair portion of the 16S rDNA region (Kim and Chun, 2014; Soliman et al., 2018), the 16S rDNA was amplified using PCR (polymerase chain reaction). The condition of the cyclical reaction was 4 min at 95°C and then 40 cycles of 40 s at 94°C, 50 s at 55°C, and 50 s at 72°C, monitored by an additional 10 min at 72°C. PCR reactions were run on an agarose gel, and the remaining mixture was purified for sequence (Alkhafaje et al., 2022).

2.2.1. Phylogenetic analysis

To evaluate the DNA similarity of the obtained 16SrDNA sequence [by using a 3,130 X DNA Sequencer (Genetic Analyzer, Applied Biosystems, Hitachi, Japan)], phylogenetic analysis was conducted using the BLAST tool.[1] Mega7 software was used to

1 www.ncbi.nlm.gov/blast

accomplish molecular phylogeny and multiple sequence alignment present in the database (NCBI). A neighbor-joining (NJ) tree and a maximum parsimony (MP) tree using bootstrapping were made using this alignment (Hassan et al., 2018; Shaaban et al., 2022).

2.3. Enzyme assay

The culture media were prepared, inoculated with lactase producers, and incubated for 24 h at 37°C. At the end of the incubation period, the fermented culture was centrifuged at 5000 rpm for 10 min at room temperature (at 25°C). 0.8 mL of the cell-free extract (crude enzyme) was incubated with 1.2 mL of 5% lactose at 37°C for 30 min. Enzyme lactase hydrolyses lactose into glucose and galactose, and this reaction was terminated by boiling the crude enzyme extract for 10 min. Glucose was then measured using a Glucose kit (Biosystem) at 540 nm (Amamcharla and Metzger, 2011). The quantity of enzyme necessary to yield 1 µg of glucose every minute under typical test circumstances was considered to be a single lactase unit.

2.4. Optimization of lactase producer using experimental design

2.4.1. Plackett-Burman screening design

Using the Plackett-Burman experimental design, the effects of various medium compositions on the production of the lactase enzyme were investigated. Constructed using a Plackett-Burman matrix (Supplementary Table S1) (Ali et al., 2013; Sorour et al., 2020), a two-level factorial design was used to examine fifteen variables at two levels, −1 for the low value and + 1 for the high value. This permits the analysis of n − 1 variables with the fewest number of tests. To determine the relative significance of 15 elements or variables ($MgSO_4$, Glucose, $NaNO_3$, $CaCl_2$, $CuSO_4$, $MnSO_4$, $ZnSO_4$, $FeSO_4$, KCL, $NaHPO_4 12H_2O$, KH_2PO_4, K_2HPO_4, yeast extract (YE), Beef extract, and Peptone), an experimental design which includes a set of 20 experiments (trials) was used. The first-order model served as the basis for the Plackett-Burman design: $Y = o + iXi$, where Y represents the response (enzyme activity), o represents the model intercept, I represents the linear coefficient, and Xi represents the degree of an independent variable. Developing the free Essential Experimental Design program, data analysis, coefficient determination, and polynomial model reduction was performed on the lactase enzyme statistics.

2.4.2. Box-Benken design

To discover the kind of response surface in the experiment and to decide the greatest circumstances for enzyme synthesis, a Box-Benken design (Ali et al., 2013; Sorour et al., 2020; Tamer et al., 2021) was adopted. The factorial design, which includes thirteen trials, was constructed to look into the most critical parameters that influence enzyme synthesis. Each variable was examined at three different levels, with low, moderate, and high values, respectively, denoted by −1, 0, and + 1 (Supplementary Table S2). A second-order polynomial equation was developed to determine the appropriate location and to connect the relationship between the independent components and the response for three parameters. The equation was:

$$Y = \beta 0 + \beta 1X1 + \beta 2X2 + \beta 3X3 + \beta 12X12 + \beta 13X13 + \beta 23X23 + \beta 11X12 + \beta 22X22 + \beta 33X32$$

Where Y is the expected response, 0 is the design constant, X1, X2, and X3 are the independent factors, 12–13 and 23 are cross-product constants, 11–22 and 33 are quadratic constants, and 12–13 and 23 are coefficients of the cross product, respectively, and 11–22 and 33 are quadratic coefficients, and 12–13 and 23 are cross product coefficients, respectively. The experimental data were subjected to a regression analysis using Microsoft Excel 2010. The constant of determination, R2, was employed to explain the polynomial model equation's grade of fit (Ali et al., 2013; Sorour et al., 2020). The tests were repeated three times, with the average results presented.

2.5. Purification of lactase enzyme

The crude enzyme was purified using the column chromatography (gel filtration) technique. Multiple columns with different pour sizes were applied to detect the molecular weight and extract the target enzyme (Amicon system). The system combines downstream sample concentration and buffer exchange with affinity-based spin column purification. The tool eliminates the requirement for numerous centrifugation processes and has a large reservoir that can hold a variety of sample quantities. For simultaneous elution, concentration, and extremely effective diafiltration (>99%) in a single spin, the included Amicon® Ultra filter (Philippines - Merck Millipore Division, an affiliate of Merck KGaA, Darmstadt, Germany) was attached. According to the protein cut-off different filters were used (UFC8010, UFC8020, UFC8030, UFC8050, UFC8070, and UFC8100 for 10, 20, 30, 50, 70, and 100 KD respectively). The concentrated protein fraction was very carefully layered on top of the pre-equilibrated and stabilized falcon tubes. The tubes were then centrifuged under cooling (4°C) for 20 min at 8000 rpm, and the upper layer was transferred to the tube with the cut-off (10, 20, 30, 50, 70, and 100 KD) as presented in the supplementary file. Protein content was estimated in each of the filter cut-offs, using the bovine serum albumin (BSA) standard curve The enzyme activity of each of the resulting various molecular weight proteins was then determined (Patel et al., 2017).

2.5.1. Characterization of purified and crude lactase

2.5.1.1. Determination of optimum temperature

At pH 7, temperatures between 30–60°C were found to be the ideal temperature for the crude and purified enzyme activity.

2.5.1.2. Obtaining the ideal pH for enzyme activity

In a trial to test the effect of pH level on crude and purified enzyme activities one at a time, different buffers, namely sodium phosphate buffer, Tris–HCl buffer, and potassium phosphate buffer with varied pH ranges (5.8–8), (6–8.5), and (5.8–8) respectively, were used.

2.6. The antibiotics sensitivity of ALSZ2

Seventeen antibiotic disks were tested, namely amikacin (AMK, 30 µg), amoxicillin-clavulanic acid (AMC, 20 µg/10 µg), ampicillin

(AMP, 10 μg), aztreonam (ATM, 30 μg), cefepime (FEP, 30 μg), ceftazidime (CAZ, 30 μg), chloramphenicol (CHL, 30 μg), ciprofloxacin (CIP, 5 μg), clindamycin (CLI, 2 μg), clotrimazole (CC, 10 μg), erythromycin (ERY, 15 μg), gentamicin (GEN, 10 μg), imipenem (IPM, 10 μg), kanamycin (KAN, 30 μg), ticarcillin-clavulanic acid (TIM, 75 μg/10 μg), trimethoprim (TMP, 5 μg) and vancomycin (VAN, 30 μg). The prepared plates were incubated for 24 h at 37°C. The inhibition zone for each antibiotic was measured with a ruler. The indicator of antibiotic sensitivity has traditionally been the existence of a clear zone surrounding the disk. The diameter of the inhibitory zone was used to calculate the results of antibiotic sensitivity tests.

3. Results

In the beginning, many bacteria were isolated from different sources of dairy products, and then the isolates were compared to produce the required enzyme and determine the best one in terms of productivity.

3.1. Isolation and screening of lactase (β-galactosidase) producers

In a screening process for lactase enzyme-producing bacteria, 100 isolates were collected from dairy product samples and examined for enzyme production. Lactase-producing bacteria were screened qualitatively on X-Gal agar plates (Figure 1A) and nutrient broth media containing X-Gal (Figure 1B) at 37°C. Thirteen out of 100 bacterial isolates showed a variance in enzyme activity. Isolate ALSZ2 was the most promising lactase producer and was related for further work.

3.2. Identification of the selected bacterial isolates

The most promising isolate with the code ALSZ2 was identified using PCR-amplified 16S rDNA genes. Molecular identification and gene bank sequence isolate (ALSZ2) was *Bacillus* genus, with a 96.66 present similarity to *B. licheniformis*, according to the findings. The Mega 7 program was used to generate a phylogenetic tree, showing that isolate (ALSZ2) is more strongly related to *B. licheniformis* bacterium (acc.: MW148439.1), shown in Figure 1.

3.3. The antibiotic sensitivity of the selected bacterial isolates

The antibiotics amikacin, amoxicillin-clavulanic acid, ampicillin, aztreonam, cefepime, ceftazidime, chloramphenicol, ciprofloxacin, clindamycin, clotrimazole, erythromycin, gentamicin, imipenem, kanamycin, ticarcillin-clavulanic acid, trimethoprim, and vancomycin were all very sensitive to *B. licheniformis* ALSZ2. The strain was resistant to ampicillin and cefepime.

3.4. Improving the nutritive necessities upsetting *Bacillus licheniformis* ALSZ2 lactase production using multifactorial statistical design: Plackett-Burman and Box–Behnken designs

3.4.1. Selection of important variables upsetting lactase production using a Plackett-Burman design

The "two-phase" optimization strategy was used to apply the statistical design. The initial stage was to determine the relative relevance of the various components in the culture media, as well as the levels of variables that have a major impact on lactase synthesis. The trials were then verified to validate the results under precise, optimal experimental settings.

Plackett-Burman design for twenty trials with two concentration levels for fifteen different variables (Supplementary Table S1) was conducted based on the experimental matrix shown in Table 1. The corresponding results were summarized in Table 2. The Plackett-Burman design studies' results revealed a wide range of variations. To assess variables that affect lactase production, the Plackett-Burman statistical design was employed (*B. licheniformis* ALSZ2). Calculations and graphical representations of the primary impacts of the investigated factors on lactase activity are shown in Figure 2. A major effect value with a positive sign suggests that a variable's high concentration is close to its optimal level, whereas the main effect value with a negative sign indicates that a variable's low concentration is close to its optimal level (Figure 2 and Table 3). It was found that Peptone, $MgSO_4$, and Glucose have the greatest positive effect on the production, followed by $ZnSO_4$, Beef extract, KCl, $FeSO_4$, $MnSO_4$, and $CaCl_2$. Whereas, $NaHPO_4$ has the most negative effect, followed by K_2HPO_4, $CuSO_4$, yeast extract, KH_2PO_4, and $NaNO_3$ in order.

3.4.1.1. Verification of the model

Variables with negative main effect values were used as (−1) coded values, while variables with positive main effect values were used as (+1) coded values. Supplementary Table S3 shows the lactase activity variations X1, X2, X3, X4, X5, X6, X10, and X19. Considering the data gathered from the outcomes of the Plackett-Burman experiment, the following composition (g/L) is expected to be near to the optimal: Beef extract, 1; $MgSO_4$, 10; Glucose, 75; $NaNO_3$, 30; Yeast extract, 100; $CaCl_2$, 1; $CuSO_4$, 0; $MnSO_4$, 10; $ZnSO_4$, 15; $FeSO_4$, 20; KCl, 1; $NaHPO_4.12H_2O$, 10; KH_2PO_4,10; K_2HPO_4, 0; Peptone, 25. The medium was reformed to a pH of 7 and the flasks were incubated at 37°C for 24 and 48 h, respectively. A verification experiment was done to estimate the reliability of the Plackett-Burman screening test.

3.4.2. Optimization of medium composition by Box–Behnken design

To validate the precision of the variables identified by the Plackett-Burman design using the Box–Behnken design experimental strategy, Response Surface Methodology was used. The following three tiers of the three crucial factors were looked into: −1, 0, and + 1.

3.4.2.1. Box–Behnken design for *Bacillus licheniformis* ALSZ2

According to the Box–Behnken design, Supplementary Table S2 shows alternative combinations of the three essential variables. All

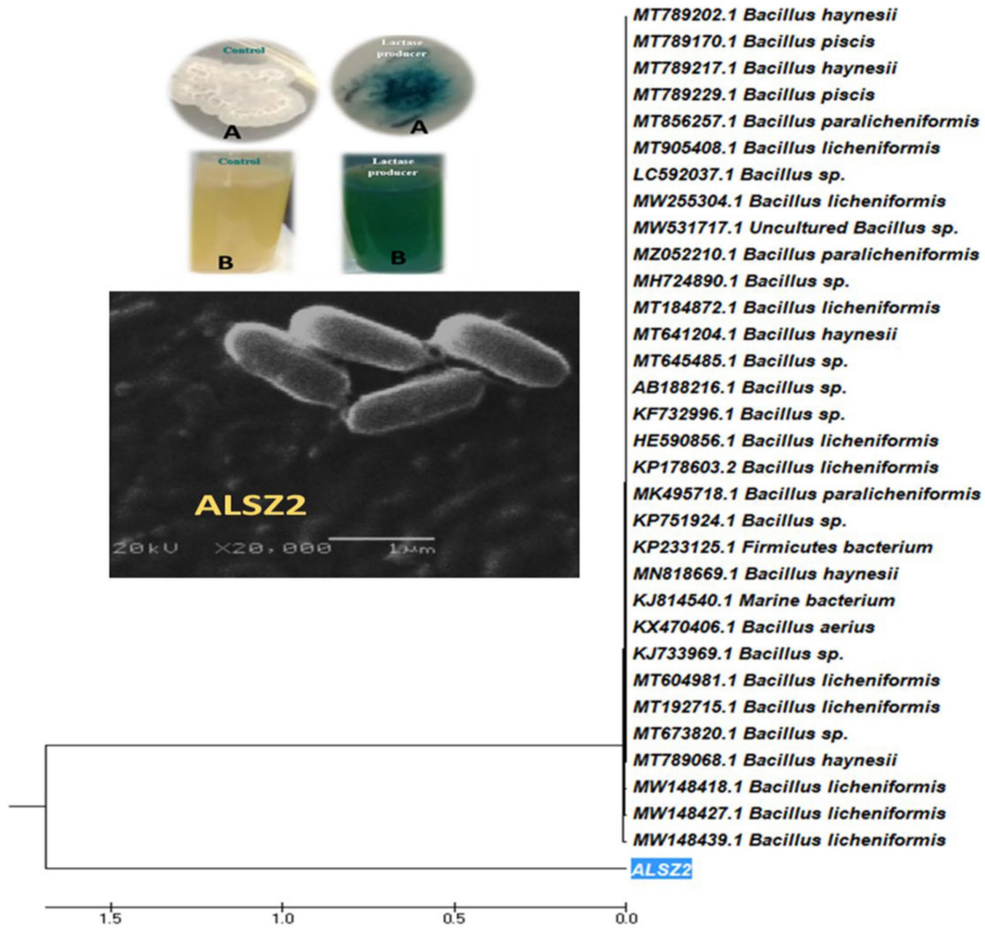

FIGURE 1
Phylogenetic tree of *Bacillus licheniformis* ALSZ2 based on 16S RNA sequence assessments. Detection of lactase production using colorimetric methods: **(A)** shows the negative control and positive lactase producer using solid media and **(B)** shows the negative control and positive lactase producer using liquid media.

assemblies had the same concentration of the remaining components as the Plackett-Burman pre-optimized medium. The Box–Behnken experimental design's results are summarized in Table 3 and the output of the surface plots formula is in (Figure 3). The optimal condition was determined by examining the connection between the individual variables and the lactase activity response. Table 3 shows the design matrix. The design indicated the optimum environmental factors as predictable lactase activity of 13.01754 U/mL, even though 13 U/mL of activity existed under ideal circumstances. As a consequence, the accuracy grade of 99.8% was used to evaluate the power of the perfect matrix under the following ideal circumstances. The medium composition contained g/L: $MgSO_4$, 10.5; Glucose, 75.4491; $NaNO_3$, 30; $CaCl_2$, 1; $CuSO_4$, 0; $MnSO_4$, 10; $ZnSO_4$, 15; $FeSO_4$, 20; KCl, 1; $NaHPO_4.12H_2O$, 10; KH_2PO_4,10; K_2HPO_4, 0; Yeast extract, 100; Beef extract, 1; Peptone, 25.249 at pH 7, and the bacteria were grown in a rotatory shaker set to 37°C and 200 rpm, for 24 h.

3.5. Purification of lactase enzyme

The cell-free extract was subjected to purification using an Amicon system to achieve the best possible result of enzyme activity with different protein molecular weight (MW) cut-offs (100, 50, 30, and 10 kDa). *Bacillus licheniformis* ALSZ2 lactase was detected in a 30–50 kDa cut-off filter.

3.6. Effect of temperature on lactase activity (crude and purified)

Bacillus licheniformis ALSZ2 lactase (crude & purified) was exposed to seven different temperatures to ascertain the enzyme's optimum temperature (30, 35, 40, 45, 50, 55, and 60°C Figure 4). Results in Figure 4 revealed that the perfect temperature for maximum enzyme activities (crude & purified) was found to be 35°C with 49 and 46.25 U/mL (30–50 kDa) respectively. Lactase synthesis reached a maximum of 90.05 IU at a temperature of 35°C.

3.7. Effect of hydrogen ion concentration on the enzyme activity (crude and purified)

To determine the ideal pH for enzyme activity, three different buffers have been used, namely sodium phosphate, potassium

TABLE 1 Plackett-Burman design matrix for fifteen variables with coded levels for *Bacillus licheniformis* ALSZ2 lactase optimization.

Trail no.	Variables															Lactase activity (U/mL)
	x1	x2	x3	x4	x5	x6	x7	x8	x9	x10	x11	x12	x13	x14	x15	
1	1	−1	−1	1	1	1	1	−1	1	−1	1	−1	−1	−1	−1	1.75
2	−1	−1	1	1	1	1	−1	1	−1	1	−1	−1	−1	−1	1	0
3	−1	1	1	1	1	−1	1	−1	1	−1	−1	−1	−1	1	1	6.125
4	1	1	1	1	−1	1	−1	1	−1	−1	−1	−1	1	1	−1	4
5	1	1	1	−1	1	−1	1	−1	−1	−1	−1	1	1	−1	−1	0
6	1	1	−1	1	−1	1	−1	−1	−1	−1	1	1	−1	−1	1	5.25
7	1	−1	1	−1	1	−1	−1	−1	−1	1	1	−1	−1	1	1	0
8	−1	1	−1	1	−1	−1	−1	−1	1	1	−1	−1	1	1	−1	0
9	1	−1	1	−1	−1	−1	−1	1	1	−1	−1	1	1	−1	−1	0
10	−1	1	−1	−1	−1	−1	1	1	−1	−1	1	1	−1	−1	1	2.5
11	1	−1	−1	−1	−1	1	1	−1	−1	1	1	−1	−1	1	1	2.75
12	−1	−1	−1	−1	1	1	−1	−1	1	1	−1	−1	1	1	1	1.5
13	−1	−1	−1	1	1	−1	−1	1	1	−1	−1	1	1	1	1	1.125
14	−1	−1	1	1	−1	−1	1	1	−1	−1	1	1	1	1	−1	1.75
15	−1	1	1	−1	−1	1	1	−1	−1	1	1	1	1	−1	1	0
16	1	1	−1	−1	1	1	−1	−1	1	1	1	1	−1	1	−1	0
17	1	−1	−1	1	1	−1	−1	1	1	1	1	−1	1	−1	1	2
18	−1	−1	1	1	−1	−1	1	1	1	1	−1	1	−1	1	−1	0.125
19	−1	1	1	−1	−1	1	1	1	1	−1	1	−11	1	−1	−1	3.625
20	1	1	−1	−1	1	1	1	1	−1	1	−1	1	−1	−1	−1	1.375

TABLE 2 Statistical analysis of Plackett–Burman design showing *p*-values, *t* stat, standard error, and coefficient values for each variable on *B. licheniformis* ALSZ2.

	Intercept	Coefficients	Standard error	*t* Stat	*p*-value
		1.69375	0.331699	5.106285	0.006952
$MgSO_4$	x1	0.775413	0.504984	1.535519	0.199455
Glucose	x2	0.86785	0.414914	2.091639	0.104637
$NaNO_3$	x3	−0.00385	0.410797	−0.00938	0.992968
$CaCl_2$	x4	0.461644	0.407376	1.133214	0.320442
$CuSO_4$	x5	−0.34818	0.412497	−0.84408	0.446148
$MnSO_4$	x6	0.493331	0.406293	1.214225	0.291444
$ZnSO_4$	x7	0.67716	0.459307	1.474306	0.214413
$FeSO_4$	x8	0.516835	0.428567	1.20596	0.294286
KCL	x9	0.519413	0.459307	1.130862	0.321323
$NaHPO_4 \cdot 12H_2O$	x10	−0.93466	0.406293	−2.30046	0.082897
$KH_2\ PO_4$	x11	−0.04708	0.412497	−0.11414	0.914629
K_2HPO_4	x12	−0.48765	0.407376	−1.19706	0.297376
Yeast extract (YE)	x13	−0.1281	0.410797	−0.31184	0.770739
Beef extract	x14	0.593642	0.414914	1.43076	0.22574

phosphate, and Tris–HCl, each with a distinct pH concentration. Sodium phosphate and potassium phosphate have a pH range of 5.8–8, while Tris–HCl buffer has a pH range of 6–8.5. Results in Figures 5A–C indicated that the optimum enzyme (crude & purified) activities were 7 with all the detected buffers with enzyme activity ranging from 30 & 27.75, 36 & 29, and 20 & 18.25 U/mL, respectively.

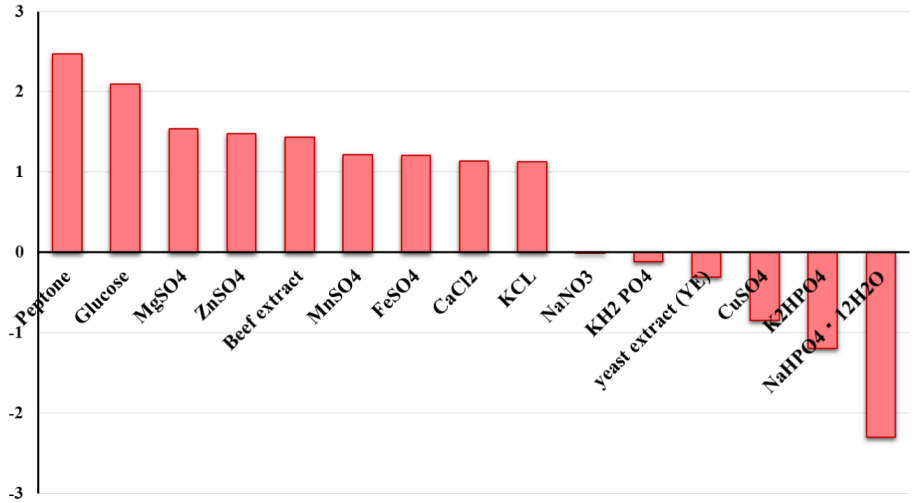

FIGURE 2
The main effect of different variables on *B. licheniformis* ALSZ2 lactase production based on Plackett-Burman design results.

TABLE 3 Box–Behnken design matrix and results for the three most significant variables that affected *B. licheniformis* ALSZ2 lactase production.

Trail	$MgSO_4$ (x1)	Glucose (x2)	Peptone (x3)	Lactase activity (IU)	Predicted IU lactase
1	0	−1	−1	7	6
2	0	+1	−1	6	7
3	0	−1	+1	7.5	7.25
4	0	+1	+1	7.25	7.5
5	−1	−1	0	8	7.75
6	−1	+1	0	8.75	8
7	+1	−1	0	8	8
8	+1	+1	0	9	8
9	−1	0	−1	8	8.75
10	−1	0	+1	7.75	8.75
11	+1	0	−1	9.25	9
12	+1	0	+1	8.75	9.25
13	0	0	0	13	13

3.8. Economic comparison between produced lactase and international products

The need for lactase medical supplements is increasing every day worldwide. The frequency of usage differed significantly between countries. This study provides a promising lactase enzyme product as the initial stage for lactase medical supplements. Comparing AlSZ2 lactase with other products available in the international market, it was found that AlSZ2 lactase is considerably more cost-effective. Many other products are expensive and often unavailable in the Egyptian market. The lactase products' cost (1,000 U) range from 5.5–8 $, due to the high cost of shipping rather than the real price of the lactase product, whereas 1,000 U of AlSZ2 lactase costs 1.2 $. Therefore, this study is of great importance to cheaply provide lactase, which leads to raising the economic value and aiding in the treatment of a prevalent digestive problem.

4. Discussion

The frequency of Middle Easterners who are lactose intolerant was 70%, with 68 percent of Egyptians affected (Silanikove et al., 2015). Therefore, this study seeks to isolate bacteria capable of producing lactase that can be accessed cheaply.

The amount of carbon in the growth media is critical for bacteria to produce extracellular lactase. Lactase biosynthesis is regulated by carbon availability in various bacteria (Konsoula and Liakopoulou-Kyriakides, 2007; Alazzeh et al., 2009; Maischberger et al., 2010; Akcan, 2018). Based on the experimental matrix, a Plackett-Burman

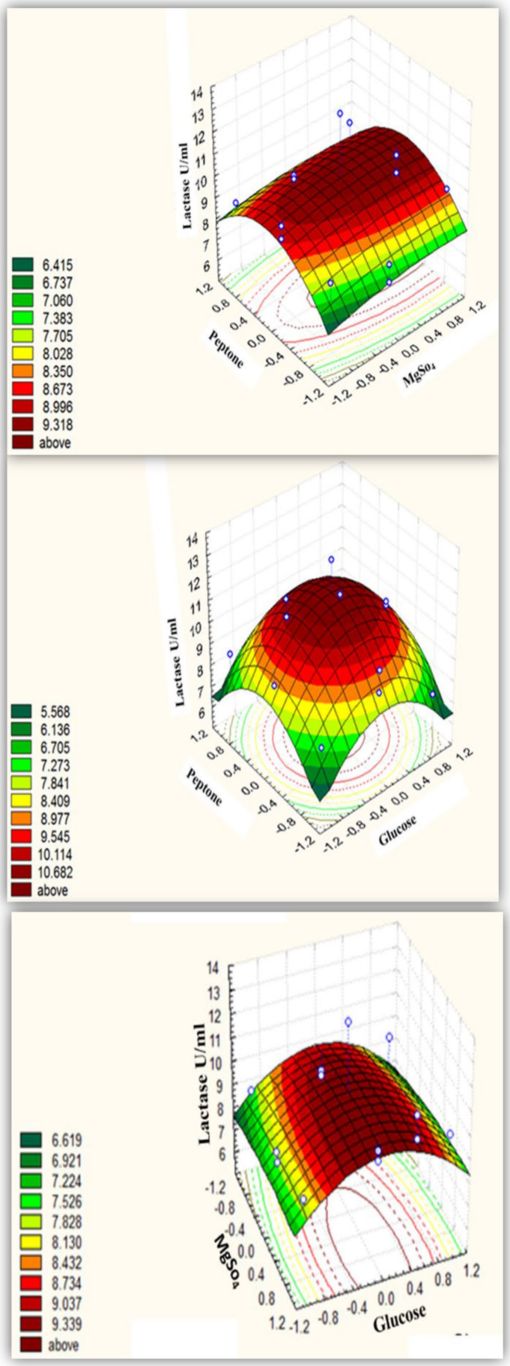

FIGURE 3
Three-dimensional response surface representing *B. licheniformis* ALSZ2 lactase enzyme as affected by culture conditions.

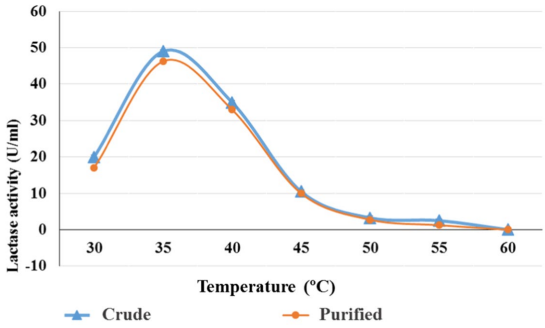

FIGURE 4
Optimum temperature for crude and purified lactase (30–50 kDa) from *B. licheniformis* AlSZ2.

design (Karlapudi et al., 2018; Sorour et al., 2020) was carried out for twenty trials with two concentration levels for fifteen distinct variables (Supplementary Table S1). When using response surface approaches, Plackett and Burman Design is a useful tool for assessing the effects of process factors on yield. It can significantly lower the number of trials that must be repeated in later optimization investigations (Ekpenyong et al., 2017).

In previous research (Manera et al., 2008), lactose was found to be an excellent substrate when used in quantities more than 28.2 g per liter, while Anumukonda and Prabhakar (2010) discovered a 1.5 percent improvement in lactase synthesis in the optimized medium. Another study using solid-state fermentation with *Aspergillus terreus* NFCCI 1840 found that supplementing the cultured medium with 2.97, 2.88, and 2.67 g per liter of ammonium sulfate, lactose, and magnesium sulfate, respectively, increased lactase production by 2.8 times when compared to the standard basal medium (Al-Jazairi et al., 2015).

Ca^{2+} and Mg^{2+} increased enzyme activity in *Pediococcus acidilacti*, *Lactobacillus acidophilus*, and *Bacillus* sp. (Ustok et al., 2010; Carevic et al., 2015; Chanalia et al., 2018). Magnesium is required for the catalytic activity and stability of β -galactosidase. $MgSO_4$ at a concentration of 0.1 percent, Ahmed, et al. (Ahmed et al., 2016) found that *Lactobacillus* sp. KLSA 22 produced the highest amount of β -galactosidase. Nitrogen sources are the most essential secondary energy molecules for bacterial growth and metabolism. The type of these compounds and the amounts used can either promote or prevent the growth of enzymes (Sharma and Singh, 2014). Sources of nitrogen's effect on *L. casei*MB2's ability to synthesize galactosidase is important. Peptone supplementation raised the enzyme activity of *L. casei*MB2 enzyme production medium to 126.24 IU/mL (specific activity of 315.60 IU/mg). Conversely, urea, sodium chloride, sodium nitrate, ammonium nitrate, and beef extract all showed a reduction in enzyme activity (Heena and Nivedita, 2020).

Numerous separation methods, such as membrane-based separation, ion exchange membrane chromatography, gel permeation chromatography, zinc chloride, protamine sulfate, and ammonium sulfate precipitation, have been investigated for the purification of beta-galactosidase from crude extract (Najer et al., 2022). β -Galactosidases with a range of molecular weights have been discovered in plant sources using the Amicon membrane system with a 100 to 30 kDa cut-off (Aulitto et al., 2021). Five enzymes with molecular weights of 87, 87, 87, 73, and 45 kDa have been recognized (Ajay et al., 2013).

The synthesis of enzymes grew continuously with increasing temperatures up to 35°C and then dropped (Ahmed et al., 2016). Natarajan et al. (2012) found that *Bacillus thuringiensis* produced the most enzymes at a temperature of 35°C. 37°C was the optimal degree of heating during fermentation, based on how temperature affects the activity of enzymes for the highest β -galactosidase yield (Husain, 2010; Huang et al., 2021).

At pH 7, the greatest enzyme activity was observed (89.94 IU), which was also a good pH for *Lactobacillus* sp. KLSA 228 growth.

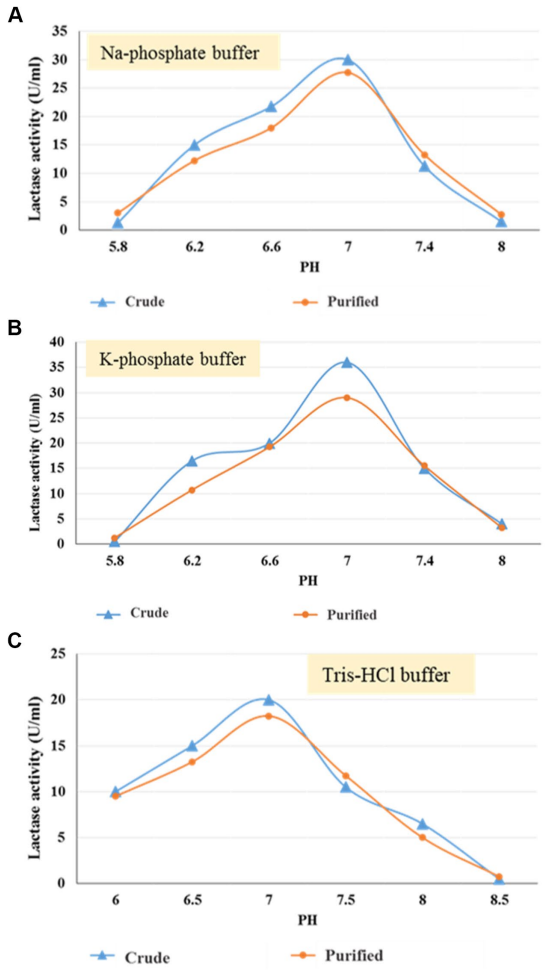

FIGURE 5
Optimum pH using Na-phosphate **(A)**, K-phosphate **(B)**, and Tris–HCl **(C)** buffer for crude and purified (30–50 kDa) lactase from *B. licheniformis* ALSZ2.

However, *L. amylophilus* GV6 was shown to produce the most lactase when grown at pH 6.513. Lactase from *L. delbrueckii* spp. ATCC 11842 was found to have the highest activity when pH was 6.8 (Ahmed et al., 2016; Venkateswarulu et al., 2020). Natarajan et al. (2012), on the other hand, found that lactase synthesis was best at a pH of 7.

5. Conclusion

Exploration of bacterial species with unique lactase capacities is critical. As a result, the current study aimed to isolate the most potent extracellular lactase-producing bacteria from various dairy products in various Alexandria locations, as well as increase lactase productivity by a local isolate *Bacillus* strain ASZ using low-cost materials via a sequential optimization strategy. The findings indicated that the chosen isolate is *B. licheniformis* ALSZ2, which is employed as a lactase-producing model. Through a two-level Plackett–Burman design, peptone, lactose, and $MgSO_4$ were chosen as investigated variables because of their strong positive influence on lactase efficiency. The lactase yield increased with the initial basal medium, allowing a quadratic polynomial model to be developed that links the relationship between all three factors and lactase production. In comparison to the un-optimized medium, the estimated ideal lactase activity was 13 U/mL, which was four times higher. Following that, the purification of experimental bacterial lactase productivity was done. When compared to comparable lactase products on the worldwide market, AlSZ2 lactase is significantly less expensive.

Data availability statement

The data presented in this study are deposited in the NCBI database under accession number OR535141.

Author contributions

SA conceived the study and funded the project. Experimental work, data analysis, and primary publication writing were all done in collaboration with AA, ZO, and SA. All authors contributed to the article and approved the submitted version.

Conflict of interest

The authors declare that the research was conducted in the absence of any commercial or financial relationships that could be construed as a potential conflict of interest.

Publisher's note

All claims expressed in this article are solely those of the authors and do not necessarily represent those of their affiliated organizations, or those of the publisher, the editors and the reviewers. Any product that may be evaluated in this article, or claim that may be made by its manufacturer, is not guaranteed or endorsed by the publisher.

Supplementary material

The Supplementary material for this article can be found online at: https://www.frontiersin.org/articles/10.3389/fmicb.2023.1180463/full#supplementary-material

References

Aggarwal, S., Chakravarty, A., and Ikram, S. (2021). A comprehensive review on ofcredible renewable carriers as promising platforms for enzyme immobilization & thereof strategies. *Int. J. Biol. Macromol.* 167, 962–986. doi: 10.1016/j.ijbiomac.2020.11.052

Ahmed, S., Kattimani, L., Divatar, M., Gajare, S., Shivalee, A., Asma, F., et al. (2016). Optimization of lactase production under submerged fermentation by *Lactobacillus* sp. KLSA 22. *Int. J. Pure App. Biosci* 4, 212–220. doi: 10.18782/2320-7051.2321

Ajay, P., Melita, L., and Farhath, K. (2013). Extraction, purification and thermodynamic characterization of almond (*Amygdalus communis*) β-Galactosidase for the preparation of delactosed milk. *Food Technol. Biotechnol.* 51, 53–61. Available at: https://hrcak.srce.hr/file/146868

Akcan, N. (2018). Cultural conditions optimization for production of β-galactosidase from *Bacillus licheniformis* ATCC 12759 under solid-state fermentation. *Turkish J. Biochem.* 43, 240–247. doi: 10.1515/tjb-2017-0153

Alazzeh, A. Y., Ibrahim, S. A., Song, D., Shahbazi, A., and AbuGhazaleh, A. A. (2009). Carbohydrate and protein sources influence the induction of α-and β-galactosidases in *Lactobacillus reuteri*. *Food Chem.* 117, 654–659. doi: 10.1016/j.foodchem.2009.04.065

Ali, S. M., Omar, S. H., and Soliman, N. A. (2013). Co-production of cellulase and xylanase enzymes by thermophilic *Bacillus subtilis* 276NS. *Int. J. Biotechnol. Wellness Indus.* 2, 65–74. Available at: https://citeseerx.ist.psu.edu/viewdoc/download?doi=10.1.1.985.9502&rep=rep1&type=pdf

Al-Jazairi, M., Abou-Ghorra, S., Bakri, Y., and Mustafa, M. (2015). Optimization of [Beta]-galactosidase production by response surface methodology using locally isolated Kluyveromyces marxianus. *Int. Food Res. J.* 22:1361. Available at: https://www.proquest.com/openview/66eb623a60fb5faadca2f12a4e4e5779/1?pq-origsite=gscholar&cbl=816390

Alkhafaje, W. K., Ali, S. M., and Olama, Z. A. (2019). Isolation and molecular differentiation of MDR bacteria isolated from dairy products. *Pollut. Res.* 38, 959–964. Available at: http://www.envirobiotechjournals.com/article_abstract.php?aid=10075&iid=286&jid=4

Alkhafaje, W. K., Ali, S. M., and Olama, Z. A. (2022). Molecular characterization of virulence factors and microbial resistance of different bacterial isolates in some dairy products. *Iraqi Journal of Veterinary Sciences*. 36, 333–339. doi: 10.33899/ijvs.2021.130206.1764

Amamcharla, J. K., and Metzger, L. E. (2011). Development of a rapid method for the measurement of lactose in milk using a blood glucose biosensor. *J. Dairy Sci.* 94, 4800–4809. doi: 10.3168/jds.2011-4416

Anumukonda, P., and Prabhakar, T. (2010). Optimization of bioprocess parameters for the production of β-galactosidase by employing statistical methods. *Int. J. Pharm. Biosci* 1, 1–9. Available at: http://citeseerx.ist.psu.edu/viewdoc/download?doi=10.1.1.437.7762&rep=rep1&type=pdf

Aulitto, M., Strazzulli, A., Sansone, F., Cozzolino, F., Monti, M., Moracci, M., et al. (2021). Prebiotic properties of *Bacillus coagulans* MA−13: production of galactoside hydrolyzing enzymes and characterization of the transglycosylation properties of a GH42 β-galactosidase. *Microb. Cell Factories* 20, 71–17. doi: 10.1186/s12934-021-01553-y

Aydin, Y., and Coin, I. (2021). Biochemical insights into structure and function of arrestins. *FEBS J.* 288, 2529–2549. doi: 10.1111/febs.15811

Cao, Y., Li, X., and Ge, J. (2021). Enzyme catalyst engineering toward the integration of biocatalysis and chemocatalysis. *Trends Biotechnol.* 39, 1173–1183. doi: 10.1016/j.tibtech.2021.01.002

Carevic, M., Vukasinovic-Sekulic, M., Grbavcic, S., Stojanovic, M., Mihailovic, M., Dimitrijevic, A., et al. (2015). Optimization of β-galactosidase production from lactic acid bacteria. *Hem. Ind* 69, 305–312. doi: 10.2298/HEMIND140303044C

Chanalia, P., Gandhi, D., Attri, P., and Dhanda, S. (2018). Purification and characterization of β-galactosidase from probiotic *Pediococcus acidilactici* and its use in milk lactose hydrolysis and galactooligosaccharide synthesis. *Bioorg. Chem.* 77, 176–189. doi: 10.1016/j.bioorg.2018.01.006

Ekpenyong, M. G., Antai, S. P., Asitok, A. D., and Ekpo, B. O. (2017). Plackett-Burman design and response surface optimization of medium trace nutrients for Glycolipopeptide biosurfactant production. *Iranian Biomed J* 21, 249–260. doi: 10.18869/acadpub.ibj.21.4.249

Hassan, S. W., Abd El Latif, H. H., and Ali, S. M. (2018). Production of cold-active lipase by free and immobilized marine *Bacillus cereus* HSS: application in wastewater treatment. *Front. Microbiol.* 9:2377. doi: 10.3389/fmicb.2018.02377

Heena, C., and Nivedita, S. (2020). Optimization of B-Galactosidase produced by a potential lactic acid Bacteria *Lactobacillus casei* MB2 isolated from traditional dairy product of Himachal Pradesh. *Int. J. Curr. Microbiol. App. Sci.* 9, 2819–2832. doi: 10.20546/ijcmas.2020.906.341

Huang, C., Feng, Y., Patel, G., Xu, X. Q., Qian, J., Liu, Q., et al. (2021). Production, immobilization and characterization of beta-glucosidase for application in cellulose degradation from a novel Aspergillus versicolor. *Int. J. Biol. Macromol.* 177, 437–446. doi: 10.1016/j.ijbiomac.2021.02.154

Husain, Q. (2010). β Galactosidases and their potential applications: a review. *Crit. Rev. Biotechnol.* 30, 41–62. doi: 10.3109/07388550903330497

Jacobson, R. H., Zhang, X. J., DuBose, R. F., and Matthews, B. W. (1994). Three-dimensional structure of β-galactosidase from *E. coli*. *Nature* 369, 761–766. doi: 10.1038/369761a0

Karlapudi, A. P., Krupanidhi, S., Reddy, R., Indira, M. M. D. N. B., and Venkateswarulu, T. C. (2018). Plackett-Burman design for screening of process components and their effects on production of lactase by newly isolated *Bacillus* sp. VUVD101 strain from dairy effluent. *Beni-Suef Univ. J. basic Appl. Sci.* 7, 543–546. doi: 10.1016/j.bjbas.2018.06.006

Kim, M., and Chun, J. (2014). 16S rRNA gene-based identification of bacteria and archaea using the EzTaxon server. *Methods Microbiol.* 41, 61–74. doi: 10.1016/bs.mim.2014.08.001

Kocabaş, D. S., Lyne, J., and Ustunol, Z. (2021). Hydrolytic enzymes in the dairy industry: applications, market and future perspectives. *Trends Food Sci. Technol.* 119, 467–475. doi: 10.1016/j.tifs.2021.12.013

Konsoula, Z., and Liakopoulou-Kyriakides, M. (2007). Co-production of α-amylase and β-galactosidase by *Bacillus subtilis* in complex organic substrates. *Bioresour. Technol.* 98, 150–157. doi: 10.1016/j.biortech.2005.11.001

Liburdi, K., and Marco, E. (2022). Galacto-oligosaccharide (GOS) synthesis during enzymatic lactose-free Milk production: state of the art and emerging opportunities. *Beverages* 8:21. doi: 10.3390/beverages8020021

Maischberger, T., Leitner, E., Nitisinprasert, S., Juajun, O., Yamabhai, M., Nguyen, T. H., et al. (2010). B-Galactosidase from *Lactobacillus pentosus*: purification, characterization and formation of galacto-oligosaccharides. *Biotechnol. J.* 5, 838–847. doi: 10.1002/biot.201000126

Manera, A. P., Ores, J. C., Ribeiro, V. A., Burkert, C. A. V., and Kalil, S. J. (2008). Optimization of the culture medium for the production of β-galactosidase from K. marxianus CCT7082. *Food Technol. Biotechnol.* 46, 66–72. Available at: https://hrcak.srce.hr/22222

Martarello, R. D. A., Cunha, L., Cardoso, S. L., de Freitas, M. M., Silveira, D., Fonseca-Bazzo, Y. M., et al. (2019). Optimization and partial purification of beta-galactosidase production by *Aspergillus Niger* isolated from Brazilian soils using soybean residue. *AMB Express* 9, 81–13. doi: 10.1186/s13568-019-0805-6

Movahedpour, A., Ahmadi, N., Ghalamfarsa, F., Ghesmati, Z., Khalifeh, M., Maleksabet, A., et al. (2022). β-Galactosidase: from its source and applications to its recombinant form. *Biotechnol. Appl. Biochem.* 69, 612–628. doi: 10.1002/bab.2137

Muzaffar, K., Jan, R., Bhat, N. A., Gani, A., and Shagoo, M. A. (2021). Commercially available probiotics and prebiotics used in human and animal nutrition. *Adv. Probiotics*, 417–435. doi: 10.1016/B978-0-12-822909-5.00025-3

Najer, A., Blight, J., Ducker, C. B., Gasbarri, M., Brown, J. C., Che, J., et al. (2022). Potent Virustatic polymer–lipid Nanomimics block viral entry and inhibit malaria parasites in vivo. *ACS Central Sci.* 8, 1238–1257. doi: 10.1021/acscentsci.1c01368

Natarajan, J., Christobell, C., Kumar, D. M., Balakumaran, M. D., Kumar, M. R., and Kalaichelvan, P. T. (2012). Isolation and characterization of b-galactosidase producing *Bacillus* sp. from dairy effluent. *World Appl. Sci. J.* 17, 1466–1474. Available at: https://www.semanticscholar.org/paper/Isolation-and-Characterization-of-%CE%B2-Galactosidase-Natarajan-Kumar/d74ae1ebf26c1ac62d865f5b5db8a500dbc76148

Patel, A. K., Singhania, R. R., and Pandey, A. (2017). Production, purification, and application of microbial enzymes. Biotechnology of microbial enzymes. *Acade. Press* 13–41. doi:10.1016/B978-0-12-803725-6.00002-9Get rights and content

Paulo, A. J. (2018). *Produção, caracterização e purificação parcial de uma nova β-Galactosidade produzida por Cladosporium tenuissimum URM 7803*. Universidade Federal de Pernambuco. Brazil

Peele, K. A., Krupanidhi, S., Reddy, E. R., Indira, M., Bobby, M. N., and Venkateswarulu, T. C. (2018). Plackett-Burman design for screening of process components and their effects on production of lactase by newly isolated *Bacillus* sp. VUVD101 strain from dairy effluent. *Beni-Suef Univer. J. Basic Appl. Sci* 7, 543–546. doi: 10.1016/j.bjbas.2018.06.006

Petassi, M. T., Hsieh, S. C., and Peters, J. E. (2020). Guide RNA categorization enables target site choice in Tn7-CRISPR-Cas transposons. *Cells* 183, 1757–1771.e18. doi: 10.1016/j.cell.2020.11.005

Piumetti, M., and Illanes, A. (2022). Enzymes and their function. *Mol. Dynamics Complex. Catalysis Biocatalysis*, 23–53. doi: 10.1007/978-3-030-88500-7.pdf

Poch, O., L'Hôte, H., Dallery, V., Debeaux, F., Fleer, R., and Sodoyer, R. (1992). Sequence of the Kluyveromyces lactis β-galactosidase: comparison with prokaryotic enzymes and secondary structure analysis. *Gene* 118, 55–63. doi: 10.1016/0378-1119(92)90248-N

Portnoy, M., and Barbano, D. M. (2021). Lactose: use, measurement, and expression of results. *J. Dairy Sci.* 104, 8314–8325. doi: 10.3168/jds.2020-18706

Ramos, O.S., and Malcata, F.X. (2011). Comprehensive biotechnology. Industrial biotechnology and commodity products 20.

Saqib, S., Akram, A., Halim, S. A., and Tassaduq, R. (2017). Sources of β-galactosidase and its applications in food industry. *Biotech* 7, 79–77. doi: 10.1007/s13205-017-0645-5

Sedzro, D. M., Bellah, S. M. F., Akbar, H., and Billah, S. M. S. (2018). Structure, function, application and modification strategy of β–Galactosidase. *J Multidis Res Rev.* 1, 10–16. Available at: https://www.researchgate.net/publication/331276005

Shaaban, M. T., Abdelhamid, R. M., Zayed, M., and Ali, S. M. (2022). Evaluation of a new antimicrobial agent production (RSMM C3) by using metagenomics approaches from Egyptian marine biotech. *Biotechnol. Reports* 34:e00706. doi: 10.1016/j.btre.2022.e00706

Shaima'a, R., and Rashid, I. M. (2017). Use and misuse of antimicrobial agents in healthcare settings of Diyala Province. *Diyala J. Med.* 12, 30–33. Available at: https://djm.uodiyala.edu.iq/index.php/djm/article/view/145

Sharma, S., and Singh, P. (2014). Isolation and characterization of β-Galactosidase enzyme producing microbe and optimization of its enzyme activity under different culture condition. *Int. J. Cur. Micro. Appl. Sci.* 3, 148–155. Available at: https://www.researchgate.net/publication/306092614_Isolation_and_Characterization_of_beta-Galactosidase_Enzyme_Producing_Microbe_and_Optimization_of_its_Enzyme_Activity_under_different_culture_condition

Shrestha, A., Samuelsson, L., Sharma, P., and Day, L. (2021). Cameron-Smith, D., and Milan, A. M. Comparing response of sheep and cow milk on acute digestive comfort and lactose malabsorption: a randomized controlled trial in female dairy avoiders. *Front. Nutr.* 8. doi:10.3389/fnut.2021.603816

Silanikove, N., Leitner, G., and Merin, U. (2015). The interrelationships between lactose intolerance and the modern dairy industry: global perspectives in evolutional and historical backgrounds. *Nutrients* 7, 7312–7331. doi: 10.3390/nu7095340

Soliman, N., Ali, S., and Omar, S. (2018). Statistical optimization for Thermostable Xylanase production by *Geobacillus stearothermophilus* NASA267 and access to sugar production from some agricultural waste. *Res. J. Biotechnol.* 13, 28–37. Available at: https://www.researchgate.net/publication/328870798_Statistical_optimization_for_thermostable_xylanase_production_by_Geobacillus_stearothermophilus_NASA267_and_access_to_sugar_production_from_some_agricultural_waste

Sorour, A. A., Ali, S. M., El-Naggar, M. Y., and Olama, Z. A. (2020). Isolation and optimization of cellulase production by *Aspergillus penicillioides* 12 ASZ using experimental design. *Eco. Env. Cons.* 26, S109–S115. Available at: http://www.envirobiotechjournals.com/EEC/Vol26AugSuppl20/EEC-17.pdf

Swentowsky, K. W. (2021). *Characterization of two meiotic drive kinesins and loci controlling perenniality in Zea* (Doctoral dissertation, University of Georgia) Georgia

Szilagyi, A., Catherine, W., and Mark, G. T. (2019). Lactose intolerance and other related food sensitivities. *Lactose*, 113–153. doi: 10.1016/B978-0-12-811720-0.00003-9

Tamer, T. M., Eweida, B. Y., Omer, A. M., Soliman, H. M., Ali, S. M., Zaatot, A. A., et al. (2021). Removal of oil spills by novel Amphiphilic chitosan-g-Octanal Schiff Base polymer developed by click grafting technique. *J. Saudi Chem. Soc.* 25:101369. doi: 10.1016/j.jscs.2021.101369

Ureta, M. M., Martins, G. N., Figueira, O., Pires, P. F., Castilho, P. C., and Gomez-Zavaglia, A. (2021). Recent advances in β-galactosidase and fructosyltransferase immobilization technology. *Crit. Rev. Food Sci. Nutr.* 61, 2659–2690. doi: 10.1080/10408398.2020.1783639

Ustok, F. I., Tari, C., and Harsa, S. (2010). Biochemical and thermal properties of β-galactosidase enzymes produced by artisanal yoghurt cultures. *Food Chemi.* 119, 1114–1120. doi: 10.1016/j.foodchem.2009.08.022

Venkateswarulu, T. C., Abraham Peele, K., Krupanidhi, S., Prakash Narayana Reddy, K., Indira, M., Ranga Rao, A., et al. (2020). Biochemical and molecular characterization of lactase producing bacterium isolated from dairy effluent. *J. King Saud Univ. Sci.* 32, 1581–1585. doi: 10.1016/j.jksus.2019.12.014

Venkateswarulu, T. C., Vidya Prabhakar, K., Bharath Kumar, R., and Krupanidhi, S. (2017). Optimization of variables for lactase production from isolated *Bacillus subtilis* strainVUVD001 through submerged fermentation. *Curr. Trend. Biotechnol. Pharm* 11, 371–375. Available at: https://agris.fao.org/agris-search/search.do?recordID=US202100049465

Wang, X., Cheng, M. T., Chen, Z. P., Jiang, Y. L., Ge, Y. S., Xia, R., et al. (2021). Structural and biochemical analyses of the tetrameric carboxypeptidase S9Cfn from *Fusobacterium nucleatum*. Acta Crystallographica section D. *Struct. Biol.* 77. doi: 10.1107/S2059798321010810/cb5129sup1.pdf

Xu, X., Zhang, D., Zhou, B., Zhen, X., and Ouyang, S. (2021). Structural and biochemical analyses of the tetrameric cell binding domain of Lys170 from enterococcal phage F170/08. *Eur. Biophys. J.* 50, 721–729. doi: 10.1007/s00249-021-01511-x

frontiers | Frontiers in Microbiology

TYPE Original Research
PUBLISHED 22 January 2024
DOI 10.3389/fmicb.2023.1280405

OPEN ACCESS

EDITED BY
Guneet Kaur,
University of Guelph, Canada

REVIEWED BY
Smith Etareri Evivie,
University of Benin, Nigeria
Rajat Kumar,
Hong Kong Baptist University,
Hong Kong SAR, China

*CORRESPONDENCE
Hamid Reza Samadlouie
✉ hsamadlouie@yahoo.com

RECEIVED 20 August 2023
ACCEPTED 21 December 2023
PUBLISHED 22 January 2024

CITATION
Tajik A, Samadlouie HR, Salek Farrokhi A and Ghasemi A (2024) Optimization of chemical conditions for metabolites production by *Ganoderma lucidum* using response surface methodology and investigation of antimicrobial as well as anticancer activities. *Front. Microbiol.* 14:1280405. doi: 10.3389/fmicb.2023.1280405

Optimization of chemical conditions for metabolites production by *Ganoderma lucidum* using response surface methodology and investigation of antimicrobial as well as anticancer activities

Alireza Tajik[1], Hamid Reza Samadlouie[1]*, Amir Salek Farrokhi[2] and Amir Ghasemi[1]

[1]Department of Food Science and Technology, Faculty of Agriculture, Shahrood University of Technology, Shahrood, Iran, [2]Department of Immunology, Pasteur Institute of Iran, Tehran, Iran

Ganoderma lucidum (*G. lucidum*) is a medicinal mushroom that is known for its ability to produce compounds with physiological effects on human health. This research was undertaken to amplify the production of bioactive components of *G. lucidum* under optimal cultivation conditions, obtained in a submerged state and utilized in solid state fermentation, with the purpose of enhancing antimicrobial and anticancer activities. The results indicated that titanium dioxide (TiO_2 NPs), magnesium oxide nanoparticles (MgO_2 NPs), and B6, along with glucose syrup and CLS syrups, were the most effective for producing GA, while wheat starch and whey protein, along with MgO_2 NPs and B6 vitamin, stimulated polysaccharide production using the One Factor at a Time (OFAT) method. After screening, the response surface method (RSM) statistically indicated that the media containing 42.11 g/L wheat starch with 22 g/L whey protein and 50 g/L glucose syrup with 30 g/L CSL were found to be the best conditions for polysaccharide (21.47% of dry weight biomass) and GA (20.35 mg/g dry weight biomass) production, respectively. The moss of the fruit body of *G. lucidum* produced under optimal GA conditions had the highest diversity in flavonoids and phenolic acids and significant antimicrobial activity against *Escherichia coli* (*E. coli*) and *Bacillus subtilis* (*B. subtilis*). In addition, the IC50 levels of shell and stem of *G. lucidum* were 465.3 and 485.7 μg/mL, respectively, while the moss did not reach 50% inhibition. In the end, the statistical approaches utilized in this research to elevate the levels of bioactive components in the fruiting body of *G. lucidum* produced a promising natural source of antimicrobial and anticancer agents.

KEYWORDS

***Ganoderma lucidum*, optimization, nanoparticles, polysaccharide, ganoderic acid, antimicrobial activity**

Introduction

Medical mushrooms as main producers of bioactive components with impressive effects on health promotion are a major area of interest within the field of biotechnology and pharmacology (Pan et al., 2022). Among various mushroom, *G. lucidum* has received considerable critical attention for its tendency to produce high-value bioactive components such as polysaccharide, many oxygenated triterpenes (especially ganoderic acid) and phenolic components with enormous medicinal properties such as anticancerous, antimicrobial and antitumor activates (Ahmad et al., 2022; Yang et al., 2022). In the past 2 decades, a number of researchers have sought to determine the GA, polysaccharide, and phenolic components as secondary metabolites of *G. lucidum* cultivated under the different formulated deciduous woods (Heleno et al., 2012; Ma et al., 2019; Lin et al., 2022; Liu et al., 2022). Physicochemical conditions of solid state fermentation found to be influencing *G. lucidum* metabolites have been explored in several studies as the formulated medium is so similar to natural habitat (Murugesan et al., 2007). Despite its efficacy, such fermentation method suffers from several major drawbacks: Dependence on the culture medium employed for secondary metabolite production and relatively long time of cultivation to harvest the fruit at the optimum stage of maturity (Fang and Zhong, 2002b). Most importantly, the production of secondary metabolites by *G. lucidum* in solid state fermentation is heavily influenced by the key substrates used in formulated media. As a primary substrate in solid state, starch plays a crucial role in promoting the production of secondary metabolites by *G. lucidum* (Zhou et al., 2012; Berovic and Zhong, 2023). Formulating a solid state media for mushroom cultivation relies heavily on the expertise of cultivators, as no statistical analysis has been conducted on solid state mediums to determine the most effective substrate for promoting *G. lucidum* growth and metabolites. The lack of precise measurements of biomass and metabolites in the solid state fermentation before the fruiting process has hindered the optimization process (Torres-Mancera et al., 2018). Previous research comparing submerge and solid state fermentation has found submerge fermentation is of series advantages over solid state such as the easy control of the physical and chemical conditions of media, the relatively lower spore contamination and cost-effective fermentation method. There is a consensus among biotechnology research scientists that the quality and quantity of macro elements such as carbon, nitrogen, and mineral elements substrates considerably affect the mushroom proliferation and secondary metabolites synthesis in submerge fermentation (Samadlouie et al., 2018). In the same vein, nanoparticles have several properties that are ideally suited to stimulate the rate of microbiological reaction (Gonabadi et al., 2021; Dong et al., 2022). Likewise, vitamins, especially the B group, as cofactor compounds, which are required in very small amounts, play a vital role in microbial growth and metabolite productions (LeBlanc et al., 2013; Miret and Munné-Bosch, 2014). A large and growing body of literature has investigated to identify the appropriate statistical method(s) for optimization of the physico-chemical conditions of medium for metabolite productions. Efficient productivity of polysaccharide and GA can be accomplished via appropriate key substrate selections and subsequently optimization methods (Ma et al., 2013). Among various statistical methods, response surface methodology (RSM) has been worldwide employed to improve the mathematics achievement of optimum conditions for key substrates affecting the responses (Malinowska et al., 2009; Ma et al., 2013). Before the optimization, key substrates with high positive impacts on responses should be detected by screening method like one a factor at a time method (Singh et al., 2011). Notably, studies on the effect of titanium dioxide (TiO_2 NPs), magnesium oxide nanoparticles (MgO_2 NPs), and vitamin B6 on secondary metabolites production in submerge conditions are scare, hence, the study provides recent updates on using these substrates in the formulated media. More importantly, the phenolic components of various parts of *G. lucidum* fruitbody, moss, stem and shell, have not been well-characterized yet. Therefore, the objective of this research was the optimization of *G. lucidum*' polysaccharide and GA production in submerge fermentation, and finally, the optimal condition was applied in solid state and then the GA, total phenol as well as phenolic components profile of the mushroom fruit-body were characterized, following that the antimicrobial and anticancer activates of the extractions of different parts of *G. lucidum* fruit were examined.

Materials and methods

Materials and chemicals

Ganoderma lucidum (Sp. GIRAN17) was obtained from Faculty of Biological Sciences, Shahid Beheshti University, Tehran, Iran. Almost all materials were purchased from Merck Company. Concentrations were obtained under low pressure in a rotary evaporator (Heidolph Laborota 4000 efficient rotary evaporator, Germany). The extracts were dried by vacuum freeze-drying (Christ Alpha 1–2 freeze-dryer). TiO_2 NPs and MgO_2 NPs were attained from United States Research Nanomaterials Inc. with a purity of ±99% and an average size of 15 and 20 nm, respectively.

Microorganisms, inoculums, and cultivation conditions

The strain was grown on potato dextrose agar (PDA), and for long-term preservation, it was maintained at a low temperature at 4°C. 250 mL Erlenmeyer flasks with 50 mL formulated medium was used to provide sufficient oxygen supply for fungi growth and metabolites production. 30 g/L glucose and 10 g/L yeast extract with macro mineral elements was served in 5 day fermentation for inoculum development to obtain maximum cell viability and concentrations. 5 percent of fresh seed culture was added to the fermentation media for growth efficiency and stimulation of secondary metabolite production (Esfandiyari Mehni et al., 2022).

Fermentation media

Various substrates such as carbon (Corn and wheat starch, glucose powder, glucose, and fructose syrup) and protein [Corn Steep Liquor (CSL), Yeast extract, meat peptone, Fat-free soya flour, and Sweet whey powder] as macro elements substrate for evaluation of their effects on the production of polysaccharide and ganoderic acid were utilized. $MgSo_4$. 7 H_20 (1 g/L), $CaCl_2$ (0.2 g/L), KH_2Po_4 (1.5 g/L), and $CaCo_3$ (1.5 g/L), a rotary shaker at 185 RPM and 30°C as constant factors were chosen (Xu et al., 2008). In a pioneering approach to improve the production of secondary metabolites, the effect of TiO_2 NPs and MgO_2 NPs in three

concentrations (0.1, 0.05, and 0.01 g/L) as well as vitamin pyridoxine (B6) in four concentrations (μl) of 100, 200, 1,000, and 3,000 on the growth and formation of secondary metabolites (GA and polysaccharide) of *G. lucidum* in liquid culture medium were investigated.

Analytical methods

Measurement of GA

Dry biomass of *G. lucidum* was used for GA extraction with 70% (v/v) ethanol and determined as previously described (Fang et al., 2002). Briefly, 10 mL of 70% (v/v) ethanol was served to extract GA from 0.1 g mycelium powder. Centrifugal separation was performed to separate the impurities, and then the supernatants were dried at 50°C under rotary evaporation. 5 mL chloroform was added to extract GA from the suspension of residues dissolved in 5 mL of water. After that, chloroform was removed and 5% (w/v) $NaHCO_3$ with pH 3 was mixed with water to extract the desired components. Chloroform was added again to extract GA from the $NaHCO_3$ solution and a relatively pure solution of GA in chloroform was dried using rotary evaporation at 40°C. The obtained precipitate was dissolved in anhydrous ethanol and the GA content was detected by spectrometric method at 245 nm wavelength. Thymol (Merck, 108,167, crystal) and absolute ethanol were used as a standard and blank solution. The concentrations of calibration thymol solutions ranged from 0.1 to 1 mg/mL.

Isolation and purification of polysaccharide

Ganoderma lucidum biomass was centrifuged (12,000 *g*, 5 min) to sediment from the formulated medium, and then distilled water (two times) was used for washing extracted biomass. Dry and crushed biomass was utilized to extract polysaccharides. The biomass was heated three times for 3 h at the boiling temperature of 96% ethanol solution to remove fats, coloring agent, free small molecules, and oligosaccharides. Polysaccharide of dry biomass was extracted thrice with distilled water at 70°C for 3 h. The supernatant was separated and purified by centrifuging at 3,000 rpm. The solution was deproteinated by sevag method (1-butanol: chloroform at a ratio of 1:4, v/v; Staub, 1965). The sevag reagent was removed and a vacuum rotary evaporator (Heidolph Laborota, Germany) was employed to remove 2/3 water phase (supernatant), and then dialyzed against deionized water for 48 h. The concentrated water-soluble polysaccharides were precipitated by using 96% ethanol maintained at 4°C for 24 h. The precipitated polysaccharides were collected by centrifugation, and a vacuum Alpha 1–2 freeze-dryer (Christ, Germany) was used to attain crude *G. lucidum* polysaccharides (CGLP; Samadlouie et al., 2020).

Preparation of *Ganoderma lucidum* solid state medium for fruit production

The optimized medium obtained by statistical methods was served to prepare the solid state medium for fruit production by *G. lucidum*. Beech wood sawdust and chips in equal amount was served as a basic substrate, detoxified by alkaline solution (NaOH) and formulated with glucose and CLS syrup. As these substrates were of a protective impact on spore contamination, naturally presented in Beech wood, a concentration of 50 ppm of NaOCl was used which had a detrimental effect on heat resistant spores (data not shown) and soaked the mixed substrates for 6 h and then sterilized at 121°C for 2.5 h. Seeds were added to a sterilized medium and incubated at appropriate conditions (Stamets, 2011) to harvest *G. lucidum* fruits.

Extraction of *Ganoderma lucidum* dry matter, total phenolic content, and analysis of phenolic compounds

Dried and fine crushed moss, stem and shell of *G. lucidum* were extracted with 90% ethanol (2,000 mL) at 25°C for 72 h. The extracts were centrifuged and then concentrated by a vacuum rotary evaporator (Heidolph Laborota, Germany; Nickavar and Esbati, 2012). The total phenolic contents (TPCs) were measured by Folin–Ciocalteu reagent and gallic acid (GAE) standard. Briefly, GAE standard dissolved in absolute ethanol was mixed with Folin Ciocalteu reagent. After 10 min, sodium carbonate solution (75 mg/mL) was mixed with the standards solution and maintained for 30 min at ambient temperature. UV–Vis spectrophotometer was employed to measure the absorbance of mixed solution at 765 nm. Exactly the same went for dry extracted ethanol solution of *G. lucidum* and the TPC was reported as mg GAE per gram of the ganoderma dry tissue (Nickavar and Esbati, 2012). *Ganoderma lucidum* dry biomass was used to extract phenolic components and phenolic profiles were determined as previously stated (Yahia et al., 2017).

The structure of the phenolic components was examined by an agilent 6410 QqQ, equipped with an Electrospray Ionization interface (ESI), with the following settings: Drying gas temperature (nitrogen): 350°C, drying gas flow rate: 9 L/min, nebulizer pressure: 40 psig, Injection Volume: 25 μL, skimmer: 60 V, fragmentor voltage: 220 V, capillary voltage: 3,500 V, and scan range of m/z: 50–1,000.

Antimicrobial activity of *Ganoderma lucidum*

The antibacterial activity of the extractions of the various parts of *G. lucidum*, shell, stem, and moss, against *E. coli* (ATCC25922) and *B. subtilis* (PTCC1715), was determined by the broth microdilution technique. Briefly, the bacteria were incubated overnight at 37°C in MHB (Mueller Hinton broth). 100 μL of the extractions of the various part of *G. lucidum* at the following concentrations: 62.5, 125, 250, 500, and 1,000 μg/mL, with 100 μL of bacteria were mixed in 96 well microplates, to reach 5×10^5 colony-forming units (CFU)/mL of the examined bacteria. Erythromycin at a concentration of 32 μg/mL was used as positive control and 5×10^5 CFU/mL of examined bacteria was served as growth control. All media was incubated at 37°C for 24 h. 20 μL of 0.5% solution (g/L) 2,3,5-triphenyl-tetrazolium chloride was added to each well after 22 h, following that 2 more hours of incubation was applied to determine microbial growth and MIC. The colorless samples were incubated in Brain Heart Infusion (BHI) agar and the lowest concentration that totally eradicated microbial growth was considered MBC (Valgas et al., 2007).

Cell culture and viability analysis

Breast cancer cell line MDA-MB-231 was purchased from National Cell Bank of Institute Pasteur of Iran. Dulbecco's Modified Eagle Medium (DMEM), supplemented with 1% penicillin/streptomycin and 10% heat-inactivated fetal bovine serum was served to culture MDA-MB-231 cells line at 37°C with 5% CO_2. To achieve high cellular viability, cells were subcultured with trypsin at the near confluency, following that 1 million cells were reseeded into a fresh T-75. MTT assay was served to determine cell viability of MDA-MB-231 and IC50 values (half maximal inhibitory concentration) of stem, shell, and moss of *G. lucidum* against MDA-MB-231. 10,000 cells per well were incubated and exposed to *G. lucidum* extractions for 48 h at 37°C in a 96-well plate. Serial dilutions of *G. lucidum* extractions 0, 62.5, 125, 250, 500, and 1,000 μg/mL were added into each of 96-well plates containing 10,000 cells. Cytotoxic evaluations

of the extractions against MDA-MB-231 cancer cell line were evaluated using MTT assay according to the previous research (Hastings and Kenealey, 2017).

Statistical method

One Factor at a Time method was served to identify the key substrates among the various substrates which exerted high influences on GA and CGLP production, and then the selected substrates were optimized using response surface method. Central composite design (CCD), a common form of response surface methodology (RSM) in statistical package Design-Expert, version 7.0.0, Stat-Ease, Inc. Minneapolis, MN, United States, was applied to design the experiments and statistically optimize the quantity of substrates influencing the responses. The ANOVA was used to verify the significance of the models, substrates, and their interactions on the responses. The least squares method was used to formulate second equation. All the experiments were conducted in triplicates. The means and standard deviations (SD) were obtained by Microsoft Excel (2023) software. The SPSS 16.0 software was used to compare the differences among means at the level of 0.05 by Duncan's multiple range test.

Results and discussion

Effect of carbon sources on biomass growth rate, CGLP, and GA productions

Carbohydrates have been identified as the main contributing factors for the *G. lucidum* growth and polysaccharide production (Hsieh et al., 2005). Simple (glucose powder, glucose syrup, and fructose syrup) and complex (corn and wheat) carbohydrates were served to evaluate their effects on biomass dry weight (BDW), CGLP, and GA productions. The highest biomass dry weight (BDW) was accumulated with glucose syrup (0.86 percentage of medium), while the lowest was accumulated in fructose substrate (0.44 percentage of medium). The results indicated that there was no significant difference between corn and wheat starch. The unit of single simple sugars such as glucose substrate found to be influencing biomass production have been explored in several studies (Xu et al., 2008; Hu et al., 2018). In term of CGLP production, the medium containing wheat starch and fructose syrup had the highest (15.1 percent of DWB) and lowest (3.5 percent of DWB) CGLP, respectively. No significant difference was observed between the three carbon sources of corn starch, glucose powder, and glucose syrup. According to recent studies, the suitability of wheat starch compared to other carbohydrate sources may be a result of the potential for these substrates to be quickly transformed into accumulated polysaccharide (Fan et al., 2007; Maalej et al., 2014). As shown in Figure 1, the highest GA was obtained in the medium containing glucose syrup. Following that, glucose powder showed the highest (12 mg/g DWB) GA. Other carbon sources supported lower GA productions. These results were supported by Wei et al. (2016) who reported that glucose is the preferred carbon source for biomass and total GA production (Wei et al., 2016). wheat starch and glucose syrup turned out at the top in impacting CGLP and GA productions, respectively, which were utilized separately to further study its effect on metabolite productions with using different substrates employed.

Effect of nitrogen source on DWB, CGLP, and GA productions

As the main substrates involved in the structure of microbial biomass and enzyme production, proteins have been successfully used as a vital macronutrient in medium to stimulate microbial growth and metabolic production (Esfandiyari Mehni et al., 2022). Two media with different carbon sources, wheat starch, and glucose syrup, were used to investigate the effects of various nitrogen sources on DWB, CGLP, and GA productions. The analysis showed that the best candidate for achieving the greatest DWB was obtained in the medium that comprised of whey

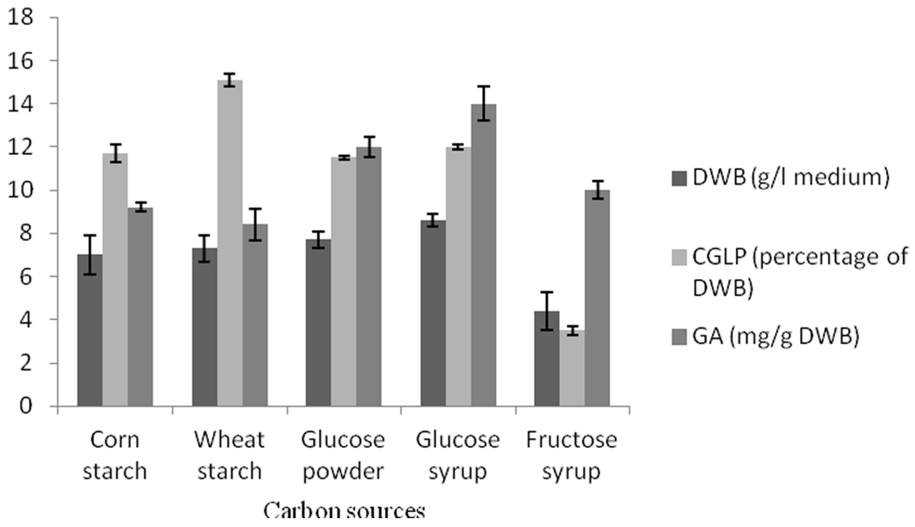

FIGURE 1
The effect of various carbon sources on DWB (percentage of medium), CGLP (percentage of DWB), and GA (mg/g DWB). The results are the mean ± SD of three independent experiments.

powder substrate, succeeding that soybean powder. However, the lowest DWB were accumulated in media containing CSL syrup nitrogen source. No significant differences were observed between meat peptone and yeast extract in biomass production. As whey protein is rich in essential amino acids, lactose and micronutrients (Patel, 2015), it is considered as the best macronutrient substrate for microbial growth. In terms of CGLP production, whey protein was the most potent, with soybean powder substrate coming in second, and CSL syrup substrate producing the least (8.5 percent of DWB) CGLP content in wheat starch medium. Detailed examination of whey protein by Song et al. (2007) and Lee et al. (2003) showed that such a protein source could be a suitable substrate for mycelia and polysaccharide productions (Lee et al., 2003; Song et al., 2007). As shown in Figure 2, culture medium containing yeast extract, meat peptone and CSL stimulated the most (17 mg/g DWB) GA formation. On the other hand, the lowest average GA was found in medium containing whey substrate and glucose syrup medium. Overall, a reasonable amount of GA was produced with CSL syrup, as this protein source is the most cost effective, and was therefore selected for further studies. No previous study has investigated the effect of CSL syrup on GA formation by *G. lucidum*.

Effect of initial pH on biomass growth rate, CGLP, and GA productions

At pH 5, the maximum DWB was obtained under the optimal conditions resulting from the OFAT method. The data show an inverse correlation between the higher initial pH and average DWB in the two formulated media, indicating that *G. lucidum* biomass tends to accumulate in slightly acidic conditions. The amount of CGLP at initial pH between 5 and 6.5 was almost close to each other and thus suitable for CGLP production. Any increase in pH toward a higher level negatively affects the CGLP content (Figure 3). Similarly, Supramani et al. (2019) showed that lowering the initial pH from 6 to

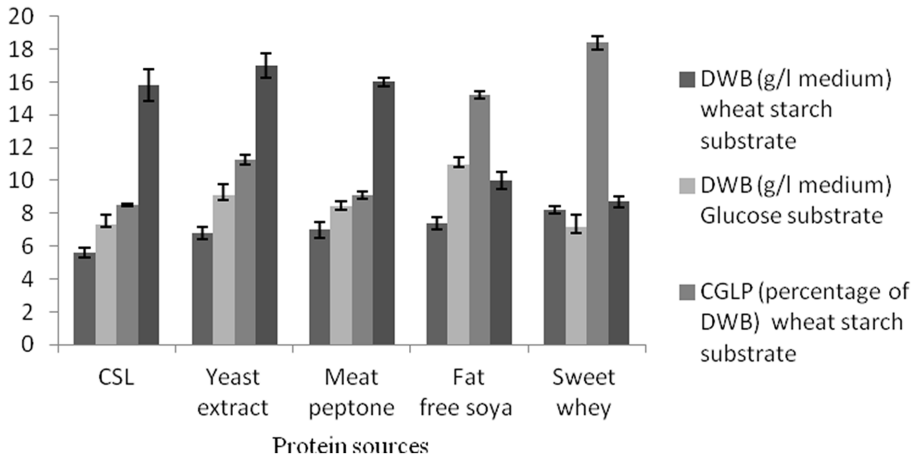

FIGURE 2
The effect of various protein sources on DWB (percentage of medium), CGLP (percentage of DWB), and GA (mg/g DWB).

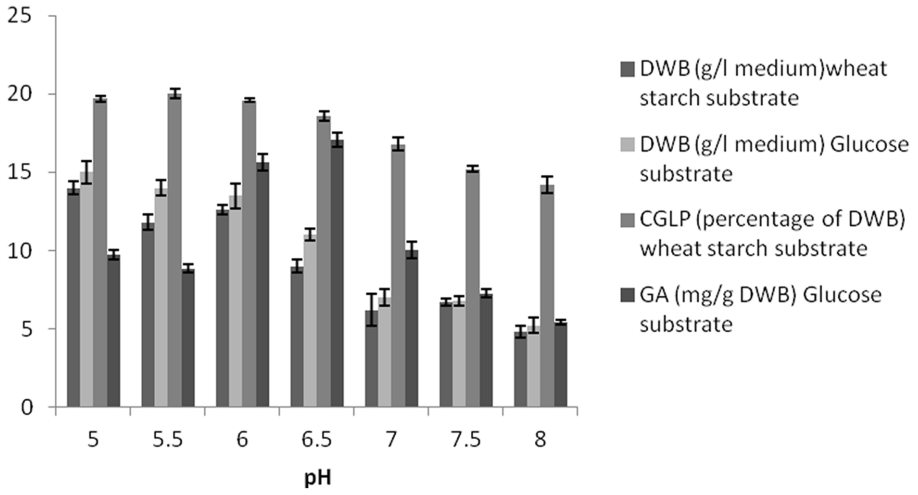

FIGURE 3
The effect of pH on DWB (percentage of medium), CGLP (percentage of DWB), and GA (mg/g DWB).

4 stimulated biomass and CGLP production. In term of GA production, medium with initial pH 6.5 and 8 had the highest (17.06 mg/g DWB) and lowest (5.41 mg/g DWB) GA, respectively. This view was supported by Fang and Zhong (2002a) who stated that maximum GA production was achieved at an initial pH of 6.5.

Effect of TiO_2 NPs on DWB, CGLP, and GA productions

Titanium dioxide nanoparticles negatively impacted biomass production. There was a strong negative correlation between the concentration of titanium dioxide nanoparticles and DWB. In the last 2 decades, a number of researchers have demonstrated the antimicrobial activity of titanium dioxide nanoparticles (Mesgari et al., 2021). As far as CGLP production was concerned, the control sample showed the highest internal CGLP formation (16 percent of DWB). TiO_2 NPs had a negative effect on the formation of CGLP. As shown in Figure 4, the culture supplemented with 0.05 g/L titanium dioxide had the highest GA content (18.2 mg/g DWB). It can be concluded that the antimicrobial activity of TiO_2 NPs (de Dicastillo et al., 2020) stimulated GA production. The stimulatory effect of TiO_2 NPs on the GA production as a secondary metabolite could be strongly attributed to the chemical defense of cells already exposed to harmful components like nanoparticles. In the same vein, Gu et al. (2018) in their review article reported that the biosynthesis of GA in *G. lucidum* was triggered by stressors (Gu et al., 2018), so 0.05 g/L titanium dioxide was used in the experiment to optimize the carbon to nitrogen level for GA production.

The effect of MgO_2 NPs on DWB, CGLP, and GA productions

As shown in Figure 5, MgO_2 NPs had positive impacts on DWB in all concentrations compared to the control sample. Importantly, maximum CGLP was produced with 0.01 g/L nanoparticles of magnesium oxide, followed by 0.05 g/L of MgO_2 NPs. The amount of CGLP in the control sample was higher than that of the medium containing 0.1 g/L MgO_2 NPs. In general, the highest concentration of MgO_2 NPs adversely affected the formation of CGLP. Therefore, in the experiment to optimize the ratio of carbon to nitrogen to produce the maximum internal CGLP of biomass, a concentration of 0.01 g/L of MgO_2 NPs was considered for further studies. As shown in Figure 5, 0.05 g/L MgO_2 NPs was the best concentration of nanoparticles to stimulate GA (18.6 mg/g DWB). No significant difference was observed between the medium containing 0.1 g/L magnesium oxide nanoparticles and the control sample. Various factors have influenced the toxicity of nanoparticles on microorganisms, including the characteristics of nanoparticles, species of microorganisms, physicochemical conditions of the media and its concentration (Pareek et al., 2018). Therefore, in the experiment of optimizing the carbon to nitrogen ratio to produce the maximum GA of biomass, a concentration of 0.05 g/L of MgO_2 NPs was utilized.

Effect of vitamin pyridoxine on DWB, CGLP, and GA productions

There is a growing trend toward the use of micronutrients such as vitamins, which have significant effects on the effectiveness and efficiency of fermentation success. Pyridoxine exerts a considerable influence on carbon utilization and therefore promotes microbial growth and metabolites (Du Preez et al., 1985). Several studies were demonstrated that pyridoxin stimulated growth and secondary metabolites (Yang et al., 2008; Tripathi et al., 2012), however what is not yet clear is the impact of pyridoxine present and its concentration in the media on the growth and metabolites of *G. lucidum*. Based on this, pyridoxine at different concentrations was utilized to investigate its effect on microbial growth and secondary metabolites. A substantial increase in DWB (19.1 g/L in glucose syrup medium and 17.5 g/L in

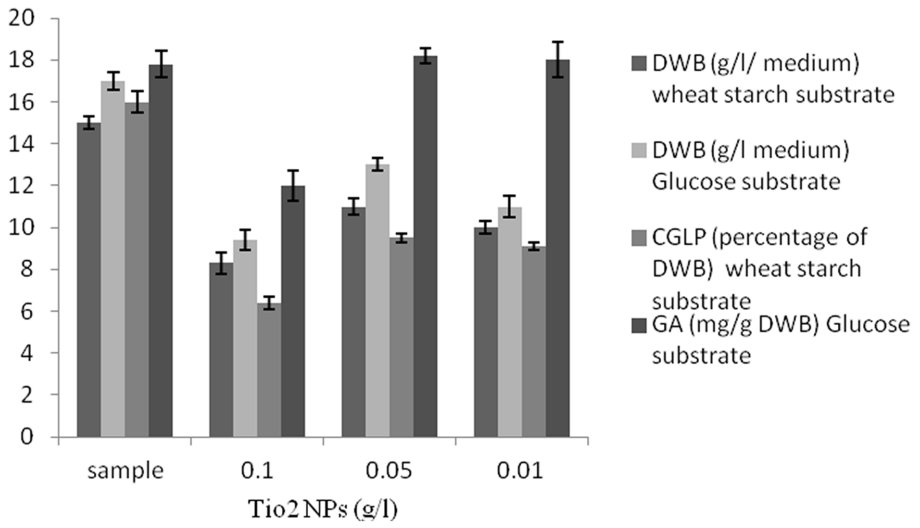

FIGURE 4
The effect of various concentrations of TiO_2 NPs (g/L) on DWB (percentage of medium), CGLP (percentage of DWB), and GA (mg/g DWB).

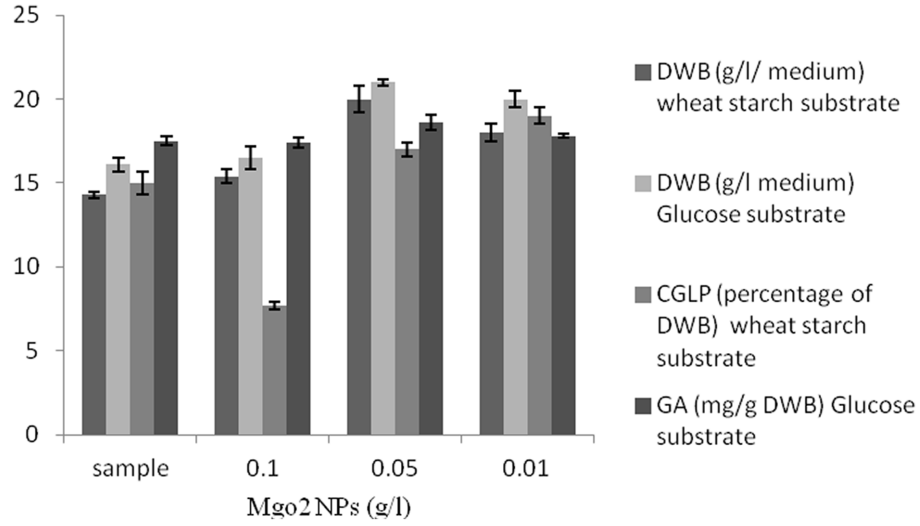

FIGURE 5
The effect of various concentration of magnesium oxide nanoparticles (g/L) on DWB (percentage of medium), CGLP (percentage of DWB), and GA (mg/g DWB).

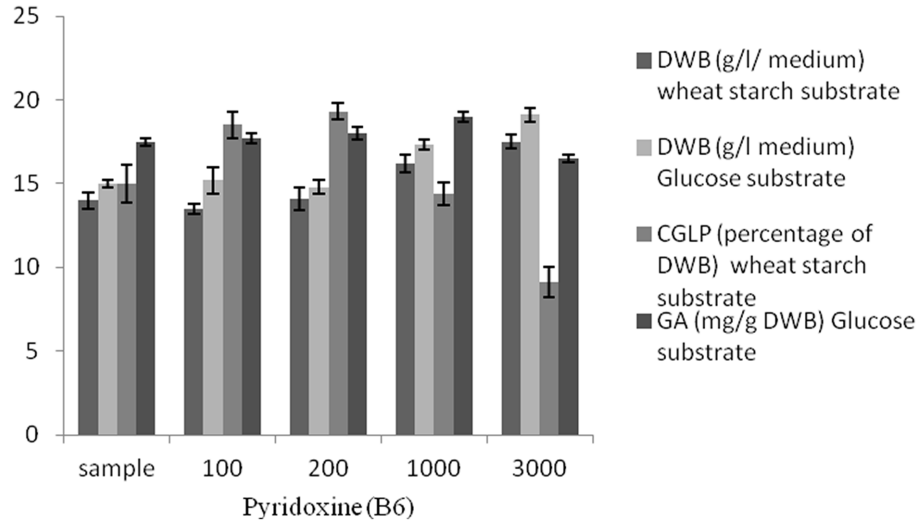

FIGURE 6
The effect of various concentration of pyridoxine (B6) μL on DWB (percentage of medium), CGLP (percentage of DWB), and GA (mg/g DWB).

wheat starch medium) was observed at the maximum concentration of pyridoxine (3,000 μL). Maximum CGLP (19%) was attained at 200 μL pyridoxine. However, a further increase in pyridoxine concentrations was detrimental to CGLP production. As shown in Figure 6, 1,000 μL vitamin pyridoxine provoked the highest GA formation (19 mg/g DWB), while 3,000 μL vitamin pyridoxine resulted in the lowest GA content (16.5 mg/g DWB). In general, there was a positive correlation between vitamin pyridoxine concentration up to 1,000 μL and GA production, while a further increase in pyridoxine concentration up to 3,000 μL caused the formation of GA to decrease its lowest content. Therefore, vitamin pyridoxine with a concentration of 1,000 μL was considered in optimizing the carbon-nitrogen ratio to produce maximum GA content.

Optimization of CGLP production using RSM

The main aim of this investigation was to optimize the amount of CGLP in DWB of *G. lucidum* in submerge fermentation. A wide range of amounts of wheat starch and whey powder, identified as key substrates by OFAT method, were optimized by CCD. OFAT indicated that pH 6.5, 0.05 g/L magnesium oxide nanoparticles and 200 μL of pyridoxine were suitable for CGLP production, selected as constant factors. The results of ANOVA showed that the linear, interaction and quadratic effects of whey powder (A) and wheat starch (B) on the amount of CGLP in liquid culture medium were significant ($p < 0.05$). As shown in Table 1, the *F* value of wheat starch was higher than that

10.3389/fmicb.2023.1280405

TABLE 1 ANOVA for polysaccharide surface quadratic.

Source	Sum of squares	df	Mean square	*F* value	*p* value Prob > *F*
Model	40.26071	5	8.052143	17.2859	0.0082
A-whey	7.065748	1	7.065748	15.16836	0.0176
B-wheat	12.09222	1	12.09222	25.95891	0.0070
AB	0.7225	1	0.7225	1.551024	0.2810
A^2	17.49446	1	17.49446	37.55616	0.0036
B^2	11.07161	1	11.07161	23.76792	0.0082
Residual	1.863286	4	0.465821		
Lack of Fit	1.618286	3	0.539429	2.201749	0.4514
Pure Error	0.245	1	0.245		
Cor Total	42.124	9			

TABLE 2 Results of CCD using two variables demonstrating observed polysaccharide.

Sample	Wheat starch g/L	Whey g/L	Actual polysaccharide percentage of DWB	Predicted polysaccharide
1	20	37.5	21.5	21.1
2	34.14214	37.5	18.3	18.5
3	5.857864	37.5	15.6	15.9
4	10	25	15	15
5	10	50	19	19.7
6	30	50	20	19.4
7	20	19.82233	16.5	16.3
8	20	37.5	20.8	21.1
9	20	55.17767	19	18.3
10	30	25	17.7	17.7

of whey powder. Wheat starch was found to be quantitatively superior to whey powder in the formation of CGLP.

ANOVA was employed to determine a second order polynomial equation. The fitted second order polynomial equation of CGLP production at different concentrations of wheat starch and whey powder has demonstrated as Y is CGLP production, A and B are wheat starch and whey powder, respectively.

$$Y = -8.79917 + 1.00398 \times B + 0.91336 \times A - 3.40000E - 003 \times A \times B - 0.019563 \times B^2 - 9.96000E - 003 \times A^2$$

The numerical value of the coefficient of determination (R^2) for the CGLP production formula with non-significant lack of fit values ($p > 0.05$) was 0.9558; which indicates the degree of compliance of the data in the regression model (Table 1). From the numerical value of the coefficient of determination, it can be concluded that the regression models have been able to show and predict the relationship between the culture conditions (wheat starch and whey powder) and the formation of intracellular CGLP of the fungal biomass in the liquid culture medium. Hereupon, as the amount of wheat starch was increased from 25 g/L to 50, while keeping the nitrogen source of whey powder at a low concentration of 10 g/L, the quantity of CGLP climbed steeply from 15 to the highest value of 19 percentage of DWB (samples 4 and 5). On the other hand, when the quantity of whey powder was kept constant at the highest value of 30 g/L and the quantity of wheat starch was climbed up to the same quantity, the amount of CGLP formation started increasing at a lower rate from 17.7 up to 20 percent of DWB (sample 6 and 10). Such results indicated the adverse impact of high quantity of protein sources on increasing the rate of CGLP production (Table 2). Previous research has indicated that the higher content of nitrogen source has a negative impact on polysaccharide production (Hsieh et al., 2005).

Moreover, the result showed that keeping whey powder constant at an average concentration of 20 g/L, when wheat starch climbed from 19.82 g/L up to 37.5, the formation of CGLP raised with an increase rate from 16.3 up to 21.1 percentage of DWB (sample 7 and 1) (Table 2).

Similarly, Hsieh et al. (2006) found that low nitrogen level stimulated polysaccharide production. The maximum rate of CGLP was reached when the quantity of wheat starch was headed toward 37.5 g/L, after which production started to irreversible decline at higher concentrations. This result was supported by Hsieh et al. (2006)

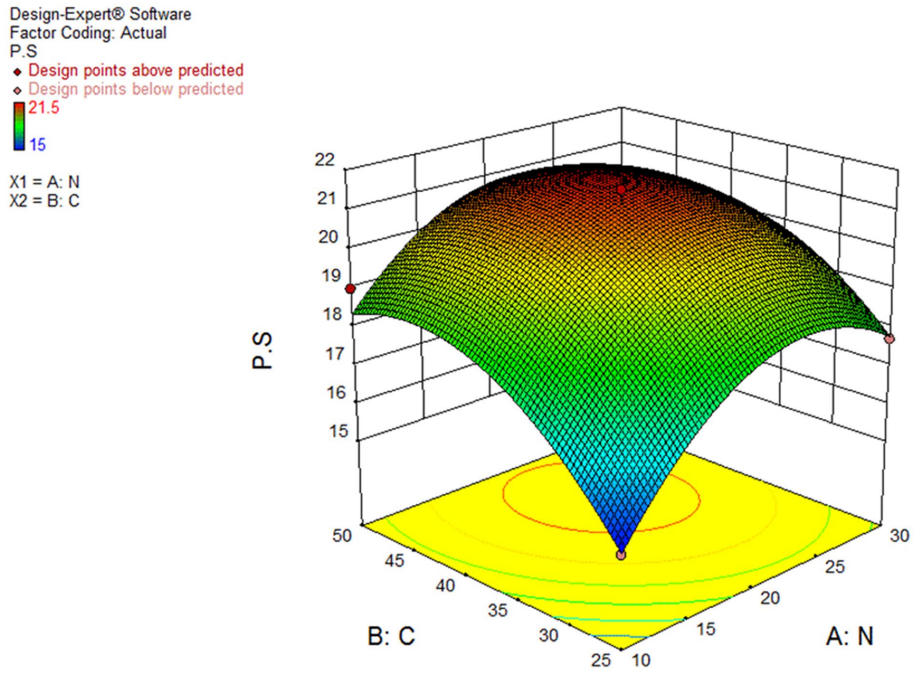

FIGURE 7
Curve of RSM for polysaccharide (PS) production by *Ganoderma lucidum* using wheat starch (C) and whey powder (N) as variable factors. PS (percentage of media), C and N (G/L).

TABLE 3 ANOVA for linear model.

Source	Sum of squares	df	Mean square	*F* value	*p* value	
Model	19.56	2	9.78	31.00	0.0003	Significant
A-G.S	11.09	1	11.09	35.17	0.0006	
B-CSL	8.47	1	8.47	26.84	0.0013	
Residual	2.21	7	0.3154			
Lack of fit	2.20	6	0.3671	73.42	0.0891	Not significant
Pure error	0.0050	1	0.0050			
Cor. total	21.76	9				

and Supramani et al. (2019) who stated that higher concentration of carbon and nitrogen source were of a negative impacts on CGLP production by *G. lucidum*.

CGLP production

Figure 7 demonstrated the effect of different levels of wheat starch and whey powder on CGLP production. As the response surface curve shows, the content of CGLP in DWB was stimulated by increasing the concentration up to middle content of both substrates in the liquid culture medium. The highest of CGLP content was obtained (21.47 percent of DWB) in medium containing (g/L) 42.11 wheat starch and 22 whey. The predicted value was implemented and the actual CGLP content of 22.5 percentage of DWB was achieved, significantly close to the result obtained by the RSM model. The lowest amount of CGLP, 15.04 (percentage of DWB), was observed in the medium containing 25 g/L of wheat starch and 10 g/L of whey protein.

Optimization of GA production using RSM

A range of two key substrates were applied: glucose syrup as a carbon source and CSL syrup as a nitrogen source based on the results of OFAT. Then, the amount of these two substrates was optimized by RSM method. pH 6.5, 1,000 µL of vitamin pyridoxine, 0.05 g/L TiO_2 and MgO_2 NPs were suitable for GA production so these factors were selected as constant factors.

ANOVA was employed to indicate a second order polynomial equation (Table 3). The fitted second-order polynomial equation of GA accumulation over glucose syrup and CSL syrup was demonstrated as where Y was GA production and A and B were glucose syrup and CSL syrup, respectively.

$$Y = +125.56230 + 0.94196 \times A + 1.02872 \times B$$

The coefficients of the linear polynomial model were obtained after analysis with the software and eliminating nonsense terms using the Forward method in the software.

The numerical value of the determination coefficient (R^2) for the formula of GA production is 0.89; which indicates the degree of compliance of the data in the regression model. From the numerical value of the coefficient of determination, it can be concluded that regression models have been able to show and predict the relationship between culture conditions (glucose syrup and CSL syrup) and GA accumulation.

As shown in Table 4, GA content was stimulated by keeping the nitrogen source of CSL syrup constant and increasing the glucose syrup concentration (samples 1 and 2). The same result was obtained when glucose syrup concentration was kept constant and CSL syrup was slightly increased (samples 1 and 6). Higher concentrations of glucose syrup and CSL syrup had the greatest effect on GA formation. It was found that quality and quantity of carbon, especially simple carbohydrate and nitrogen sources, effectively stimulated GA production (Xu et al., 2008; Hu et al., 2017).

GA production

Figure 8 showed the effect of different levels of glucose syrup (B) and CSL syrup (A) on GA production. As the response surface curve showed, GA content in DWB was stimulated by increasing the concentration of both sources in the liquid culture medium. The highest GA content (20.35 mg/g DWB) was obtained in the medium containing 50 g/L glucose syrups and 30 g/L CSL syrups (Fang and Zhong, 2002b) supported the hypothesis that simple carbohydrate such as glucose at 50 g/L induced GA production. While the lowest content of GA, 16.08 mg/g DWB, was observed in the medium containing 25.92 g/L glucose syrup and 10.51 g/L CSL syrup. The predicted amount of selected substrates was run with the aim of producing maximum GA content, and the actual GA content was equal to 20 mg/g DWB, significantly close to the result obtained by the RSM model. Response surface methodology has been widespreadly used to optimize key substrates for the growth and

TABLE 4 Results of CCD using two variables demonstrating observed GA.

Sample	Glucose syrup (g/L)	CSL (g/L)	GA (mg/g DWB)
1	50	10	18.9
2	25	10	16.2
3	37.5	20	17.9
4	37.5	20	18
5	37.5	34.14214	19.6
6	50	30	21
7	25	30	17.4
8	19.82233	20	17
9	37.5	5.857864	16.1
10	55.17767	20	19.2

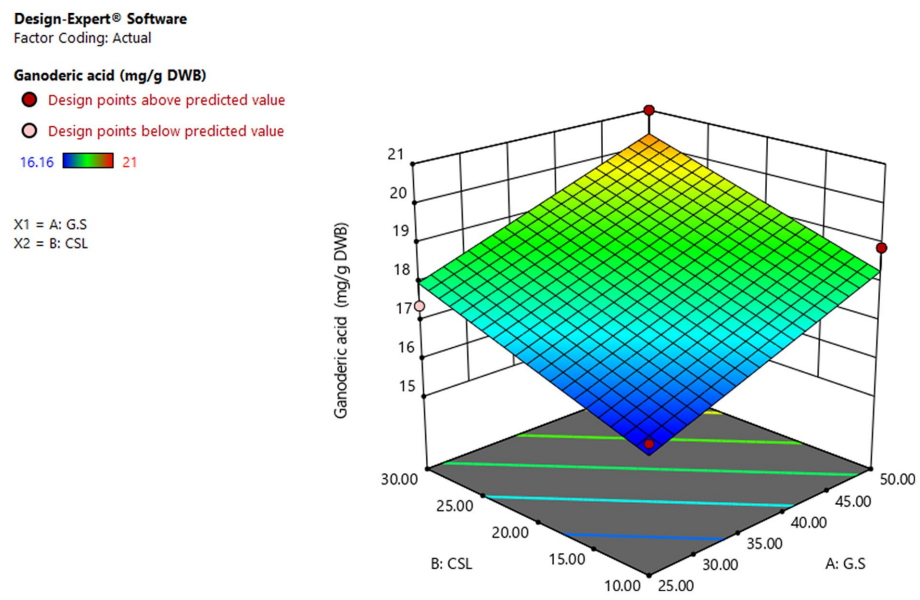

FIGURE 8
Curve of RSM for GA production by *Ganoderma lucidum* using glucose syrup (A) and CSL syrup (N) as variable factors.GA (μg/g DWB), C and N (g/L).

metabolites production of fungi, but no research on glucose syrup and CLS syrup have been used to optimize GA production with such a statistical method. The lower production of GA in submerge fermentation compared to solid state fermentation (Tang and Zhong, 2002) was the main reason for applying optimal condition in solid state fermentation with basic media of Beech wood sawdust and chips.

Solid state formulation toward *Ganoderma lucidum* fruiting

Optimum GA production condition was used to prepare solid state medium. Beech wood sawdust and chips in equal amount as basic medium was enriched with glucose and CLS syrup. Nutrient components added to wood chips had protective effects on heat-resistant spores, so in initial test, the formulated media were invaded by heat-resistant spores, despite the fact that the formulated medium was sterilized at 120°c for 2.5 h. To solve the problem of contamination and reduce the resistance of resistant spores before the sterilization process, all substrates were soaked in 50 ppm NaOCl for 6 h. Optimal condition for fruit production by *G. lucidum* was prepared based on book of Stamets (2011), and after 2 months all fruits were harvested (Figure 9). The optimal condition applied led to the production of maximum GA, 32.64 ± 0.5 mg/g.

The results indicated that solid state fermentation led to a significant increase in GA production compared to submerge fermentation (more than 63%: from 20 to 32.64 mg/g DWB). Dry matter, total phenolic component, and phenolic profiles of the moss, shell, and stem of the *G. lucidum* fruiting body were investigated. The results showed that solid state fermentation led to a significant increase in GA production compared to submerged fermentation (more than 63%: from 20 to 32.64 mg/g DWB). Dry matter, total phenolic components, and phenolic profiles of moss, shell, and stem of *G. lucidum* fruiting body were investigated.

FIGURE 9
Fruiting body of *Ganoderma lucidum* cultivated under optimal condition predicted by RSM.

Total phenolic content and phenolic profiles

The dry matters of *G. lucidum* tissue extracted with 90% ethanol were between 6 and 11%, most of which was in shell (11%), followed by stems (10%) and then moss (6%), respectively. To measure the amount of phenolic components, the dried matters of *G. lucidum* tissue were dissolved in ethanol and brought to a concentration of 400 μg/mL. At this concentrations, 8.84 μg/mL total phenol was obtained in moss, 29.98 in shell and 30.26 in mushroom stems.

So that 2.21% of meat, 7.49% of skin, and 7.56% of mushroom stems were made up of phenolic compounds. These results indicated that the highest amount of phenolic compounds was obtained in the stem and the lowest amount was obtained in the fungal moss. Several attempts have been made to measure the content of *G. lucidum* phenolic compounds and its anioxidant activates. In these studies, conducted to determine the phenolic compounds of *G. lucidum*, it was discovered to be between 3.3 and 7.14/100 g GAE (Yuen and Gohel, 2005; Ferreira et al., 2009; Veljović et al., 2017).

What is not yet clear is the impact of various part of *G. lucidum* on phenolic content and their phenolic profiles. The ethanol extracts of *G. lucidum* phenolic profiles were determined by an Agilent 6410 QqQ, equipped with an Electrospray Ionization interface (ESI) and the results were showed in Table 5. The moss of *G. lucidum* fruit had the highest diversity variation in phenolic components, namely 16 phenolic compounds from the list of phenolic compounds, followed by 11 phenolic compounds in the skin and nine phenolic compounds in the stem. Previous studies have reported that phenolic acids (gallic acid and trans-cinnamic acid) and flavonoids (quercetin, kaempferol, hesperetin, and naringenin) were the major phenolic compounds identified in Ganoderma by Veljović et al. (2017). The present results showed that the moss, skin, and stem of *G. lucidum* fruit contained nine flavonoids and seven phenolic acids, seven flavonoids and three phenolic acids and five flavonoids and four phenolic acids, respectively. In the last 2 decades, a number of researchers have sought to determine the profile of phenolic acids and flavonoids of *G. lucidum* fruit (Karaman et al., 2010; Heleno et al., 2012; Saltarelli et al., 2015; Dong et al., 2019), However researchers have not addressed the phenolic acids profiles in various parts of *G. lucidum* fruit in much detail. Naringin and Myricetin and 3,4-Dihydroxybenzaldehyde were observed only in the shell of *G. lucidum* fruit. Protocatechuic acid, on the other hand, was the only phenolic acid found in the stem. Gallic acid, Kaempferol, Isoramnethin, Homogentisic acid, p-Coumaric acid, o-Coumaric acid, Quercetin, and Coumaric acid were specifically found in the fruit moss of *G. lucidum* (Table 5).

Antibacterial activates of ethanol extraction of *Ganoderma lucidum* shell, stem and moss against *Esherichia coli* (ATCC 25922) and *Bacillus subtilis* (PTCC 1715)

Antimicrobial potentiality of *G. lucidum* fruit body has long been of great interest in a wide range of biotechnology fields. In this research, six initial concentrations (μg/mL), 10,000, 5,000, 2,500, 1,250, 625, and 312 of *G. lucidum* shell, stem and moss were

10.3389/fmicb.2023.1280405

TABLE 5 Phenolic acids and flavonoids extracted from moss, shell and stem of *Ganoderma lucidum*.

Phenolic compounds	Polyphenol classes	Moss	Shell	Stem
1 Malic acid	Phenolic acids	+	+	+
2 Protocatechuic acid	Phenolic acids	–	–	+
3 Gallic acid	Phenolic acids	+	–	–
4 Kaempferol	Flavonoids	+	–	–
5 Isorhamnetin	Flavonoids	+	–	–
6 Sinapic acid	Phenolic acids	–	–	–
7 Pyrogallol	Other polyphenols	–	–	–
8 Homogentisic acid	Phenolic acids	+	–	–
9 5-Sulfosalicylic acid	Phenolic acids	–	–	–
10 Gentisic acid	Phenolic acids	–	–	–
11 p-Hydroxybenzoic acid	Phenolic acids	–	–	–
12 Catechin	Flavonoids	+	+	+
13 Chlorogenic acid	Phenolic acids	+	+	+
14 Vanillic acid	Phenolic acids	–	–	–
15 Caffeic acid	Phenolic acids	–	–	–
16 Syringic acid	Phenolic acids	–	–	–
17 Vanillin	Other polyphenols	–	–	–
18 Cinnamic acid	Phenolic acids	–	–	–
19 p-Coumaric acid	Phenolic acids	+	–	–
20 Ferulic acid	Phenolic acids	–	+	+
21 Veratric acid	Phenolic acids	–	–	–
22 Rutin	Flavonoids	+	+	+
23 Salicylic acid (2-Hydroxybenzoic acid)	Phenolic acids	–	–	–
24 Benzoic acid	Phenolic acids	–	–	–
25 Naringin	Flavonoids	–	+	–
26 o-Coumaric acid	Phenolic acids	+	–	–
27 Myricetin	Flavonoids	–	+	–
28 Resveratrol	Stilbenes	–	–	–
29 Quercetin	Flavonoids	+	–	–
30 Naringenin	Flavonoids	+	–	+
31 Hesperetin	Flavonoids	+	–	–
32 Formononetin	Flavonoids	–	+	+
33 Biochanin A	Flavonoids	+	+	–
34 Epicatechin	Flavonoids	+	+	+
35 Syringaldehyde	Other polyphenols	–	–	–
36 2,3,4-Trihydroxybenzoic acid	Phenolic acids	–	–	–
37 3,4-Dihydroxybenzoic aldehyde (Protocatechuic aldehyde)	Other polyphenols	–	+	–
38 m-Coumaric acid	Phenolic acids	+	–	–
39 Quercetin 3-D-galactoside	Flavonoids	–	–	–
40 Abscisic acid	hormone	+	+	+

utilized to evaluate their antibacterial activity against *E. coli* and *B. subtilis* by McFarland standards. According to the results of Table 6, the MBC of shell, stem, and moss was 625, 625, and 312 μg/mL, respectively, which eradicated the entire population of *E. coli* after 48 h. At the concentration of 375 μg/mL shell, 500 μg/mL stem, and 250 μg/mL moss, only two colonies were observed,

10.3389/fmicb.2023.1280405

TABLE 6 The effect of various concentrations of stem, shell and moss of *Ganoderma lucidum* against *Esherichia coli* (ATCC25922), and *Bacillus subtilis* (PTCC1715).

							Erythromycin concentration
Concentration µg/mL shell	10,000	5,000	2,500	1,250	625	312	32 µg/mL
E. coli	–	–	–	–	–	+	–
B. subtilis	–	–	+	+	+	+	–
Concentration µg/mL stem	10,000	5,000	2,500	1,250	625	312	32 µg/mL
E. coli	–	–	–	–	–	+	–
B. subtilis	–	–	+	+	+	+	–
Concentration µg/mL moss	10,000	5,000	2,500	1,250	625	312	32 µg/mL
E. coli	–	–	–	–	–	–	–
B. subtilis	–	–	+	+	+	+	–
Concentration µg/mL shell	8,000	4,000	2,000	1,000	500	250	32 µg/mL
E. coli	–	–	–	–	+	+	–
B. subtilis	–	–	+	+	+	+	–
Concentration µg/mL stem	8,000	4,000	2,000	1,000	500	250	32 µg/mL
E. coli	–	–	–	–	+	+	–
B. subtilis	_	–	+	+	+	+	–
Concentration µg/mL moss	8,000	4,000	2,000	1,000	500	250	32 µg/mL
E. coli	–	–	–	–	–	+	–
B. subtilis	–	–	+	+	+	+	–
Concentration µg/mL shell	6,000	3,000	1,500	750	375	182	32 mL/ µg
E. coli	–	–	–	–	+	+	–
B. subtilis	–	+	+	+	+	+	–
Concentration µg/mL stem	6,000	3,000	1,500	750	375	182	32 µg/mL
E. coli	–	–	–	–	+	+	–
B. subtilis	_	+	+	+	+	+	–
Concentration µg/mL moss	6,000	3,000	1,500	750	375	182	32 µg/mL
E. coli	–	–	–	–	–	+	–
B. subtilis	_	–	+	+	+	+	–

and these concentrations were considered as MIC, respectively. As far as *B. subtilis* was concerned, the phenolic extract at a concentration of 4,000 µg/mL shell, 4,000 µg/mL stem, and 3,000 µg/mL moss was able to kill the entire population of *B. subtilis*, even after 48 h no colony was observed. Only two colonies were observed at concentration of 3,000 µg/mL shell, 3,000 µg/mL stem, and 2,500 µg/mL moss, which were considered as MBC and MIC, respectively, (Table 5). The highest antibacterial activity with the lowest MIC and MBC of *G. lucidum* moss against *E. coli* and *B. subtilis* was most likely attributed to the greatest variation in the phenolic components of the moss compared to those of shell and stem. *Esherichia coli* as a germ negative Bacteria showed more susceptibility than *B. subtilis* at the lowest concentration of 312 µg/mL of *G. lucidum* moss. Data from several studies suggested that the fruiting body of *G.lucidum* exhibited inhibitory activity against *E. coli*, most importantly, the MIC were reported (mg/mL) 1.25 (Shah et al., 2014), 8 (Quereshi et al., 2010), and 15 (Mehta and Jandaik, 2012).

The same was reported for *B. subtilis* and MIC between 8 and 20 mg/mL were declared (Keypour et al., 2008; Quereshi et al., 2010; Mehta and Jandaik, 2012). Surprisingly, the culture conditions attained through the statistical method stimulated bioactive compounds with valuable antimicrobial activity in the fruiting body. Therefore, the highest antimicrobial activity compared to the previous research was obtained in this research. Consequently, antimicrobial compounds from *G. lucidum* moss could be proposed as good therapeutic potential.

Cytotoxicity *of Ganoderma lucidum* against human breast cancer cell line MDA-MB-231

The impact of different concentrations (0–1,000 µg/mL) of different part of *G. lucidum* on the growth of highly invasive, estrogen-independent (MDA-MB-231) breast cancer cells was evaluated in a dose dependent manner for 48 h. Although extensive research has been

carried out on antitumor potential of *G. lucidum* extract (Jiang et al., 2004, 2006; de Camargo et al., 2022), What is still unclear is the impact of extracting different parts of the fruiting body of *G. lucidum* in against breast cancer cell line MDA-MB-231. MTT assay was performed to evaluate the cytotoxicity capacity of *G. lucidum* shell, stem, and, moss against MDA-MB-231 cells. This study delved into the potential anti-cancer benefits of different parts of the *Ganoderma* mushroom fruit for the first time. The result indicated that the stem and shell of *G. lucidum* significantly aggravated cell death at a dose of 500 µg/mL. The IC50 levels of shell and stem of *G. lucidum* were found to be around 465.3 and 485.7 µg/mL, for 48 h incubation while moss did not reach IC50 levels at inhibitor concentrations (Figures 10, 11, 12).

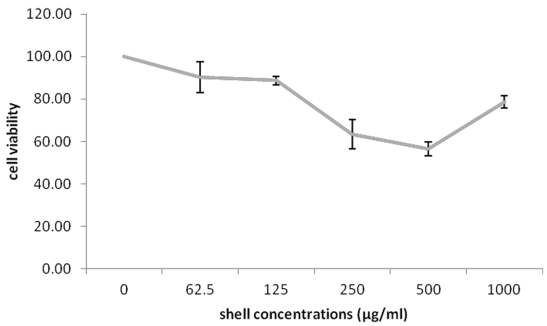

FIGURE 10
Cytotoxic impact of *Ganoderma lucidum* shell on MDA-MB-231 cells. Each bar indicated the mean ± SD of three experiments.

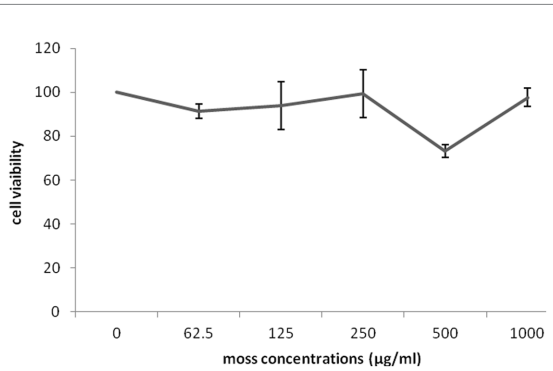

FIGURE 11
Cytotoxic impact of *Ganoderma lucidum* moss on MDA-MB-231 cells. Each bar indicated the mean ± SD of three experiments.

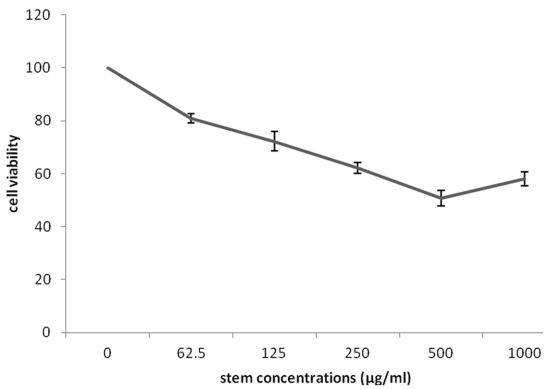

FIGURE 12
Cytotoxic impact of *Ganoderma lucidum* stem on MDA-MB-231 cells. Each bar represented the mean ± SD of three experiments.

To date, more than 300 bioactive compounds have been isolated from various parts of *G. lucidum*, including peptides, fatty acids, polysaccharides, and especially triterpenoids (Sharma et al., 2019). Studies indicate that different extracts or isolated compounds from *G. lucidum* act as a carcinostatic on different cancer cell lines, such as, lung (Li et al., 2013), colon (Li et al., 2020), pancreas (Chen et al., 2023), liver (Li et al., 2005), breast (Barbieri et al., 2017), skin (Shahid et al., 2022), and prostate (Wang et al., 2020). Among these compounds, triterpenoids are the most important bioactive compounds of *G. lucidum*, whose inhibitory effects on many cancers have been widely studied (Zhao et al., 2023). In this research, glucose as a carbon substrate and CSL syrup as a protein substrate was rated as the best substrates for stimulating an important biological compound, namely ganoderic acids. These optimal conditions led to an increased in the amount of the biologically active compound in the *G. lucidum* fruit. So that stem and shell of *G. lucidum* showed a significant control effect on MDA-MB-231 cells.

Conclusion

The objectives of this research are to find out the effect of the key substrates and their concentrations on CGLP and GA productions using OFAT as screening method prior to RSM. The highest content of GA in TiO_2 NPs with the highest content of glucose syrups and CSL syrups indicated that biosynthesis of GA in *G. lucidum* was triggered by chemical stressors. The moss of *G. lucidum* fruit-body with a wide variety of flavonoids and phenolic acids had the highest antimicrobial activity against *E. coli* and *B. subtilis*. The shell of *G. lucidum* induced the most prominent cytotoxicity against the MDA-MB-231 cell line with the lowest IC50. In conclusion, the optimized methods employed enhanced the quality and quantity of the bioactive components of the shell and moss of *G. lucidum* fruit body with the highest prominent cytotoxicity against cancer cells and significant antimicrobial activity, respectively, and probably performs the same way for the other medical mushroom.

Data availability statement

The original contributions presented in the study are included in the article; further inquiries can be directed to the corresponding author.

Ethics statement

This is an observational study. The XYZ Research Ethics Committee has confirmed that no ethical approval is required.

Author contributions

AT: Data curation, Formal analysis, Investigation, Project administration, Resources, Software, Writing – review & editing.

HS: Conceptualization, Data curation, Formal analysis, Investigation, Methodology, Project administration, Software, Supervision, Validation, Visualization, Writing – review & editing. AS: Conceptualization, Data curation, Formal analysis, Investigation, Methodology, Project administration, Software, Supervision, Validation, Visualization, Writing – review & editing. AG: Data curation, Investigation, Project administration, Resources, Writing – review & editing.

Funding

The author(s) declare that no financial support was received for the research, authorship, and/or publication of this article.

Conflict of interest

The authors declare that the research was conducted in the absence of any commercial or financial relationships that could be construed as a potential conflict of interest.

Publisher's note

All claims expressed in this article are solely those of the authors and do not necessarily represent those of their affiliated organizations, or those of the publisher, the editors and the reviewers. Any product that may be evaluated in this article, or claim that may be made by its manufacturer, is not guaranteed or endorsed by the publisher.

References

Ahmad, M. F., Wahab, S., Ahmad, F. A., Ashraf, S. A., Abullais, S. S., and Saad, H. H. (2022). Ganoderma lucidum: a potential pleiotropic approach of ganoderic acids in health reinforcement and factors influencing their production. *Fungal Biol. Rev.* 39, 100–125. doi: 10.1016/j.fbr.2021.12.003

Barbieri, A., Quagliariello, V., Del Vecchio, V., Falco, M., Luciano, A., Amruthraj, N. J., et al. (2017). Anticancer and anti-inflammatory properties of Ganoderma lucidum extract effects on melanoma and triple-negative breast cancer treatment. *Nutrients* 9:210. doi: 10.3390/nu9030210

Berovic, M., and Zhong, J.-J. (2023). Advances in Production of Medicinal Mushrooms Biomass in Solid State and Submerged Bioreactors. *Biochemical Engineering and Biotechnology of Medicinal Mushrooms*. 3:125–61.

Chen, H.-Y., Lei, J.-Y., Li, S.-L., Guo, L.-Q., Lin, J.-F., Wu, G.-H., et al. (2023). Progress in biological activities and biosynthesis of edible fungi terpenoids. *Crit. Rev. Food Sci. Nutr.* 63, 7288–7310. doi: 10.1080/10408398.2022.2045559

de Camargo, M. R., Frazon, T. F., Inacio, K. K., Smiderle, F. R., Amôr, N. G., Dionisio, T. J., et al. (2022). Ganoderma lucidum polysaccharides inhibit in vitro tumorigenesis, cancer stem cell properties and epithelial-mesenchymal transition in oral squamous cell carcinoma. *J. Ethnopharmacol.* 286:114891. doi: 10.1016/j.jep.2021.114891

de Dicastillo, C. L., Correa, M. G., Martinez, F. B., Streitt, C., and Galotto, M. J. (2020). Antimicrobial effect of titanium dioxide nanoparticles. *Antimicrob. Resist. One Heal. Perspect*

Dong, Z., Guo, H., Zhang, M., Xia, D., Yin, X., and Lv, J. (2022). Enhancing biomethane yield of coal in anaerobic digestion using iron/copper nanoparticles synthesized from corn straw extract. *Fuel* 319:123664. doi: 10.1016/j.fuel.2022.123664

Dong, Q., Li, Y., Liu, G., Zhang, Z., Zhou, H., and Yang, H. (2019). High oxygen treatments enhance the contents of phenolic compound and ganoderic acid, and the antioxidant and DNA damage protective activities of Ganoderma lingzhi fruiting body. *Front. Microbiol.* 10:2363. doi: 10.3389/fmicb.2019.02363

Du Preez, J. C., Kock, J. L. F., Monteiro, A. M. T., and Prior, B. A. (1985). The vitamin requirements of Candida shehatae for xylose fermentation. *FEMS Microbiol. Lett.* 28, 271–275. doi: 10.1111/j.1574-6968.1985.tb00804.x

Esfandiyari Mehni, M., Samadlouie, H. R., and Rajaei, A. (2022). Enhancement of oil productivity of Mortierella alpine and investigation into the potential of Pickering oil-in-water emulsions to improve its oxidative stability. *Food Sci. Nutr.* 10, 103–114. doi: 10.1002/fsn3.2651

Fan, L., Soccol, A. T., Pandey, A., and Soccol, C. R. (2007). Effect of nutritional and environmental conditions on the production of exo-polysaccharide of agaricus brasiliensis by submerged fermentation and its antitumor activity. *LWT-Food Sci. Technol.* 40, 30–35. doi: 10.1016/j.lwt.2005.09.006

Fang, Q.-H., Tang, Y.-J., and Zhong, J.-J. (2002). Significance of inoculation density control in production of polysaccharide and ganoderic acid by submerged culture of Ganoderma lucidum. *Process Biochem.* 37, 1375–1379. doi: 10.1016/S0032-9592(02)00017-1

Fang, Q.-H., and Zhong, J.-J. (2002a). Effect of initial pH on production of ganoderic acid and polysaccharide by submerged fermentation of Ganoderma lucidum. *Process Biochem.* 37, 769–774. doi: 10.1016/S0032-9592(01)00278-3

Fang, Q.-H., and Zhong, J.-J. (2002b). Submerged fermentation of higher fungus Ganoderma lucidum for production of valuable bioactive metabolites—ganoderic acid and polysaccharide. *Biochem. Eng. J.* 10, 61–65. doi: 10.1016/S1369-703X(01)00158-9

Ferreira, I. C. F. R., Barros, L., and Abreu, R. (2009). Antioxidants in wild mushrooms. *Curr. Med. Chem.* 16, 1543–1560. doi: 10.2174/092986709787909587

Gonabadi, E., Samadlouie, H. R., and Shafafi Zenoozian, M. (2021). Optimization of culture conditions for enhanced *Dunaliella salina* productions in mixotrophic culture. *Prep. Biochem. Biotechnol.* 52, 1–9. doi: 10.1080/10826068.2021.1922917

Gu, L., Zheng, Y., Lian, D., Zhong, X., and Liu, X. (2018). Production of triterpenoids from Ganoderma lucidum: elicitation strategy and signal transduction. *Process Biochem.* 69, 22–32. doi: 10.1016/j.procbio.2018.03.019

Hastings, J., and Kenealey, J. (2017). Avenanthramide-C reduces the viability of MDA-MB-231 breast cancer cells through an apoptotic mechanism. *Cancer Cell Int.* 17, 1–12. doi: 10.1186/s12935-017-0464-0

Heleno, S. A., Barros, L., Martins, A., Queiroz, M. J. R. P., Santos-Buelga, C., and Ferreira, I. C. F. R. (2012). Fruiting body, spores and in vitro produced mycelium of Ganoderma lucidum from Northeast Portugal: a comparative study of the antioxidant potential of phenolic and polysaccharidic extracts. *Food Res. Int.* 46, 135–140. doi: 10.1016/j.foodres.2011.12.009

Hsieh, C., Hsu, T.-H., and Yang, F.-C. (2005). Production of polysaccharides of Ganoderma lucidum (CCRC36021) by reusing thin stillage. *Process Biochem.* 40, 909–916. doi: 10.1016/j.procbio.2004.02.004

Hsieh, C., Tseng, M.-H., and Liu, C.-J. (2006). Production of polysaccharides from Ganoderma lucidum (CCRC 36041) under limitations of nutrients. *Enzym. Microb. Technol.* 38, 109–117. doi: 10.1016/j.enzmictec.2005.05.004

Hu, Y., Ahmed, S., Li, J., Luo, B., Gao, Z., Zhang, Q., et al. (2017). Improved ganoderic acids production in Ganoderma lucidum by wood decaying components. *Sci. Rep.* 7, 1–10. doi: 10.1038/srep46623

Hu, G., Zhai, M., Niu, R., Xu, X., Liu, Q., and Jia, J. (2018). Optimization of culture condition for ganoderic acid production in Ganoderma lucidum liquid static culture and design of a suitable bioreactor. *Molecules* 23:2563. doi: 10.3390/molecules23102563

Jiang, J., Slivova, V., Harvey, K., Valachovicova, T., and Sliva, D. (2004). Ganoderma lucidum suppresses growth of breast cancer cells through the inhibition of Akt/NF-$κ$B signaling. *Nutr. Cancer* 49, 209–216. doi: 10.1207/s15327914nc4902_13

Jiang, J., Slivova, V., and Sliva, D. (2006). Ganoderma lucidum inhibits proliferation of human breast cancer cells by down-regulation of estrogen receptor and NF-$κ$B signaling. *Int. J. Oncol.* 29, 695–703. doi: 10.3892/ijo.29.3.695

Karaman, M., Jovin, E., Malbaša, R., Matavuly, M., and Popović, M. (2010). Medicinal and edible lignicolous fungi as natural sources of antioxidative and antibacterial agents. *Phyther. Res.* 24, 1473–1481. doi: 10.1002/ptr.2969

Keypour, S., Riahi, H., Moradali, M.-F., and Rafati, H. (2008). Investigation of the antibacterial activity of a chloroform extract of Ling Zhi or Reishi medicinal mushroom, Ganoderma lucidum (W. Curt.: Fr.) P. Karst.(Aphyllophoromycetideae), from Iran. *Int. J. Med. Mushrooms* 10, 345–349. doi: 10.1615/IntJMedMushr.v10.i4.70

LeBlanc, J. G., Milani, C., De Giori, G. S., Sesma, F., Van Sinderen, D., and Ventura, M. (2013). Bacteria as vitamin suppliers to their host: a gut microbiota perspective. *Curr. Opin. Biotechnol.* 24, 160–168. doi: 10.1016/j.copbio.2012.08.005

Lee, H., Song, M., and Hwang, S. (2003). Optimizing bioconversion of deproteinated cheese whey to mycelia of Ganoderma lucidum. *Process Biochem.* 38, 1685–1693. doi: 10.1016/S0032-9592(02)00259-5

Li, C.-H., Chen, P.-Y., Chang, U.-M., Kan, L.-S., Fang, W.-H., Tsai, K.-S., et al. (2005). Ganoderic acid X, a lanostanoid triterpene, inhibits topoisomerases and induces apoptosis of cancer cells. *Life Sci.* 77, 252–265. doi: 10.1016/j.lfs.2004.09.045

Li, P., Liu, L., Huang, S., Zhang, Y., Xu, J., and Zhang, Z. (2020). Anti-cancer effects of a neutral triterpene fraction from Ganoderma lucidum and its active constituents on SW620 human colorectal cancer cells. *Anti Cancer Agents Med. Chem.* 20, 237–244. doi: 10.2174/1871520619666191015102442

Li, Y.-B., Liu, R.-M., and Zhong, J.-J. (2013). A new ganoderic acid from Ganoderma lucidum mycelia and its stability. *Fitoterapia* 84, 115–122. doi: 10.1016/j.fitote.2012.11.008

Lin, Y.-X., Sun, J.-T., Liao, Z.-Z., Sun, Y., Tian, X.-G., Jin, L.-L., et al. (2022). Triterpenoids from the fruiting bodies of Ganoderma lucidum and their inhibitory activity against FAAH. *Fitoterapia* 158:105161. doi: 10.1016/j.fitote.2022.105161

Liu, Y., Long, Y., Liu, H., Lan, Y., Long, T., Kuang, R., et al. (2022). Polysaccharide prediction in Ganoderma lucidum fruiting body by hyperspectral imaging. *Food Chem. X* 13:100199. doi: 10.1016/j.fochx.2021.100199

Ma, Y., Mao, D., Geng, L., Wang, Z., and Xu, C. (2013). Production, fractionation, characterization of extracellular polysaccharide from a newly isolated Trametes gibbosa and its hypoglycemic activity. *Carbohydr. Polym.* 96, 460–465. doi: 10.1016/j.carbpol.2013.04.019

Ma, Z., Xu, M., Wang, Q., Wang, F., Zheng, H., Gu, Z., et al. (2019). Development of an efficient strategy to improve extracellular polysaccharide production of Ganoderma lucidum using l-phenylalanine as an enhancer. *Front. Microbiol.* 10:2306. doi: 10.3389/fmicb.2019.02306

Maalej, H., Boisset, C., Hmidet, N., Buon, L., Heyraud, A., and Nasri, M. (2014). Purification and structural data of a highly substituted exopolysaccharide from *Pseudomonas stutzeri* AS22. *Carbohydr. Polym.* 112, 404–411. doi: 10.1016/j.carbpol.2014.06.003

Malinowska, E., Krzyczkowski, W., Łapienis, G., and Herold, F. (2009). Improved simultaneous production of mycelial biomass and polysaccharides by submerged culture of Hericium erinaceum: optimization using a central composite rotatable design (CCRD). *J. Ind. Microbiol. Biotechnol.* 36, 1513–1527. doi: 10.1007/s10295-009-0640-x

Mehta, S., and Jandaik, S. (2012). In vitro comparative evaluation of antibacterial activity of fruiting body and mycelial extracts of Ganoderma lucidum against pathogenic bacteria. *J. Pure Appl. Microbiol.* 6, 1997–2001.

Mesgari, M., Aalami, A. H., and Sahebkar, A. (2021). Antimicrobial activities of chitosan/titanium dioxide composites as a biological nanolayer for food preservation: a review. *Int. J. Biol. Macromol.* 176, 530–539. doi: 10.1016/j.ijbiomac.2021.02.099

Miret, J. A., and Munné-Bosch, S. (2014). Plant amino acid-derived vitamins: biosynthesis and function. *Amino Acids* 46, 809–824. doi: 10.1007/s00726-013-1653-3

Murugesan, K., Nam, I.-H., Kim, Y.-M., and Chang, Y.-S. (2007). Decolorization of reactive dyes by a thermostable laccase produced by Ganoderma lucidum in solid state culture. *Enzym. Microb. Technol.* 40, 1662–1672. doi: 10.1016/j.enzmictec.2006.08.028

Nickavar, B., and Esbati, N. (2012). Evaluation of the antioxidant capacity and phenolic content of three Thymus species. *J. Acupunct. Meridian Stud.* 5, 119–125. doi: 10.1016/j.jams.2012.03.003

Pan, X., Yin, M., Guo, M., Niu, X., and Han, L. (2022). The latest progress of natural food polysaccharides preventing ulcerative colitis by regulating intestinal microbiota. *J. Funct. Foods* 96:105201. doi: 10.1016/j.jff.2022.105201

Pareek, V., Gupta, R., and Panwar, J. (2018). Do physico-chemical properties of silver nanoparticles decide their interaction with biological media and bactericidal action? *A review. Mater. Sci. Eng. C* 90, 739–749. doi: 10.1016/j.msec.2018.04.093

Patel, S. (2015). Functional food relevance of whey protein: a review of recent findings and scopes ahead. *J. Funct. Foods* 19, 308–319. doi: 10.1016/j.jff.2015.09.040

Quereshi, S., Pandey, A. K., and Sandhu, S. S. (2010). Evaluation of antibacterial activity of different Ganoderma lucidum extracts. *J. Sci. Res.* 3, 9–13.

Saltarelli, R., Ceccaroli, P., Buffalini, M., Vallorani, L., Casadei, L., Zambonelli, A., et al. (2015). Biochemical characterization and antioxidant and antiproliferative activities of different Ganoderma collections. *Microb. Physiol.* 25, 16–25. doi: 10.1159/000369212

Samadlouie, H. R., Jahanbin, K., and Jalali, P. (2020). Production, medium optimization, and structural characterization of an extracellular polysaccharide produced by *Rhodotorula minuta* ATCC 10658. *Food Sci. Nutr.* 8, 4957–4964. doi: 10.1002/fsn3.1792

Samadlouie, H. R., Nurmohamadi, S., Moradpoor, F., and Gharanjik, S. (2018). Effect of low-cost substrate on the fatty acid profiles of Mortierella alpina CBS 754.68 and Wickerhamomyces siamensis SAKSG. *Biotechnol. Biotechnol. Equip.* 32, 1228–1235. doi: 10.1080/13102818.2018.1471360

Shah, P., Modi, H. A., Shukla, M. D., and Lahiri, S. K. (2014). Preliminary phytochemical analysis and antibacterial activity of Ganoderma lucidum collected from Dang District of Gujarat, India. *Int. J. Curr. Microbiol. App. Sci.* 3, 246–255.

Shahid, A., Huang, M., Liu, M., Shamim, M. A., Parsa, C., Orlando, R., et al. (2022). The medicinal mushroom Ganoderma lucidum attenuates UV-induced skin carcinogenesis and immunosuppression. *PLoS One* 17:e0265615. doi: 10.1371/journal.pone.0265615

Sharma, C., Bhardwaj, N., Sharma, A., Tuli, H. S., Batra, P., Beniwal, V., et al. (2019). Bioactive metabolites of Ganoderma lucidum: factors, mechanism and broad spectrum therapeutic potential. *J. Herb. Med.* 17-18:100268. doi: 10.1016/j.hermed.2019.100268

Singh, S. K., Singh, S. K., Tripathi, V. R., Khare, S. K., and Garg, S. K. (2011). Comparative one-factor-at-a-time, response surface (statistical) and bench-scale bioreactor level optimization of thermoalkaline protease production from a psychrotrophic *Pseudomonas putida* SKG-1 isolate. *Microb. Cell Factories* 10:114. doi: 10.1186/1475-2859-10-114

Song, M., Kim, N., Lee, S., and Hwang, S. (2007). Use of whey permeate for cultivating Ganoderma lucidum mycelia. *J. Dairy Sci.* 90, 2141–2146. doi: 10.3168/jds.2006-690

Stamets, P. (2011). *Growing Gourmet and Medicinal Mushrooms*. Berkeley: Ten Speed Press.

Staub, A. M. (1965). Removeal of protein-Sevag method. *Methods Carbohydr. Chem.* 5, 5–6.

Supramani, S., Rahayu Ahmad, Z. I., Annuar, M. S. M., Klaus, A., and Wan, W. A. A. Q. I., and others (2019). Optimisation of biomass, exopolysaccharide and intracellular polysaccharide production from the mycelium of an identified Ganoderma lucidum strain QRS 5120 using response surface methodology. *AIMS Microbiol.* 5::19. doi: 10.3934/microbiol.2019.1.19

Tang, Y.-J., and Zhong, J.-J. (2002). Fed-batch fermentation of Ganoderma lucidum for hyperproduction of polysaccharide and ganoderic acid. *Enzym. Microb. Technol.* 31, 20–28. doi: 10.1016/S0141-0229(02)00066-2

Torres-Mancera, M. T., Figueroa-Montero, A., Favela-Torres, E., Rosales-Zamora, G., Nampoothiri, K. M., and Saucedo-Castañeda, G. (2018). "Online monitoring of solid-state fermentation using respirometry" in *Current Developments in Biotechnology and Bioengineering* (Elsevier), 97–108.

Tripathi, A. D., Yadav, A., Jha, A., and Srivastava, S. K. (2012). Utilizing of sugar refinery waste (cane molasses) for production of bio-plastic under submerged fermentation process. *J. Polym. Environ.* 20, 446–453. doi: 10.1007/s10924-011-0394-1

Valgas, C., De Souza, S. M., Smânia, E. F. A., and Smânia, A. Jr. (2007). Screening methods to determine antibacterial activity of natural products. *Braz. J. Microbiol.* 38, 369–380. doi: 10.1590/S1517-83822007000200034

Veljović, S., Veljović, M., Nikićević, N., Despotović, S., Radulović, S., Nikšić, M., et al. (2017). Chemical composition, antiproliferative and antioxidant activity of differently processed Ganoderma lucidum ethanol extracts. *J. Food Sci. Technol.* 54, 1312–1320. doi: 10.1007/s13197-017-2559-y

Wang, X., Wang, B., Zhou, L., Wang, X., Veeraraghavan, V. P., Mohan, S. K., et al. (2020). Ganoderma lucidum put forth anti-tumor activity against PC-3 prostate cancer cells via inhibition of Jak-1/STAT-3 activity. *Saudi J. Biol. Sci.* 27, 2632–2637. doi: 10.1016/j.sjbs.2020.05.044

Wei, Z., Liu, L., Guo, X., Li, Y., Hou, B., Fan, Q., et al. (2016). Sucrose fed-batch strategy enhanced biomass, polysaccharide, and ganoderic acids production in fermentation of Ganoderma lucidum 5.26. *Bioprocess Biosyst. Eng.* 39, 37–44. doi: 10.1007/s00449-015-1480-x

Xu, P., Ding, Z.-Y., Qian, Z., Zhao, C.-X., and Zhang, K.-C. (2008). Improved production of mycelial biomass and ganoderic acid by submerged culture of Ganoderma lucidum SB97 using complex media. *Enzym. Microb. Technol.* 42, 325–331. doi: 10.1016/j.enzmictec.2007.10.016

Yahia, E. M., Gutiérrez-Orozco, F., and Moreno-Pérez, M. A. (2017). Identification of phenolic compounds by liquid chromatography-mass spectrometry in seventeen species of wild mushrooms in Central Mexico and determination of their antioxidant activity and bioactive compounds. *Food Chem.* 226, 14–22. doi: 10.1016/j.foodchem.2017.01.044

Yang, L., Kang, X., Dong, W., Wang, L., Liu, S., Zhong, X., et al. (2022). Prebiotic properties of Ganoderma lucidum polysaccharides with special enrichment of Bacteroides ovatus and *B. uniformis* in vitro. *J. Funct. Foods* 92:105069. doi: 10.1016/j.jff.2022.105069

Yang, S.-Y., Lü, F.-X., Lu, Z.-X., Bie, X.-M., Jiao, Y., Sun, L.-J., et al. (2008). Production of $γ$-aminobutyric acid by *Streptococcus salivarius* subsp. thermophilus Y2 under submerged fermentation. *Amino Acids* 34, 473–478. doi: 10.1007/s00726-007-0544-x

Yuen, J. W. M., and Gohel, M. D. I. (2005). Anticancer effects of Ganoderma lucidum: a review of scientific evidence. *Nutr. Cancer* 53, 11–17. doi: 10.1207/s15327914nc5301_2

Zhao, P., Guan, M., Tang, W., Walayat, N., Ding, Y., and Liu, J. (2023). Structural diversity, fermentation production, bioactivities and applications of triterpenoids from several common medicinal fungi: recent advances and future perspectives. *Fitoterapia* 166:105470. doi: 10.1016/j.fitote.2023.105470

Zhou, X.-W., Su, K.-Q., and Zhang, Y.-M. (2012). Applied modern biotechnology for cultivation of Ganoderma and development of their products. *Appl. Microbiol. Biotechnol.* 93, 941–963. doi: 10.1007/s00253-011-3780-7

frontiers | Frontiers in Microbiology

TYPE Original Research
PUBLISHED 31 January 2024
DOI 10.3389/fmicb.2024.1341179

OPEN ACCESS

EDITED BY
Monika Prakash Rai,
Amity University, India

REVIEWED BY
Guanhua Xun,
University of Illinois at Urbana-Champaign, United States
Arun Karnwal,
Lovely Professional University, India

*CORRESPONDENCE
Qing-Shan Shi
✉ shiqingshan@hotmail.com
Gang Zhou
✉ zgbees@gdim.cn
Xiao-Bao Xie
✉ xiexb@gdim.cn
Jie Wang
✉ jiewang@scau.edu.cn

†These authors have contributed equally to this work

RECEIVED 20 November 2023
ACCEPTED 09 January 2024
PUBLISHED 31 January 2024

CITATION
Zhu X-X, Wang Y-S, Li S-J, Peng R-Q, Wen X, Peng H, Shi Q-S, Zhou G, Xie X-B and Wang J (2024) Rapid detection of *mexX* in *Pseudomonas aeruginosa* based on CRISPR-Cas13a coupled with recombinase polymerase amplification.
Front. Microbiol. 15:1341179.
doi: 10.3389/fmicb.2024.1341179

Rapid detection of *mexX* in *Pseudomonas aeruginosa* based on CRISPR-Cas13a coupled with recombinase polymerase amplification

Xiao-Xuan Zhu[1,2†], Ying-Si Wang[1,2†], Su-Juan Li[2], Ru-Qun Peng[2], Xia Wen[2], Hong Peng[2], Qing-Shan Shi[1,2*], Gang Zhou[1,2*], Xiao-Bao Xie[1,2*] and Jie Wang[1*]

[1]Guangdong Provincial Key Laboratory of Nutraceuticals and Functional Foods, College of Food Science, South China Agricultural University, Guangzhou, Guangdong, China, [2]Guangdong Provincial Key Laboratory of Microbial Culture Collection and Application, State Key Laboratory of Applied Microbiology Southern China, Institute of Microbiology, Guangdong Academy of Sciences, Guangzhou, Guangdong, China

The principal pathogen responsible for chronic urinary tract infections, immunocompromised hosts, and cystic fibrosis patients is *Pseudomonas aeruginosa*, which is difficult to eradicate. Due to the extensive use of antibiotics, multidrug-resistant *P. aeruginosa* has evolved, complicating clinical therapy. Therefore, a rapid and efficient approach for detecting *P. aeruginosa* strains and their resistance genes is necessary for early clinical diagnosis and appropriate treatment. This study combines recombinase polymerase amplification (RPA) and clustered regularly interspaced short palindromic repeats-association protein 13a (CRISPR-Cas13a) to establish a one-tube and two-step reaction systems for detecting the *mexX* gene in *P. aeruginosa*. The test times for one-tube and two-step RPA-Cas13a methods were 5 and 40 min (including a 30 min RPA amplification reaction), respectively. Both methods outperform Quantitative Real-time Polymerase Chain Reactions (qRT-PCR) and traditional PCR. The limit of detection (LoD) of *P. aeruginosa* genome in one-tube and two-step RPA-Cas13a is 10 aM and 1 aM, respectively. Meanwhile, the designed primers have a high specificity for *P. aeruginosa mexX* gene. These two methods were also verified with actual samples isolated from industrial settings and demonstrated great accuracy. Furthermore, the results of the two-step RPA-Cas13a assay could also be visualized using a commercial lateral flow dipstick with a LoD of 10 fM, which is a useful adjunt to the gold-standard qRT-PCR assay in field detection. Taken together, the procedure developed in this study using RPA and CRISPR-Cas13a provides a simple and fast way for detecting resistance genes.

KEYWORDS

***Pseudomonas aeruginosa*, MexX, Crispr-cas13a, recombinase polymerase amplification, detection**

1 Introduction

Pseudomonas aeruginosa is an opportunistic pathogen that is commonly found in hospitals. It can cause a variety of chronic infections, including urinary tract infections, bronchial dilation, and cystic fibrosis, all of which have a high recurrence rate and are difficult to treat (Gellatly and Hancock, 2013; Diggle and Whiteley, 2020; Shi et al., 2023). In addition, *P. aeruginosa* can cling to various surfaces of food processing equipment to form biofilms, endangering food safety and quality and potentially causing food-borne diseases (Teng et al., 2022; Ingrid et al., 2023; Silvia et al., 2023; Wu et al., 2023). Under the pressure of drug selection, *P. aeruginosa* continuously evolves and varies in its tolerance to a variety of commonly used antibiotics. Meanwhile, the drug-resistant mechanisms of *P. aeruginosa* are quite complex. However, excessive expression of efflux pumps' bacterial active external discharge system is regarded to be one of the primary drug resistance mechanisms of *P. aeruginosa* (Eichenberger and Thaden, 2019). These efflux systems can pump out a wide range of molecules, including antibiotics with diverse structures and foreign biological substances, in order to reduce the concentration of intracellular antibacterial chemicals and prevent the development of multi-drug resistance in bacteria (Cunrath et al., 2019). There are at least 12 varieties of resistance nodulation division (RND) external pumps in *P.aeruginosa*, including MexAB-OprM, MexCD-OprJ, MexEF-OprN, MexXY-OprM, MexJK-OprM, MexGHI-OprM, MexMN-OprM, with MexAB-OprM, and MexXY-OprM being the most prevalent (Pesingi et al., 2019; Tsutsumi et al., 2019). In particular, MexXY over-expression is frequently found in the clinical isolates of drug-resistant *P. aeruginosa*, and it is becoming widely accepted that MexXY plays a substantial role in *P. aeruginosa* aminoglycoside resistance (Henríquez et al., 2020; Kei et al., 2021). A mutant missing MexXY showed increased resistance to aminoglycosides, erythromycin, and tetracycline but not to ß-lactams, chloramphenicol, or quinolones (Morita et al., 2001). Because of their significance in the drug tolerance mechanism, efflux pumps have emerged as a crucial therapeutic target. Antibiotic resistance can be combated by preventing these efflux pumps from working (Avakh et al., 2023). However, the modern quick and effective detection methods for efflux pump genes are scarce, limiting the prompt detection and treatment of resistant *P. aeruginosa*.

In prokaryotes, clustered regularly interspaced short palindromic repeats (CRISPR) and association protein (Cas) are immunological defensive mechanisms that resist the invasion of foreign genetic material (Manghwar et al., 2019). The nucleic acid enzyme domain in Cas13a has RNA endonuclease activity and the ability to cut RNA non-specifically. Cas13a can precisely identify and cut the target RNA in the case of the processed RNA molecule (crRNA). Cas13a randomly cuts adjacent RNA after its collateral-cutting capabilities is activated. This motivates Cas13a to create novel RNA-targeting tools and expand the application of CRISPR systems for gene detection (Abudayyeh et al., 2016; Zhao et al., 2022). By labeling RNA probes with fluorophores at both ends, CRISPR/Cas13a can detect RNA templates and amplify signals to achieve specific detection of target molecules (Abudayyeh et al., 2016; Kellner et al., 2019). More specifically, CRISPR-Cas13a-based detection techniques provide the following benefits and advantages: Cas13a has no protospacer adjacent motif (PAM) site limit, allowing it to target any sequences (Escalona-Noguero et al., 2021). Therefore, CRISPR-Cas13a has a promising application prospect in pathogenic testing.

Antibiotics overuse and misuse have been linked to the rapid emergence of drug-resistant bacteria (Tacconelli et al., 2018; Ranjbar et al., 2024). Bacterial resistance has grown to be an urgent issue that must be tackled. The Antimicrobial Susceptibility Test (AST) is a classic method for determining microbial drug resistance (Antimicrobial Resistance, AMR; Paul et al., 2022). Then physical, chemical, and molecular biology detection technologies emerged, including flow cytometry (Williams et al., 2017), Raman spectroscopy (Duan et al., 2016), and mass spectrometers (Lee et al., 2016), as well as immune hybridization (Shahid et al., 2021). For nucleic acid amplification, molecular biological detection technologies, such as Polymerase Chain Reaction (PCR; Niu et al., 2020), Quantitative Real-time PCR (qRT-PCR; Abramova et al., 2023), and whole-genome/metagenome sequencing (Boolchandani et al., 2019), are commonly used. Although most of the tactics outlined above are commonly utilized in practical settings, they are either ineffectual or necessitate complex apparatus. A developed isothermal nucleic acid amplification technique of Recombinase polymerase amplification (RPA) has significant advantages in terms of reaction time and equipment (Tan et al., 2022). Numerous researchers have imaginatively created novel nucleic acid detection technologies based on CRISPR-Cas13a and RPA (Gao et al., 2021; He et al., 2022; MacGregor et al., 2023; Miao et al., 2023). However, greater improvement of the sensitivity, precision, and experimental protocols of the RPA coupled Cas13a detection approach is required for visual molecular diagnostics.

Therefore, this study uses CRISPR/Cas13a with RPA technology to develop specific primers and probes for the identification of *mexX* in *P. aeruginosa*. The easy operation method with great sensitivity to the presence of *mexX* provides technical support for preventing and controlling *P. aeruginosa* resistance.

2 Materials and methods

2.1 Chemical reagents and materials

LwCas13a protein and its corresponding buffer were purchased from Magigen Biotech Co. Ltd. (Guangzhou, China). DNase I, T7 RNA polymerase, and recombinant RNase inhibitor were obtained from TaKaRa (Dalian, China). ChamQ Universal SYBR qPCR Master Mix was purchased from Vazyme (Guangzhou, China). Sangon Biotech (Shanghai, China) provided the NTP mixture (10 mM each), dNTP mixture (25 mM each), and Spin Column RNA Cleanup & Concentration Kit. DNA Constant Temperature Rapid Amplification Kit (Liquid Basic Type) and CRISPR Cas12/13 Hybridetect Test Note were purchased from Warbio Biotech (Nanjing, China).

2.2 Bacterial strains and nucleic acid preparation

In our laboratory, *P. aeruginosa* was isolated from spoiled wood paint lotion. Other pathogenic bacteria obtained from American Type Culture Collection (ATCC) and German Collection of Microorganisms and Cell Cultures included *Staphylococcus aureus* ATCC 6538P, *Escherichia coli* ATCC 8739, *Vibrio parahaemolyticus* ATCC 17802, *Salmonella enterica* ATCC 9115, *Klebsiella pneumoniae* ATCC 4352, *Lactobacillus paracasei* ATCC 334, *Bacillus*

paralicheniformis ATCC 9945, *and Bacillus subtilis* DSM 23778. The nucleic acids of the above strains were extracted using the HiPure Bacterial DNA Kit (Magen Biotech Co., Ltd.; Guangzhou, China) according to the manufacturer's instructions. The concentration of DNA was quantified using the Nanodrop One instrument (Thermo Fisher Scientific, Shanghai, China). Until they were used, all DNA samples were stored at-20°C.

2.3 Primer design for crRNA and RPA

The *mexX* gene sequences of *P. aeruginosa* were downloaded from the GenBank database of the National Center for Biotechnology Information (NCBI).[1] After aligning gene sequences to identify conserved regions, 10 crRNAs were designed using the online Cas13 design tool.[2] According to the selected target sequence design and relevant works of literatures (Liu et al., 2017; Gootenberg et al., 2018; Yang et al., 2023), a T7 promoter binding sequence was attached to the 5′-end of the designed crRNAs. Simultaneously, the PRIMER 5 program was used to design equivalent RPA primers between the upstream and downstream clips of the candidate target DNA. The RNA probe 1 is tagged with 6-FAM at the 5′ -end and uses BHQ1 at the 3′ -end (Zhou et al., 2020), whereas RNA probe 2 is designated with 6-FAM at the 5′ end and uses BIO at the 3′ end (Wang et al., 2023). The designed primers, probes, and oligonucleotides were synthesized by TsingkeBiotech (Beijing, China). All of the nucleic acid sequences used in this study are listed in Table 1.

2.4 crRNA preparation

The templates for an oligonucleotide incorporating T7 promoters, repetitive sequences, and interval sequences have been developed to create the double strand DNA (dsDNA). Forward and reverse oligonucleotide DNA (5 μmol/L) were added to produce dsDNA templates for transcription. And each single-chain template was then mixed, annealed for 5 min at 95°C and naturally cooled to room temperature naturally. The crRNA was synthesized by incubating the above mixtures for 2 h at 42°C with T7 RNA polymerase (TaKaRa). To carry out the process, the synthesized crRNA was digested with DNase I (TaKaRa) at 37°C for 1 h to remove DNA templates, and then purified using the RNA Rapid Concentration and Purification kit (Sangon Biotech, Shanghai, China) in accordance with the manufacturer's instructions. The crRNA concentration was then determined using the NanoDrop spectrophotometer (Thermo Fisher Scientific, Shanghai, China) and was subsequently kept at-80°C until use.

2.5 One-tube RPA-Cas13a

For the one-tube RPA-Cas13a assay, RPA amplification and CRISPR-Cas13a were coupled in a one-tube reaction system (Figure 1). Briefly, the 50 μL one-tube reaction system consisted of 18 μL C buffer (Warbio Biotech Co. Ltd.; Guangzhou, China), 5 μL L buffer (Warbio), 12 μL P-core (Warbio), 1 μL each of 10 μM forward and reverse primers, 1.5 μL 10 mM dNTPs, 1 μL target DNA template, 2 μL 25 mM NTP mix, 1 μL recombinant RNase inhibitor, 1 μL 10 μM RNA-probe, 1 μL T7 RNA polymerase, 0.4 μL 2 μM Cas13a, 1 μL 12 nM crRNA, and added RNase-free ddH_2O to 50 μL. After gently spinning the reaction mixtures, 2.5 μL of 280 mM magnesium acetate (MgOAc) was added. Finally, the reactions were then run at 39°C for 20 min, and the fluorescence signal was collected every 1 min on a QuantStudio™ Real-Time PCR Software (Applied Biosystems, Waltham, MA, United States) with three replicates set for each sample.

2.6 Two-step RPA-Cas13a

In the two-step RPA-Cas13a assay, the crucial RPA reactions were first conducted according to the instructions of the DNA constant temperature rapid amplification kit (Warbio, China; Figure 1). Each 50 μL RPA reaction volume contained the following elements: 20 μL C buffer, 5 μL L buffer, 12 μL P-core, 2 μL each of 10 μM forward and reversed primers, 1.5 μL 10 mM dNTPs, 1 μL target DNA template, and 4 μL RNase-free ddH_2O. The reaction mixtures were gently vortexed and spun. Then, 2.5 μL of 280 mM MgOAc was added and thoroughly mixed to start the reaction, which would last for 30 min at 39°C. Subsequently, a 50 μL CRISPR-Cas13a reaction system was performed with 5 μL 10 × reaction buffer, 2 μL 25 mM NTP mix, 0.8 μL recombinant RNase inhibitor, 1 μL PA-crRNA, 1 μL 10 μM RNA-probe, 0.6 μL T7 RNA polymerase, 0.4 μL 2 μM Cas13a, 4 μL RPA products and added RNase-free ddH_2O to 50 μL. Three replicates were set up for each sample, and the reactions were carried out at 39°C for 20 min after mixing. The fluorescence signal was collected every minute using the QuantStudio™ Real-Time PCR program.

2.7 LwCas13a feasibility analysis for nucleic detection

The crRNA 1 with the highest predicted score in online website design was selected for the detection system to confirm the activity of the LwCas13a protein and examine if a detection system could be successfully established. In the first, second, and third groups, equivalent amounts of RNase-free H_2O were introduced to the reaction system in place of crRNA 1, DNA, and LwCas13a, which served as negative controls. Instead of DNA, crRNA 1, and LwCas13a protein, the blank control group received an equal amount of RNase-free H_2O. After mixing, the reactions were run for 20 min at 39°C, and the fluorescence signal was collected every 1 min on a QuantStudio™ Real-Time PCR Software with three replicates.

2.8 Target crRNA screening

To ensure the excellent activity of the Cas13a protein, 10 crRNAs were obtained via the online Cas13 design tool. And three pairs of RPA isothermal amplification primers were designed based on the conserved sequence to match the crRNA. Using the same batch of extracted DNA products, the CRISPR-Cas13a system, which contains

1 http://www.ncbi.nlm.nih.gov/

2 https://cas13design.nygenoMe.org/

TABLE 1 Sequence of primers, oligonucleotides and RNA probes in this study.

Name	Sequence (5′-3′)
mexX-crRNA 1	TAATACGACTCACTATAGGGGATTTAGACTACCCCAAAAACGAAGGGGACTAAAACATCGATCCGATCTACGTGAACTT
mexX-crRNA 2	TAATACGACTCACTATAGGGGATTTAGACTACCCCAAAAACGAAGGGGACTAAAACGAAGTTCACGTAGATCGGATCGA
mexX-crRNA 3	TAATACGACTCACTATAGGGGATTTAGACTACCCCAAAAACGAAGGGGACTAAAACGCGACACCCTTCACCTGGCCTTC
mexX-crRNA 4	TAATACGACTCACTATAGGGGATTTAGACTACCCCAAAAACGAAGGGGACTAAAACTCCACGTCTTCCACCACGCCCTG
mexX-crRNA 5	TAATACGACTCACTATAGGGGATTTAGACTACCCCAAAAACGAAGGGGACTAAAACCCACGTCTTCCACCACGCCCTGT
mexX-crRNA 6	TAATACGACTCACTATAGGGGATTTAGACTACCCCAAAAACGAAGGGGACTAAAACGATGATCCAGTCACGGCCCTGCA
mexX-crRNA 7	TAATACGACTCACTATAGGGGATTTAGACTACCCCAAAAACGAAGGGGACTAAAACCCAGCAGGAATAGGGCGACCAGG
mexX-crRNA 8	TAATACGACTCACTATAGGGGATTTAGACTACCCCAAAAACGAAGGGGACTAAAACCTGATGATCCAGTCACGGCCCTG
mexX-crRNA 9	TAATACGACTCACTATAGGGGATTTAGACTACCCCAAAAACGAAGGGGACTAAAACTGATGATCCAGTCACGGCCCTGC
mexX-crRNA 10 F	TAATACGACTCACTATAGGGGATTTAGACTACCCCAAAAACGAAGGGGACTAAAACATGATCCAGTCACGGCCCTGCAG
mexX-crRNA 1 R	AAGTTCACGTAGATCGGATCGATGTTTTAGTCCCCTTCGTTTTTGGGGTAGTCTAAATC
mexX-crRNA 2 R	TCGATCCGATCTACGTGAACTTCGTTTTAGTCCCCTTCGTTTTTGGGGTAGTCTAAATC
mexX-crRNA 3 R	GAAGGCCAGGTGAAGGGTGTCGCGTTTTAGTCCCCTTCGTTTTTGGGGTAGTCTAAATC
mexX-crRNA 4 R	CAGGGCGTGGTGGAAGACGTGGAGTTTTAGTCCCCTTCGTTTTTGGGGTAGTCTAAATC
mexX-crRNA 5 R	ACAGGGCGTGGTGGAAGACGTGGGTTTTAGTCCCCTTCGTTTTTGGGGTAGTCTAAATC
mexX-crRNA 6 R	TGCAGGGCCGTGACTGGATCATCGTTTTAGTCCCCTTCGTTTTTGGGGTAGTCTAAATC
mexX-crRNA 7 R	CCTGGTCGCCCTATTCCTGCTGGGTTTTAGTCCCCTTCGTTTTTGGGGTAGTCTAAATC
mexX-crRNA 8 R	CAGGGCCGTGACTGGATCATCAGGTTTTAGTCCCCTTCGTTTTTGGGGTAGTCTAAATC
mexX-crRNA 9 R	GCAGGGCCGTGACTGGATCATCAGTTTTAGTCCCCTTCGTTTTTGGGGTAGTCTAAATC
mexX-crRNA 10 R	CTGCAGGGCCGTGACTGGATCATGTTTTAGTCCCCTTCGTTTTTGGGGTAGTCTAAATC
mexX-RPA-F1	TAATACGACTCACTATAGGGAGCGAACGCGAGTACACCGAAGCGCAGAC
mexX-RPA-R1	ATGTCCTTGTCGGCGACACCCTTCACCTGG
mexX-RPA-F2	TAATACGACTCACTATAGGGCATCCAATGGACCGGCTCGCTGCGCGGGCT
mexX-RPA-R2	CTTCCAGGCGTCCGGGCAGCTCGCTGGTGATG
mexX-RPA-F3	TAATACGACTCACTATAGGGCTGATCCGTACCGCCCAGTCCGCCGTGGTC
mexX-RPA-R3	CGGCATGCTGGGCGGCGTTCTCGACGATC
mexX-qRT-PCR F	CCGTGCTGTTCCAGATC
mexX-qRT-PCR R	TCCTTGATCAGGTCGGCG
mexX-PCR F	GCGGAAGGTCAGGGTCAG
mexX-PCR R	GGTTTTCTGGGATTCCTCTTTG
RNA probe 1	6-FAM-UUGGCGUAAUCAUGGUCAUA-BHQ1
RNA probe 2	6-FAM-UUUUUUUUUUUUUUUUUUUU-BIO

F, forward primer; R, reverse primer. The T7 promoter is underlined; GGG is required for T7 transcription.

10 distinct crRNAs, was next tested for detection efficiency. The endpoint fluorescence value was recorded for comparison.

2.9 Reaction condition optimization

The Cas13a-crRNA-fluorescent measurement signal was used to optimize the detection system, and the fluorescence value was simultaneously selected for comparison. The samples for the optimization procedure are *P. aeruginosa* DNA samples with the same initial concentration. A single variable should be controlled to optimize the following parameters: reaction temperatures (37, 38, 39, 40, and 41°C), primer concentrations (0.6–1 μM), LwCas13a concentrations (0–40 nM), and crRNA concentrations (0–48 nM).

2.10 Sensitivity and specificity of one-tube and two-step RPA-Cas13a

To compare the minimal LoD of these two approaches, the extracted *P. aeruginosa* nucleic acids are employed as a template to dilute a series of gradients 10 times, resulting in distinct concentration standards. The gradient diluted dsDNA standards were detected using the one-tube and two-step RPA-Cas13a methods. We used qRT-PCR as the reference test, which was conducted according to the guidelines provided in the following section. The specificity of the one-tube and two-step RPA-Cas13a methods was tested by using the genomes extracted from *P. aeruginosa*, *S. aureus* ATCC 6538P, *E. coli* ATCC 8739, *V. parahaemolyticus* ATCC 17802, *S. enterica* ATCC 9115,

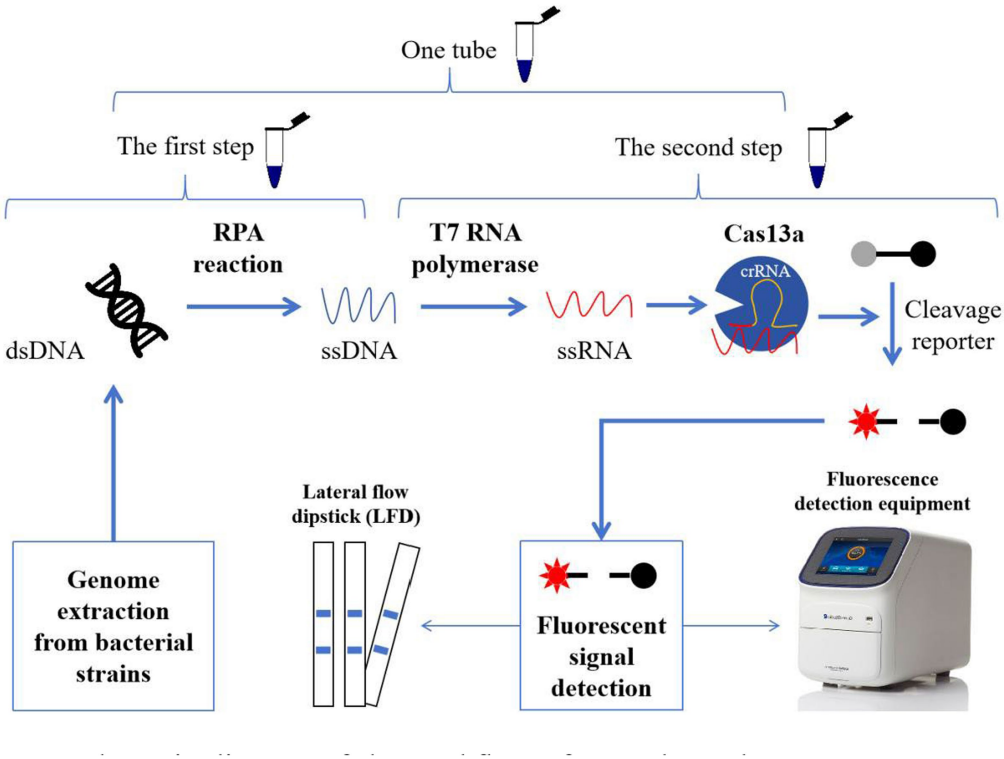

FIGURE 1
Schematic diagram of the workflow of one-tube and two-step RPA-Cas13a detection methods. In the two-step process, the extracted genomes from bacterial strains were introduced to the RPA reaction to amplify the targeted sequences (ssDNA). And then, the acquired ssDNAs were translated into ssRNA using T7 RNA polymerase. Cas13a activity was initiated when the target sequences in ssRNA were identified by crRNA. Meanwhile, the active Cas13a exhibits the auxiliary cleavage activity to cleave the RNA fluorescence probe, which could be detected by fluorescence detection equipment (fluorescence quantitative PCR instrument or enzyme-linked immunosorbent assay instrument) or LFD. If the first and second steps were performed in one tube, we referred to this as one-tube RPA-Cas13a detection method.

K. pneumoniae ATCC 4352, *L. paracasei* ATCC 334, *B. paracaeniformis* ATCC 9945, and *B. subtilis* DSM 23778.

2.11 Verification of RPA-Cas13a using industrial products

In our laboratory, 38 *P. aeruginosa* were previously isolated from industrial products (spoiled daily chemical products and coatings; Supplementary Table 1). To validate the usefulness and practicality of the RPA-Cas13a assay, nucleic acids from these real specimens were extracted and detected using the one-tube and two-step RPA-Cas13a assay methods mentioned above. Meanwhile, qRT-PCR and PCR were also employed to detect these samples, and the results were finally compared with those obtained using RPA-Cas13a.

2.12 qRT-PCR

After a 10-fold gradient dilution, the DNA template was detected using a fluorescence quantitative PCR kit (TaKaRa). The reaction mixture contains 10 μL 2 × ChamQ Universal SYBR qPCR Master Mix, 0.4 μL of each primer pair at 10 μM, 1 μL template DNA, and ddH_2O to 20.0 μL. qRT-PCR was performed on the QuantStudio™ Real-Time PCR software instrument, and the reaction was run as follows: 95°C for 30 s, followed by 40 cycles of 95°C for 10 s, and then 60°C for 30s.

2.13 PCR detection

For comparison with RPA-Cas13a, the traditional PCR was also used to amplify the targeted *mexX* gene from the strains used in this study. The following steps were taken to prepare the PCR reaction system: 5 μL 2 × Rapid Taq Master Mix (Vazyme, Nanjing, China), 0.2 μL of each primer (10 μmol/L), 4.4 μL ddH_2O, and 0.2 μL template DNA. The mixtures were subsequently subjected to 30 cycles of PCR using a PCR instrument (T100 Thermal Cycler; Bio-Rad Laboratories) with the following reaction parameters: 95°C for 5 min, 95°C for 15 s, annealing at 57°C for 15 s, and 30 s extending at 72°C. One more extension cycle at 72°C for 5 min was needed to complete the reaction.

2.14 Establishment of Cas13a lateral flow dipstick

The practical workflow for this test consists of three steps. First, the gene was amplified using RPA and translated to ssRNA. Then, this nuclease recognized crRNA and cut off the reporter molecule using its collateral cutting capability. Lastly, lateral flow dipstick assays were

performed using the identical reaction components as the fluorescent detection assays, but using 400 nM FAM-20 U-Biotin instead of the fluorescent reporter. And the reaction was incubated for 30 min at 39°C. A lateral flow dipstick (Warbio, Nanjing, China) was then inserted into the tube and incubated at room temperature for 5 min, during which the result was recorded. It was noteworthy that, whereas negative samples should only have a C line, positive samples should display two lines (T and C lines).

2.15 Statistical analysis

The Cas13a-crRNA-fluorescence test signals were recorded and expressed as the mean of at least three independent reactions plus standard deviation (SD). GraphPad Prism 9.0 was used to do the analysis of variance and create the figures.

3 Results

3.1 Feasibility analysis of LwCas13a for nucleic detection

To verify whether the LwCas13a protein exhibited the expected ribonuclease activity, a comprehensive Cas13a reaction system is developed using positive genes as the detection template. Additionally, in order to quantify fluorescence kinetics, negative and blank control groups were set up. The results demonstrated that when any of the following elements were not present in the detection system: LwCas13a, crRNA 1, or DNA/RPA product, the fluorescence signal remained essentially unchanged (Figure 2). When LwCas13a, crRNA 1, and DNA/RPA products were all present at the same time, the fluorescence signal increased noticeably, indicating that the Cas13a protein was performing its collateral cleavage activity in this circumstance (Figure 2). The fluorescence signal developed quickly over time and it only took 5 min for a single tube to react (Figure 2A), whereas the two-step method took roughly 10 min (Figure 2B). Following that, whether utilizing a single tube or a two-step procedure, the fluorescence kinetic curves approached a plateaued stage (Figure 2). These results demonstrated that the LwCas13a protein can precisely recognize target RNA and exhibits the anticipated auxiliary cleavage activity to cleave the RNA fluorescence probe in the system, resulting in a signal with high fluorescence intensity. The one-tube and two-step Cas13a fluorescence detection systems based on RPA and Cas13a have been effectively constructed.

3.2 Different crRNAs exhibit varying *mexX* detection efficiencies

According to the earlier researches, crRNA is the primary factor affecting Cas13a cleavage activity (Liu et al., 2017; Yang et al., 2023). To improve the cleavage activity of LwCas13a, 10 crRNAs targeting the *mexX* gene were designed based on the Cas13a protospacer flanking site (PFS) motif. To identify the optimal crRNA for further research, the one-tube and two-step RPA-Cas13a fluorescence assays were performed. The fluorescence signals were recorded at 1 min intervals using a QuantStudio™ Real-Time PCR. The results demonstrated that the activity of the 10 different crRNA candidates is much higher than the no-target control (Figure 3). Within 10 min, all crRNAs produced fluorescence signals. However, crRNA 7 generated the maximum fluorescence intensity in both one-tube (Figure 3A) and two-step (Figure 3B) RPA-Cas13a detection systems, implying that crRNA 7 had enhanced activity for target DNA detection. Therefore, crRNA 7 was chosen as the optimal crRNA for the subsequent one-tube and two-step RPA-Cas13a detection optimizations.

3.3 RPA-Cas13a detection system can be affected by different parameters

In the one-tube RPA-Cas13a detection system, we first evaluated the effect of temperatures (37, 38, 39, 40, and 41°C) on fluorescence excitation of probes and discovered that 39°C exhibited the greatest fluorescence signals (Figure 4A). Then, the best fluorescence signal was obtained at an RPA primer concentration of 0.4 μM at 39°C conditions (Figure 4B). At 39°C and 0.4 μM primers, the optimum LwCas13a concentration was then determined. The results demonstrated that raising the LwCas13a concentration increased the fluorescence signal from 0 to 16 nM. There was only a minor fluorescence enhancement at LwCas13a concentrations greater than 16 nM (Figure 4C). Finally, we investigated the ideal crRNA concentration at 39°C, 0.4 μM primer, and 16 nM LwCas13a. Despite using less crRNA, the fluorescence generated is equivalent to 48 nM. Thus, the optimal crRNA concentration was determined to be 36 nM (Figure 4D). As a result, for one-tube, the ideal RPA-Cas13a conditions were 39°C, 0.40 μM primer, 16 nM LwCas13, and 36 nM crRNA concentration.

We first investigated the ideal reaction temperature for the two-step RPA-Cas13a reaction using a 0.40 μM primer concentration. The fluorescent signal reaches its maximum at 39°C, which was considered as the optimal temperature (Figure 5A). At 39°C, the ideal primer concentration was 0.2 μM (Figure 5B). Meanwhile, the fluorescence signal was enhanced at LwCas13a concentration between 0 and 16 nM, and this value hardly changed when the Cas13a concentration was over 16 nM (Figure 5C). Finally, at 39°C, 0.2 μM primer concentration, and 16 nM LwCas13a concentration, we explored the optimal crRNA concentration. It generated fluorescence comparable to the concentration range of 24–48 nM (Figure 5D). Thus, we determined that 24 nM was the optimal crRNA concentration (Figure 5D). Consequently, the optimal parameters for the two-step RPA-Cas13a were 39°C, 0.2 μM primer concentration, 16 nM LwCas13a, and 24 nM crRNA.

3.4 Sensitivity of one-tube and two-step RPA-Cas13a detection systems

The DNA at a starting concentration of 100 pM was diluted 10 times with RNase-free H_2O to generate the detection concentration gradient. The sensitivity of one-tube and two-step RPA-Cas13a for *P. aeruginosa* was assessed using this gradient. The results demonstrated that the LoD for one-tube RPA-Cas13a was 10 aM (Figure 6A), slightly less than the LoD for two-step RPA-Cas13a (1 aM; Figure 6B). However, qRT-PCR exhibited a higher LoD of 100 aM (Figure 6C).

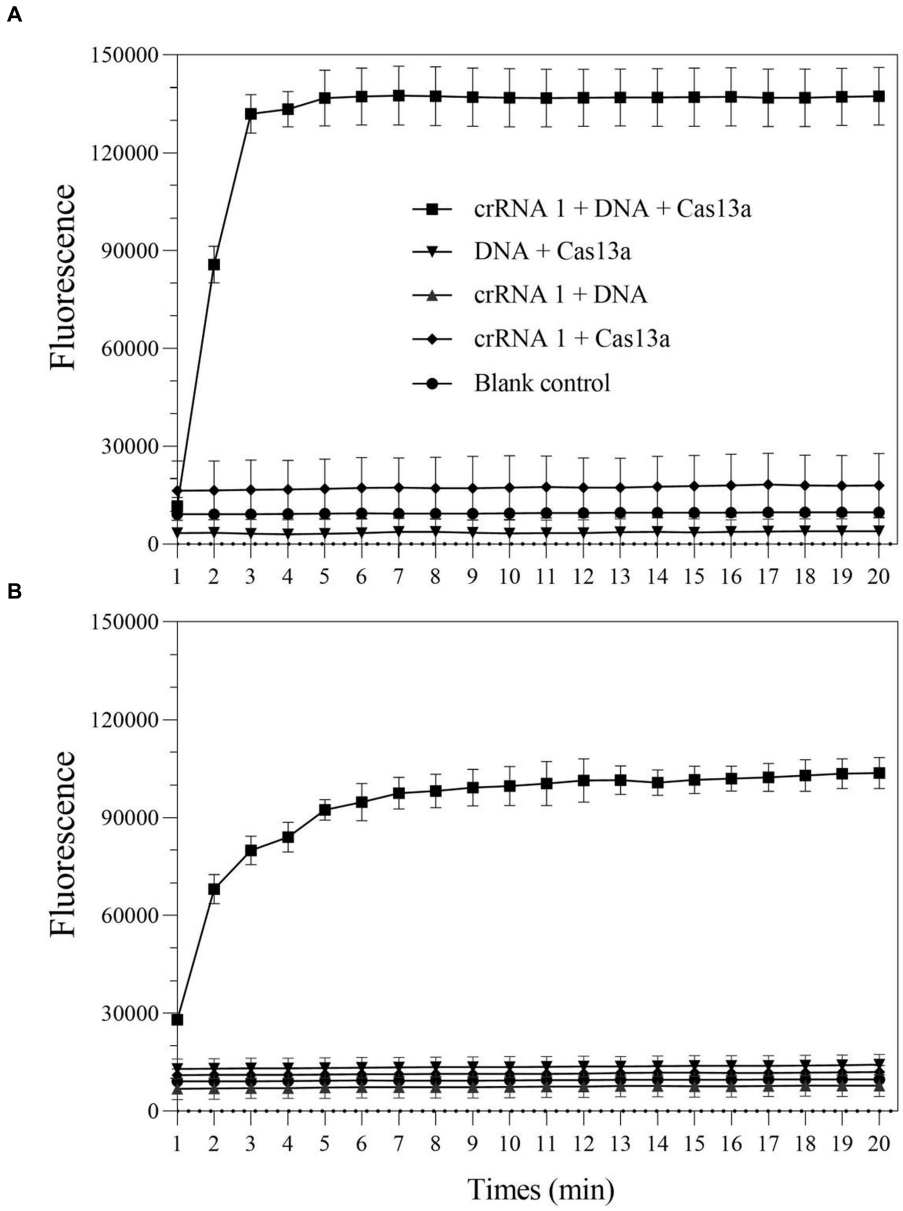

FIGURE 2
The collateral-cutting activity of CRISPR-Cas13a. **(A)** one-tube RPA-Cas13a detection; **(B)** two-step RPA-Cas13a detection.

3.5 Specificity of one-tube and two-step RPA-Cas13a detection systems

In nucleic acid testing, specificity is a fundamental issue: a suitable level of specificity improves detection accuracy by lowering false positive results and inaccurate conclusions (Antropov and Stepanov, 2023). Under optimal conditions, a particular experimental investigation was carried out to assay the degree of specificity of the RPA-Cas13a nucleic acid detection method. Only *P. aeruginosa* displayed detection signals among the nine common bacteria for specificity assessment without cross-reactions whether using one-tube (Figure 7A) or two-step RPA-Cas13a (Figure 7B). A comparable degree of specificity was also shown by qRT-PCR (Figure 7C). Thus, the target gene of *mexX* can be precisely identified using one-tube or two-step CRISPR/Cas13a-based detection method, which exhibits the same specificity as qRT-PCR.

3.6 Actual sample detection performance using RPA-Cas13a

The one-tube and two-step RPA-Cas13a methods were used to select and detect a total of 38 actual samples from various

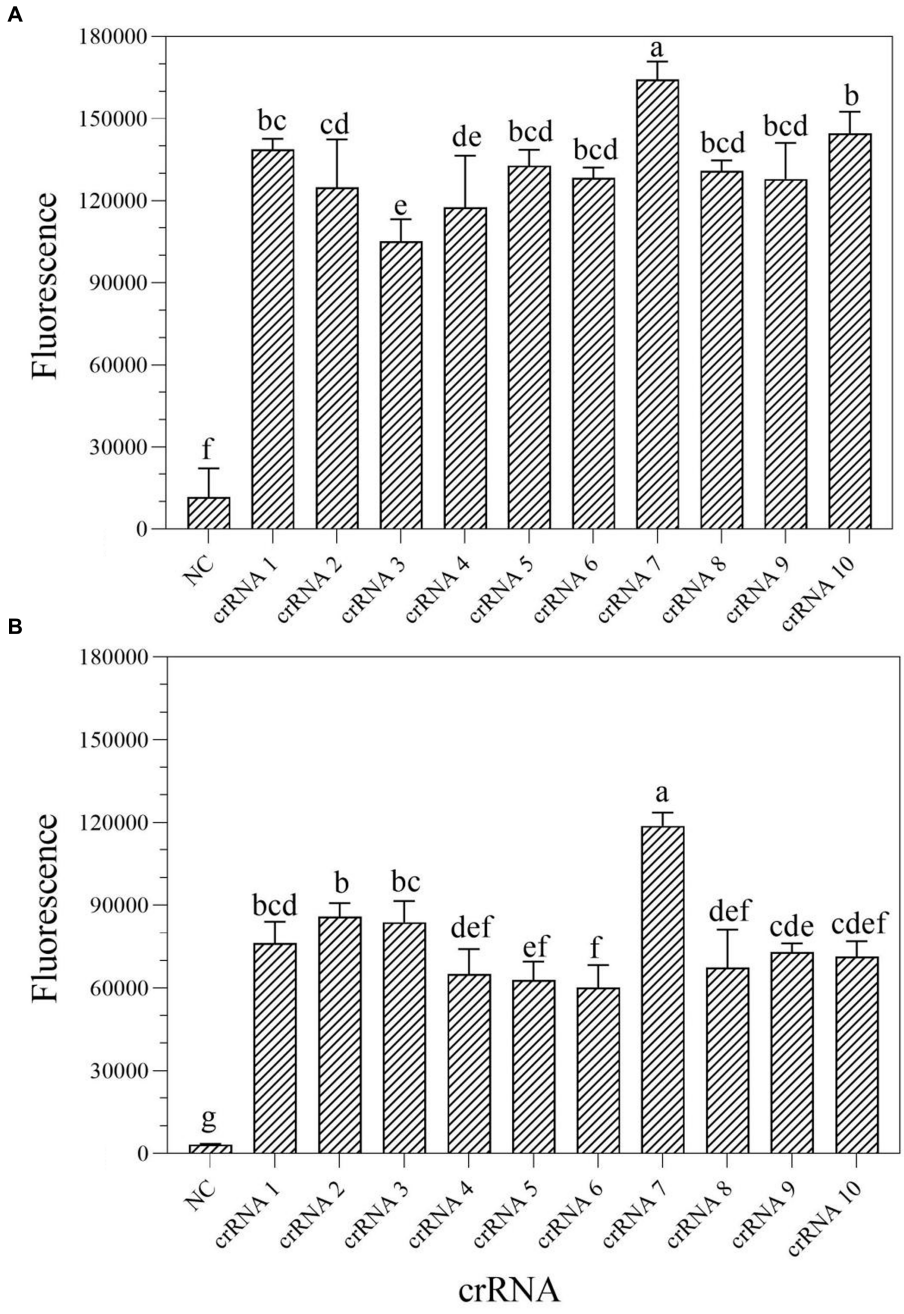

FIGURE 3
Screen of crRNAs for one-tube **(A)** and two-step **(B)** RPA-Cas13a detection systems. When Cas13a reacted with different crRNAs, all of the fluorescence signals were obtained at 10 min. All assays were performed in triplicate. Mean values and standard deviations are shown. Values with different letters are statistically different from each other for a given gene according to Fisher's LSD test ($p < 0.05$). NC, negative control.

industrial products in order to assess the applicability of these two detection methods for *P. aeruginosa* in real samples. The results demonstrated that 38 samples, using both one-tube (Figure 8A) and two-step RPA-Cas13a (Figure 8B), tested positive for the target gene of *mexX*. Additionally, qRT-PCR (Figure 8C) and traditional PCR (Figure 8D) also demonstrated the same efficiency. We conclude that the one-tube and two-step procedures exhibit high agreement with qRT-PCR and traditional PCR, suggesting that these two RPA-Cas13a detection methods could be used to real samples.

3.7 Establishment of RPA-Cas13a-LFD

To assess if the RPA-Cas13a detection method established in this study can directly apply the commercialized LFD to detect its results, a more practical and visually appealing detection strip method called RPA-Cas13a-LFD was developed. The results indicated that the initial template concentration affected the appearance of two lines and the LoD of the two-step RPA-Cas13a was 10 fM (Figure 9). The investigation demonstrated that commercial flow strips can be used to identify diagnostic results.

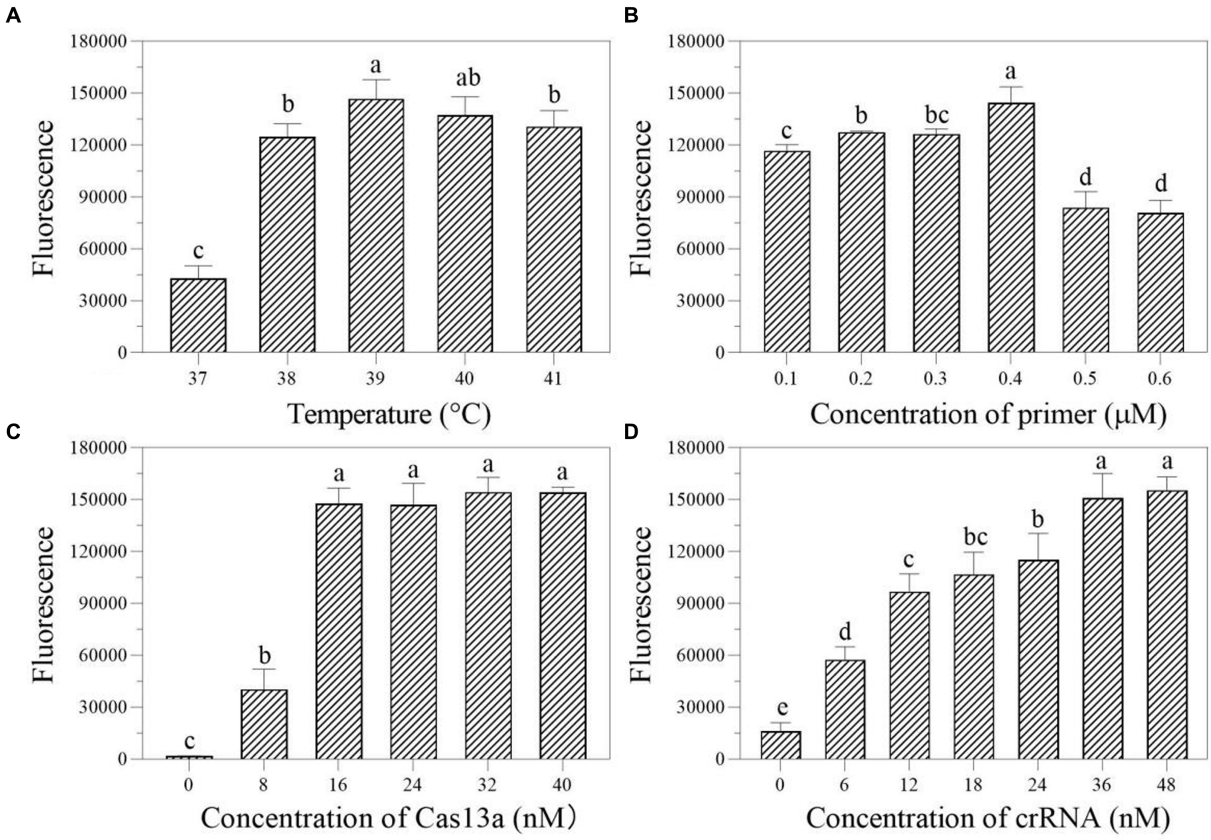

FIGURE 4
The effect of temperature (**A**; °C), primer concentration (**B**; μM), Cas13a concentration (**C**; nM), and crRNA concentration (**D**; nM) on the fluorescence in one-tube RPA-Cas13a detection system. All assays were performed in triplicate. Mean values and standard deviations are provided. Values with different letters are statistically different from each other for a given gene according to Fisher's LSD test ($p < 0.05$).

4 Discussion

Rapid, low-cost, and sensitive nucleic acid detection could help with pathogen identification, genotyping analysis, and disease monitoring at the point of care. Since the CRISPR-Cas13a-based molecular detection platform termed SHERLOCK was established with RPA in 2017 (Gootenberg et al., 2017), many research groups have attempted to optimize, improve, and extend this system. Up to now, this platform has been used to detect a number of viruses, such as syndrome coronavirus 2 (SARS-CoV-2; Cao et al., 2022; López-Valls et al., 2022; Su et al., 2022) and coronavirus disease (COVID-19). Meanwhile, CRISPR-Cas13a was also used to identify a number of bacterial strains, including *Aspergillus fumigatus* (Li et al., 2022), *Staphylococcus aureus* (Zhou et al., 2020), *Salmonella* spp. (An et al., 2021), *Neisseria gonorrhoeae* (Allan-Blitz et al., 2023) and *Group B Streptococci* (GBS; Li Z. et al., 2023). Moreover, the CRISPR-Cas13a technology was also utilized to identify multiple genes, such as toxin genes in *Clostridioides difficile* (Jiang et al., 2023), the *mecA* and *clfA* genes in *methicillin-resistant S. aureus* (MRSA; Liu et al., 2023), the *blaKPC* gene in *Enterobacterales* (Liang et al., 2023), the *lcrV* gene in *Yersinia pestis* (Schultzhaus et al., 2021). Similarly, in this study, we established a one-tube and two-step RPA-Cas13a platform (Figure 1) to detect the *mexX* gene from *P. aeruginosa*, with respectable sensitivity and reasonable specificity.

Several factors can influence the efficacy of one-tube and two-step RPA-Cas13a detection methods, including the reagent buffer used and the sequence of the RNA reporter (Gootenberg et al., 2018), as well as the concentration of Cas13a and used crRNA, reaction temperature, and RNA report probe concentration (Hu et al., 2022; Huang et al., 2022). The results of this study show that while the ideal crRNA, reaction temperature, and Cas13a concentrations of one-tube and two-step RPA-Cas13a techniques remain consistent, the optimal primer and crRNA concentrations varied somewhat between these two methods (Figures 3–5). Similar results were also discovered in prior references, which indicated that the optimal temperature and primer concentration for the one-tube and two-step methods are the same (An et al., 2021). The fundamental cause of the differences in optimum reaction conditions between this study and previous findings is the concentration of individual reagents in the systems, such as RNase inhibitors and total buffer. More diluted primer concentrations were found to improve both raw signal and quantitative accuracy in two methods, indicating that the reaction does not saturate at lower primer concentrations (Gootenberg et al., 2018). When it is insufficient, many Cas enzymes are unable to bind to crRNA to form complexes, leaving

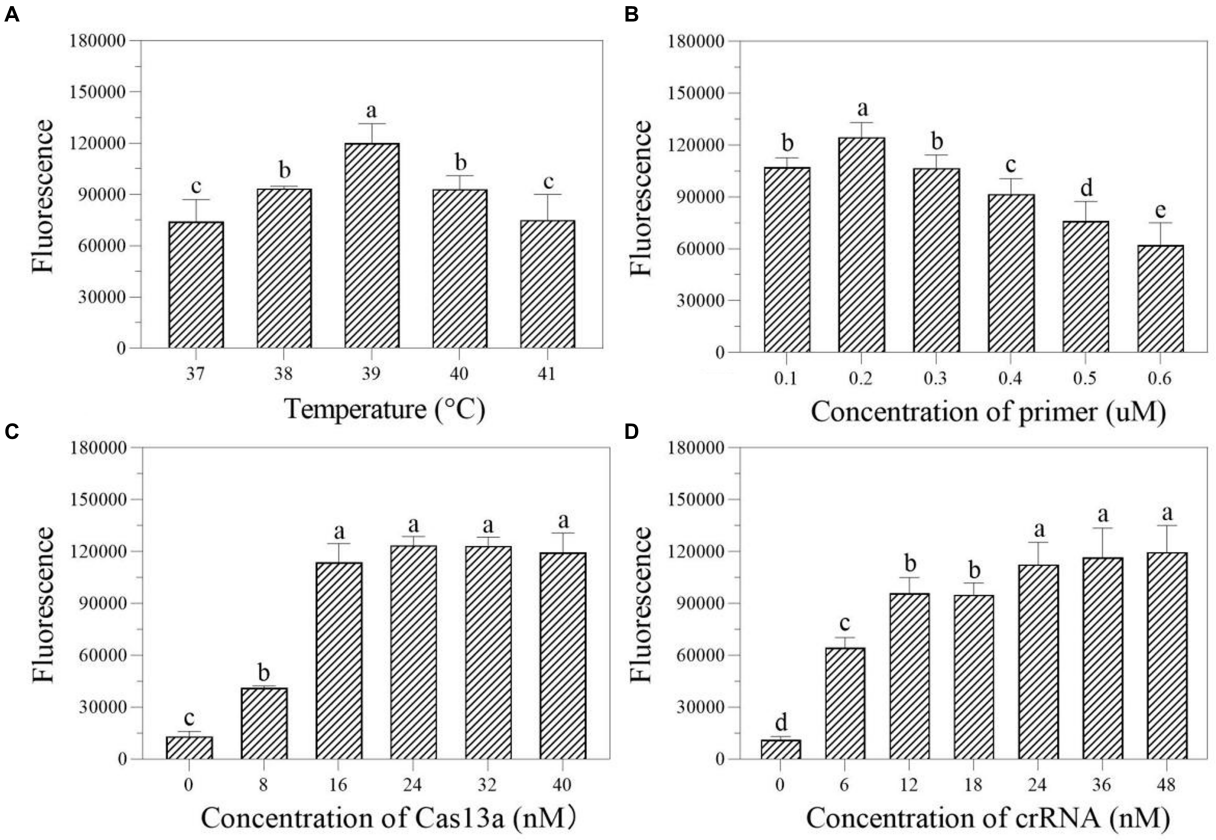

FIGURE 5
The effect of temperature (**A**; °C), primer concentration (**B**; μM), Cas13a concentration (**C**; nM), and crRNA concentration (**D**; nM) on the fluorescence in two-step RPA-Cas13a detection system. All assays were performed in triplicate. Mean values and standard deviations are shown. Values with different letters are statistically different from each other for a given gene according to Fisher's LSD test ($p < 0.05$).

only a small number of active Cas enzymes, reducing the reaction's efficiency (Hu et al., 2022). The Cas13a nuclease was fully activated throughout the system since the Cas13a concentration selected following the optimization of the two methods was the same (16 nM; Figures 4, 5), indicating that this concentration is sufficient to cut the RNA probe.

In this study, the LoD of the RPA-Cas13a platform can reach the fM or even aM level (Figure 6), which is comparable to or greater than previous studies. For example, the LoDs for hemagglutinin (HA) and neuraminidase (NA) genes of the H7N9 virus are 1 fM (Liu et al., 2019). Max J. Kellner detected synthetic DNA with a LoD of 20 aM (Kellner et al., 2019). In this study, one-tube and two-step RPA-Cas13a detection methods can detect DNA targets at concentrations as low as 10 aM (Figure 6A) and 1 aM (Figure 6B), respectively. Obviously, the sensitivity of the two-step RPA-Cas13a method is higher than that of the one-tube method in these two methods, which is consistent with the discoveries of An et al. (2021) and Arizti-Sanz et al. (2020).

The one-step method reduces nucleic acid detection sensitivity, owing to certain components of the CRISPR reagent buffer that limit nucleic acid amplification (Arizti-Sanz et al., 2020). For instance, magnesium ions in the CRISPR-Cas buffer may have an effect on the RPA reaction, reducing or stopping the RPA reaction's ability to replicate. Furthermore, the Cas13a enzyme can identify and specifically cleave sample nucleic acid during the RPA amplification in conjunction with Cas13a detection, reducing the efficiency of the nucleic acid amplification and thus the sensitivity and detection efficiency (Wang et al., 2019). Moreover, the T7 RNA polymerase in the CRISPR-Cas13a reagent can impair the efficiency of the RPA-amplified dsDNA to ssRNA, hence hindering the nucleic acid amplification step. They fundamentally reduce the sensitivity and detection efficacy of the one-tube RPA-Cas13a technique. In the conventional two-step SHERLOCK test, transcription is separated from the RPA amplification reaction, allowing complete independence and unrestricted access to the use of their dsDNA templates (Hu et al., 2022). Additionally, the efficiency of RPA amplification and Cas13a's cutting capability are the primary determinants influencing RPA-Cas13a's sensitivity (Gootenberg et al., 2017).

In addition, the one-tube and two-step RPA-Cas13a detection methods reported in this study demonstrated strong specificity (Figure 7), and these two methods can reliably detect real samples (Figure 8). Using recombinase-aided amplification SHERLOCK

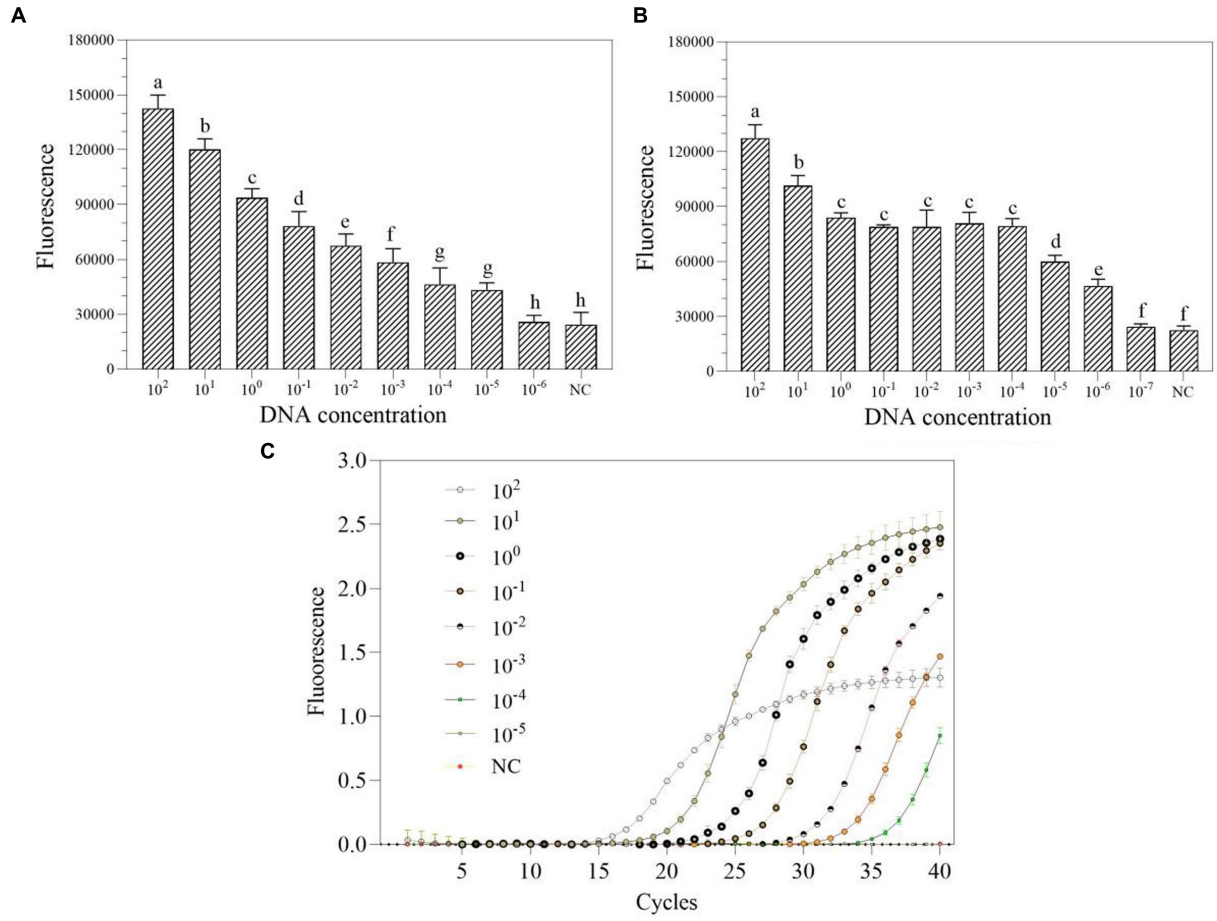

FIGURE 6
The sensitivity of one-tube **(A)** and two-step **(B)** RPA-Cas13a detection systems as well as real-time PCR **(C)**. 10^{2}–10^{-7} (pM) represented the concentration of *P. aeruginosa* DNA standards. All assays were performed in triplicate. Mean values and standard deviations are shown. Values with different letters are statistically different from each other for a given gene according to Fisher's LSD test ($p < 0.05$). NC, negative control.

(RAA-SHERLOCK) with a lateral-flow report, the African swine fever virus (ASFV) was successfully identified and this assay demonstrated excellent ASFV specificity, no reactivity with other swine viruses, and 100% concordance with the PCR data (Wei et al., 2022). To detect smoke mold, this two-step RPA-SHERLOCK method is also used. Compared to other molds, only the genes of tobacco mold and the plasmid DNA containing target sequences can be detected with higher specificity (Li et al., 2022). There was no discernible difference between the PCR and CRISPR methods (Li et al., 2022). In this study, we also found that the typical PCR method showed identical results with RPA-Cas13a methods in the detection of actual samples (Figure 8). Finally, since fluorescence detection is frequently more sensitive than LFD detection (Wang et al., 2020), the fluorescent technique developed in this work has a LoD of 1–10 aM (6×10^{-2}–6×10^{-1} copies/μL; Figure 9), which is greater than LFD detection. The Ebola and Lassa virus of LASV-II was identified using the same crRNA, which had a sensitivity of 10 copies/μL with fluorescence and 100 copies/μL with LFD (Barnes et al., 2020). In fluorescence assay of another Ebola and Lassa virus of LASV-IV in the same research, the LoD was 100 copies/μL, whereas the LFD had a LoD of 1,000 copies/μL (Barnes et al., 2020). Similar phenomena were also found in the detection of dengue virus (Gootenberg et al., 2018), Porcine Circovirus Type 4 (Wang et al., 2023), SARS-CoV-2 (Su et al., 2022), epidemic diarrhea virus (PEDV; Yin et al., 2022), and hepatitis B virus (Tian et al., 2023). Even while LFD's sensitivity is slightly lower, it can evaluate detection findings directly with the human eye and eliminates the need for fluorescence detection instruments, simplifying the equipment required. Furthermore, LFD can suit the needs of rapid pathogen detection and drug resistance gene identification because its detection period takes less than an hour.

However, in this study, the RPA-Cas13a-LFD detection method of *P. aeruginosa* DNA is only appropriate for the two-step RPA-Cas13a (Figure 9). The one-tube SHERLOCK formulation is an extremely complex and packed molecular system with numerous enzymes in its reaction components (Li H. et al., 2023). For the RPA reaction, a polymer known as polyethylene glycol (PEG) is required for the RPA reaction, which creates a crowded and extremely sticky environment for the RPA protease,

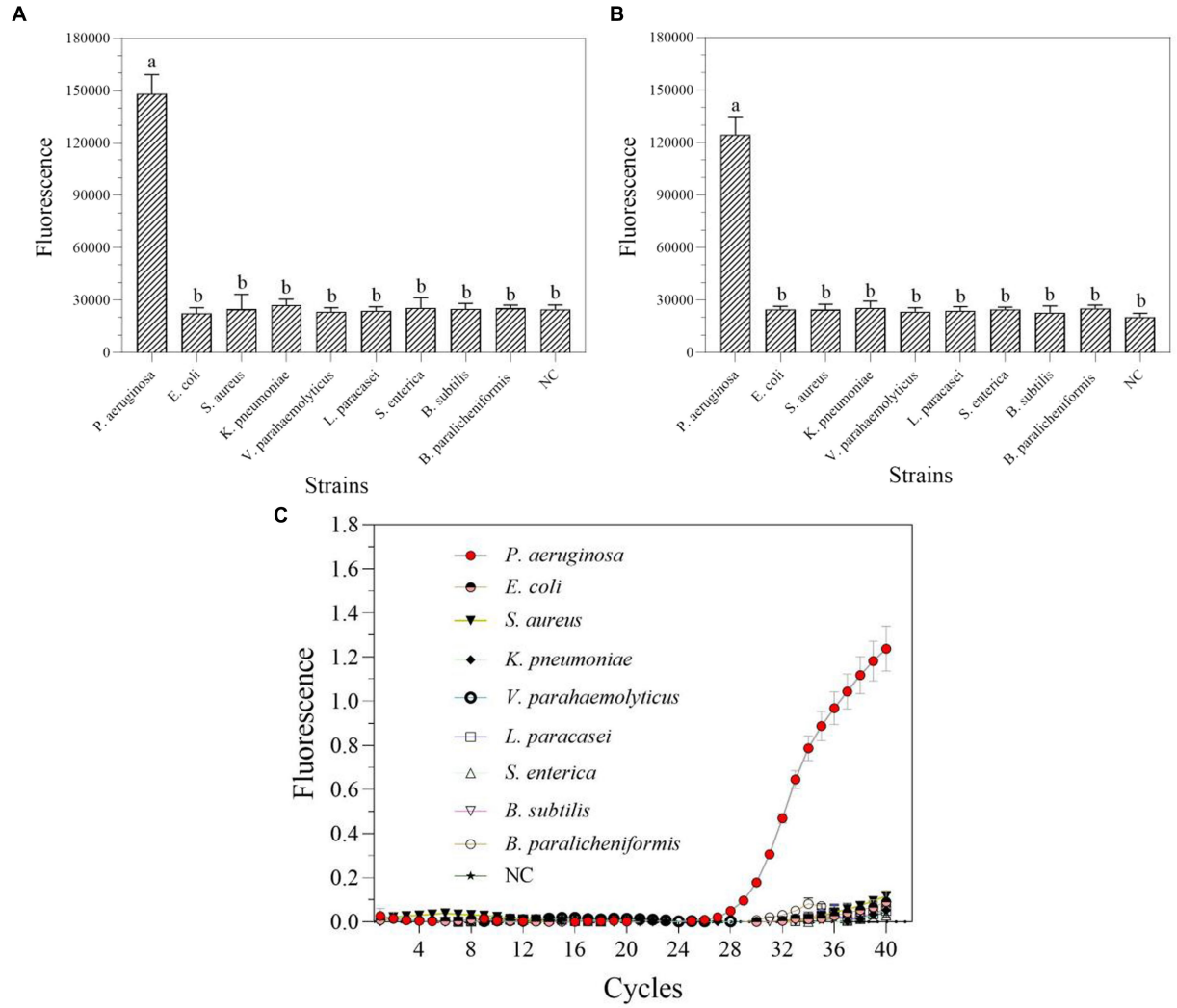

FIGURE 7
The specificity of one-tube **(A)** and two-step **(B)** RPA-Cas13a detection systems as well as real-time PCR **(C)**. All assays were performed in triplicate. Mean values and standard deviations are shown. Values with different letters are statistically different from each other for a given gene according to Fisher's LSD test ($p < 0.05$). NC, negative control.

interfering with the flow of other components in the experiments and being detrimental for other enzyme activities. Although the higher viscosity of the reaction solution has no effect on the fluorescent signal rising speed, PEG has impeded the flow of different components within the test strip, significantly impacting the one-step lateral flow dipstick method (Arizti-Sanz et al., 2022). To reduce viscosity, some groups employed one lyophilized pellet from the DNA constant temperature rapid amplification kit, which yielded approximately five individual reactions (Miao et al., 2023). In addition, a novel one-tube method SHERCOK was also exploited to deal with the viscosity (Xiong et al., 2022; Liu et al., 2023). Although this method reduces the risk of sample contamination and maintains detection sensitivity (Xiong et al., 2022; Liu et al., 2023), it is essentially a two-step method of SHERCOK in a strict sense. In subsequent work, we will investigate strategies to overcome the problems given by enzyme incompatibility and the crowding effect of one-tube molecular detection, thereby making the one-step RPA-Cas13a determination method a simple, dependable, and stable diagnostic tool.

5 Conclusion

In this study, *mexX* gene of *P. aeruginosa* was successfully detected using a one-tube and two-step RPA-Cas13a technique with reasonable specificity and sensitivity as well as lower LoD. Meanwhile, temperature, reaction time, RPA primer concentration, crRNA type and concentration all have effects on these two detection methods. In addition, a lateral flow strip measurement was also established to make this RPA-Cas13a nucleic acid detection platform rapid, affordable, and visually appealing. These platforms also demonstrate that they can detect target genes swiftly at a constant temperature of 39°C, indicating their potential for instantaneous detection. Overall, these platforms eliminate the requirement for specialized detection

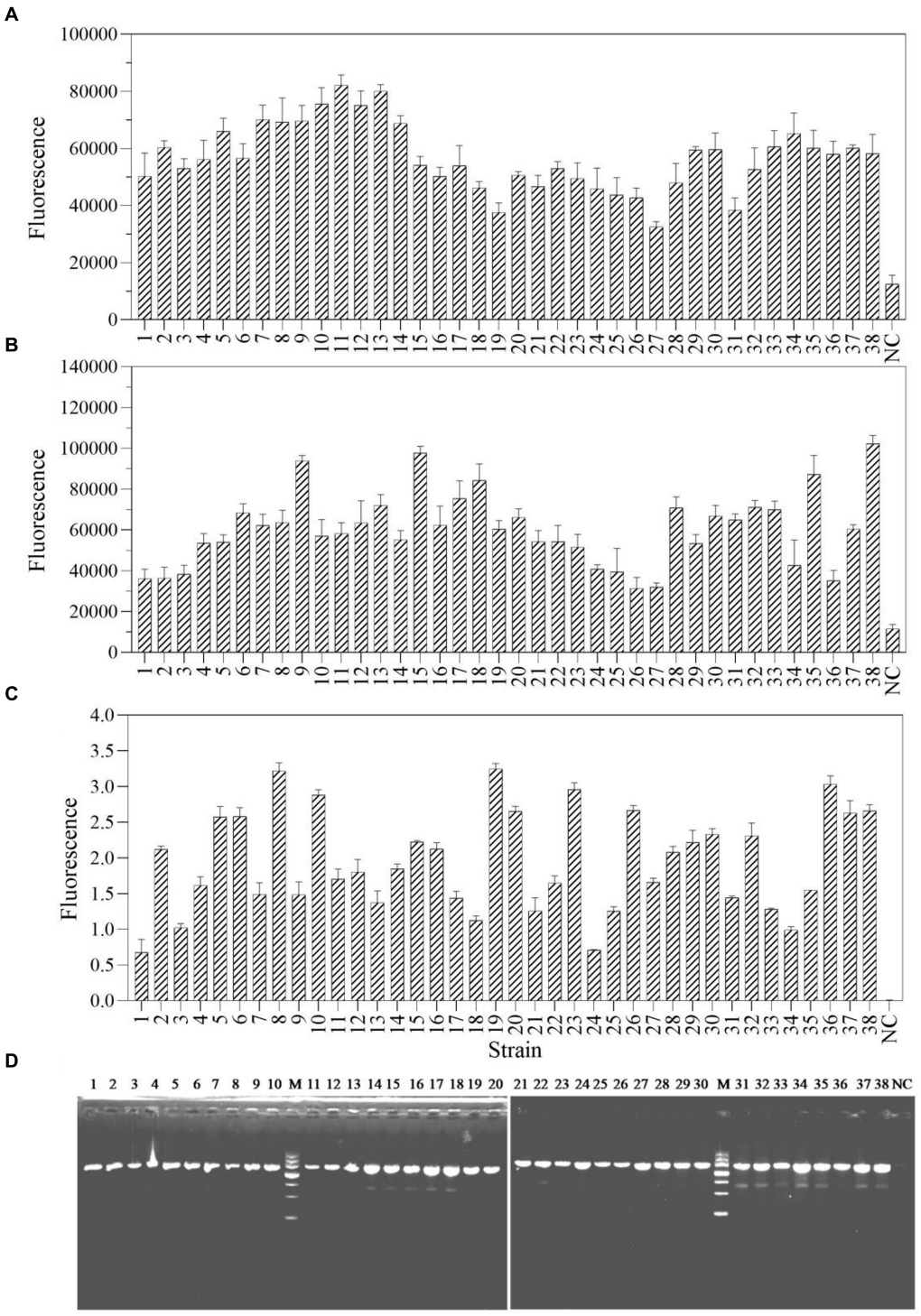

FIGURE 8
The sample consistency of four different detection methods: one-tube RPA-Cas13a **(A)**, two-step RPA-Cas13a **(B)**, qRT-PCR **(C)** at the 40 cycles, and traditional PCR **(D)**. M: DNA marker III, Tiangen Biotech Co. Ltd., China (from bottom to top: 200 bp, 500 bp, 800 bp, 1,200 bp, 2,000 bp, 3,000 bp, and 4,500 bp). NC, negative control.

instruments while also making the process of detecting bacterial resistance genes easier, indicating a promising prospect for monitoring bacterial resistance on site and preventing the spread of drug-resistant microorganisms on time. However, the nucleic acid in bacterial sample must be extracted prior to detection, which necessitates the use of centrifuges and other equipment, complicating the detection procedure. Therefore, the primary focus of future research on this method should be on sample front processing technology to allow rapid environmental sample detection.

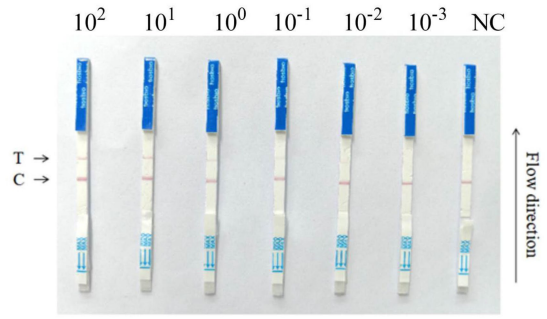

FIGURE 9
RPA-Cas13a-LFD detection of the *P. aeruginosa* DNA at various concentrations. 10-fold serial dilution of target DNA was used as the detection template. A RPA-Cas13a-LFD assay for on-site detection was developed using RPA, LwCas13a, and LFD. A biotin-tagged FAM-RNA reporter was used to create the LFD. For the negative control, an anti-FAM antibody-gold nanoparticle was conjugated to the FAM-RNA-biotin reporter, and the conjugation was intercepted by a biotin ligand at the control line. For the positive control, the FAM-RNA-biotin reporter was cleaved, and the anti-FAM antibody-gold nanoparticle conjugate accumulated at the test line. The two-step RPA-Cas13a-LFD detection reactions were performed using the following LoDs: 100 pM, 10 pM, 1 pM, 100 fM, 10 fM, 1 fM; NC, negative control; T, test line; C, control line.

Data availability statement

The original contributions presented in the study are included in the article/Supplementary material, further inquiries can be directed to the corresponding authors.

Author contributions

X-XZ: Writing – original draft, Investigation, Methodology. Y-SW: Formal analysis, Methodology, Writing – review & editing. S-JL: Methodology, Resources, Writing – review & editing. R-QP: Methodology, Resources, Writing – review & editing. XW: Methodology, Resources, Writing – review & editing. HP: Data curation, Methodology, Writing – review & editing. Q-SS: Supervision, Visualization, Writing – review & editing. GZ: Formal analysis, Supervision, Validation, Writing – review & editing. X-BX: Supervision, Visualization, Writing – review & editing. JW: Supervision, Validation, Visualization, Writing – review & editing.

Funding

The author(s) declare financial support was received for the research, authorship, and/or publication of this article. This work was funded by the Research and Development Plan in Key Areas of Guangdong Province (No. 2022B1111040002), Key-Area Research and Development Program of Guangdong Province (Nos. 2020B020226008, 2022B0202040002, and 2018B020206001), Guangdong Basic and Applied Basic Research Foundation (No. 2023A1515030059), Natural Science Foundation of Guangdong Province (No. 2023A1515012057), and GDAS' Project of Science and Technology Development (No. 2022GDASZH-2022010202).

Conflict of interest

The authors declare that the research was conducted in the absence of any commercial or financial relationships that could be construed as a potential conflict of interest.

Publisher's note

All claims expressed in this article are solely those of the authors and do not necessarily represent those of their affiliated organizations, or those of the publisher, the editors and the reviewers. Any product that may be evaluated in this article, or claim that may be made by its manufacturer, is not guaranteed or endorsed by the publisher.

Supplementary material

The Supplementary material for this article can be found online at: https://www.frontiersin.org/articles/10.3389/fmicb.2024.1341179/full#supplementary-material

SUPPLEMENTARY TABLE 1
The related information of actual samples from industrial settings.

References

Abramova, A., Berendonk, T. U., and Bengtsson-Palme, J. (2023). A global baseline for qPCR-determined antimicrobial resistance gene prevalence across environments. *Environ. Int.* 178:108084. doi: 10.1016/j.envint.2023.108084

Abudayyeh, O. O., Gootenberg, J. S., Konermann, S., Joung, J., Slaymaker, I. M., Cox, D. B., et al. (2016). C2c2 is a single-component programmable RNA-guided RNA-targeting CRISPR effector. *Science* 353:aaf5573. doi: 10.1126/science.aaf5573

Allan-Blitz, L. T., Shah, P., Adams, G., Branda, J. A., Klausner, J. D., Goldstein, R., et al. (2023). Development of Cas13a-based assays for *Neisseria gonorrhoeae* detection and gyrase a determination. *mSphere.* 8:e41623. doi: 10.1128/msphere.00416-23

An, B., Zhang, H., Su, X., Guo, Y., Wu, T., Ge, Y., et al. (2021). Rapid and sensitive detection of *Salmonella spp.* using CRISPR-Cas13a combined with recombinase polymerase amplification. *Front. Microbiol.* 12:732426. doi: 10.3389/fmicb.2021.732426

Antropov, D. N., and Stepanov, G. A. (2023). Molecular mechanisms underlying CRISPR/Cas-based assays for nucleic acid detection. *Curr. Issues Mol. Biol.* 45, 649–662. doi: 10.3390/cimb45010043

Arizti-Sanz, J., Bradley, A., Zhang, Y. B., Boehm, C. K., Freije, C. A., Grunberg, M. E., et al. (2022). Simplified Cas13-based assays for the fast identification of SARS-CoV-2 and its variants. *Nat. Biomed. Eng.* 6, 932–943. doi: 10.1038/s41551-022-00889-z

Arizti-Sanz, J., Freije, C. A., Stanton, A. C., Petros, B. A., Boehm, C. K., Siddiqui, S., et al. (2020). Streamlined inactivation, amplification, and Cas13-based detection of SARS-CoV-2. *Nat. Commun.* 11:5921. doi: 10.1038/s41467-020-19097-x

Avakh, A., Grant, G. D., Cheesman, M. J., Kalkundri, T., and Hall, S. (2023). The art of war with *Pseudomonas aeruginosa*: targeting Mex efflux pumps directly to strategically enhance antipseudomonal drug efficacy. *Antibiotics-Basel.* 12:1304. doi: 10.3390/antibiotics12081304

Barnes, K. G., Lachenauer, A. E., Nitido, A., Siddiqui, S., Gross, R., Beitzel, B., et al. (2020). Deployable CRISPR-Cas13a diagnostic tools to detect and report Ebola and Lassa virus cases in real-time. *Nat. Commun.* 11:4131. doi: 10.1038/s41467-020-17994-9

Boolchandani, M., D'Souza, A. W., and Dantas, G. (2019). Sequencing-based methods and resources to study antimicrobial resistance. *Nat. Rev. Genet.* 20, 356–370. doi: 10.1038/s41576-019-0108-4

Cao, G., Huo, D., Chen, X., Wang, X., Zhou, S., Zhao, S., et al. (2022). Automated, portable, and high-throughput fluorescence analyzer (APHF-analyzer) and lateral flow strip based on CRISPR/Cas13a for sensitive and visual detection of SARS-CoV-2. *Talanta* 248:123594. doi: 10.1016/j.talanta.2022.123594

Cunrath, O., Meinel, D. M., Maturana, P., Fanous, J., Buyck, J. M., Saint, A. P., et al. (2019). Quantitative contribution of efflux to multi-drug resistance of clinical *Escherichia coli* and *Pseudomonas aeruginosa* strains. *EBioMedicine* 41, 479–487. doi: 10.1016/j.ebiom.2019.02.061

Diggle, S. P., and Whiteley, M. (2020). Microbe profile: *Pseudomonas aeruginosa*: opportunistic pathogen and lab rat. *Microbiology.* 166, 30–33. doi: 10.1099/mic.0.000860

Duan, N., Chang, B., Zhang, H., Wang, Z., and Wu, S. (2016). *Salmonella typhimurium* detection using a surface-enhanced Raman scattering-based aptasensor. *Int. J. Food Microbiol.* 218, 38–43. doi: 10.1016/j.ijfoodmicro.2015.11.006

Eichenberger, E. M., and Thaden, J. T. (2019). Epidemiology and mechanisms of resistance of extensively drug resistant gram-negative bacteria. *Antibiotics-Basel.* 8:37. doi: 10.3390/antibiotics8020037

Escalona-Noguero, C., López-Valls, M., and Sot, B. (2021). CRISPR/Cas technology as a promising weapon to combat viral infections. *BioEssays* 43:e2000315. doi: 10.1002/bies.202000315

Gao, S., Liu, J., Li, Z., Ma, Y., and Wang, J. (2021). Sensitive detection of foodborne pathogens based on CRISPR-Cas13a. *J. Food Sci.* 86, 2615–2625. doi: 10.1111/1750-3841.15745

Gellatly, S. L., and Hancock, R. E. (2013). *Pseudomonas aeruginosa*: new insights into pathogenesis and host defenses. *Pathog. Dis.* 67, 159–173. doi: 10.1111/2049-632X.12033

Gootenberg, J. S., Abudayyeh, O. O., Kellner, M. J., Joung, J., Collins, J. J., and Zhang, F. (2018). Multiplexed and portable nucleic acid detection platform with Cas13, Cas12a, and Csm6. *Science* 360, 439–444. doi: 10.1126/science.aaq0179

Gootenberg, J. S., Abudayyeh, O. O., Lee, J. W., Essletzbichler, P., Dy, A. J., Joung, J., et al. (2017). Nucleic acid detection with CRISPR-Cas13a/C2c2. *Science* 356, 438–442. doi: 10.1126/science.aam9321

He, D., Liu, G., Yang, J., Jiang, X., Wang, H., Fan, Y., et al. (2022). Specific high-sensitivity enzymatic molecular detection system termed RPA-based CRISPR-Cas13a for duck tembusu virus diagnostics. *Bioconjug. Chem.* 33, 1232–1240. doi: 10.1021/acs.bioconjchem.2c00200

Henríquez, T., Stein, N. V., and Jung, H. (2020). Resistance to bipyridyls mediated by the TtgABC efflux system in *Pseudomonas putida* KT2440. *Front. Microbiol.* 11:1974. doi: 10.3389/fmicb.2020.01974

Hu, F., Liu, Y., Zhao, S., Zhang, Z., Li, X., Peng, N., et al. (2022). A one-pot CRISPR/Cas13a-based contamination-free biosensor for low-cost and rapid nucleic acid diagnostics. *Biosens. Bioelectron.* 202:113994. doi: 10.1016/j.bios.2022.113994

Huang, F., Shan, J., Liang, K., Yang, M., Zhou, X., Duan, X., et al. (2022). A new method to detect red spotted grouper neuro necrosis virus (RGNNV) based on CRISPR/Cas13a. *Aquaculture* 555:738217. doi: 10.1016/j.aquaculture.2022.738217

Ingrid, D. C., Dana, D. D. P., Valérie, S. N. H., Possi, K. C., Leina, D. B. F., Celianthe, G., et al. (2023). Phenotypic characterization and prevalence of carbapenemase-producing *Pseudomonas aeruginosa* isolates in six health facilities in Cameroon. *BioMed.* 3, 77–88. doi: 10.3390/biomed3010006

Jiang, T., Hu, X., and Shen, J. (2023). Establishment of a novel detection platform for *Clostridioides difficile* toxin genes based on orthogonal CRISPR. *Microbiol. Spectr.* 11:e188623. doi: 10.1128/spectrum.01886-23

Kei, I., Ryo, K., Junko, T., Yoshiaki, K., and Yuji, M. (2021). Overexpression of the MexXY multidrug efflux system correlates with deficient pyoverdine production in *Pseudomonas aeruginosa*. *Antibiotics.* 10:658. doi: 10.3390/antibiotics10060658

Kellner, M. J., Koob, J. G., Gootenberg, J. S., Abudayyeh, O. O., and Zhang, F. (2019). SHERLOCK: nucleic acid detection with CRISPR nucleases. *Nat. Protoc.* 14, 2986–3012. doi: 10.1038/s41596-019-0210-2

Lee, C. H., Rimesso, G., Reynolds, D. M., Cai, J., and Baker, N. E. (2016). Whole-genome sequencing and iPLEX MassARRAY genotyping map an EMS-induced mutation affecting cell competition in *drosophila melanogaster*. *G3-Genes Genomes Genet.* 6, 3207–3217. doi: 10.1534/g3.116.029421

Li, Z., Hua, L., Xie, L., Wang, D., and Jiang, X. (2023). Automated microfluidic nucleic acid detection platform-integrated RPA-T7-Cas13a for pathogen diagnosis. *Anal. Chem.* 95, 6940–6947. doi: 10.1021/acs.analchem.3c00242

Li, H., Kielich, D., Liu, G., Smith, G., Bello, A., Strong, J. E., et al. (2023). Strategies to improve multi-enzyme compatibility and coordination in one-pot SHERLOCK. *Anal. Chem.* 95, 10522–10531. doi: 10.1021/acs.analchem.2c05032

Li, Z., Wang, M., Xu, T., Zhan, Y., Chen, F., Lin, Y., et al. (2022). Development and clinical implications of a novel CRISPR-based diagnostic test for pulmonary *Aspergillus fumigatus* infection. *J. Microbiol. Immunol. Infect.* 55, 749–756. doi: 10.1016/j.jmii.2021.11.008

Liang, M., Xiao, B., Chen, L., Huang, X., Li, J., Kuang, Z., et al. (2023). Rapid detection of Bla(KPC) in carbapenem-resistant enterobacterales based on CRISPR/Cas13a. *Curr. Microbiol.* 80:352. doi: 10.1007/s00284-023-03457-z

Liu, L., Li, X., Ma, J., Li, Z., You, L., Wang, J., et al. (2017). The molecular architecture for RNA-guided RNA cleavage by Cas13a. *Cell* 170, 714–726.e10. doi: 10.1016/j.cell.2017.06.050

Liu, Y., Liu, H., Yu, G., Sun, W., Aizaz, M., Yang, G., et al. (2023). One-tube RPA-CRISPR Cas12a/Cas13a rapid detection of methicillin-resistant *Staphylococcus aureus*. *Anal. Chim. Acta* 1278:341757. doi: 10.1016/j.aca.2023.341757

Liu, Y., Xu, H., Liu, C., Peng, L., Khan, H., Cui, L., et al. (2019). CRISPR-Cas13a nanomachine based simple technology for avian influenza a (H7N9) virus on-site detection. *J. Biomed. Nanotechnol.* 15, 790–798. doi: 10.1166/jbn.2019.2742

López-Valls, M., Escalona-Noguero, C., Rodríguez-Díaz, C., Pardo, D., Castellanos, M., Milán-Rois, P., et al. (2022). CASCADE: naked eye-detection of SARS-CoV-2 using Cas13a and gold nanoparticles. *Anal. Chim. Acta* 1205:339749. doi: 10.1016/j.aca.2022.339749

MacGregor, S. R., McManus, D. P., Sivakumaran, H., Egwang, T. G., Adriko, M., Cai, P., et al. (2023). Development of CRISPR/Cas13a-based assays for the diagnosis of schistosomiasis. *EBioMedicine* 94:104730. doi: 10.1016/j.ebiom.2023.104730

Manghwar, H., Lindsey, K., Zhang, X., and Jin, S. (2019). CRISPR/Cas system: recent advances and future prospects for genome editing. *Trends Plant Sci.* 24, 1102–1125. doi: 10.1016/j.tplants.2019.09.006

Miao, J., Zuo, L., He, D., Fang, Z., Berthet, N., Yu, C., et al. (2023). Rapid detection of Nipah virus using the one-pot RPA-CRISPR/Cas13a assay. *Virus Res.* 332:199130. doi: 10.1016/j.virusres.2023.199130

Morita, Y., Kimura, N., Mima, T., Mizushima, T., and Tsuchiya, T. (2001). Roles of MexXY- and MexAB-multidrug efflux pumps in intrinsic multidrug resistance of *Pseudomonas aeruginosa* PAO1. *J. Gen. Appl. Microbiol.* 47, 27–32. doi: 10.2323/jgam.47.27

Niu, J. L., Peng, J. J., Ming, Y. Y., Ma, Q. C., Liu, W. C., and Ma, Y. (2020). Identification of drug resistance genes and drug resistance analysis of *Salmonella* in the duck farm environment of Zhanjiang. *China. Environ. Sci. Pollut. Res.* 27, 24999–25008. doi: 10.1007/s11356-020-09007-5

Paul, M., Carrara, E., Retamar, P., Tängdén, T., Bitterman, R., Bonomo, R. A., et al. (2022). European society of clinical microbiology and infectious diseases (ESCMID) guidelines for the treatment of infections caused by multidrug-resistant gram-negative bacilli (endorsed by European society of intensive care medicine). *Clin. Microbiol. Infect.* 28, 521–547. doi: 10.1016/j.cmi.2021.11.025

Pesingi, P. V., Singh, B. R., Pesingi, P. K., Bhardwaj, M., Singh, S. V., Kumawat, M., et al. (2019). MexAB-OprM efflux pump of *Pseudomonas aeruginosa* offers resistance to carvacrol: a herbal antimicrobial agent. *Front. Microbiol.* 10:2664. doi: 10.3389/fmicb.2019.02664

Ranjbar, R., and Alam, M.Antimicrobial Resistance Collaborators (2024). Global burden of bacterial antimicrobial resistance in 2019: a systematic analysis. *Evid Based Nurs* 27:16. doi: 10.1136/ebnurs-2022-103540

Schultzhaus, Z., Wang, Z., and Stenger, D. (2021). Systematic analysis, identification, and use of CRISPR/Cas13a-associated crRNAs for sensitive and specific detection of the lcrV gene of *Yersinia pestis*. *Diagn. Microbiol. Infect. Dis.* 99:115275. doi: 10.1016/j.diagmicrobio.2020.115275

Shahid, M. F., Yaqub, T., Ali, M., Ul-Rahman, A., and Bente, D. A. (2021). Prevalence and phylogenetic analysis of Crimean-Congo hemorrhagic fever virus in ticks collected from Punjab province of Pakistan. *Acta Trop.* 218:105892. doi: 10.1016/j.actatropica.2021.105892

Shi, Y., Cao, Q., Sun, J., Hu, X., Su, Z., Xu, Y., et al. (2023). The opportunistic pathogen *Pseudomonas aeruginosa* exploits bacterial biotin synthesis pathway to benefit its infectivity. *PLoS Pathog.* 19:e1011110. doi: 10.1371/journal.ppat.1011110

Silvia, D., Federica, P., Antonio, V., Roberto, G. D., and Matteo, B. (2023). Severe infections caused by difficult-to-treat gram-negative bacteria. *Curr. Opin. Crit. Care* 29, 438–445. doi: 10.1097/MCC.0000000000001074

Su, G., Zhu, M., Li, D., Xu, M., Zhu, Y., Zhang, Y., et al. (2022). Multiplexed lateral flow assay integrated with orthogonal CRISPR-Cas system for SARS-CoV-2 detection. *Sens. Actuator B-Chem.* 371:132537. doi: 10.1016/j.snb.2022.132537

Tacconelli, E., Carrara, E., Savoldi, A., Harbarth, S., Mendelson, M., Monnet, D. L., et al. (2018). Discovery, research, and development of new antibiotics: the WHO priority list of antibiotic-resistant bacteria and tuberculosis. *Lancet Infect. Dis.* 18, 318–327. doi: 10.1016/S1473-3099(17)30753-3

Tan, M., Liao, C., Liang, L., Yi, X., Zhou, Z., and Wei, G. (2022). Recent advances in recombinase polymerase amplification: principle, advantages, disadvantages and applications. *Front. Cell. Infect. Microbiol.* 12:1019071. doi: 10.3389/fcimb.2022.1019071

Teng, X., Zhang, M., Mujumdar, A. S., and Wang, H. (2022). Inhibition of nitrite in prepared dish of *Brassica chinensis* L. during storage via non-extractable phenols in hawthorn pomace: a comparison of different extraction methods. *Food Chem.* 393:133344. doi: 10.1016/j.foodchem.2022.133344

Tian, Y., Fan, Z., Xu, L., Cao, Y., Chen, S., Pan, Z., et al. (2023). CRISPR/Cas13a-assisted rapid and portable HBV DNA detection for low-level viremia patients. *Emerg. Microbes Infect.* 12:e2177088. doi: 10.1080/22221751.2023.2177088

Tsutsumi, K., Yonehara, R., Ishizaka-Ikeda, E., Miyazaki, N., Maeda, S., Iwasaki, K., et al. (2019). Structures of the wild-type MexAB-OprM tripartite pump reveal its complex formation and drug efflux mechanism. *Nat. Commun.* 10:1520. doi: 10.1038/s41467-019-09463-9

Wang, W., Wang, C., Bai, Y., Zhang, P., Yao, S., Liu, J., et al. (2020). Establishment of reverse transcription recombinase-aided amplification-lateral-flow dipstick and real-time fluorescence-based reverse transcription recombinase-aided amplification methods for detection of the Newcastle disease virus in chickens. *Poult. Sci.* 99, 3393–3401. doi: 10.1016/j.psj.2020.03.018

Wang, B., Wang, R., Wang, D., Wu, J., Li, J., Wang, J., et al. (2019). Cas12aVDet: a CRISPR/Cas12a-based platform for rapid and visual nucleic acid detection. *Anal. Chem.* 91, 12156–12161. doi: 10.1021/acs.analchem.9b01526

Wang, J., Zhu, X., Yin, D., Cai, C., Liu, H., Yang, Y., et al. (2023). Rapid and easy-read porcine circovirus type 4 detection with CRISPR-Cas13a-based lateral flow strip. *Microorganisms.* 11:354. doi: 10.3390/microorganisms11020354

Wei, N., Zheng, B., Niu, J., Chen, T., Ye, J., Si, Y., et al. (2022). Rapid detection of genotype II african swine fever virus using CRISPR Cas13a-based lateral flow strip. *Viruses* 14:179. doi: 10.3390/v14020179

Williams, A. J., Cooper, W. M., Ramsaroop, S., Alusta, P., Buzatu, D. A., and Wilkes, J. G. (2017). Rapid flow cytometry detection of a single viable *Escherichia coli* O157:H7 cell in raw spinach using a simplified sample preparation technique. *Front. Microbiol.* 8:1493. doi: 10.3389/fmicb.2017.01493

Wu, X., Yang, L., Wu, Y., Li, H., and Shao, B. (2023). Spread of multidrug-resistant *Pseudomonas aeruginosa* in animal-derived foods in Beijing. *China. Int. J. Food Microbiol.* 403:110296. doi: 10.1016/j.ijfoodmicro.2023.110296

Xiong, Y., Cao, G., Chen, X., Yang, J., Shi, M., Wang, Y., et al. (2022). One-pot platform for rapid detecting virus utilizing recombinase polymerase amplification and CRISPR/Cas12a. *Appl. Microbiol. Biotechnol.* 106, 4607–4616. doi: 10.1007/s00253-022-12015-9

Yang, L., Zhang, Y., Yi, W., Dong, X., Niu, M., Song, Y., et al. (2023). A rapid and efficient platform for antiviral crRNA screening using CRISPR-Cas13a-based nucleic acid detection. *Front. Immunol.* 14:1116230. doi: 10.3389/fimmu.2023.1116230

Yin, D., Yin, L., Guo, H., Wang, J., Shen, X., Zhao, R., et al. (2022). Visual detection and differentiation of porcine epidemic diarrhea virus wild-type strains and attenuated vaccine strains using CRISPR/Cas13a-based lateral flow strip. *Front. Cell. Infect. Microbiol.* 12:976137. doi: 10.3389/fcimb.2022.976137

Zhao, L., Qiu, M., Li, X., Yang, J., and Li, J. (2022). CRISPR-Cas13a system: a novel tool for molecular diagnostics. *Front. Microbiol.* 13:1060947. doi: 10.3389/fmicb.2022.1060947

Zhou, J., Yin, L., Dong, Y., Peng, L., Liu, G., Man, S., et al. (2020). CRISPR-Cas13a based bacterial detection platform: sensing pathogen *Staphylococcus aureus* in food samples. *Anal. Chim. Acta* 1127, 225–233. doi: 10.1016/j.aca.2020.06.041

frontiers | Frontiers in Microbiology

TYPE Original Research
PUBLISHED 09 February 2024
DOI 10.3389/fmicb.2024.1322758

OPEN ACCESS

EDITED BY
Guneet Kaur,
University of Guelph, Canada

REVIEWED BY
Francesco Fancello,
University of Sassari, Italy
Arun Karnwal,
Lovely Professional University, India

*CORRESPONDENCE
M. Y. Sreenivasa
✉ sreenivasamy@gmail.com;
✉ mys@microbiology.uni-mysore.ac.in

RECEIVED 16 October 2023
ACCEPTED 15 January 2024
PUBLISHED 09 February 2024

CITATION
Vasundaradevi R, Sarvajith M, Somashekaraiah R, Gunduraj A and Sreenivasa MY (2024) Antagonistic properties of *Lactiplantibacillus plantarum* MYSVB1 against *Alternaria alternata*: a putative probiotic strain isolated from the banyan tree fruit. *Front. Microbiol.* 15:1322758. doi: 10.3389/fmicb.2024.1322758

Antagonistic properties of *Lactiplantibacillus plantarum* MYSVB1 against *Alternaria alternata*: a putative probiotic strain isolated from the banyan tree fruit

R. Vasundaradevi, M. Sarvajith, Rakesh Somashekaraiah, Adithi Gunduraj and M. Y. Sreenivasa*

Applied Mycology Laboratory, Department of Studies in Microbiology, University of Mysore, Mysuru, India

Alternaria alternata, a notorious phytopathogenic fungus, has been documented to infect several plant species, leading to the loss of agricultural commodities and resulting in significant economic losses. Lactic acid bacteria (LAB) hold immense promise as biocontrol candidates. However, the potential of LABs derived from fruits remains largely unexplored. In this study, several LABs were isolated from tropical fruit and assessed for their probiotic and antifungal properties. A total of fifty-five LABs were successfully isolated from seven distinct fruits. Among these, seven isolates showed inhibition to growth of *A. alternata*. Two strains, isolated from fruits: *Ficus benghalensis*, and *Tinospora cordifolia* exhibited promising antifungal properties against *A. alternata*. Molecular identification confirmed their identities as *Lactiplantibacillus plantarum* MYSVB1 and MYSVA7, respectively. Both strains showed adaptability to a wide temperature range (10–45°C), and salt concentrations (up to 7%), with optimal growth around 37 °C and high survival rates under simulated gastrointestinal conditions. Among these two strains, *Lpb. plantarum* MYSVB1 demonstrated significant inhibition ($p < 0.01$) of the growth of *A. alternata*. The inhibitory effects of cell-free supernatant (CFS) were strong, with 5% crude CFS sufficient to reduce fungal growth by >70% and complete inhibition by 10% CFS. Moreover, the CFS was inhibitory for both mycelial growth and conidial germination. CFS retained its activity even after long cold storage. The chromatographic analysis identified organic acids in CFS, with succinic acid as the predominant constituent, with lactic acid, and malic acid in descending order. LAB strains isolated from tropical fruits showed promising probiotic and antifungal properties, making them potential candidates for various applications in food and agriculture.

KEYWORDS

tropical fruits, phytopathogen, *Alternaria* conidia, antifungal activity, cell-free supernatant, organic acids, succinic acid

1 Introduction

Alternaria, a widespread fungus encompassing both pathogenic and saprophytic species, poses a substantial threat to agriculture and the economy. It causes an extensive loss and spoilage of postharvest fruits, vegetables, and cereals (Gabriel et al., 2017). There are more than 60 known species of *Alternaria,* of which *A. alternata* comprises seven distinct pathotypes, each producing host-specific toxins, that result in severe diseases in different host plants (Gai et al., 2023). *A. alternata* frequently contaminates agricultural produce such as tomatoes, potatoes, melons, cucumbers, citrus, and apples (Stewart et al., 2013; Tanahashi et al., 2016; Armitage et al., 2020). Notably, *A. alternata* colonization primarily exploits the pre-existing surface lesions, caused by bruising, or ripe-fruit cracking and eventually causes diseases like Alternaria black rot, leaf spot, and brown spot (Masunaka et al., 2005; Armitage et al., 2020). Currently, chemical agents are recommended to manage or prevent *Alternaria* infection (Steglińska et al., 2022). However, most of the chemicals carry risks of toxicity to both humans and the environment. It can deplete the local microbial community and develop resistance in pathogens (Steglińska et al., 2022). To mitigate these impacts, there is a growing need for environmentally friendly alternatives to chemical treatments.

Lactic acid bacteria (LAB) represent a promising option for biocontrol applications. They are commonly encountered in a wide array of sources such as dairy products, meat, vegetables, fruits, and wine (Somashekaraiah et al., 2019, 2021; Kumari et al., 2022). The widespread distribution of LAB suggests a greater adaptability to diverse environments and versatile metabolic pathways (Garcia et al., 2016). Notably, LAB holds the status of both Generally Recognized as Safe (GRAS) and Qualified Presumption of Safety (QPS), which accentuates their significance in the probiotics and biological control agents (Adithi et al., 2022). LABs exhibit a remarkable ability to produce multiple antimicrobial compounds, offering an environmentally friendly and effective means of countering specific microbial threats, thereby playing a pivotal role in developing biocontrol capabilities. Certain LAB strains, known for their antifungal properties, have also demonstrated as natural preservatives in food applications. For instance, LAB isolated from kimchi showed greater inhibition to growth of *Cladosporium* sp. YS1, *Penicillium crustosum* YS2, and *Neurospora* sp. YS3 than calcium propionate. While *Pediococcus pentosaceus* and *Lactobacillus plantarum* isolated from Tunisian grapes showed greater detoxification capability to ochratoxin A produced by *Aspergillus niger aggrégats* and *Aspergillus carbonarius* (Taroub et al., 2019).

Fruits, among all sources of probiotics, are naturally safe and necessitate minimal processing (Garcia et al., 2016; Rodríguez et al., 2021). The distinctive chemical composition of fruits provides a unique microbial niche, fostering the isolation of a wide variety of LABs with diverse metabolic functions, including antifungal properties. Raw fruits and their byproducts exhibit inherent similarities with the human gastrointestinal tract, particularly, acidity, and the presence of antinutritional factors such as tannins and phenols (Vitali et al., 2012). It is important to note that tropical fruits have the potential to be a natural source of bioactive compounds with antimicrobial properties (Maria, do Socorro et al., 2010). Furthermore, these fruits are naturally adapted to their intrinsic characteristics, which could potentially enhance their survival during processing and storage (Garcia et al., 2016). Despite this, most of the studies involving LAB are derived from dairy or fermented food products. There is still lack of investigations on antifungal properties of LAB, sourced from fruits (Garcia et al., 2016). Given that *A. alternata* is a cosmopolitan, endophytic fungus primarily found in soil, we sought to explore tropical fruits as a source for selecting LAB for antifungal properties against *A. alternata.* By exploring these fruits, it is possible to reduce dependency on synthetic antimicrobials and promote natural alternatives. Moreover, the probiotic property of LAB strains offers an added advantage for its safe consumption by humans.

Accordingly, the objectives of this study were designed to (i) isolate LAB from previously unexplored tropical fruits, (ii) evaluate the isolated LAB for *in vitro* probiotic properties, (iii) screen and evaluate antifungal activity against *A. alternata*, and (iv) discern and identify the specific antifungal component produced by LAB. The isolation process targeted seven distinct tropical fruits as potential sources of LAB. The selected LAB was studied for growth kinetics, tolerance to bile, salt, and phenol, aggregation ability, and a comprehensive safety evaluation including antibiotic resistance and hemolytic activity. Following a rigorous screening and meticulous selection process, the most potent LAB strain was studied *in vitro* to evaluate its antifungal activity against *A. alternata*.

2 Materials and methods

2.1 Isolation and characterization of LAB

2.1.1 Isolation of LAB from tropical fruits

The LAB was isolated from locally grown fruits in Karnataka, India specifically in the Mysuru and Mandya districts. Most of the fruits were picked during the Spring of 2020 for isolation. The fruits were selected primarily based on local availability, and rarity, emphasizing the exploration of previously unexplored varieties. The selected fruits included: *Musa* sp. cv. Nanjangud rasa bale (Nanjangud rasabale), *Annona muricata* (soursop), *Ficus glomerata* (cluster fig), *Couroupita guianensis* (cannonball tree), *Solanum nigrum* (black nightshade), *Ficus benghalensis* (Banyan tree), *Tinospora cordifolia* (Amrutha balli) (**Supplementary Figure 1**). Prior to isolation, the selected fruits were first washed using 70% (v/v) ethanol, and sterile demineralized water for 2–3 min. About 1 g of the fruit pulp was suspended in 0.1 M phosphate-buffered saline (PBS) and homogenized to obtain a slurry. 1 mL of this slurry was enriched in 9 mL de Mann, Rogosa Sharpe (MRS) broth at 37 °C under anaerobic conditions for 48 h in multiple replicates. Following enrichment, 1 mL of this mixture was serially diluted (up to 10^{-10}) in 0.1 M PBS and plated onto MRS agar plates. After incubation at 37 °C under anaerobic conditions for 48 h, morphologically distinct and pinpoint colonies were randomly selected and were repeatedly streaked onto MRS agar plates until pure colonies were obtained.

2.1.2 Preliminary screening of LAB for antifungal activity

To evaluate the inhibitory activity of the isolated LAB against *A. alternata*, a dual confrontation assay was conducted with slight modifications (Gkarmiri et al., 2015). For this, overnight-grown isolates were first streak-plated in the center of the agar plate forming an 8.5 cm line. Subsequently, a 5 mm diameter fungal plug from the edge of an actively growing colony of *A. alternata* was placed on either side of the bacterial streak line. Control plates containing only *A. alternata* were also prepared. After 5 days of incubation at room temperature, the plates were examined for the growth of *A. alternata* and zone of inhibition (ZoI) around the isolates. The ZoI was defined by the distance, in millimeters, between the LAB and *A. alternata* (**Figure 1B** inset). The changes in the morphology of *A. alternata* in the presence of LAB were quantified by increase/decrease in the length and width of the colony with reference to control (**Figure 1C** inset).

2.2 Molecular identification of selected LABs having antifungal activity

Genomic DNA from overnight-grown LAB strains was extracted using GeNei^{TM} kit following the manufacturer's instructions. The 16S region of rDNA was amplified using universal primer sets: 8F-5′AGAGTTTGATCCTGGCTCAG 3′ and 1391 R-5′ GACGGGCGGTGWGTRCA 3′ (Somashekaraiah et al., 2021). The obtained amplicon was sequenced at Eurofins PVT. Ltd. Following identification, the sequences were submitted to the GenBank database to obtain accession IDs. A phylogenetic tree was constructed to further understand the evolutionary relationship between the identified LAB strains and the related species from the NCBI database. The tree was constructed by neighbor-joining method with a bootstrap value of 1,000 repetitions using MEGA 11 software.

2.3 Bacterial growth parameters

The LAB isolates were grown in MRS broth for 24–48 h at 37°C. After incubation, the cells were serially diluted and plated on MRS agar plates. The bacterial viability was calculated using the plate count method and expressed as logCFU.mL^{-1} (Reuben et al., 2019). Alternatively, the optical density at 600 nm at every hour was also measured to evaluate the growth of LAB.

Average division rate (R), the number of generations related to the growth time of the population was determined by $R = (1/\log 2)x(\log N_t - \log N_0/t\text{-}t_0)$. To determine the generation time (τ) or doubling time, the data points corresponding to the exponential phase of the growth curves were utilized in the following formula: $N = [log(N_t)\text{-}log(N_0)/log2]$. Where $\log(N_0)$ and $\log(N_t)$ represent the logarithm of the number of cells at early and later time points during the exponential phase, respectively. The variable N signifies the number of generations within the specified time frame. Subsequently, the generation time (τ) was calculated using the formula: $\tau = T/N$ where, T denotes the time interval between N_0 and N_t, while N stands for the number of generations determined by the previous formula. The specific growth rate (μ), growth rate per unit of CFU was calculated using the formula: $\mu = 2.3[\log N_t - \log N_0/t\text{-}t_o]$ (Kushkevych et al., 2019). The acidifying capacity was calculated as a function of the decrease in pH values during the growth (Rodríguez et al., 2021). The pH was determined at intervals of 1 h. Maximum acidification was determined as the lowest pH observed during the bacterial growth period. while acidification rate is characterized as the rate of change in pH within a specified time interval. For instance: $\Delta pH/\ \Delta t = (pH_t\text{-}pH_0/t_1\text{-}t_0)$ (Rodríguez et al., 2021).

2.4 Probiotic attributes of selected LAB

The LAB isolates were initially characterized for phenotypic and biochemical traits, including Gram staining, catalase activity, bile salt hydrolase activity, osmotic tolerance (ranging from 3 to 7% NaCl), and carbohydrate fermentation (glucose, lactose, sucrose, xylose, maltose, D-arabinose, sorbitol, and D-raffinose) according to Cappuccino and Sherman (1999), Hedberg et al. (2008), and Shehata et al. (2016). The viability of the LAB strains was determined by calculating the logarithm of colony-forming units (CFU) per milliliter (mL) on MRS agar.

The LAB strains were grown in MRS broth under the anaerobic condition at 37°C for 16–20 h (~7 log CFU/mL). The cell suspension was centrifuged at 8,000 rpm for 10 min, washed, and resuspended in 0.1M PBS, pH 7.4. The cell-pellet or resuspended pellet in PBS was used in the following assays unless specified otherwise.

2.4.1 Cell surface hydrophobicity and auto-aggregation

To a 5 mL bacterial suspension in PBS, an equal volume of xylene was added, and mixed thoroughly. The mixture was allowed to stand undisturbed for 30 min, after which the absorbance of the aqueous phase measured at 600 nm. Percent hydrophobicity was calculated as $[(A_0\text{-}A_t)/A_0]x100$, where A_t and A_0 represent absorbance at 600 nm at a given time interval and at time 0, respectively.

To determine auto-aggregation, the cellular suspension in 0.1 M PBS was transferred to a glass cuvette. The change in optical density at 600 nm was measured every 1h intervals in a UV-Vis spectrophotometer. Percent aggregation at each time was calculated as $[1\text{-}(A_t/A_0) \times 100]$.

2.4.2 Tolerance to temperatures and osmotic stress

About 50 μL of overnight grown active cell culture (~7 log CFU/mL) was inoculated to a 5 mL previously salt-amended sterile MRS [3–7% (w/v)] and incubated at 37°C for 24 h. For assessing the growth at different temperatures, 50 μL of active cell culture was used to inoculate sterile MRS broth. The cultures were subsequently incubated for 24 h at 4, 10, 30, 37, and 60°C (Reuben et al., 2019). After incubation, 0.1 mL of the culture suspension was serially diluted and plated on MRS agar plates. The plates were incubated at 37°C for 24 to 48 h. The growth or viability was calculated as colony-forming units: $(\log.CFU.T_t/\ \log.CFU.T_0) \times 100$. Where T_t is the viable count after incubation and T_0 is the initial viable count.

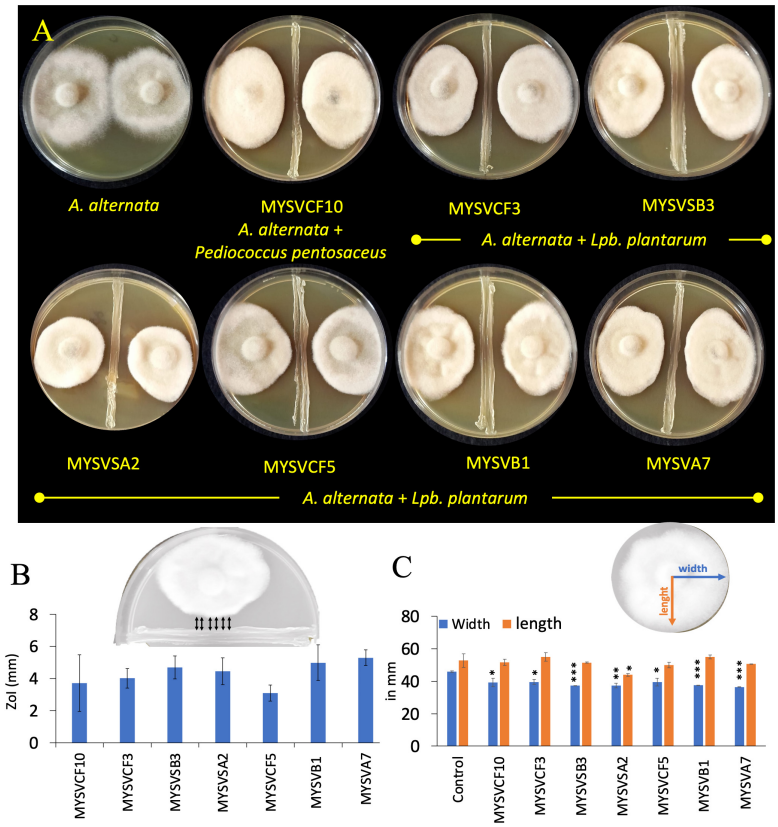

FIGURE 1
In vitro, dual confrontation assays showing the inhibition of the growth of *Alternaria alternata* by isolated LAB strains from various fruits **(A)**. The distinct area devoid of fungal growth between the LAB and *A. alternata*, were identified as the zone of inhibition (ZoI) **(B)**. Inset **(B)** provides a depiction of ZoI measurement highlighted in black arrows. Changes in the morphology of *A. alternata* were assessed by quantifying alterations in colony length and width in the presence of LAB **(C)**. Inset **(C)** features blue and orange lines representing width and length measurements. The x-axis in panels **(B,C)** represents the strain identity. Statistical significance at $*p \leq 0.05$, $**p \leq 0.01$, $***p \leq 0.001$.

2.4.3 Tolerance to low pH, bile salt, and phenol

To assess growth and tolerance at varying low pH levels, the washed cell pellet was resuspended in 5 mL of previously pH-adjusted sterile MRS broth. pH values of 2, 3, and 4 were achieved by adding 1 N HCl to the initial pH 6. For bile salt tolerance, the cell pellet was resuspended in sterile MRS broth (Hi media, India) supplemented with 0.3% (w/v) bile salt (ox gall) (Loba Chemie, India). Alternatively, for the phenol tolerance test, the isolates were grown in MRS broth supplemented with 0.3–0.6% phenol (Adithi et al., 2022).

The LAB cultures under various experimental conditions were incubated for 1–4 or 24 h under anaerobic conditions at 37°C. At each 1 h time interval, the cultures were serially diluted and plated on MRS agar plates to determine the bacterial viability as described above.

2.5 Safety evaluation of the selected LAB

2.5.1 Hemolytic activity

Blood agar plates were prepared using nutrient agar (Hi Media, India) supplemented with 5% (v/v) blood. The active LAB isolates were streak-plated forming a 3 cm line at the center of the plate. After 48 h of incubation at 37°C, the plates were examined to detect the presence of a distinct hemolysis pattern around the LAB colonies. The plates were classified as clean (β-hemolysis), greenish (α-hemolysis), and no hemolysis (γ-hemolysis). *Staphylococcus aureus* (ATCC 6538) served as a reference strain for hemolysis (Vanitha et al., 2023).

2.5.2 Antibiotic susceptibility

The susceptibility of LAB strains to antibiotics was determined following Charteris et al. (1998) with minor modifications. The selected LAB isolates (100 μL) were spread-plated on MRS agar plates and air-dried aseptically. Antibiotic discs containing 2 μg/disc of clindamycin, 10 μg/disc each of ampicillin, gentamycin, streptomycin, 15 μg/disc erythromycin, and 30 μg/disc each of vancomycin, kanamycin, chloramphenicol, and tetracycline were placed on inoculated plates. After 48 h of incubation at 37°C, the plates were examined for the zone of inhibition. The interpretive criteria for breakpoints were based on potential *Lactobacillus* sp. as outlined in Charteris et al. (1998) (**Table 1**).

2.6 Antibacterial activity

The antibacterial properties of LAB isolates and their CFS against specific indicator bacteria: *Escherichia coli* (ATCC 25922),

TABLE 1 Antibiotic sensitivity of selected LAB isolates from tropical fruits.

Antibiotics (μg/disc)		Concentration (μg/disc)	*Lpb. plantarum*		Breakpoint criteria (mm)*		
			MYSVA7	MYSVB1	*R*	MS	*S*
Ampicillin	Amp	10	S	S	≤12	13–15	≥16
Clindamycin	Cli	2	S	S	≤8	9–11	≥12
Chloramphenicol	Chl	30	S	S	≤13	14–17	≥18
Erythromycin	Ery	15	S	S	≤13	14–17	≥18
Kanamycin	Kan	30	MS	MS	≤13	14–17	≥18
Streptomycin	Ste	10	MS	MS	≤11	12–14	≥15
Tetracycline	Tet	30	S	S	≤14	15–18	≥19
Vancomycin	Van	30	R	R	-	-	15

*Antibiotic susceptibly expressed as R (Resistant), MS (Moderately Susceptible) and S (Susceptible). The interpretive criteria for breakpoints of disc diffusion for potential *Lactobacillus* species as outlined in Charteris et al. (1998).

Pseudomonas aeruginosa (ATCC 15422), *Salmonella paratyphi* (ATCC 27820) and *Staphylococcus aureus* (ATCC 27870) was evaluated. For this, LAB cells and their CFS (both treated and untreated) were incubated with the indicator organisms. A part of the extracted CFS was neutralized to pH 7 (n-CFS) or proteinase K (1 mg.mL^{-1}) treated (pCFS), or heat treated (100°C, 15 min) (hCFS) before use in the experiments (Rao et al., 2019).

2.7 Antifungal activity of LAB cells by co-inoculation assay

Experiments were conducted in a 100 mL Erlenmeyer flask containing 50 mL of modified MRS broth. Modified MRS broth was prepared by dissolving the following in demineralized water: 5 g/L Bacteriological peptone, 5 g/L mycological peptone, 5 g/L beef extract, 10 g/L yeast extract, 5 g/L dextrose, 0.1 g/L $MgSO_4$, 0.05 g/L MnSO4, 2 g/L K_2HPO_4. The modified MRS was devoid of antifungal substances such as polysorbate 80, ammonium citrate and sodium acetate (Deepthi et al., 2016). Each flask was inoculated with 100 μL of LAB isolates and 100 μL of *A. alternata* (10^6 spores/mL) and incubated at 37°C for 3, 7, 10, and 14 days. At the end of each pre-determined time interval, the mycelial biomass was harvested by filtration using Whatman no. 1 filter paper and dried at 60°C for 24 h. Simultaneously, the bacterial population in terms of log CFU/mL was determined by plate count technique. The flasks with bacterial cells and the spores of *A. alternata* alone served as control.

2.8 Antifungal activity of CFS of LAB isolates

2.8.1 Biomass inhibition

Experiments were conducted in a 100 mL Erlenmeyer flask, each containing 50 mL of different ratios of CFS (5 to 20%, v/v). The desired CFS ratio was achieved by directly mixing CFS and sterile potato dextrose broth. Subsequently, *A. alternata* fungal discs with a diameter of approximately 7.5 mm were introduced into these flasks, followed by incubation at room temperature. Flasks without CFS served as control. After 10 days, the fungal mat was harvested as described above by filtration. The dry weight of each treatment was then compared to that of the control.

2.8.2 Conidial germination inhibition

The experiments were conducted in a 24-well microtiter plate, using either LAB isolates or their CFS. In each well, 100 μL of LAB culture (~10^6 CFU/mL) and 100 μL of *A. alternata* spores (10^6 spores/mL) in a 1:1 ratio were combined to reach a final volume of 1 mL, using 0.1 M PBS at pH 7.4. For the CFS, a mixture of 200 μL of CFS and *A. alternata* spores (10^6 spores/mL) was prepared. The microtiter plate was then placed in an incubator at 30°C for 24 to 48 h. At each 2 h time interval, the germination of conidia was observed using a phase contrast microscope (Carl Zeiss AXIO, Germany). Briefly, 10 μL of conidial suspension (in triplicates) was transferred to a hemocytometer and directly observed under the microscope without any staining with brightfield illumination. The percentage of conidia germinated was determined by counting in a hemocytometer and calculated using the formula: Percentage = (Number of germinated conidia / Total conidia counted) x 100.

2.9 Stability and activity of CFS of LAB isolates

The stability of the CFS to inhibit *A. alternata* following proteinase K, pH neutralization, and high-temperature treatments was evaluated. For proteinase K, the CFS was treated with proteinase K (1 mg mL^{-1}) at 37°C for 2 h, followed by enzyme inactivation at 80°C for 10 min. As for evaluating thermal stability, the CFS was heated to 100°C for 15 min and then cooled to room temperature. For the effect of pH, the CFS was neutralized to pH of 7 with 1 M NaOH. The pre-treated CFS was relabeled as heat-deactivated CFS (hCFS), proteinase K treatment (pCFS), and pH-neutralization (nCFS). The residual antifungal activity was measured in triplicate after each treatment in a 24-well microtiter plate, as detailed below. CFS shelf-life test was also conducted to evaluate the stability and antifungal activity after long storage and freeze-thaw conditions. The extracted crude CFS was stored at −20

or 4°C for >8 months. After which, conidial germination assay was conducted using the stored CFS as detailed above.

2.10 Identification of antifungal compounds

The CFS was recovered from LAB isolates after 72 h in modified MRS broth by centrifugation at 8,000 rpm for 15 min. The obtained supernatant was filter sterilized using a 0.22 μm syringe filter. Following this, the CFS was extracted using methanol and resuspended in the mobile phase before injection to Liquid chromatography with tandem mass spectrometry (LC-MS). For LC-MS analysis, the UPLC BEH-amide column was used at 25°C using organic and aqueous phases as mobile phases at 0.1 mL/min flow rate. The mobile phase consisted of 10 mM ammonium citrate and acetonitrile (1:1), pH 8.5. The initial flow conditions included 100% aqueous phase for 30 s, after which the gradient was changed to the ratio of 95:5 aqueous and organic phases for 6 min. After separation, the eluant from the column was directly pumped to a tandem quadrupole mass detector (TQD-MS/MS) without split for quantification of organic acids (Oliveira et al., 2008).

2.11 Microdilution method to evaluate the antifungal activity of succinic and lactic acids

The experiments were conducted in a 24-well microtiter plate, using different concentrations of organic acids in PDA broth. To each well, succinic acid (0–3 mg/mL), lactic acid (0–9 mg/mL), or a combination of succinic (0–1 mg/mL) and lactic acid (0–5 mg/mL) were added to the final volume of 2 mL. *A. alternata* plugs, measuring 3 mm in diameter, were introduced into each well. Wells with PDA alone, CFS, *A. alternata* plugs were considered as control. The plate was incubated at 30°C for 5 days. After incubation % inhibition was calculated as (biomass in control-biomass in treated/ biomass in control × 100). The Inhibitory Concentration (IC50) is determined as the concentration at which fungal growth is reduced by 50% compared to the control in the absence of an antifungal agent, in this case, organic acids or CFS (Pierce et al., 2008).

2.12 Statistical analysis

Experiments were conducted in a minimum of three replicates. The average and standard deviation from the replicates were used to plot the graphs in origin. The effect of LAB or its CFS extracts on *A. alternata* was determined using a student's *t*-test. ANOVA was used to determine the variations in growth at different low pH and in antibacterial assays. Statistical analysis was performed using Microsoft Excel 2019. Statistical significance was determined at $p \leq 0.05$.

3 Results

3.1 Isolation and screening of LAB from tropical fruits for antifungal activity

Lactic acid bacteria was successfully isolated from seven types of fruits. An average of 10^5 CFU per g of fruit was obtained on MRS agar plates. Colonies that were pinpoint/small, circular, opaque, and displayed either white or colored morphological characteristics were selected for further screening and identification. After preliminary screening for negative catalase and positive gram tests, a total of fifty-five isolates were obtained with the highest counts (14) for *Solanum nigrum* and the lowest counts (4 each) for *Musa* and *Couroupita guianensis*.

Of the fifty-five LAB isolates obtained, only seven isolates exhibited inhibition against *A. alternata* (**Figure 1**). The inhibition was evident as irregular but compact growth near the area of LAB confrontation. The inhibitory zones produced by the LAB strains varied between 2- and 6-mm. Strains MYSVSB3 and MYSVA7 exhibited the highest inhibitory zones at >5.5 mm, while the strain MYSVCF5 exhibited the lowest at 2.3 mm among the seven isolates (**Figures 1A, B**). To ascertain the influence of LAB on the changes in the growth of *A. alternata*, the length, and width of the fungal colony were also measured (**Figure 1C**). All seven strains showed a significant reduction in the width of the fungal colony ($p < 0.01$), with the highest reduction with strains MYSVSB3, MYSVB1, and MYSVA7. Although the height or the length differed it was not statistically significant except for strain MYSVSA2 ($p < 0.05$). Strain MYSVSB3 did not show consistent results. Hence, it was screened out from further studies. Strains MYSVB1 and MYSVA7 showed promising and consistent inhibition against *A. alternata*. Moreover, a constriction in the morphology of the fungal colony was observed with these two strains (**Figure 1A**). Therefore, further studies were conducted with strains MYSVB1 and MYSVA7.

3.2 Molecular identification and growth kinetics of LAB from fruits

The 16S rRNA sequence of seven LAB isolates positive for antifungal activity was successfully obtained and analyzed. The genomic sequences confirmed the identity of six strains belonging to *Lactiplantibacillus* and one strain belonging to the *Pediococcus* genus. Each of the 16S rDNA sequences from these strains was assigned accession IDs. The identities, encompassing genus species and strain are *Pediococcus pentosaceus* MYSVCF10 (GenBank ID: OP563857), *Lpb. plantarum* MYSVCF3 (GenBank ID: OL347999), *Lpb. plantarum* MYSVSB3 (GenBank ID: OL691142), *Lpb. plantarum* MYSVSA2 (GenBank ID: OL691141), *Lpb. plantarum* MYSVCF5 (GenBank ID: OP563855), *Lpb. plantarum* MYSVB1 (GenBank ID: OL347991), and *Lpb. plantarum* MYSVA7 (GenBank ID: OL347927). With the selected *Lpb. plantarum* strains MYSVA7 and MYSVB1, a phylogenetic tree was constructed to visualize the relationship within the *Lactiplantibacillus* genus and other LABs reported in the literature (**Figure 2**). Based on sequence similarity and phylogenetic analysis, the next closest match was

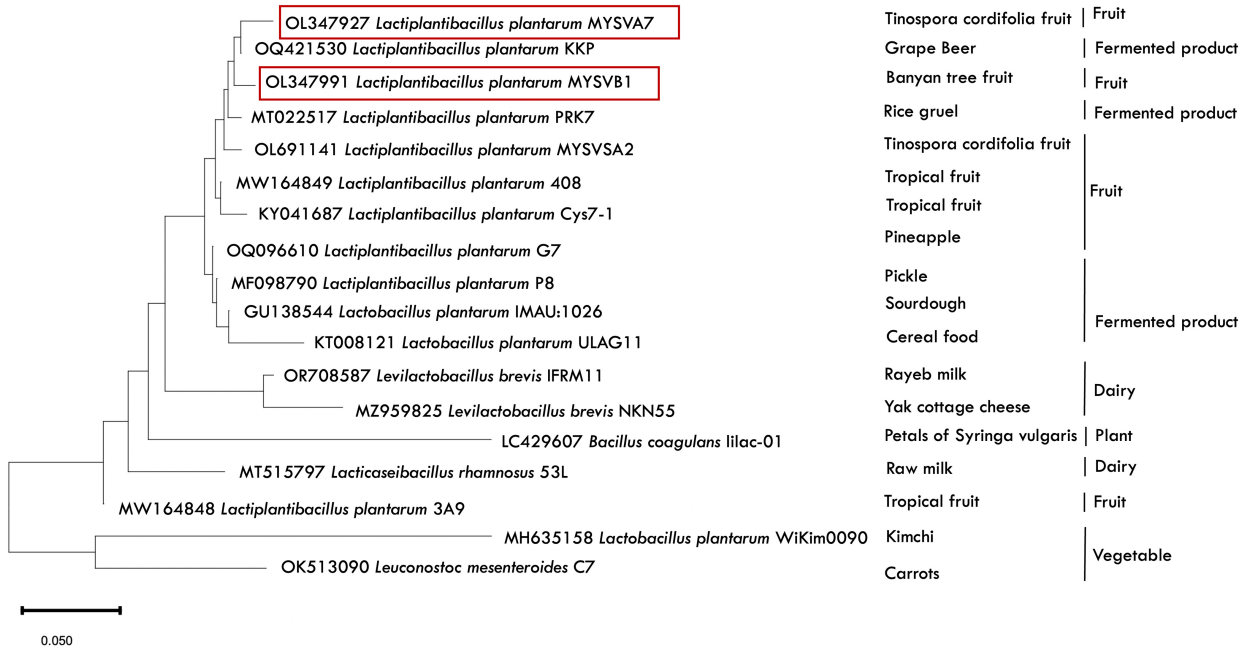

FIGURE 2
Phylogenetic analysis depicting the relative position of LAB isolates (MYSVA7 and MYSVB1) in comparison to other previously reported strains. The tree was built using 16S rDNA sequences (available in NCBI database) in Mega 11 software using maximum parsimony analysis. Strains isolated in this study are highlighted in red, with the source of isolation specified next to the strain identity. The alphanumerical (OL347927) represent the NCBI accession IDs for reference.

found to be *L. brevis* for isolates MYSVB1 and MYSVA7 (Figure 2). The strains MYSVA7 and MYSVB1 could be morphologically described as rods, non-spore-forming bacteria. Both the strains were able to ferment all the sugars without the formation of gas (Table 2). The growth kinetics of LAB strains MYSVA7 and MYSVB1 are shown in Figure 3. With the lag time of 2 h, the average division rate was observed to be 0.83 and 1 generation per h, respectively. Further, the LAB isolates' acidification coincided with the growth due to the ability to ferment sugars and production of organic acids (data not shown). A strong association was observed between the growth rate and acidifying capacity. As the growth rate increased, the pH level of the medium decreased, ultimately reaching pH < 4 (Supplementary Table 1). Previous studies have established time required for fermentation of fruits and vegetables by autochthonous bacteria between 8 and 24 h (Di Cagno et al., 2013; Rodríguez et al., 2021). The maximum acidification in this study was obtained at time 10 h, and the maximum specific growth rate of 0.57 and 0.73 for strains MYSVB1 and MYSVA7 respectively (Supplementary Table 1). LAB strains were also evaluated for growth and cell viability at different temperatures. Variability of the growth kinetics was evident among the LAB strains. Both the strains exhibited the highest growth at >30°C. Although slight differences in the growth between 30 and 37 °C were observed, it was statistically insignificant ($p > 0.05$) for both temperatures. Therefore, the optimal temperature for LAB was >30°C. Growth at suboptimal temperatures at 10 and 4°C displayed a reduced growth ($p < 0.001$). An average reduction of >1 log CFU/ mL was observed for both temperatures (Figures 3A, B). Similar results were observed at high-temperature tolerance at 45 °C. In this case, a reduction by > 2 log CFU/mL ($p < 0.001$) was observed (Figures 3C, D).

TABLE 2 Carbohydrate fermentation ability of selected LAB isolates from fruits.

Carbohydrate fermentation	LAB isolates	
	MYSVA7	MYSVB1
Glucose	+	+
Lactose	+	+
Sucrose	+	+
Xylose	+	+
Maltose	+	+
D-Arabinose	+	+
Sorbitol	+	+
D-Raffinose	+	+

3.3 Probiotic attributes of selected LABs

3.3.1 Cell surface properties

To evaluate the adhesive property, the cell surface hydrophobicity was measured. Notably, the hydrophobicity of the isolates exhibited consistency across the strains, at 25% (±3) for MYSVA7 and 28% (±2) for MYSVB1. Moreover, there was a discernible increase in percent aggregation over time. (Supplementary Figure 2). Particularly, both strains exhibited

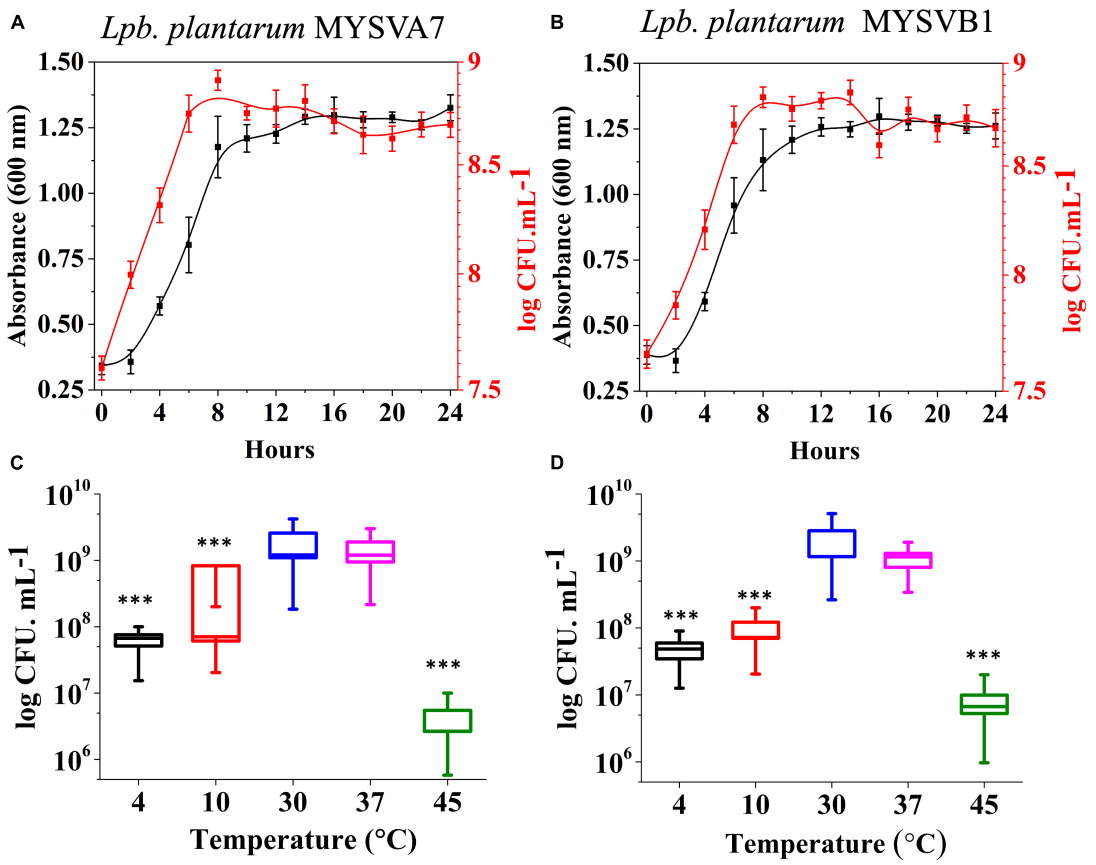

FIGURE 3
Growth kinetics **(A,B)** and growth at different temperatures **(C,D)** of strains *Lactiplantibacillus plantarum* MYSVA7 **(A,C)** and MYSVB1 **(B,D)**. The growth kinetics was studied at 37°C **(A,B)**. Statistical significance at ***$p \leq 0.001$.

25% aggregation after 5 h. Following a 24 h incubation, a further increase in aggregation index was observed, with percentages of 53 and 68%, respectively.

3.3.2 Survival ability to osmotic stress and simulated gastrointestinal conditions

Figures 4A, B shows the tolerance of LAB isolates to different concentrations of salt. Both the isolates were tolerant to salt concentrations up to 7%. The cell viability was not affected by up to 5% salt concentration. An increase in salt to 7%, decreased the viability by 1 log CFU/mL ($p < 0.05$). On the other hand, with up to 0.6% phenol (Figures 4C, D) or 0.3% bile (Figures 4E, F), the viability of both strains was not compromised. The cellular viability of both strains was maintained above 9 log CFU/mL demonstrating >95% viability. Further, the LAB strains under simulated gastrointestinal conditions exhibited high tolerance, with minimal loss in viability (Figures 4G, H). Both strains MYSVA7 and MYSVB1 showed tolerance to pH 2. The cell counts of strain MYSVA7 at pH 3 and pH 2 after 4 h showed only 4 to 6 log CFU/mL as compared to pH 4 and above at 8 log CFU/mL. However, after 24 h, the cell counts reached 5 to 6 log CFU/mL at pH < 3 (Figure 4G). This was attributed to the combination of acidic pH and extended lag phase. No significant reduction ($p > 0.05$) was observed for strain MYSVA7 at pH < 3. Similar cell counts were observed for strain MYSVB1. At pH < 3, after 4 h, the viability decreased to 4 log CFU/mL from 7 log CFU/mL. However, after 24 h, the cell count increased to 7 log CFU/mL suggesting high tolerance and growth even at pH as low as 2 (Figure 4H). Overall, the isolated LAB showed high tolerance to osmotic stress and simulated gastrointestinal conditions.

3.3.3 Antibacterial activity

The antibacterial effectiveness of the strain MYSVB1 and its CFS was also evaluated against various pathogens including ESKAPE pathogens. The zone of inhibition for *E. coli*, *P. aeruginosa*, *S. paratyphi*, and *S. aureus* are shown in Figure 5. Notably, the cells of MYSVB1 and its crude CFS exhibited the highest inhibition against all the tested pathogens. The zone of inhibition ranged from 3 to 3.6 mm. However, antibacterial activity significantly declined after heat treatment ($p < 0.001$) (Figure 5). While treatment of proteinase K reduced the inhibition significantly ($p < 0.05$) for *E. coli*, *P. aeruginosa*, *S. paratyphi*, and *S. aureus* did not show any inhibition for growth (Figure 5). No inhibition was observed for CFS at pH 7 to any tested pathogens.

3.3.4 The safety aspect of LABs

Both strains MYSVA7 and MYSVB1 showed no clear zone formation on blood agar. *Staphylococcus aureus* showed complete lysis of red blood cells evident by yellow coloration around its colony suggesting β-hemolysis (Supplementary Figure 3).

10.3389/fmicb.2024.1322758

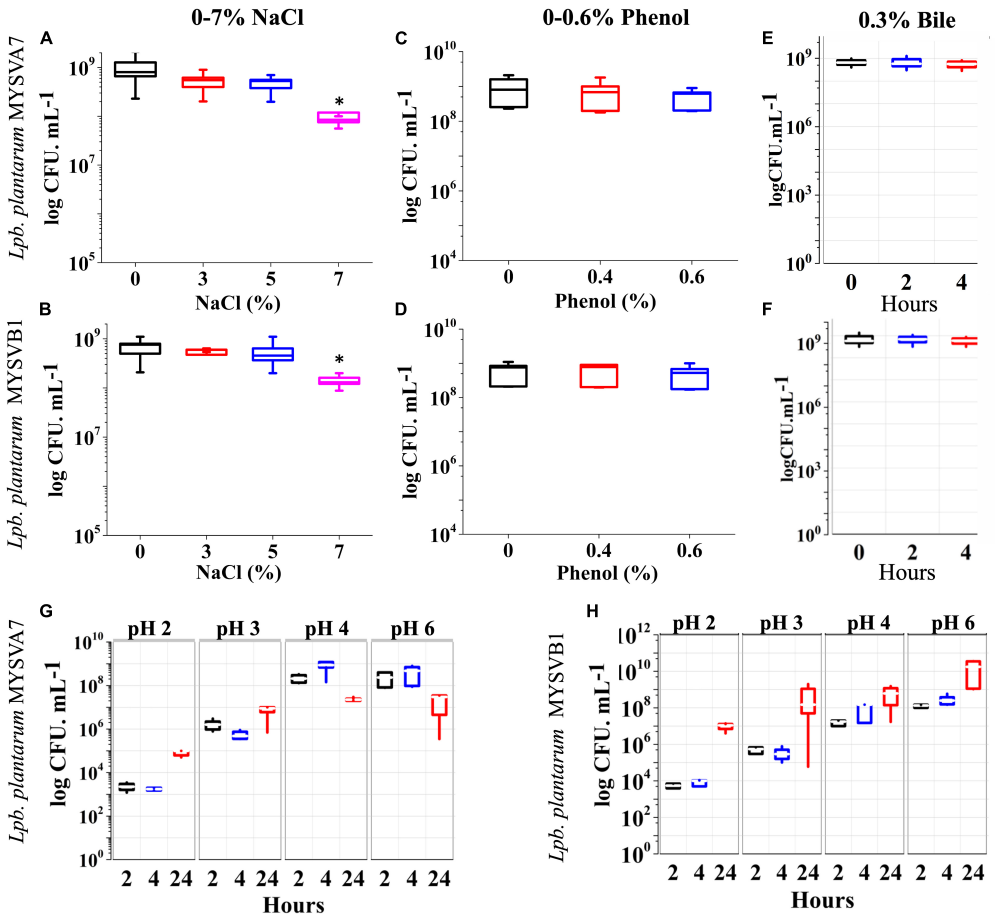

FIGURE 4
Probiotic properties of *Lactiplantibacillus plantarum* strains isolated from tropical fruits. The growth of LAB was assessed under various conditions, including different salinity levels (0–7% NaCl) **(A,B)**, phenol concentrations (0–0.6%) **(C,D)**, bile salt concentrations (0–0.3%) **(E,F)**, and varying pH conditions (pH 2–6) **(G,H)**. The properties for strains MYSVA7 are presented in panels **(A,C,E,G)**, while those for MYSVB1 are shown in panels **(B,D,F,H)**. Statistical significance at $^{*}p \leq 0.05$.

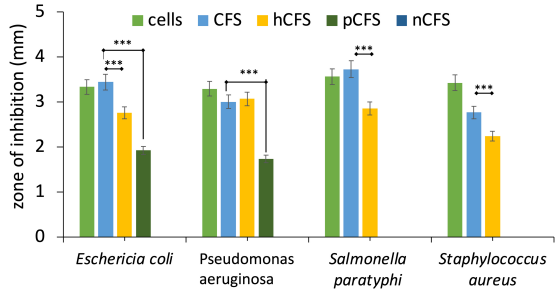

FIGURE 5
Antibacterial activity of *Lactiplantibacillus plantarum* MYSVB1. The target pathogen was inoculated with both viable cells of *Lpb. plantarum* MYSVB1 or its crude CFS. The CFS was pre-treated: heat-deactivated CFS (hCFS), proteinase K treated CFS (pCFS), and pH-neutralized CFS (nCFS) before use in the experiment. Statistical significance at $^{***}p \leq 0.001$.

Differences in susceptibility and resistance to common antibiotics were observed. Both strains showed similar sensitivity (Table 1). The strains were susceptible to ampicillin, clindamycin, chloramphenicol, erythromycin, and tetracycline. While kanamycin and streptomycin showed moderate sensitivity and complete resistance was observed with vancomycin. Nevertheless, the isolated strains were non-hemolytic and were susceptible to most of the common antibiotics tested.

3.4 Antifungal activity

Figure 6 illustrates the growth of *A. alternata* over a 14-day period. By day 3, visible thick mat growth was observed which continued to increase until day 14. By day 10 the fungal mat reached its maximum growth and the density of the mat remained unchanged thereafter. The weight of biomass exhibited progressive growth from day 1 until day 10, before reaching 1.8 g (dry weight). However, the introduction of viable cells of MYSVA7 (Figure 6B) and MYSVB1 (Figure 6C) significantly inhibited ($p < 0.001$) the growth of *A. alternata* by 87 and 75%, respectively, by day 3 (Figures 6D, E). As a result, no observable expansion or growth of fungal biomass was observed. Notably, the viability of the strain MYSVA7 and MYSVB1 during the 14-day period in the presence of *A. alternata* was not

10.3389/fmicb.2024.1322758

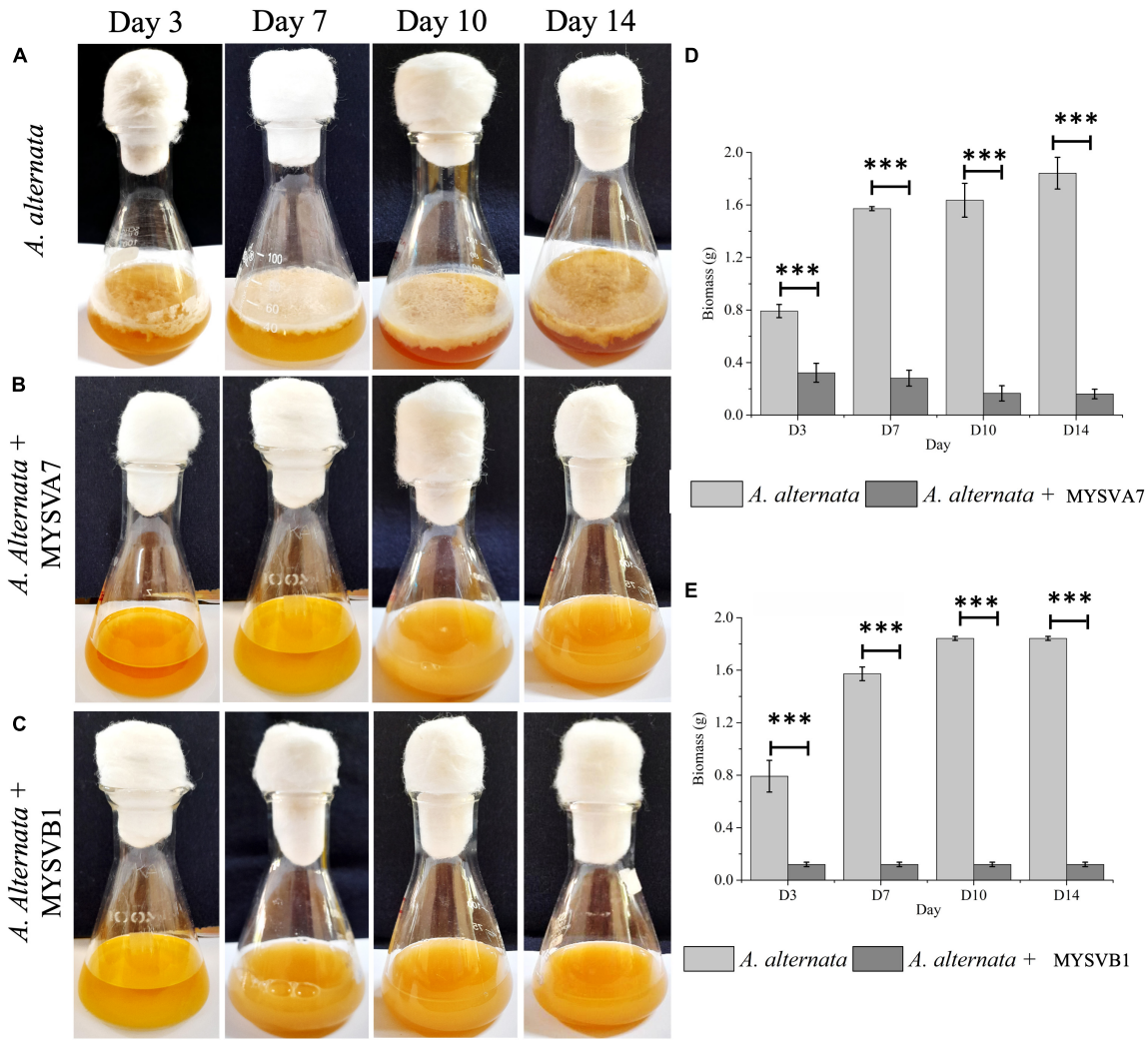

FIGURE 6
Co-inoculation assay demonstrating the inhibition of *A. alternata* by strains *Lactiplantibacillus plantarum* MYSVA7 and MYSVB1 on different days **(A–C)**. Time course the growth of mycelial mat in control **(A)** and in the presence of *Lpb. plantarum* MYSVA7 **(B)** and *Lpb. plantarum* MYSVB1 **(C)** are shown. The corresponding biomass yield harvested on different days are shown in panels **(D,E)**. Statistical significance at ***$p \leq 0.001$.

affected but displayed an exponential growth, lasting 3 days followed by a gradual decline over time (data not shown). These findings clearly demonstrate the effectiveness of strains in suppressing the growth of *A. alternata*, while maintaining its viability.

Alternatively, when different ratios of crude CFS were used, differential inhibition was observed between the two strains (Figure 7). With just 5% of crude CFS, a significant inhibition ($p < 0.01$) in the growth of *A. alternata* was observed, with MYSVB1 displaying greater inhibition ($p = 0.003$). When the concentration of CFS from MYSVA7 was increased to 15%, the biomass yield of *A. alternata* decreased substantially by 94% (Figure 7B). Similarly, using only ≤ 10% CFS from strain MYSVB1 resulted in a comparable reduction in the yield. In fact, >70% decrease in biomass yield was recorded when only 5% of CFS of MYSVB1 was used (Figure 7D). Therefore, the CFS of strain MYSVB1 was considered the most potent inhibitor of *A. alternata*.

The presence of viable cells of MYSVB1 had a pronounced inhibitory effect on both conidial germination and mycelial development. Microscopic examination revealed that even after 48 h, the germination of conidia impeded with viable cells or its CFS, with no observable germ tube formation (Figure 8). In striking contrast, the control groups exhibited rapid formation of germ tube within 4 h, followed by luxurious growth of mycelium (Figure 8A). By 16 h, 90% (of 10^6 spores/mL) produced germ tubes, accompanied by the formation of mycelia (Figure 8B). It is worth noting that under nutrient-rich conditions, PDB medium, the germination of conidia and mycelial development occurred at an even faster rate (data not shown).

3.5 Tentative determination of antifungal substances

To identify the active components of CFS, following different treatments, antifungal assays were performed (Supplementary Figure 4). Heat treatment preserved the inhibitory properties,

10.3389/fmicb.2024.1322758

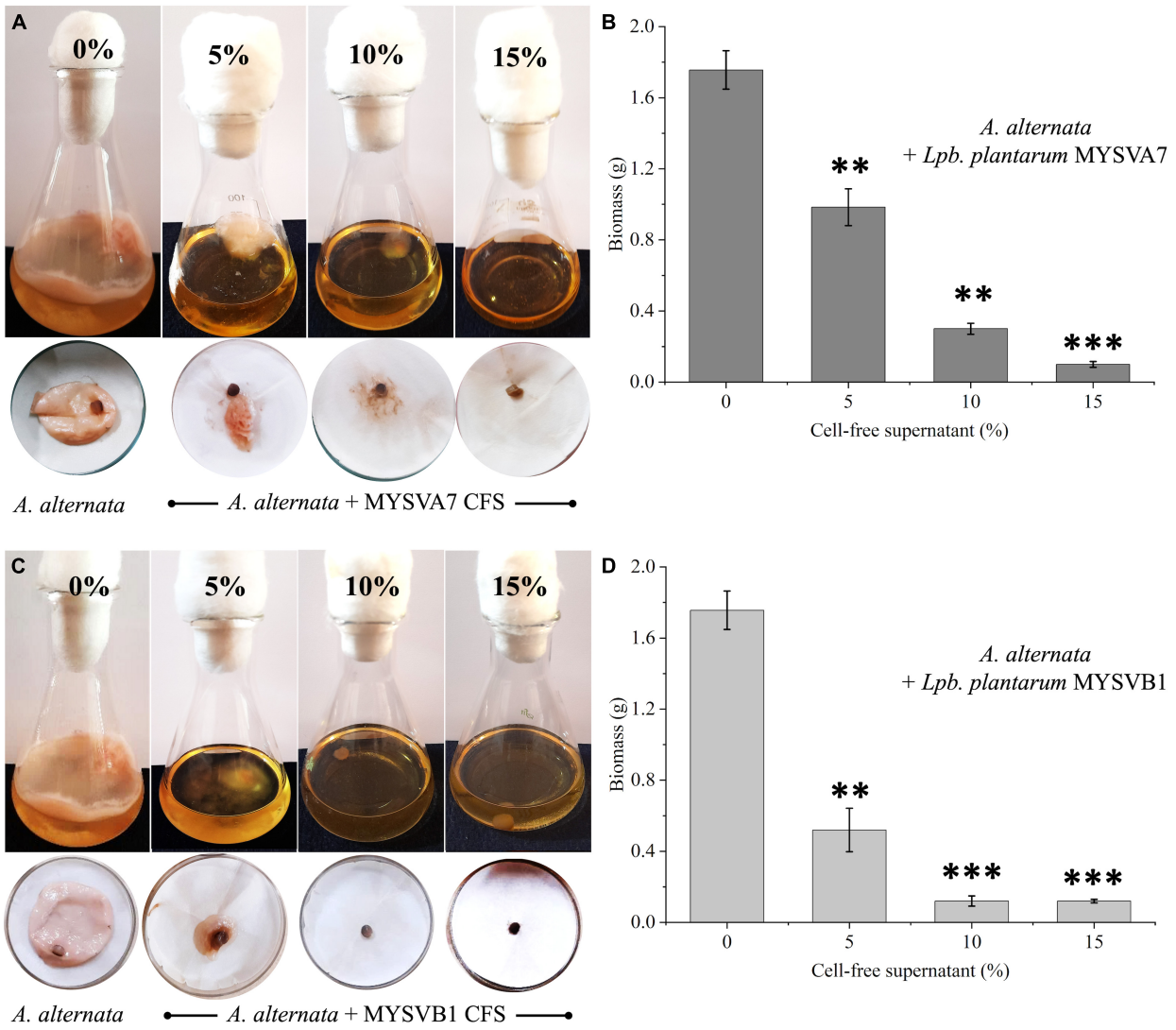

FIGURE 7
Antifungal activity of cell-free supernatant (CFS) extracted from *Lactiplantibacillus plantarum* MYSVA7 **(A,B)** and *Lpb. plantarum* MYSVB1 **(C,D)** against Alternaria alternata. Experiments were performed with different concentrations (%) of CFS. Flasks showing growth of *Alternaria alternata* with CFS of strain MYSVA7 **(A)** and MYSVB1 **(C)**. The corresponding fungal biomass yield harvested after 10 days of incubation at room temperature **(B,D)**. Statistical significance at $^{**}p \leq 0.01$, $^{***}p \leq 0.001$.

while pH neutralization and proteinase K treatment rendered them ineffective (Supplementary Figure 4). Both treatments showed no difference in inhibition compared to control without CFS, allowing fungal growth and sporulation. A pivotal role of the LAB's acidic environment in its antifungal properties against *A. alternata*. Thus, the antifungal metabolites present in the culture filtrate (CFS) likely consist of acidic compounds, which may include organic acids and proteinaceous substances that are resistant to heat, possibly even a combination of components. With LC-MS, several organic acids were successfully identified in the CFS (Table 3). Specifically, lactic acid, pyruvic acid, succinic acid, malonic acid, fumaric acid, citric acid, hydroxy-citric acid, and shikimic acid were identified. Notably, Succinic acid was a predominant fraction, making up 63% (3.7 $mg.mL^{-1}$) of the total organic acids identified, following lactic acid, and malic acid each at 9% (Table 3).

3.6 In vitro antifungal activity of organic acid

Succinic acid, identified as the predominant organic acid in CFS through LC-MS, was further investigated for its *in vitro* antifungal activity against *A. alternata*. As the concentration of succinic acid increased, a corresponding increase in percent inhibition was observed. At a concentration of 0.8 mg/mL succinic acid, mirroring the observed concentration in 20% CFS, the percent inhibition ranged from 38 to 40%. A further increase in concentration to > 2.5 mg/mL resulted in inhibition exceeding 90% (Supplementary Figure 4A). The IC_{50} for succinic acid was determined to be between 1.8 and 1.9 mg/mL, which was more than four times the concentration found in 20% CFS. Consequently, additional experiments were conducted to explore lactic acid, the second most prevalent organic acid in CFS.

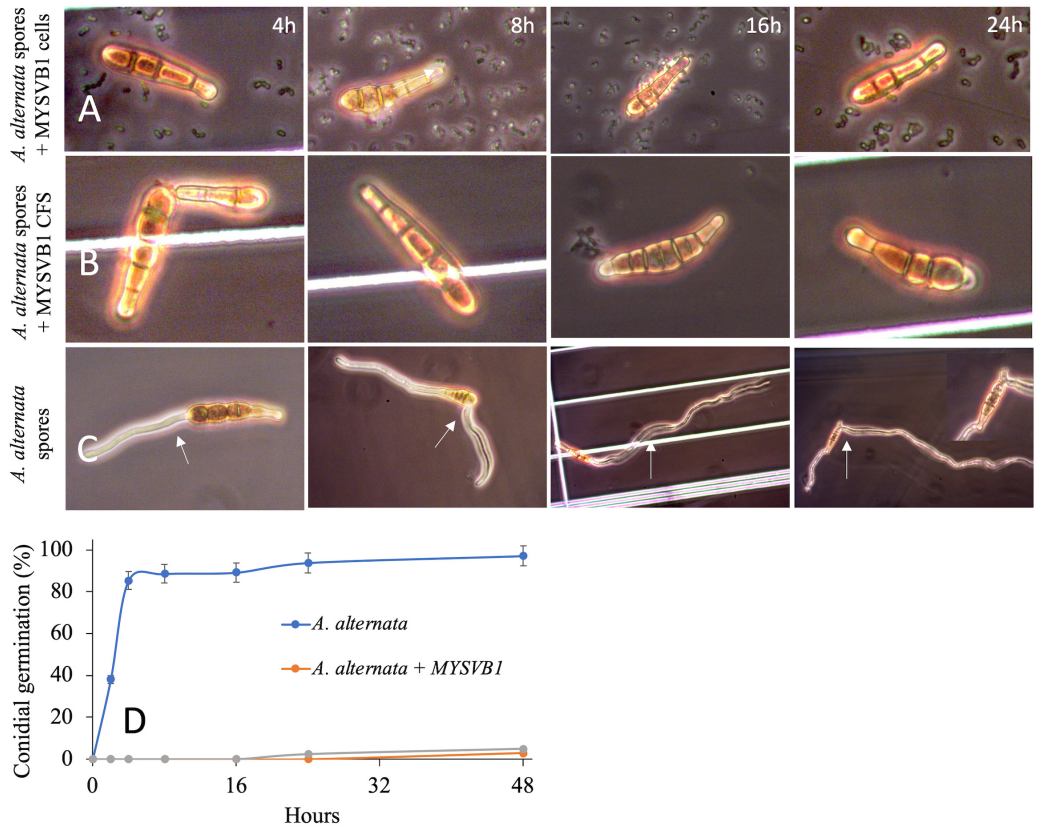

FIGURE 8
Germination of conidia of *Alternaria alternata* co-cultured with *Lactiplantibacillus plantarum* MYSVB1 **(A)** and its CFS **(B)** against control **(C)**. Panel **(D)** displays the corresponding time course of percentages of germinated conidia, measured at regular intervals. The white arrow shows the germination or formation of the germ tube.

With the addition of 0.1 mg/mL lactic acid, corresponding to the concentration in 20% CFS, no discernible differences were noted. Even with an increase in concentration to 0.6 mg/mL lactic acid in conjunction with 1 mg/mL succinic acid, no variations were observed (**Supplementary Figure 4C**). However, upon further increasing the concentration of lactic acid to 9 mg/mL, complete inhibition of *A. alternata* was achieved (**Supplementary Figure 4B**). The IC_{50} for lactic acid was determined to be >5 mg/mL. Consequently, the observed concentration of succinic acid in CFS alone could not replicate the inhibition observed in CFS, even when combined with lactic acid. Thus, succinic acid appears to contribute partially to the growth inhibition, possibly through a synergistic interaction with other organic acids.

TABLE 3 Major organic acids composition of cell-free supernatant (CFS) of strain *Lpb. plantarum* MYSVB1.

Organic acids	Molecular weight ($g.mol^{-1}$)	CFS ($mg.mL^{-1}$)	% distribution
Succinic acid	118.09	3.7 ± 0.02	63.8
Lactic acid	90.08	0.5 ± 0.004	9.3
Malic acid	116.1	0.54 ± 0.02	9.2
Malonic acid	104.06	0.39 ± 0.02	6.6
Citric acid	192.12	0.38 ± 0.3	6.4
Pyruvic acid	88.06	0.12 ± 0.01	2.0

4 Discussion

Enhancing crop yield through effective protection against plant pathogens has long been a pivotal objective in agriculture. *Alternaria* sp. is responsible for causing severe foliar disease, known as blight in several plants. Combatting the infection of *Alternaria* sp. is crucial for ensuring agricultural productivity (Stewart et al., 2013; Tanahashi et al., 2016). In this context, the role of beneficial microorganisms, such as LABs are important players. LAB, with its well-documented antimicrobial properties, can play a vital role in strengthening plant health and combating phytopathogens like *Alternaria*. Moreover, LABs have gained prominence as probiotics for fostering balance in the intestinal microbiota of humans and animals and for their ability to inhibit or fight against pathogenic or infectious diseases (Argyri et al., 2013). With growing interest in green alternatives for improved health, fruits and vegetables are an important source of probiotics (Di Cagno et al., 2010; Garcia et al., 2016; Zhang et al., 2022). As fruits are

traditionally safe for consumption without requiring processing, LAB from fruits are natural choices for probiotics. In this study, a total of fifty-five isolates were obtained from seven different tropical and previously unexplored fruits. Of these LAB strains, seven strains showed antagonistic activity against phytopathogen *A. alternata*. Two strains, namely MYSVA7 and MYSVB1 showed sustained inhibition against *A. alternata*. The analysis revealed that these strains exhibited several characteristics morphological and biochemical traits such as the genus *Lactiplantibacillus* including Gram-positive, rod, catalase-negative, and non-spore-forming, and the tendency to aggregate and demonstrated facultative hetero-type fermentation. 16S rDNA sequencing confirmed this observation with *L. plantarum* having the highest (>99%) homology. To the best of our knowledge, this is the first report, to isolate and evaluate probiotic characteristics for tropical fruits having antifungal activity against a phytopathogen *A. alternata*.

The ability to maintain viability and adhere to is a determinant factor in many recommendations regarding probiotics (Zhang et al., 2022). The intestinal bile salts and the acidic environments of the stomach have been identified as the primary challenges to the survival of LAB within the GI tract (Hsu et al., 2018). The growth of MYSVA7 and MYSVB1 was not affected under conditions of salt up to 7% and temperature ranging from 4 to 45°C. Despite a minor growth delay at higher mesophilic temperatures ($T = 45°C$), the notable tolerance and adaptability exhibited by these two strains strongly support their capability for both high- and low-temperature fermentation. Moreover, under the condition of pH 2 to 6, and in the presence of bile (up to 0.6%) the growth was not affected. At pH 4–6, the pH of the fermentation broth decreased in pH value rapidly. It is widely documented that LAB can decrease the pH by the production of organic acids (Hsu et al., 2018). It is important to note that these strains displayed resilience within a broad pH range, from pH 2 to 6, and even in the presence of bile concentrations up to 0.6% bile. The differing levels of survivability in acidic conditions can likely be attributed to species- or strain-specific mechanisms of acid tolerance potentially involving specific bacterial proteins that confer resistance (Nami et al., 2019).

One of the hallmark characteristics of LABs is the ability for auto aggregation that allows the microorganisms of the same species to form cohesive groups, often binding to the intestinal mucosa (Lukic et al., 2014) or co-aggregation with other strains enabling interactions, potentially with pathogens serving as a host defense against infections (Goh and Klaenhammer, 2010). The strains in this study displayed varying degrees of auto-aggregation. However, with high tolerance to GI conditions and aggregation ability, the isolates could significantly contribute to intestinal health. Several studies have highlighted certain probiotic strains can potentially combat intestinal pathogens effectively (Kumar et al., 2010; Campana et al., 2017; Mirzaei et al., 2018). Considering growing concerns surrounding antibiotic resistance, the antimicrobial capabilities against pathogenic bacteria have gained significant attention (Lee et al., 2013). Within the isolates, the strains exhibited robust antibacterial activity. Notably, the CFS exerted the same efficacy of viable cells in inhibiting the pathogenic bacteria suggesting the production and release of antimicrobial substances. Moreover, the CFS could inhibit both Gram-positive and Gram-negative pathogens. LABs are known for their health-promoting attributes, beyond their antibacterial activity, which encompasses antiviral and potential anticancer properties (Drider et al., 2016; Kaur et al., 2017). While this study did not explore these specific aspects, it is an intriguing avenue for future research, where LAB's broader therapeutic potential in the context of viral infections and cancer could be studied.

Despite the long history of safe usage of LAB as food-grade microorganisms, it remains essential to consider and assess the potential virulence-associated factors (Li et al., 2020). In this study, none of the isolated strains exhibited erythrocyte lysis confirming the safety aspect but does not confirm the absence of virulence factors. The strains were also susceptible to common antibiotics. Notably, both strains were resistant to vancomycin antibiotics. Vancomycin resistance within the genus *Lactiplantibacillus* is typically classified as intrinsic, primarily due to the peptidoglycan structure of the bacterial cell wall. Similar reports of probiotics from dietary supplements and dairy products also exhibited resistance to vancomycin, kanamycin, and gentamycin (Li et al., 2020). Overall, the isolates were deemed safe as potential probiotics. Following the antibacterial activity, the strains *Lpb. plantarum* MYSVA7 and MYSVB1 consistently demonstrated the most significant antifungal activity in both solid and liquid substrate-based models. It is worth noting that many species within the genus have been previously documented to exhibit antifungal properties in dairy products, silage fermentation, etc. (Li et al., 2020). Strains belonging to *L. plantarum* have shown inhibition against *Fusarium*, *Penicillium*, and *Aspergillus*, among others (Wang et al., 2012; Deepthi et al., 2016; Adithi et al., 2022). In this study, it's worth noting that despite both strains belonging to *Lpb. plantarum* species, the antifungal activity displayed strain-specific variations. Specifically, MYSVB1 showed robust inhibition against *A. alternata*. This variance in antifungal efficacy observed in previous research was attributed to the strains' potential to produce antifungal molecules, which might be limited by their ability to attain higher population levels (Leyva Salas et al., 2017). However, both strains displayed an optimal growing temperature between 30–37°C with comparable generation time (0.8–1 generation per h). These differences were consistent when crude CFS was used instead of viable cells. For instance, 5% CFS derived from strain MYSVB1 was sufficient to inhibit the fungal growth by 70% while it required ~8–10% CFS from MYSVA7 to inhibit fungal growth by 70%. viz., strain MYSVB1 was more potent by at least a factor of two than MYSVA7 in inhibiting the growth of *A. alternata*. Further, the inhibitory effects on spore germination were also confirmed. Previous research has consistently shown that the antimicrobial compounds present in CFS produced by LAB tend to specifically target the cell membranes of pathogenic microorganisms. This interaction results in a range of effects, including changes in cellular morphology, and disruption of surface structures on conidia, ultimately damaging the cell membranes (Xu et al., 2019). The modulation of cell membrane permeability stands out as a fundamental antimicrobial mechanism employed by LAB. Zhao et al. (2022) suggested that intracellular substance leakage resulting from peroxidation damage to hyphae is a major mechanism of action. Although this is well-documented in different *Lactiplantibacillus* strains (He et al., 2020), the changes in the conidial morphology due to cells or its CFS were not observed in this study, but rather complete inhibition was observed.

The CFS of MYSVB1 demonstrated excellent thermostability, and stability in an acidic environment but poor enzymatic stability (**Supplementary Figure 4**). The antimicrobial properties

exhibited by the CFS tend to remain across a wide range of temperatures. This is primarily attributed to the low molecular weight antimicrobial compounds (Girma and Aemiro, 2021). In addition to this, the loss of antifungal activity after protease treatment suggests the presence of proteinaceous substances in CFS. The present investigation confirmed succinic acid as the predominant antifungal molecule synthesized by MYSVB1. Notably, its accumulation was found to reach higher concentrations than MIC for bacteria at 320 μg/mL (Kumar et al., 2018) to inhibit the *A. alternata* spore growth effectively. Under anaerobic conditions, succinic acid and lactic acid serve as the primary fermentation products. Among the three possible routes for succinic acid production, the conversion of malic acid into succinic acid, facilitated by succinate dehydrogenase, is the most favorable reaction (Wang et al., 2021). Besides, lactic acid and malic acid are the second most abundant organic acids produced by the MYSVB1 strain. The generation of lactic acid may arise from the decarboxylation of malic acid through malolactic enzyme activity or the reduction of pyruvate by lactate dehydrogenase (Wang et al., 2021). Markedly, the absence of acetic acid and the presence of pyruvic acid suggest succinic acid production via the malic acid pathway. This insight adds depth to our understanding of the metabolic processes involved. However, further experiments are needed to confirm the actual pathway. When succinic acid was evaluated independently, the inhibitory concentration for succinic acid was determined to be approximately 1.9 mg/mL, which is twice the concentration identified in CFS. Nevertheless, when combined with a higher concentration of lactic acid, the inhibitory effect was observed to increase. Consequently, it can be concluded that succinic acid, at the observed concentration alone, only contributes partially to the antifungal activity. Succinic acid has already been described for its ability to cause loss of viability and cell destruction as a weak acid (Orij et al., 2012). The enhanced inhibition observed in combination with lactic acids suggests that a synergistic interaction among organic acid compounds providing a more comprehensive explanation for the observed activity. Moreover, the observed poor efficacy at both alkaline and neutral pH may be due to the dissociation of organic acids. Therefore, when contemplating the application in CFS, it is important to account for acid-base conditions of the food matrix. Nevertheless, CFS demonstrated robust stability and can be safely stored for extended durations, ranging up to 10 months, within a temperature range spanning from 4 to 35°C.

It is important to acknowledge that the observed antifungal activity is attributed to organic acids, specifically succinic acid. It is also suggested that the compound may also contain proteinaceous molecules. However, at this point, the proteinaceous content in the CFS could not be confirmed. For a comprehensive understanding of the applicability of *Lpb. plantarum* strain MYSVB1 or its CFS, it is essential to conduct further studies aimed at elucidating the antimicrobial components, factors influencing their stability, and *in vivo* assays in field conditions.

5 Practical implications

Alternaria disease has been a global problem since its first report of leaf blotch in apple trees in 1926. The disease is typically prevalent in regions with dry, warm weather conditions. But more recently it has emerged in temperate zones. *Alternaria* disease appears during warm weather and heat periods, with initial symptoms showing up in early summer. As the summer progresses and temperatures drop, the symptoms worsen, leading to severe defoliation and the appearance of fruit spots. This results in 85% defoliation and 80% infested fruits per orchard. Besides, *Alternaria* sp. can also cause other diseases like moldy core during postharvest storage. Therefore, the incidence of *Alternaria* disease can occur both during cultivation and post-harvest, leading to significant economic losses. Hence, effective strategies are necessary to manage *Alternaria*-related diseases for sustainable agriculture. *Alternaria* disease is traditionally managed by applying chemical fungicides through spray treatments. Few studies reported success in controlling the disease in various crops, including *Solanum tuberosum*, *Capsicum annuum*, sunflower, and Jerusalem artichoke (Viriyasuthee et al., 2019). However, due to evolving agricultural policies, aiming to reduce pesticide use by up to 50% by 2030 and the adverse effects of such fungicides, there is a need for innovative strategies. The use of resistant genotypes and biocontrol methods involving *Trichoderma* sp., however, have proven effective in peanuts, sunflower, chili, and aloe vera (Viriyasuthee et al., 2019) but not widely studied.

Using LABs as antifungal agents for crop protection is a promising prospect. LABs are naturally occurring microorganisms that have been found to offer a range of health benefits to humans, such as improving digestive health and boosting the immune system. As a probiotic, LABs can support the growth of beneficial bacteria in the gut, leading to improved overall health and wellbeing. By leveraging the natural properties of LABs, it is possible to protect the crops against harmful fungi while simultaneously promoting sustainable agricultural practices. The diverse population of LAB found in fruits can be a valuable resource for producing various probiotic products. The two novel LAB strains, isolated from *Tinospora cordifolia and Ficus benghalensis*: *Lpb. plantarum* MYSVA7 and *Lpb. plantarum* MYSVB1, respectively, offers an alternative solution against *A. alternata*. *Lpb. plantarum* MYSVB1 and its CFS showed imbibition of both mycelial growth and conidial germination. Moreover, it demonstrated in-vitro probiotic attributes, suggesting its potential as a probiotic strain. To ensure their suitability for industrial processing and storage, LAB strains, including the novel *Lpb. plantarum* MYSVB1 must undergo essential technological assessments. Further research should be focused on understanding their mechanisms of action and assessing their antifungal properties against other *Alternaria* sp. including the human pathogenic strains. In addition, it is important to study the *in vivo* efficacy of LAB as a probiotic and in-planta experiment of CFS as a biocontrol agent. This exploration has the potential to promote sustainable agricultural practices while capitalizing on the probiotic advantages offered by LABs.

6 Conclusion

A total of fifty-five LAB strains were isolated from seven different tropical fruits. Among these, seven isolates showed inhibition to *A. alternata*. Two strains, *Lactiplantibacillus*

plantarum MYSVA7, and *Lpb. plantarum* MYSVB1, showed promise as probiotics isolated from *Tinospora cordifolia* and *Ficus benghalensis* fruits, respectively. These strains demonstrated robust probiotic characteristics, including resistance to acidic pH (pH 4–6), 0.3% bile salt, 0.6% phenol and osmolarity (3–7% salt), as well as antibacterial activities against selected pathogens. Notably, these strains exhibited antifungal activity against *Alternaria alternata*, with strain MYSVB1 showing stable inhibition. The crude cell-free supernatant (CFS) from MYSVB1 exhibited superior inhibition, achieving a 70% growth reduction of *A. alternata* at 5%, and > 95% at 10% CFS. Additionally, the CFS also suppressed the germination of conidia. The specificity of MYSVB1 in inhibiting *A. alternata* suggested the involvement of a combination of several organic acids and proteinaceous substances. Succinic acid was the predominant organic acid present in CFS at 63%. yet it partly contributed to the inhibition. Further studies are needed to identify the antifungal molecule in CFS and test its efficacy in-planta experiments. This study contributes to the knowledge of LAB diversity in tropical fruits and their potential applications in probiotics and biocontrol against fungal phytopathogens.

Data availability statement

The data presented in the study are deposited in the National Center for Biotechnology Information (NCBI) repository and accession numbers can be found in the article.

Author contributions

RV: Conceptualization, Data curation, Formal analysis, Methodology, Writing—original draft. MS: Data curation, Validation, Writing—review and editing. RS: Resources, Writing—review and editing. AG: Resources, Writing—review and editing. MYS: Supervision, Writing—review and editing.

Funding

The author(s) declare that no financial support was received for the research, authorship, and/or publication of this article.

Conflict of interest

The authors declare that the research was conducted in the absence of any commercial or financial relationships that could be construed as a potential conflict of interest.

Publisher's note

All claims expressed in this article are solely those of the authors and do not necessarily represent those of their affiliated organizations, or those of the publisher, the editors and the reviewers. Any product that may be evaluated in this article, or claim that may be made by its manufacturer, is not guaranteed or endorsed by the publisher.

Supplementary material

The Supplementary Material for this article can be found online at: https://www.frontiersin.org/articles/10.3389/fmicb.2024.1322758/full#supplementary-material

References

Adithi, G., Somashekaraiah, R., Divyashree, S., Shruthi, B., and Sreenivasa, M. Y. (2022). Assessment of probiotic and antifungal activity of *Lactiplantibacillus plantarum* MYSAGT3 isolated from locally available herbal juice against mycotoxigenic *Aspergillus* species. *Food Biosci.* 50:102118.

Argyri, A. A., Zoumpopoulou, G., Karatzas, K. A. G., Tsakalidou, E., Nychas, G. J. E., Panagou, E. Z., et al. (2013). Selection of potential probiotic lactic acid bacteria from fermented olives by in vitro tests. *Food Microbiol.* 33, 282–291.

Armitage, A. D., Cockerton, H. M., Sreenivasaprasad, S., Woodhall, J., Lane, C. R., Harrison, R. J., et al. (2020). Genomics evolutionary history and diagnostics of the *Alternaria alternata* species group including apple and Asian pear pathotypes. *Front. Microbiol.* 10:3124. doi: 10.3389/fmicb.2019.03124

Campana, R., van Hemert, S., and Baffone, W. (2017). Strain-specific probiotic properties of lactic acid bacteria and their interference with human intestinal pathogens invasion. *Gut Pathog.* 9:12. doi: 10.1186/s13099-017-0162-4

Cappuccino, J. G. S., and Sherman, N. (1999). *Microbiology: a Laboratory Manual*, 10th Edn. : California, CA: Pearson Benjamin Cummings.

Charteris, W. P., Kelly, P. M., Morelli, L., and Collins, J. K. (1998). Antibiotic susceptibility of potentially probiotic Lactobacillus species. *J. Food Prot.* 61, 1636–1643.

Deepthi, B. V., Rao, P., Chennapa, M. K. N., Chandrashekara, K. T., and Sreenivasa, M. Y. (2016). Antifungal attributes of *Lactobacillus plantarum* MYS6 against Fumonisin producing *Fusarium proliferatum* associated with poultry feeds. *PLoS One* 11:e0155122. doi: 10.1371/journal.pone.0155122

Di Cagno, R., Cardinali, G., Minervini, G., Antonielli, L., Rizzello, C. G., Ricciuti, P., et al. (2010). Taxonomic structure of the yeasts and lactic acid bacteria microbiota of pineapple (*Ananas comosus* L. Merr.) and use of autochthonous starters for minimally processing. *Food Microbiol.* 27, 381–389. doi: 10.1016/j.fm.2009.11.012

Di Cagno, R., Coda, R., De Angelis, M., and Gobbetti, M. (2013). Exploitation of vegetables and fruits through lactic acid fermentation. *Food Microbiol.* 33, 1–10.

Drider, D., Bendali, F., Naghmouchi, K., and Chikindas, M. L. (2016). Bacteriocins: not only antibacterial agents. *Probiotics Antimicrob.* 8, 177–182.

Gabriel, M. F., Uriel, N., Teifoori, F., Postigo, I., Suñén, E., and Martínez, J. (2017). The major *Alternaria alternata* allergen, Alt a 1: a reliable and specific marker of fungal contamination in citrus fruits. *Int. J. Food Microbiol.* 257, 26–30. doi: 10.1016/j.ijfoodmicro.2017.06.006

Gai, Y., Niu, Q., Kong, J., Li, L., Liang, X., Cao, Y., et al. (2023). Genomic and transcriptomic characterization of *Alternaria alternata* during infection. *Agronomy* 13:809.

Garcia, E. F., Luciano, W. A., Xavier, D. E., da Costa, W. C., de Sousa Oliveira, K., Franco, O. L., et al. (2016). Identification of lactic acid bacteria in fruit pulp processing byproducts and potential probiotic properties of selected *Lactobacillus* strains. *Front. Microbiol.* 7:1371. doi: 10.3389/fmicb.2016.01371

Girma, A., and Aemiro, A. (2021). Antibacterial activity of lactic acid bacteria isolated from fermented Ethiopian traditional dairy products against food spoilage and pathogenic bacterial strains. *J. Food Qual.* 2021:9978561.

Gkarmiri, K., Finlay, R. D., Alström, S., Thomas, E., Cubeta, M. A., and Högberg, N. (2015). Transcriptomic changes in the plant pathogenic fungus *Rhizoctonia solani* AG-3 in response to the antagonistic bacteria *Serratia proteamaculans* and *Serratia plymuthica*. *BMC Genom.* 16:630. doi: 10.1186/s12864-015-1758-z

Goh, Y. J., and Klaenhammer, T. R. (2010). Functional roles of aggregation-promoting-like factor in stress tolerance and adherence of *Lactobacillus acidophilus* NCFM. *Appl. Environ. Microbiol.* 76, 5005–5012. doi: 10.1128/AEM.00030-10

He, J.-F., Jin, D.-X., Luo, X.-G., and Zhang, T.-C. (2020). LHH1, a novel antimicrobial peptide with anti-cancer cell activity identified from *Lactobacillus casei* HZ1. *AMB Express*, 10, 1–15. doi: 10.1186/s13568-020-01139-8

Hedberg, M., Hasslöf, P., Sjöström, I., Twetman, S., and Stecksén-Blicks, C. (2008). Sugar fermentation in probiotic bacteria–an in vitro study. *Oral Microbiol. Immunol.* 23, 482–485. doi: 10.1111/j.1399-302X.2008.00457.x

Hsu, T. C., Yi, P. J., Lee, T. Y., and Liu, J. R. (2018). Probiotic characteristics and zearalenone-removal ability of a *Bacillus licheniformis* strain. *PLoS One* 13:e0194866. doi: 10.1371/journal.pone.0194866

Kaur, M., Singh, H., Jangra, M., Kaur, L., Jaswal, P., Dureja, C., et al. (2017). Lactic acid bacteria isolated from yak milk show probiotic potential. *Appl. Microbiol. Biotechnol.* 101, 7635–7652.

Kumar, R., Chandar, B., and Parani, M. (2018). Use of succinic & oxalic acid in reducing the dosage of colistin against New Delhi metallo-β-lactamase-1 bacteria. *Indian J. Med. Res.* 147, 97–101.

Kumar, V. J. R., Seo, B. J., Mun, M. R., Kim, C. J., Lee, I., Kim, H., et al. (2010). Putative probiotic *Lactobacillus* spp. from porcine gastrointestinal tract inhibit transmissible gastroenteritis coronavirus and enteric bacterial pathogens. *Trop. Anim. Health Prod.* 42, 1855–1860. doi: 10.1007/s11250-010-9648-5

Kumari, V. B., Huligere, S. S., Ramu, R., Naik Bajpe, S., Sreenivasa, M. Y., Silina, E., et al. (2022). Evaluation of probiotic and antidiabetic attributes of *Lactobacillus* strains isolated from fermented beetroot. *Front. Microbiol.* 13:911243. doi: 10.3389/fmicb.2022.911243

Kushkevych, I., Kotrsová, V., Dordević, D., Buňková, L., Vítězová, M., and Amedei, A. (2019). Hydrogen sulfide effects on the survival of lactobacilli with emphasis on the development of inflammatory bowel diseases. *Biomolecules* 9:752. doi: 10.3390/biom9120752

Lee, J. S., Chung, M. J., and Seo, J. G. (2013). In vitro evaluation of antimicrobial activity of lactic acid bacteria against *Clostridium difficile*. *Toxicol. Res.* 29, 99–106.

Leyva Salas, M., Mounier, J., Valence, F., Coton, M., Thierry, A., and Coton, E. (2017). Antifungal microbial agents for food biopreservation—a review. *Microorganisms* 5:37. doi: 10.3390/microorganisms5030037

Li, M., Wang, Y., Cui, H., Li, Y., Sun, Y., and Qiu, H. J. (2020). Characterization of lactic acid bacteria isolated from the gastrointestinal tract of a wild boar as potential probiotics. *Front. Vet. Sci.* 7:49. doi: 10.3389/fvets.2020.00049

Lukic, J., Strahinic, I., Milenkovic, M., Nikolic, M., Tolinacki, M., Kojic, M., et al. (2014). Aggregation factor as an inhibitor of bacterial binding to gut mucosa. *Microb. Ecol.* 68, 633–644. doi: 10.1007/s00248-014-0426-1

Maria, do Socorro, M. R., Alves, R. E., de Brito, E. S., Pérez-Jiménez, J., Saura-Calixto, F., et al. (2010). Bioactive compounds and antioxidant capacities of 18 non-traditional tropical fruits from Brazil. *Food Chem.* 121, 996–1002.

Masunaka, A., Ohtani, K., Peever, T. L., Timmer, L. W., Tsuge, T., Yamamoto, M., et al. (2005). An isolate of *Alternaria alternata* that is pathogenic to both tangerines and rough lemon and produces two host-selective toxins, ACT- and ACR-toxins. *Phytopathology* 95, 241–247.

Mirzaei, E. Z., Lashani, E., and Davoodabadi, A. (2018). Antimicrobial properties of lactic acid bacteria isolated from traditional yogurt and milk against *Shigella* strains. *GMS Hyg. Infect. Control* 13:Doc01. doi: 10.3205/dgkh000307

Nami, Y., Vaseghi Bakhshayesh, R., Mohammadzadeh Jalaly, H., Lotfi, H., Eslami, S., and Hejazi, M. A. (2019). Probiotic properties of *Enterococcus* isolated from artisanal dairy products. *Front. Microbiol.* 10:300. doi: 10.3389/fmicb.2019.00300

Oliveira, A. P., Pereira, J. A., Andrade, P. B., Valentão, P., Seabra, R. M., and Silva, B. M. (2008). Organic acids composition of *Cydonia oblonga* Miller leaf. *Food Chem.* 111, 393–399. doi: 10.1016/j.foodchem.2008.04.004

Orij, R., Urbanus, M. L., Vizeacoumar, F. J., Giaever, G., Boone, C., Nislow, C. C., et al. (2012). Genome-wide analysis of intracellular pH reveals quantitative control of cell division rate by pH in *Saccharomyces cerevisiae*. *Genome Biol.* 13:R80. doi: 10.1186/gb-2012-13-9-r80

Pierce, C. G., Uppuluri, P., Tristan, A. R., Wormley, F. L., Mowat, E., Ramage, G., et al. (2008). A simple and reproducible 96-well plate-based method for the formation of fungal biofilms and its application to antifungal susceptibility testing. *Nat. Protoc.* 3, 1494–1500. doi: 10.1038/nport.2008.141

Rao, P. K., Deepthi, B. V., Rakesh, S., Ganesh, T., Achar, P., and Sreenivasa, M. Y. (2019). Antiaflatoxigenic potential of cell-free supernatant from *Lactobacillus plantarum* MYS44 against *Aspergillus parasiticus*. *Probiotics Antimicrob.* 11, 55–64. doi: 10.1007/s12602-017-9338-y

Reuben, R. C., Roy, P. C., Sarkar, S. L., Alam, R. U., and Jahid, I. K. (2019). Isolation, characterization, and assessment of lactic acid bacteria toward their selection as poultry probiotics. *BMC Microbiol.* 19:253. doi: 10.1186/s12866-019-1626-0

Rodríguez, L. G. R., Gasga, V. M. Z., Pescuma, M., Van Nieuwenhove, C., Mozzi, F., and Burgos, J. A. S. (2021). Fruits and fruit by-products as sources of bioactive compounds. benefits and trends of lactic acid fermentation in the development of novel fruit-based functional beverages. *Food Res. Int.* 140:109854. doi: 10.1016/j.foodres.2020.109854

Shehata, M. G., El Sohaimy, S. A., El-Sahn, M. A., and Youssef, M. M. (2016). Screening of isolated potential probiotic lactic acid bacteria for cholesterol lowering property and bile salt hydrolase activity. *Ann. Agric. Sci.* 61, 65–75.

Somashekaraiah, R., Mottawea, W., Gunduraj, A., Joshi, U., Hammami, R., and Sreenivasa, M. Y. (2021). Probiotic and antifungal attributes of *Levilactobacillus brevis* MYSN105, isolated from an Indian traditional fermented food Pozha. *Front. Microbiol.* 12:696267. doi: 10.3389/fmicb.2021.696267

Somashekaraiah, R., Shruthi, B., Deepthi, B. V., and Sreenivasa, M. Y. (2019). Probiotic properties of lactic acid bacteria isolated from neera: a naturally fermenting coconut palm nectar. *Front. Microbiol.* 10:1382. doi: 10.3389/fmicb.2019.01382

Steglińska, A., Kołtuniak, A., Motyl, I., Berłowska, J., Czyżowska, A., Cieciura-Włoch, W., et al. (2022). Lactic acid bacteria as biocontrol agents against potato (*Solanum tuberosum* l.) pathogens. *Appl. Sci.* 12:7763.

Stewart, J. E., Thomas, K. A., Lawrence, C. B., Dang, H., Pryor, B. M., Timmer, L. M., et al. (2013). Signatures of recombination in clonal lineages of the citrus brown spot pathogen, *Alternaria alternata sensu* lato. *Phytopathology* 103, 741–749. doi: 10.1094/PHYTO-08-12-0211-R

Tanahashi, M., Nakano, T., Akamatsu, H., Kodama, M., Otani, H., and Osaki-Oka, K. (2016). *Alternaria alternata* apple pathotype (*A. mali*) causes black spot of European pear. *Eur. J. Plant Pathol.* 145, 787–795.

Taroub, B., Salma, L., Manel, Z., Ouzari, H. I., Hamdi, Z., and Moktar, H. (2019). Isolation of lactic acid bacteria from grape fruit: antifungal activities, probiotic properties, and in vitro detoxification of ochratoxin A. *Ann. Microbiol.* 69, 17–27.

Vanitha, P. R., Somashekaraiah, R., Divyashree, S., Pan, I., and Sreenivasa, M. Y. (2023). Antifungal activity of probiotic strain *Lactiplantibacillus plantarum* MYSN7 against *Trichophyton tonsurans*. *Front. Microbiol.* 14:1192449. doi: 10.3389/fmicb.2023.1192449

Viriyasuthee, W., Jogloy, S., Saksirirat, W., Saepaisan, S., Gleason, M. L., and Chen, R. S. (2019). Biological control of Alternaria leaf spot caused by *Alternaria* spp. in Jerusalem artichoke (*Helianthus tuberosus* L.) under two fertilization regimes. *Plants* 8:463. doi: 10.3390/plants8110463

Vitali, B., Minervini, G., Rizzello, C. G., Spisni, E., Maccaferri, S., Brigidi, P., et al. (2012). Novel probiotic candidates for humans isolated from raw fruits and vegetables. *Food Microbiol.* 31, 116–125. doi: 10.1016/j.fm.2011.12.027

Wang, H., Yan, Y., Wang, J., Zhang, H., and Qi, W. (2012). Production and characterization of antifungal compounds produced by *Lactobacillus plantarum* IMAU10014. *PLoS One* 7:e29452. doi: 10.1371/journal.pone.0029452

Wang, Y., Wu, J., Lv, M., Shao, Z., Hungwe, M., Wang, J., et al. (2021). Metabolism characteristics of lactic acid bacteria and the expanding applications in food industry. *Front. Bioeng. Biotechnol.* 9:612285. doi: 10.3389/fbioe.2021.612285

Xu, W., Wang, H., Lv, Z., Shi, Y., and Wang, Z. (2019). Antifungal activity and functional components of cell-free supernatant from *Bacillus amyloliquefaciens* LZN01 inhibit *Fusarium oxysporum* f. sp. niveum growth. *Biotechnol. Biotechnol. Equip.* 33, 1042–1052.

Zhang, Y., Yang, H., Huang, R., Wang, X., Ma, C., and Zhang, F. (2022). Effects of *Lactiplantibacillus plantarum* and *Lactiplantibacillus brevis* on fermentation, aerobic stability, and the bacterial community of paper mulberry silage. *Front. Microbiol.* 13:1063914. doi: 10.3389/fmicb.2022.1063914

Zhao, H., Liu, K., Fan, Y., Cao, J., Li, H., Song, W., et al. (2022). Cell-free supernatant of *Bacillus velezensis* suppresses mycelial growth and reduces virulence of *Botrytis cinerea* by inducing oxidative stress. *Front. Microbiol.* 13:980022. doi: 10.3389/fmicb.2022.980022

frontiers | Frontiers in Microbiology

TYPE Review
PUBLISHED 13 March 2024
DOI 10.3389/fmicb.2024.1269282

OPEN ACCESS

EDITED BY
Monika Prakash Rai,
Motilal Nehru National Institute of Technology Allahabad, India

REVIEWED BY
Arun Karnwal,
Lovely Professional University, India
Leonardo Teixeira Dall'Agnol,
Federal University of Maranhão, Brazil
Nigel Richards,
Cardiff University, United Kingdom

*CORRESPONDENCE
Kindu Tsegaye
✉ kindu.nibret@uog.edu.et

RECEIVED 29 July 2023
ACCEPTED 20 February 2024
PUBLISHED 13 March 2024

CITATION
Tsegaye K, Tsehai BA and Getie B (2024) Desirable L-asparaginases for treating cancer and current research trends.
Front. Microbiol. 15:1269282.
doi: 10.3389/fmicb.2024.1269282

Desirable L-asparaginases for treating cancer and current research trends

Kindu Tsegaye[1]*, Berhanu Andualem Tsehai[2] and Birhan Getie[3]

[1]Department of Industrial Biotechnology, Institute of Biotechnology, University of Gondar, Gondar, Ethiopia, [2]Department of Biotechnology, University of Gondar, Gondar, Ethiopia, [3]Department of Industrial Biotechnology, Institute of Biotechnology, University of Gondar, Gondar, Ethiopia

Amino acid depletion therapy is a promising approach for cancer treatment. It exploits the differences in the metabolic processes between healthy and cancerous cells. Certain microbial enzymes induce cancer cell apoptosis by removing essential amino acids. L-asparaginase is an enzyme approved by the FDA for the treatment of acute lymphoblastic leukemia. The enzymes currently employed in clinics come from two different sources: *Escherichia coli* and *Erwinia chrysanthemi*. Nevertheless, the search for improved enzymes and other sources continues because of several factors, including immunogenicity, *in vivo* instability, and protease degradation. Before determining whether L-asparaginase is clinically useful, research should consider the Michaelis constant, turnover number, and maximal velocity. The identification of L-asparaginase from microbial sources has been the subject of various studies. The primary goals of this review are to explore the most current approaches used in the search for therapeutically useful L-asparaginases and to establish whether these investigations identified the crucial characteristics of L-asparaginases before declaring their therapeutic potential.

KEYWORDS

acute lympho blastic leukemia, cancer, kinetic properties, L-asparaginase, Michaelis constant

Introduction

Amino acid deprivation is an approach that shows promise for the development of novel cancer therapies. This natural remedy relies on the difference in metabolic processes between healthy and cancerous cells (Dhankhar et al., 2020). Because of their rapid growth, cancer cells produce fewer enzymes overall, which leads to auxotrophy for a subset of amino acids and makes them a target for enzymes that deplete amino acids. Therapeutic enzymes can only suppress tumor cells by cutting off amino acids, since normal cells can make their own. Amino acid deprivation therapy requires the use of certain enzymes, such as L-asparaginase, arginine deiminase, methionine, lysine oxidase, glutaminase, and phenylalanine ammonia-lyase (Dhankhar et al., 2020). L-asparaginases were first discovered as anticancer enzymes in 1922 (El-fakharany et al., 2020). The 22nd World Health Organization List of Essential Medicines now includes L-asparaginase as a cytotoxic therapy for acute lymphoblastic leukemia (WHO, 2021).

Leukemia is usually a cancer that causes an overabundance of aberrant white blood cells (blasts) in the bone marrow. Lymphoblastic leukemia affects lymphocytes that make up the lymph tissues 4. Acute lymphoblastic leukemia (ALL) is characterized by unchecked

lymphocyte immature growth. L-asparaginase is one of the most widely used medications for treating ALL (Díaz-Barriga et al., 2021).

Antineoplastic drug successfully treated acute lymphoblastic leukemia (Radadiya et al., 2020; Sobat et al., 2020). L-asparaginase converts L-asparagine into aspartic acid and ammonia. When administered systemically, L-asparaginase (L-ASNase) reduces the availability of L-asparagine and prevents cancer cells from multiplying quickly and with a prime need for exogenous asparagine (van Trimpont et al., 2022). Lymphoblasts do not express asparagine synthetase (ASNS); hence, these cells must take extracellular asparagine to survive.

The L-asparaginases from *Escherichia coli* and *Erwinia chrysanthemi* have been used extensively in medicine, but growing complications like hypersensitivity, antigenicity, short half-life, temporary blood clearance, and unfavorable L-glutaminase-dependent neurotoxicity require ongoing research to find more suitable alternatives (Nguyen et al., 2018; Radadiya et al., 2020; Sobat et al., 2020). Problems with commercial L-ASNases have prompted research into better sources of the enzyme. This article summarizes the bacterial and fungal based L-asparaginases that are medically significant.

L-asparaginases in the modern clinics

Today's clinics use five distinct L-ASNase preparations (van Trimpont et al., 2022). The two ansB gene products from *E. chrysanthemi* are in the market under the trade names Erwinase and Rylaze. The ansB gene from *E. coli* was the source of the remaining three. Two of the three type II *E. coli* ASNases are stabilized formulations produced by the covalent conjugation of monomethoxy polyethylene glycol (PEG) to lysine on the enzyme via a succinimidyl succinate linker (Oncaspar) or succinimidyl carbonate linker (Asparlas). One of the three type II *E. coli* ASNases is a native formulation (Elspar and Kidrol). The addition of a PEG tag to L-ASNases prolongs their half-life and delays their removal from the body (van Trimpont et al., 2022).

The primary treatment for most ALL patients is PEG-native *E. coli* L-ASNase (EcA); unfortunately, many patients experience hypersensitivity reactions. This hypersensitivity may result from either a negative immunological response to the enzyme or the formation of neutralizing antibodies (often known as silent inactivation; Modi and Gervais, 2022). Native *E. chrysanthemi* L-ASNase (ErA) differs immunologically from PEG-native EcA and does not react with PEG-nEcA-derived antibodies. Therefore, patients who acquired an allergy to PEG-native EcA were administered native ErA (or, starting in July 2021, recombinant ErA) as second-line treatment (Modi and Gervais, 2022).

L-asparaginases important in clinics

Type-I L-asparaginase, which has a low affinity for asparagine, is encoded by ansA in *E. coli*, whereas type-II L-asparaginase, which has a higher affinity for asparagine, is encoded by ansB. Acute lymphoblastic leukemia treatment employs type-II enzymes (Vimal and Kumar, 2017). The activity of an enzyme is often determined by adding a substrate to L-asparaginase and quantifying the amount of the output produced. While this measurement is a useful indicator for comparing activity between multiple enzymes within the same study, it is not always possible to compare this type of measurement to those from other studies. It is challenging to compare results from different research organizations because experiment-to-experiment variations in temperature, pH, and substrate quantity exist. In order to truly understand the therapeutic potential of a novel L-asparaginase, the kinetic parameters offer better insights (Beckett and Gervais, 2019).

The kinetic parameters provide insight into substrate affinity and turnover, which are unconditional values that can be consistently compared between study groups, and are essential for fully appreciating the therapeutic potential of a novel L-asparaginase. Before making claims regarding the therapeutic potential of a novel enzyme, Beckett and Gervais (2019) state that, at the very least, Michaelis constant (K_m), turnover number (K_{cat}), and maximum velocity (V_{max}) should be established. However, many of the articles published in recent years lack this information (Abdelrazek et al., 2019; Kumar et al., 2019; Moguel et al., 2020; Prakash et al., 2020; Chakraborty and Shivakumar, 2021). In this review, few L-asparaginases from bacterial and fungal origin are reviewed, along with their corresponding kinetic properties and other characteristics.

Michaelis constant (K_m value)

One requirement for the therapeutic effectiveness of L-asparaginases is the K_m value. Michaelis constant (K_m) is the amount of a substrate at which the reaction rate is half of the maximum reaction rate. A lower K_m value shows that the enzyme is more active toward that substrate and can perform at half its maximum rate at lower substrate concentrations (Baral et al., 2020). For L-asparagine to completely disappear from circulation, a micromolar K_m is needed.

The K_m value is a quantifiable measure of the enzyme's affinity for a substrate; the lower the K_m value, the greater the affinity of the enzyme for that substrate, and, in a therapeutic setting, the more effective the enzyme (Beckett and Gervais, 2019; Baral et al., 2020). Because intravenous L-asparaginase must be able to remove circulating pools of L-asparagine, which are not high (approximately 50 M), a low K_m (at least micromolar) of L-asparaginase is necessary (Loch and Jaskolski, 2021).

Turnover number (K_{cat})

Turnover number, often known as K_{cat}, is another helpful indicator for assessing enzyme activity. It provides the number of substrates that a single enzyme molecule converts into a product per unit of time (Baral et al., 2020). The substrate fully occupied the catalytic sites of the enzyme at the maximum reaction speed (V_{max}). V_{max} is the amount of substrate that an enzyme can convert into a product in a second. The turnover number (K_{cat}) is therefore the V_{max} divided by the enzyme concentration. The rate of transforming substrates into products increases as K_{cat} increases. A good therapeutic L-asparaginase must have a low K_m value and a high K_{cat} value to lower endogenous asparagine levels from 40 to 80 M to 0.02 M (Beckett and Gervais, 2019). Oncaspar and Erwinase, the two L-asparaginases that are currently on the market, have asparagine K_m and K_{cat} values of roughly

0.05 mM and 200–560 s^{-1}, respectively (Beckett and Gervais, 2019; Baral et al., 2020).

Glutaminase coactivity

The literature contains conflicting information regarding the secondary glutaminase activity of L-ASNases. From the FDA (United States)-approved *E. chrysanthemi* L-asparaginase, Nguyen et al. (2018) created a novel low glutaminase enzyme that was highly effective against T and B cell ALL (Nguyen et al., 2018). However, Chan et al. (2019) examined both the wild-type ASNase and its glutaminase-deficient mutant. They discovered that L-ASNase glutaminase activity, rather than ASNase activity alone, contributed to substantial anticancer efficacy against xenografts of the ASNS-negative leukemia cell line in NSG mice (Chan et al., 2019). This finding implies that, even against ASNS-negative cancer types, long-lasting, single-agent anticancer efficacy *in vivo* requires ASNase glutaminase activity. Horvath et al. (2019) investigated the pharmacodynamics of ASNase in a mouse model of cancer. They showed that asparagine was detected after L-ASNase treatment, in contrast to previously published methods that produced post-ASNase asparagine levels below the detection threshold (Horvath et al., 2019). They ascribed these differences to the use of whole blood, which collects the target analyte in both the red blood cell and plasma, as opposed to only serum or plasma.

A different study by Nguyen et al. (2017) suggested that a single-point mutation controls the substrate selection of L-asparaginases. They claimed that whereas the L-glutaminase activities of *Wolinella succinogenes* L-asparaginase (WoA) with proline at position 121 (WoA-P121) and WoA with serine at position 121 (WoA-S121) were noticeably different, their kinetic characteristics were identical. L-glutaminase activity is present in the WoA variant with a proline at position 121 but not in WoA-S121 (Nguyen et al., 2017). Nguyen et al. (2017) concluded that the residue at position 121 controls Asn vs. Gln selectivity via a mechanism other than substrate binding, which calls for further research.

Toxicity

L-asparaginase's toxicity is caused by either a secondary L-glutaminase activity or a hypersensitivity to the foreign protein (Baral et al., 2020; Fonseca et al., 2021; van Trimpont et al., 2022). When the body perceives an enzyme as foreign, it triggers an immunological reaction that results in a minor allergic reaction to anaphylactic shock (Baral et al., 2020). Glutaminase coactivity results in the hydroxylation of glutamine to glutamate and ammonia. Excessive ammonia generation may cause neurotoxicity and liver malfunction (van Trimpont et al., 2022). Ashok et al. (2019) eliminated toxicity caused by *E. coli* and *E. chrysanthemi* L-ASNases by purifying the urease (Ashok et al., 2019). Urease catalyzes the hydrolysis of urea, which results in the production of ammonia and carbon dioxide. As a result, ammonia is excreted from the bloodstream as urea is converted back to ammonia, resulting in hyperammonemia, a condition that damages the brain (Ashok et al., 2019). Chakraborty and Shivakumar (2021) also described a glutaminase and urease-free L-asparaginase from *Agaricomycete* sp. *Ganoderma australe* GPC191 (Chakraborty and Shivakumar, 2021). The urease activity of L-ASNases was not, however, reported in many of the studies.

The need for exogenous sources of L-asparaginases

Humans possess a type III L-asparaginase that needs a threonine residue at the N-terminus to catalyze reactions. Unfortunately, because of its millimolar K_m value for L-asparagine, natural human L-asparaginase is not suitable for therapeutic uses. L-asparaginases must have a micromolar K_m for asparagine in order to remove it from the blood (Rigouin et al., 2017). To get rid of the circulating L-asparagine in ALL patients, type II L-asparaginases from *E. coli* or *E. chrysanthemi* are utilized (Radadiya et al., 2020; Andrade et al., 2021). Wild type II L-asparaginases exhibit high selectivity for L-asparagine and low glutaminase side activity (2%–10%).

Kinetic parameters of microbial L-asparaginases in recent studies

L-asparaginase is a therapeutic enzyme used to treat cancer. The major obstacles to the therapeutic potential of this enzyme are immunogenicity, short plasma half-life, and glutaminase activity (Vidya et al., 2017). Several research and development projects are underway to address these problems. To identify a novel therapeutic L-asparaginase, studies must consider V_{max}, K_m, and K_{cat} values comparable to or superior to those of current therapeutic therapies (Beckett and Gervais, 2019). Plants, animals, and microbes naturally produce L-asparaginases. Compared to plant and animal sources, microbes are more cost-effective and easier to modify, optimize, extract, and purify for enzyme synthesis (Fazeli et al., 2021). In addition, genetically altering microbes to boost yields is simple (Costa-Silva et al., 2019). Because bacterial and fungal L-asparaginases are thought to be important in both medicine and industry, this review focuses on their kinetic properties.

Kinetic parameters of bacterial L-asparaginases

Although other bacterial species can produce L-asparaginases, only type-II L-asparaginases from *E. coli* and *E. chrysanthemi* have been produced on an industrial scale (Vimal and Kumar, 2017). There are two forms of bacterial L-asparaginases: intracellularly produced type I, or cytosolic, and extracellularly created type II, or periplasmic (El-fakharany et al., 2020). Most bacteria produce type I, or cytosolic, L-asparaginases within their cells, but a few secrets type II, or periplasmic, L-asparaginases outside. Since gram-positive bacteria do not have a periplasmic gap, they secrete much more enzymes into the environment than gram-negative bacteria (Vimal and Kumar, 2017).

The production of extracellularly secreted enzymes is more beneficial for industrial processes because these can be made in large quantities in a culture of ideal conditions, and it takes less money and effort to purify them (Vimal and Kumar, 2017; El-fakharany et al., 2020). As a result, it would be more profitable to test for extracellular enzymes in gram-positive bacteria. The type II bacterial L-asparaginases are the focus of this review since they are crucial for clinical outcomes. Table 1 shows bacterial strains that produce L-ASNase, along with their characteristics. The review includes studies from 2017 to present and reported the kinetic property of L-ASNases.

According to the data in Table 1, *Bacillus velezensis*, *Streptomyces brollosae* NEAE-115, and *Bacillus halotolerans* OHEM18 have low K_m values as compared to commercial L-ASNases, signifying that they might be potential candidates. L-ASNase from *Bacillus halotolerans* OHEM18 also showed an antioxidant activity against 2, 2′-azino-bis [3-ethylbenzothiazoline-6-sulfonic acid (ABTS) and 2, 2′-diphenyl-1-picrylhydrazyl (DPPH) radicals (Table 1)].

Kinetic parameters of fungi-derived L-asparaginases

Bacterial sources of L-asparaginase have been linked to a variety of immunological reactions, including hypersensitivity, irregular clotting, and allergic reactions. To reduce these immunological issues, a different supply is required. Fungi have evolved more closely with humans than bacteria, so it is likely that the enzymes they produce will have lower immunogenicity than bacteria (Ashok et al., 2019; Costa-Silva et al., 2019).

It has been claimed that a different source of L-asparaginases with fewer negative effects comes from fungi. Fungal species can be employed more successfully than other microbes to cure cancer because of their eukaryotic origin and their ability to reproduce the actions of human cells (Ashok et al., 2019). There may be fewer negative effects because yeast ASNase is more similar to human congeners (Karla et al., 2020). A variety of yeast genera, including *Candida, Pichia, Rhodosporidium, Saccharomyces*, and *Yarrowia*, have been reported to generate ASNase (Karla et al., 2020). Owing to appropriate post-translational protein modification and glycosylation, yeasts are good eukaryotic candidates for the production of asparaginase (Darvishi et al., 2018). The kinetic characteristics of L-asparaginases from fungi, as reported in recent literature, are shown in Table 2. According to Table 2, *Aspergillus terreus*, a marine sediment isolate, had a significantly high K_m compared to *E. coli* and *E. chrysanthemi*. Due to its kinetic characteristics, $K_m = 9.37$ M, $V_{max} = 127$ M/ML/min, and specific activity of 468.03 U/mg, the plant parasitic fungus *Lasiodiplodia theobromae* appears to be a suitable candidate for L-ASNase synthesis (Table 3).

The search for L-asparaginase is still ongoing

The *E. chrysanthemi* (ErAII) enzyme is only utilized when there are immunological reactions to *E. coli*-derived ASNases, and *E. coli* (EcAII) type II ASNase, whether in its native or PEGylated form, is currently the medication of choice. However, these L-ASNases have a high degree of *in vivo* instability, a short half-life, and require many administrations to be therapeutically effective (Maggi et al., 2017). Additionally, the immunological response, proteolytic degradation, and toxic side effects of type II bacterial L-ASNases limit their clinical usage (Radadiya et al., 2020). Numerous trials have been conducted worldwide in an attempt to reduce these problems.

Different strategies have been used to produce L-asparaginases with the best qualities for medicinal use. Recombinant ASNase synthesis, enzyme encapsulation, structural alteration of the enzyme, and the hunt for new ASNase-producing microbes are some of these methods (Sobat et al., 2020; Belén et al., 2021; Díaz-Barriga et al., 2021). L-asparaginase is found throughout all spheres of life; thus, a variety of sources, including bacteria, fungi, plants, and mammals, have been screened to identify enzymes with superior characteristics (Sobat et al., 2020).

TABLE 1 Kinetic parameters and other features of bacterial type-II L-asparaginase.

Bacterial species	K_m for Asn	V_{max} for Asn	Spec. activity U mg^{-1}	Half-life or stability	Other properties	Source	Effect on	Ref.
Bacillus altitudinis	9.09×10^{-2} M	0.09 Ms^{-1}	800	Opt. 37°C	Glutaminase free	Soil	Leukemia	Prakash et al. (2019)
Bacillus velezensis	3.6×10^{-5} M	41.49 µmol mL^{-1} min^{-1}	31.77	Opt. 37°C	Glutaminase free	Marine sediments	Breast cancer	Mostafa et al. (2019)
Bacillus licheniformis	0.049995 M	45.45 µmol mL^{-1} min^{-1}	36.08	Stable at 70°C for 1 h	Glutaminase free Stabile at 70°C for 1 h	Water Red sea	Breast, colon HepG2 live	Alrumman et al. (2019)
Streptomyces brollosae NEAE-115	2.139×10^{-3} M	152.6 UmL^{-1} min^{-1}	76.671	65.02 min at 50^0C	Glutaminase free extracellular Reduced immunogenicity	Soil	Ehrlich Ascites Carcinoma	El-naggar et al. (2018)
Bacillus halotolerans OHEM18	0.0047 M	92.74Uml^{-1} min^{-1}	215.33	70% activity for 1 h at 50°C	Extracellular antioxidant against DPPH* and ABTS** radicals	Soil	Leukemia, breast, hepatoma cells	El-fakharany et al. (2020)
Streptomyces sp.	0.065 mM	20.80 IU ml^{-1}	390 IU mg^{-1}	Stable till 50°C	Thermostable at 50°C	Soil	Not reported	Desai and Hungund (2018)

*DPPH, 2, 2 diphenyl-1-picrylhydrazyl. **ABTS, 2, 2′-azino-bis (3-ethylbenzothiazoline-6-sulfonic acid).

TABLE 2 The table lists recent studies that include recombinant microbial L-asparaginases and their accompanying characteristics.

Original microbe	Source	Gene	Host	K_m	V_{max}	Half-life or stability	Other properties	Ref.
Bacillus sp. *SL-1*	Salt lake	ansA1	*E. coli* BL21	10.30 µM	Not reported K_{cat} 23.96 s^{-1}	Stable at −20°C for 1 year	−Glutaminase pH range 4.5–10	Safary et al. (2019)
Cobetia amphilecti AMI6	Mangrove (shore line plant) sediments	CobAsnase AMI6 gene	*E. coli*	2.05 mM	11,641 µM min^{-1} mg^{-1}	68.26% activity after 60 min at 50°C	No detectable glutamine activity	Farahat et al. (2020)
Melioribacter roseus	Oil exploration well—Russia	L-ASNase-MrAIII Plant type	*E. coli BL21(DE3)*	1.4 mM	5,573 µM min^{-1}	70% activity after 1 h at 40°C	+Glutaminase (19%)	Dumina et al. (2021a)
Thermococcus kodakarensis	Thermophilic archaea	TK2246 gene*	*E. coli BL21(DE3)*	3.1 mM	833µmol mg^{-1} min^{-1}		Thermostable −80°C, Negligible glutaminase	Chohan et al. (2020)
Pyrococcus furiosus	NCBI CP003685.1	L-ASNase gene Uniprot Q8U4E6	*E. coli BL21(DE3)*	1.623 mM	105 µmol min^{-1} mg^{-1}	98.3% activity after 1 h at 37°C	Glutaminase free Urease free Shelf-life—56 days at 4°C	Saeed et al. (2020)
Bacillus subtilis strain R5	Culture from Osaka	Asn-R5 gene	*E. coli.*	2.4 mM	265 µmol min^{-1} mg^{-1},	180 min at 35°C	low glutaminase activities, thermal stability	Chohan and Rashid (2018)
Pseudomonas fluorescens MTCC 8127	Culture collection	ANS gene	*E. coli BL21 (DE3)*	0.050 M	4.032 mol min^{-1}	40 h	Minimal Glutaminase activity	Sindhu and Manonmani (2017)
Lactobacillus casei subsp. casei ATCC 393	Culture collection	ansB gene	*E. coli*	0.01235 mM	1.576 mM/min	serum -44 h trypsin—15 min	Active from 10 to 80°C	Aishwarya et al. (2019)
Bacillus tequilensis PV9W	Gene bank KR261609	ansA	*E. coli BL21 (DE3)*	0.04 mM	10.21 µmol mL^{-1} min^{-1}	Trypsin-120 min	Cervical cancer stable for 25 days at 25°C, least immunogenicity	Shakambari et al. (2018)
Halomonas elongata	Culture collection Iran	L-ASNase gene	*E. coli BL21 (DE3)*	5.6 mM	2.2 µmol min^{-1}, K_{cat} 1.96×10^3 s^{-1}	Serum-90 min	L-glutaminase activity-1%	Ghasemi et al. (2017)
Lactobacillus reuteri DSM 20016	Culture collection	ORF LREU_ RS09880	*E. coli BL21(DE3)*	0.3332 mM	14.06 mM min^{-1}	human serum-44 h trypsin—15 min	leukemic cell lines	Aishwarya et al. (2017)
Bacillus sonorensis	Soil	L-ASNase gene	*E. coli BL21(DE3)*	2.004 mM	3,723 µmol min^{-1}	Retain 92% activity at 37°C	No urease activity	Aly et al. (2020)
Pyrobaculum calidifontis-Archaea	NCBI CP000561.1	Pcal_0970 gene	*E. coli BL21-CodonPlus (DE3)-RIL*	4.5 mmol/L	355 µmol min^{-1} mg^{-1}	150 min at 100°C	Undetectable Glutaminase activity	Chohan et al. (2018)
Thermococcus sibiricus	Oil reservoir Serbia	*tsA_wt Gene bank WP_015849943.1*	*E. coli BL21 (DE3)*	2.8 mM	1,200 µM min^{-1}	86% activity after 20 min at 90°C	Low glutaminase activity	Dumina et al. (2021b)

Finding new L-asparaginases from new sources

Extreme conditions, such as salinity or high temperature, which cause the inactivation of enzymes isolated from terrestrial microorganisms, are widely used to produce enzymatic operations on an industrial scale. The marine environment attracts special interest in the search for new sources for economically significant products due to its extraordinary diversity and harsh circumstances (Alrumman et al., 2019; Mostafa et al., 2019; Sharma et al., 2019; Sobat et al., 2020; Bhargavi and Madhuri, 2021). Bacteria that are halotolerant or halophilic often express and synthesize enzymes that can withstand

TABLE 3 Features of fungal L-asparaginases in current research articles

Fungal/yeast species	K_m	V_{max}	Spec. activity	Half-life or stability	Other properties	Source	Ref.
Lasiodiplodia theobromae	9.37 μM	127.00 μM $mL^{-1}min^{-1}$	468.03 U/mg	Stable at 37 °C for 4 h	Extracellular	Culture collection-Egypt	Moubasher et al. (2022)
A.oryzae CCT 3940	2.10 mM	35.8 U mL^{-1}	Note reported	Stable after 60 min at 50°C	Glutaminase free	Culture collections (Brazil)	Dias et al. (2019)
A.oryzae LBA 01	5.07 mM	57.14 U mL^{-1}	Note reported	Only 60% after 60 min at 50 °C	Glutaminase free		
A. niger LBA 02	1.41 mM	39.22 U mL^{-1}	Note reported	stable after 60 min at 50°C	Low Glutaminase activity		
Aspergillus terreus	31.5 mM	500U mL^{-1}	268.5U Mg^{-1}	2826.90 min at 50°C	Glutaminase activity absent	Marine environment	Hassan et al. (2018)
Sarocladium strictum (yeast)	9.74 mM	8.19 μmol min^{-1}	Note reported	Note reported	Glutaminase free Mostly extracellular	Soil	Golbabaie et al. (2020)
Fusarium equiseti AHMF4	Not reported	Not reported	488.1 Umg^{-1}	100% activity for 1 h from 20°C to 40°C	Antioxidant—DPPH* anti-proliferative—cervical, hepatocellular, colorectal, breast	Soil	El-Gendy et al. (2021)
A. oryzae IOC 3999	3.28 mMol L^{-1}	45.04 U mL^{-1}	742.22 Umg^{-1} K_{cat} 0.93s^{-1}	Stable at 50°C for 1 h	Not reported	Culture collection-FioCruz	Da Cunha et al. (2021)
Sarocladium kiliense	0.025 mM	0.30 μmol $ml^{-1}min^{-1}$	919	Stable in human serum for48 h	Not reported	Marine water	Bhargavi and Madhuri (2021)

*DPPH, 2, 2 diphenyl-1-picrylhydrazyl.

extreme conditions, such as high temperatures, high salt concentrations, the presence of organic solvents, pH, and non-physiological values (Dumina et al., 2020; El-fakharany et al., 2020). Given that these enzymes are naturally exposed to large levels of osmolytes, such as NaCl or other suitable solutes, it would make sense to anticipate enhanced biological activity and/or osmolarity tolerance in physiological circumstances of blood serum (Ghasemi et al., 2017).

A new L-asparaginase from the hyperthermophilic archaeon *Thermococcus sibiricus* has been described by Dumina et al. (2021a). They cloned the L-ASNase gene of *Thermococcus sibiricus* into *E. coli* and studied its kinetics. The findings indicated a good contender, with K_m and V_{max} for the enzyme being 2.8 mM and 1,200 M/min, respectively (Dumina et al., 2021b). El-fakharany et al. (2020) discovered Bacillus halotolerans OHEM18, which can produce L-ASNases with $K_m = 0.0047$ M and $V_{max} = 92.74$ 2. This strain makes an essential extracellular L-ASNase, which is crucial for industry. In addition, Chakravarty et al. (2021) found *Bacillus australimaris* NJB19 in oceanic sediments and cloned the ASNase genes into *E. coli* to produce enzyme (Chakravarty et al., 2021). They discovered that the enzyme was effective against leukemic cells and had high affinity for asparagine. Tables 2, 3 show the results of several other investigations into the search for novel L-ASNases.

Reduced or absent co-activity in L-ASNase variants

The glutaminase co-activity of L-ASNase therapy has been implicated in the majority of its non-immune-related severe side effects. Thus, a decrease in glutaminase coactivity might significantly enhance the toxicity profile of L-ASNase. Alrumman et al. (2019) isolated *Bacillus licheniformis* from the Red Sea, which produces a glutaminase-free ASNase and may be a future candidate for pharmaceutical use as an anticancer medication *34*. Ashok et al. (2019) screened fungal species from Antarctic soil and moss that generate L-asparaginase devoid of glutaminase and urease (Ashok et al., 2019). Glutaminase-free L-ASNase has been tested in numerous investigations from various sources (El-naggar et al., 2018; Ashok et al., 2019; Mostafa et al., 2019; Safary et al., 2019; Karla et al., 2020; Prakash et al., 2020; Saeed et al., 2020; Prihanto et al., 2022). Further studies are necessary because there is still controversy regarding the coactivity of L-glutaminase asparaginase.

Encapsulation

Encapsulation is a promising and innovative strategy to improve the *in vivo* performance of ASNase because it prevents the enzyme from coming into direct contact with the environment, shields it from protease degradation, extends the enzyme's catalytic half-life, and, in some cases, lowers immunogenicity (Villanueva-flores et al., 2021; Guimarães et al., 2022). Shakambari et al. (2018) encapsulated L-ASNase from *Bacillus tequilensis* PV9W in solid lipid particles made from palmitic acid (Shakambari et al., 2018). In comparison to the natural L-asparaginase, the lipid particle-encapsulated version had increased V_{max} (7.790.34 to 10.211.43), a K_m that was cut in half (0.0700.01 to 0.040.001), a better half-life (50.19 to 120.56 min), and was stable for 25 days when stored at 25°C (Shakambari et al., 2018).

Encapsidation in a scaffold or substrate is another highly effective method to enhance the pharmacodynamics and pharmacokinetics of ASNase. ASNase II from *E. coli* was genetically engineered by Dáz-Barriga and colleagues into virus-like proteins of the bacteriophage P22. According to their findings, the encapsulated ASNase had a 15-fold and a 2-fold increase in K_m and K_{cat} compared to the unbound enzyme (Díaz-Barriga et al., 2021). These virus-like particles are made up of numerous copies of self-assembling proteins, but because they lack genetic material, they are unable to spread diseases. Their self-assembly abilities enable the development of a nanoparticle that is identical to the original viral capsid, except that it does not contain genetic material and instead includes an interesting chemical, in this example L-ASNase (Díaz-Barriga et al., 2021). The key findings, limitations, and existing knowledge gaps related to ASNase nano- and micro-encapsulation are well-reviewed in Villanueva-flores et al. (2021).

Site-directed mutagenesis

Site-directed mutagenesis can be used to generate EcAII variants with improved characteristics (Maggi et al., 2017). The stability, immunogenicity, and substrate specificity of L-ASNases can be significantly enhanced by using this method. According to a study by Maggi et al. (2017), Asn24 plays a critical role in maintaining EcAII active sites. For proteases that break down, asn24 serves as a cleavage point. Maggi et al. created the EcAII N24S variant through site-directed mutagenesis, which maintains asparaginase and glutaminase functions while exhibiting long-term storage stability and protease resistance (Maggi et al., 2017).

Structure-based rational design

Structure-based rational design is a potent protein engineering strategy to enhance the enzymatic capabilities of ASNases. Using bioinformatics servers (HotSpot Wizard and EVcoupling), rational design approach first screens active center residues using structural analysis, compares sequences, and identifies distal residues, allowing the construction of smart libraries for performing mutations at specific sites with less screening work (Zhou et al., 2022). Zhou et al. (2022) increased the type II ASNase from *Bacillus licheniformis's* catalytic activity by using semi-rational design (Zhou et al., 2022). According to their findings, the mutant's K_m value was 1.45 mM instead of 2.33 mM, and its K_{cat} value was 778.87 min-1 as opposed to 197.95 min^{-1} in the wild type. According to Aghaeepoor et al. (2018), the N248S mutation is linked to an appropriate L-ASNase function, while disrupting glutaminase activity due to hampered interactions. They stated that *in silico* analysis methods would provide useful information for creating mutant enzymes (Aghaeepoor et al., 2018). Yari et al. (2019) also described the significance of computational techniques for preliminary screening of appropriate mutations.

Using *in silico* screening

Traditional approaches to drug discovery are mainly based on *in vitro* drug screening and *in vivo* animal experiments; however, these methods are usually expensive and laborious. In recent years, omics data have provided an opportunity for the computational prediction of anti-cancer drugs, improving the efficiency of drug discovery (Baral et al., 2020; Li et al., 2020). Over time, there has been significant improvement in bioinformatics databases and methods used for drug screening, structural design, and immunogenicity prediction. This offers an opportunity to find anticancer medications that are less expensive and time consuming. Li et al. (2020) reviewed the databases and computational tools available for creating new cancer treatment approaches.

The basis of enzyme catalysis is the binding energy, which decreases the activation energy and circumvents the adverse entropic conditions necessary for the correct alignment of the enzyme and its substrates. Free energy was used to measure the binding energy, which is the energy generated when a substrate forms a weak connection with an enzyme's active site (Delta G). It is challenging to calculate this energy experimentally; therefore, an *in silico* method utilizing docking software would be more effective (Baral et al., 2020).

According to research by Baral et al. (2020), asnB genes from *Streptomyces griseus*, *Streptomyces venezuelae*, and *Streptomyces collinus* have higher binding energies than those from *E. coli* and *E. chrysanthemi* and were predicted to have the lowest Kms because binding energy and K_m are inversely correlate 20. As-Suhbani and Bhosale (2020) demonstrated in a different investigation that the interactions between the ligand L-asparagine and Fusarium solani CLR-36 L-asparaginase occurred at the active site with good binding energy (−6.85 kcal/mol; As-Suhbani and Bhosale, 2020).

Numerous studies have addressed the use of bioinformatics tools to analyze immune responses using *in silico* methods. Using the prediction tool EMBOSS antigenic explorer, Abdelrazek et al. (2019) identified possible antigenic areas of the L-asparaginase sequence of *Bacillus licheniformis* and compared them to those of *E. coli* and *E. chrysanthemi*. For the L-asparaginases of *E. coli*, *E. chrysanthemi,* and *Bacillus licheniformis*, 18, 16, and 17 antigenic areas, respectively, were discovered (Abdelrazek et al., 2019). Using a bioinformatics-based methodology, Belén et al. (2021) also predicted the immunogenicity of L-ASNases from nine filamentous fungi and compared the outcomes with those of *E. coli* L-ASNase (Belén et al., 2021).

Using recombinant DNA technology

Although hypersensitivity reactions frequently prevent their use, bacterial L-asparaginase has long been a crucial component of ALL treatment. For individuals with hypersensitivity, alternative asparaginase preparations are required to guarantee asparaginase availability. Recombinant technology has the potential to fill this unmet need by engineering cells to produce recombinant asparaginase with higher recovery, lower immunogenicity, and cheaper production costs (Vimal and Kumar, 2017), as well as by enhancing the characteristics of numerous commercially significant enzymes (Shakambari et al., 2018). Maese et al. (2021) described a recombinant *Erwinia asparaginase* (JZP-458) with no immunological cross-reactivity with *E. coli*-derived asparaginases *in vitro*. It was derived from a new *Pseudomonas fluorescens* production platform. The US Food

and Drug Administration approved JZP-458 (Rylaze) in June 2021 for the treatment of ALL in patients younger than 1 month old who exhibited hypersensitivity to asparaginase produced by *E. coli* (Maese et al., 2021). The process of cloning the L-asparaginase gene from an organism into *E. coli* has been attempted numerous times with success. Table 2 presents the results of a few of these attempts.

Author contributions

KT: Conceptualization, Writing – original draft, Writing – review & editing, Methodology, Validation, Investigation. BT: Validation, Writing – review & editing, Conceptualization, Supervision. BG: Validation, Writing – review & editing, Methodology.

Funding

The author(s) declare that no financial support was received for the research, authorship, and/or publication of this article.

Conflict of interest

The authors declare that the research was conducted in the absence of any commercial or financial relationships that could be construed as a potential conflict of interest.

Publisher's note

Supplementary material

The Supplementary material for this article can be found online at: https://www.frontiersin.org/articles/10.3389/fmicb.2024.1269282/full#supplementary-material

References

Abdelrazek, N. A., Elkhatib, W. F., Raafat, M. M., and Aboulwafa, M. M. (2019). Experimental and bioinformatics study for production of L-asparaginase from *Bacillus licheniformis*: a promising enzyme for medical application. *AMB Exp* 9, 1–16. doi: 10.1186/s13568-019-0751-3

Aghaeepoor, M., Akbarzadeh, A., Mirzaie, S., Hadian, A., Jamshidi Aval, S., and Dehnavi, E. (2018). Selective reduction in glutaminase activity of l'Asparaginase by asparagine 248 to serine mutation: a combined computational and experimental effort in blood cancer treatment. *Int. J. Biol. Macromol.* 120, 2448–2457. doi: 10.1016/j.ijbiomac.2018.09.015

Aishwarya, S. S., Iyappan, S., Lakshmi, K. V., and Rajnish, K. N. (2017). In silico analysis, molecular cloning, expression and characterization of l-asparaginase gene from *Lactobacillus reuteri* DSM 20016. *3 Biotech* 7:348. doi: 10.1007/s13205-017-0974-4

Aishwarya, S. S., Selvarajan, E., Iyappan, S., and Rajnish, K. (2019). Recombinant L-asparaginase II from *Lactobacillus casei* subsp.casei ATCC 393 and its anticancer activity. *Indian J. Microbiol.* 59, 313–320. doi: 10.1007/s12088-019-00806-0

Alrumman, S. A., Mostafa, Y. S., Al-izran, K. A., Alfai, M. Y., and Taha, T. H. (2019). Production and anticancer activity of an L-asparaginase from *Bacillus licheniformis* isolated from the Red Sea, Saudi Arabia. *Sci. Rep.* 9:3756. doi: 10.1038/s41598-019-40512-x

Aly, N., El-Ahwany, A., Ataya, F. A., and Saeed, H. (2020). *Bacillus sonorensis* L. Asparaginase: cloning, expression in E. Coli and characterization. *Protein J.* 39, 717–729. doi: 10.1007/s10930-020-09932-x

Andrade, K. C. R., Fernandes, R. A., Pinho, D. B., de Freitas, M. M., Filho, E. X. F., Pessoa, A., et al. (2021). Sequencing and characterization of an L-asparaginase gene from a new species of penicillium section Citrina isolated from Cerrado. *Sci. Rep.* 11:17861. doi: 10.1038/s41598-021-97316-1

Ashok, A., Doriya, K., Rao, J. V., Qureshi, A., and Tiwari, A. K. (2019). Microbes producing L-asparaginase free of glutaminase and urease isolated from extreme locations of Antarctic soil and Moss. *Sci. Rep.* 9:38094. doi: 10.1038/s41598-018-38094-1

As-Suhbani, A. E., and Bhosale, H. (2020). Homology MODELING of glutaminase free l-asparaginase from FUSARIUM SOLANI CLR-36. *J Adv. Sci. Res.* 11, 48–54.

Baral, A., Gorkhali, R., Basnet, A., Koirala, S., and Kumar, H. (2020). Selection of the optimal L-asparaginase II against acute lymphoblastic Leukemia: an in silico approach. *JMIRx Med* 2, 1–22. doi: 10.2196/29844

Beckett, A., and Gervais, D. (2019). What makes a good new therapeutic L-asparaginase? *World J. Microbiol. Biotechnol.* 9, 1–13. doi: 10.1007/s11274-019-2731-9

Belén, L. H., Lissabet, J. F. B., Rangel-Ygaui, C. O., Monteriro, G., Pessoa, A., and Farias, J. G. (2021). Immunogenicity assessment of fungal L-asparaginases: an in silico approach. *SN Appl. Sci.* 2, 1–10. doi: 10.1007/s42452-020-20

Bhargavi, M., and Madhuri, R. J. (2021). Optimization, Production, purification and characterization of anti-cancer enzyme L-asparaginase from marine Sarocladium kiliense. *Biosc.Biotech.res.Comm. Spec. Iss* 13, 93–102. doi: 10.21786/bbrc/13.15/17

Chakraborty, M., and Shivakumar, S. (2021). Bioprospecting of the agaricomycete Ganoderma australe GPC191 as novel source for l-asparaginase production. *Sci. Rep.* 11, 1–8. doi: 10.1038/s41598-021-84949-5

Chakravarty, N., Singh, J., and Singh, R. P. (2021). A potential type-II L-asparaginase from marine isolate bacillus australimaris NJB19: statistical optimization, in silico analysis and structural modeling. *Int. J. Biol. Macromol.* 174, 527–539. doi: 10.1016/j.ijbiomac.2021.01.130

Chan, W. K., Horvath, T. D., Tan, L., Link, T., Harutyunyan, K. G., Pontikos, M. A., et al. (2019). Glutaminase activity of L-asparaginase contributes to durable preclinical activity against acute lymphoblastic leukemia. *Mol. Cancer Ther.* 18, 1587–1592. doi: 10.1158/1535-7163.MCT-18-1329

Chohan, S. M., and Rashid, N. (2018). Gene cloning and characterization of recombinant L-asparaginase from *Bacillus subtilis* strain R5. *Biologia* 73, 537–543. doi: 10.2478/s11756-018-0054-1

Chohan, S. M., Rashid, N., Sajed, M., and Imanaka, T. (2018). Pcal _ 0970: an extremely thermostable L-asparaginase from *Pyrobaculum calidifontis* with no detectable glutaminase activity. *Folia Microbiol.* 64, 313–320. doi: 10.1007/s12223-018-0656-6

Chohan, S. M., Sajed, M., Naeem, S., and Rashid, N. (2020). Heterologous gene expression and characterization of TK2246, a highly active and thermostable plant type l-asparaginase from *Thermococcus kodakarensis*. *Int. J. Biol. Macromol.* 147, 131–137. doi: 10.1016/j.ijbiomac.2020.01.012

Costa-Silva, T. A., Camacho-Córdova, D. I., Agamez-Montalvo, G. S., Parizotto, L. A., Sánchez-Moguel, I., and Pessoa-Jr, A. (2019). Optimization of culture conditions and bench-scale production of anticancer enzyme L-asparaginase by submerged fermentation from aspergillus terreus CCT 7693. *Prep. Biochem. Biotechnol.* 49, 95–104. doi: 10.1080/10826068.2018.1536990

Da Cunha, M. C., Aguilar, J. G., Lindo, M., Castro, R. J. S., and Sato, H. H. (2021). L-asparaginase from Aspergillus oryzae spp.: effects of production process and biochemical parameters. *Prep. Biochem. Biotechnol.* 52, 1–11. doi: 10.1080/10826068.2021.1931881

Darvishi, F., Faraji, N., and Shamsi, F. (2018). Production and structural modeling of a novel asparaginase in Yarrowia lipolytica. *Int. J. Biol. Macromol.* 125, 955–961. doi: 10.1016/j.ijbiomac.2018.12.162

Desai, S. S., and Hungund, B. S. (2018). Submerged fermentation, purification, and characterization of L-asparaginase from streptomyces sp. isolated from soil. *J. Appl. Biol. Biotechnol.* 6, 17–23. doi: 10.7324/JABB.2018.60503

Dhankhar, R., Gupta, V., Kumar, S., Kapoor, R. K., and Gulati, P. (2020). Microbial enzymes for deprivation of amino acid metabolism in malignant cells: biological strategy for cancer treatment. *Appl. Microbiol. Biotechnol.* 104, 2857–2869. doi: 10.1007/s00253-020-10432-2

Dias, F. F. G., Gonçalves, J., Helia, A., and Sato, H. (2019). L-asparaginase from aspergillus spp.: production based on kinetics. *3 Biotech* 9, 1–10. doi: 10.1007/s13205-019-1814-5

Díaz-Barriga, C., Villanueva-Flores, F., Quester, K., Zárate-Romero, A., Cadena-Nava, R. D., and Huerta-Saquero, A. (2021). Asparaginase-phage P22 nanoreactors: toward a biobetter development for acute lymphoblastic Leukemia treatment. *Pharmaceutics* 13, 1–16. doi: 10.3390/pharmaceutics13050604

Dumina, M. V., Eldarov, M. A., Zdanov, D. D., and Sokolov, N. N. (2020). L-asparaginases of extremophilic microorganisms in biomedicine. *Biochem. Chem.* 14, 277–296. doi: 10.1134/S1990750820040046

Dumina, M., Zhgun, A., Pokrovskaya, M., Aleksandrova, S., Zhdanov, D., Sokolov, N., et al. (2021b). Highly active thermophilic L-asparaginase from Melioribacter roseus represents a novel large Group of Type II bacterial L-asparaginases from Chlorobi-Ignavibacteriae-Bacteroidetes clade. *Int. J. Mol. Sci.* 22:632. doi: 10.3390/ijms222413632

Dumina, M., Zhgun, A., Pokrovskaya, M., Aleksandrova, S., Zhdanov, D., Sokolov, N., et al. (2021a). A novel l-asparaginase from hyperthermophilic archaeon *thermococcus sibiricus*: heterologous expression and characterization for biotechnology application. *Int. J. Mol. Sci.* 22, 1–17. doi: 10.3390/ijms22189894

El-fakharany, E., Orabi, H., Abdelkhalek, E., and Sidkey, N. (2020). Purification and biotechnological applications of L-asparaginase from newly isolated bacillus halotolerans OHEM18 as antitumor and antioxidant agent. *J. Biomol. Struct. Dyn.* 40, 1–13. doi: 10.1080/07391102.2020.1851300

El-Gendy, M. M. A. A., Awad, M. F., El-Shenawy, F. S., El-Bondkly, A. M. A., and El-bondkly, A. M. A. (2021). Production, purification, characterization, antioxidant and antiproliferative activities of extracellular L-asparaginase produced by Fusarium equiseti AHMF4. *Saudi J. Biol. Sci.* 28, 2540–2548. doi: 10.1016/j.sjbs.2021.01.058

El-naggar, N. E., Deraz, S. F., El-ewasy, S. M., and Suddek, G. M. (2018). Purification, characterization and immunogenicity assessment of glutaminase free L-asparaginase from streptomyces brollosae NEAE-115. *BMC Pharmacol. Toxicol.* 19, 1–15. doi: 10.1186/s40360-018-0242-1

Farahat, M. G., Amr, D., and Galal, A. (2020). Molecular cloning, structural modeling and characterization of a novel glutaminase-free L-asparaginase from Cobetia amphilecti AMI6. *Int. J. Biol. Macromol.* 143, 685–695. doi: 10.1016/j.ijbiomac.2019.10.258

Fazeli, N., Alimadadi, N., and Nasr, S. (2021). Screening and optimization of process parameters for the production of L-asparaginase by indigenous fungal-type strains. *Iran. J. Sci. Technol. Trans. A Sci.* 45, 409–416. doi: 10.1007/s40995-020-01056-2

Fonseca, M. H. G., Fiúza, T. D. S., De Morais, S. B., De Souza, T. D. A. C. B., and Trevizani, R. (2021). Circumventing the side effects of L-asparaginase. *Biomed. Pharmacother.* 139:111616. doi: 10.1016/j.biopha.2021.111616

Ghasemi, A., Asad, S., Kabiri, M., and Dabirmanesh, B. (2017). Cloning and characterization of *Halomonas elongata* L-asparaginase, a promising chemotherapeutic agent. *Appl. Microbiol. Biotechnol.* 101, 7227–7238. doi: 10.1007/s00253-017-8456-5

Golbabaie, A., Nouri, H., Moghimi, H., and Khaleghian, A. (2020). L-asparaginase production and enhancement by Sarocladium strictum: in vitro evaluation of anti-cancerous properties. *J. Appl. Microbiol.* 129, 356–366. doi: 10.1111/jam.14623

Guimarães, M., JJM, C., Bueno, C. Z., Torres-Obreque, K. M., GVR, L., Monteiro, G., et al. (2022). Peg-grafted liposomes for L-asparaginase encapsulation. *Pharmaceutics* 14, 1–18. doi: 10.3390/pharmaceutics14091819

Hassan, S. W. M., Farag, A. M., and Beltagy, E. A. (2018). Purification, characterization and anticancer activity of L-asparaginase produced by marine aspergillus terreus. *J Pure Appl Microbiol* 12, 1845–1854. doi: 10.22207/JPAM.12.4.19

Horvath, T. D., Chan, W. K., Pontikos, M. A., Martin, L. A., du, D., Tan, L., et al. (2019). Assessment of L-asparaginase pharmacodynamics in mouse models of cancer. *Metabolites* 9:10. doi: 10.3390/metabo9010010

Karla, R., CMN, M., Ferraro, R. B., Moguel, I. S., Tonso, A., Lourenço, F. R., et al. (2020). Glutaminase-free L-asparaginase production by Leucosporidium muscorum isolated from Antarctic glutaminase-free L-asparaginase production by Leucosporidium muscorum. *Prep. Biochem. Biotechnol.* 51, 1–12. doi: 10.1080/10826068.2020.1815053

Kumar, V., Kumar, S., Darnal, S., Patial, V., Singh, A., Thakur, V., et al. (2019). Optimized chromogenic dyes—based identification and quantitative evaluation of bacterial L-asparaginase with low/no glutaminase activity bioprospected from pristine niches in Indian trans—Himalaya. *3 Biotech* 9, 1–9. doi: 10.1007/s13205-019-1810-9

Li, K., Du, Y., Li, L., and Wei, D. (2020). Bioinformatics approaches for anti-cancer drug discovery. *Curr. Drug Targets* 21, 3–17. doi: 10.2174/1389450120666190923162203

Loch, J. I., and Jaskolski, M. (2021). Structural and biophysical aspects of l-asparaginases: a growing family with amazing diversity. *IUCrJ* 8, 514–531. doi: 10.1107/S2052252521006011

Maese, L., Rizzari, C., Coleman, R., Power, A., van der Sluis, I., and Rau, R. E. (2021). Can recombinant technology address asparaginase *Erwinia chrysanthemi* shortages? *Pediatr. Blood Cancer* 68, 1–7. doi: 10.1002/pbc.29169

Maggi, M., Mittelman, S. D., Parmentier, J. H., Colombo, G., Meli, M., Whitmire, J. M., et al. (2017). A protease-resistant *Escherichia coli* asparaginase with outstanding stability and enhanced anti-leukaemic activity in vitro. *Sci. Rep.* 7:4. doi: 10.1038/s41598-017-15075-4

Modi, T., and Gervais, D. (2022). Improved pharmacokinetic and pharmacodynamic profile of a novel PEGylated native *Erwinia chrysanthemi* L-asparaginase. *Invest. New Drugs* 40, 21–29. doi: 10.1007/s10637-021-01173-8

Moguel, I. S., Yamakawa, C. K., Pessoa, A., and Mussatto, S. I. (2020). L-asparaginase production by *Leucosporidium scottii* in a bench-scale bioreactor with co-production of lipids. *Front. Bioeng. Biotechnol.* 8, 1–11. doi: 10.3389/fbioe.2020.576511

Mostafa, Y., Alrumman, S., Alamri, S., Hashem, M., al-izran, K., Alfaifi, M., et al. (2019). Enhanced production of glutaminase-free L-asparaginase by marine bacillus velezensis and cytotoxic activity against breast cancer cell lines. *Electron. J. Biotechnol.* 42, 6–15. doi: 10.1016/j.ejbt.2019.10.001

Moubasher, H. A., Balbool, B. A., Helmy, Y. A., Alsuhaibani, A. M., Atta, A. A., Sheir, D. H., et al. (2022). Insights into asparaginase from endophytic fungus Lasiodiplodia theobromae: purification, characterization and antileukemic activity. *Int. J. Environ. Res. Public Health* 19, 1–14. doi: 10.3390/ijerph19020680

Nguyen, H. A., Durden, D. L., and Lavie, A. (2017). The differential ability of asparagine and glutamine in promoting the closed/active enzyme conformation rationalizes the *Wolinella succinogenes* L-asparaginase substrate specificity. *Sci. Rep.* 7, 1–14. doi: 10.1038/srep41643

Nguyen, H. A., Su, Y., Zhang, J. Y., Antanasijevic, A., Caffrey, M., Schalk, A. M., et al. (2018). A novel L-asparaginase with low L-glutaminase coactivity is highly Ef fi cacious against both T- and B-cell acute lymphoblastic Leukemias in vivo. *Cancer Res.* 78, 1549–1560. doi: 10.1158/0008-5472.CAN-17-2106

Prakash, P., Singh, H. R., and Jha, S. K. (2019). Production, purification and kinetic characterization of glutaminase free anti-leukemic L-asparaginase with low endotoxin level from novel soil isolate. *Prep. Biochem. Biotechnol.* 50, 1–12. doi: 10.1080/10826068.2019.1692221

Prakash, P., Singh, H. R., and Jha, S. K. (2020). Indicator dye based screening of glutaminase free L-asparaginase producer and kinetic evaluation of enzyme production process. *Prep. Biochem. Biotechnol.* 50, 803–813. doi: 10.1080/10826068.2020.1737942

Prihanto, A. A., Jatmiko, Y. D., Yanti, I., and Murtazam, M. A. (2022). Optimization of glutaminase-free L-asparaginase production using mangrove endophytic *Lysinibacillus fusiformis* B27 [version 2; peer review: 2 approved]. *F1000Res* 8, 1–18. doi: 10.12688/f1000research.21178.2

Radadiya, A., Zhu, W., Coricello, A., Alcaro, S., and Richards, N. G. J. (2020). Improving the treatment of acute lymphoblastic Leukemia. *Biochemistry* 59, 3193–3200. doi: 10.1021/acs.biochem.0c00354

Rigouin, C., Nguyen, H. A., Schalk, A. M., and Lavie, A. (2017). Discovery of human-like L-asparaginases with potential clinical use by directed evolution. *Sci. Rep.* 7:10224. doi: 10.1038/s41598-017-10758-4

Saeed, H., Hemida, A., El-Nikhely, N., Abdel-Fattah, M., Shalaby, M., Hussein, A., et al. (2020). Highly efficient Pyrococcus furiosus recombinant L-asparaginase with no glutaminase activity: expression, purification, functional characterization, and cytotoxicity on THP-1, A549 and Caco-2 cell lines. *Int. J. Biol. Macromol.* 156, 812–828. doi: 10.1016/j.ijbiomac.2020.04.080

Safary, A., Moniri, R., Hamzeh-mivehroud, M., and Dastmalchi, S. (2019). Highly efficient novel recombinant L-asparaginase with no glutaminase activity from a new halo-thermotolerant bacillus strain. *Bioimpacts* 9, 15–23. doi: 10.15171/bi.2019.03

Shakambari, G., Sameer Kumar, R., Ashokkumar, B., Ganesh, V., Vasantha, V. S., and Varalakshmi, P. (2018). Cloning and expression of L-asparaginase from *Bacillus tequilensis* PV9W and therapeutic efficacy of solid lipid particle formulations against cancer. *Sci. Rep.* 8:18013. doi: 10.1038/s41598-018-36161-1

Sharma, S., Fulke, A. B., and Chaubey, A. (2019). Bioprospection of marine actinomycetes: recent advances, challenges and future perspectives. *Acta Ocean. Sin* 38, 1–17. doi: 10.1007/s13131-018-1340-z

Sindhu, R., and Manonmani, H. K. (2017). Expression and characterization of recombinant L-asparaginase from *Pseudomonas fluorescens*. *Protein Expr. Purif.* 143, 83–91. doi: 10.1016/j.pep.2017.09.009

Sobat, M., Asad, S., Kabiri, M., and Mehrshad, M. (2020). Metagenomic discovery and functional validation of L-asparaginases with anti-leukemic effect from the Caspian Sea. *iScience* 24:101973. doi: 10.1016/j.isci.2020.101973

van Trimpont, M., Peeters, E., de Visser, Y., Schalk, A. M., Mondelaers, V., de Moerloose, B., et al. (2022). Novel insights on the use of L-asparaginase as an efficient and safe anti-cancer therapy. *Cancers* 14:902. doi: 10.3390/cancers14040902

Vidya, J., Sajitha, S., Ushasree, M. V., Sindhu, R., Binod, P., Madhavan, A., et al. (2017). Genetic and metabolic engineering approaches for the production and delivery of L-asparaginases: an overview. *Bioresour. Technol.* 245, 1775–1781. doi: 10.1016/j.biortech.2017.05.057

Villanueva-flores, F., Zárate-Romero, A., Torres, A. G., and Huerta-Saquero, A. (2021). Encapsulation of asparaginase as a promising strategy to improve in vivo drug performance. *Pharmaceutics* 13:1965. doi: 10.3390/pharmaceutics13111965

Vimal, A., and Kumar, A. (2017). Biotechnological production and practical application of L-asparaginase enzyme. *Biotechnol. Genet. Eng. Rev.* 33, 40–61. doi: 10.1080/02648725.2017.1357294

WHO (2021). *World Health Organization model list of essential medicines 22nd list* Geneva: World Health Organization, 1–66.

Yari, M., Eslami, M., Ghoshoon, M. B., Nezafat, N., and Ghasemi, Y. (2019). Decreasing the immunogenicity of *Erwinia chrysanthemi* asparaginase via protein engineering: computational approach. *Mol. Biol. Rep.* 46, 4751–4761. doi: 10.1007/s11033-019-04921-5

Zhou, Y., Jiao, L., Shen, J., Chi, H., Lu, Z., Liu, H., et al. (2022). Enhancing the catalytic activity of type II L-asparaginase from *Bacillus licheniformis* through semi-rational design. *Int. J. Mol. Sci.* 23, 1–16. doi: 10.3390/ijms23179663

frontiers | Frontiers in Microbiology

TYPE Review
PUBLISHED 15 April 2024
DOI 10.3389/fmicb.2024.1266510

OPEN ACCESS

EDITED BY
Monika Prakash Rai,
Motilal Nehru National Institute of Technology Allahabad, India

REVIEWED BY
Maria de los Angeles Serradell,
Universidad Nacional de La Plata, Argentina
Rajat Kumar,
Hong Kong Baptist University, Hong Kong SAR, China

*CORRESPONDENCE
Rui Liu
✉ liurcau@naver.com

RECEIVED 25 July 2023
ACCEPTED 22 March 2024
PUBLISHED 15 April 2024

CITATION
Liu R (2024) A promising area of research in medicine: recent advances in properties and applications of Lactobacillus-derived exosomes.
Front. Microbiol. 15:1266510.
doi: 10.3389/fmicb.2024.1266510

A promising area of research in medicine: recent advances in properties and applications of Lactobacillus-derived exosomes

Rui Liu*

School of Food Engineering, Ludong University, Yantai, Shandong, China

Lactobacillus-derived exosomes, small extracellular vesicles released by bacteria, have emerged as a promising area of research in recent years. These exosomes possess a unique structural and functional diversity that allows them to regulate the immune response and promote gut health. The isolation and purification of these exosomes are crucial for their effective use as a therapeutic agent. Several isolation and purification methods have been developed, including differential ultracentrifugation, density gradient centrifugation, and size-exclusion chromatography. Lactobacillus-derived exosomes have been demonstrated to have therapeutic potential in various diseases, such as inflammatory bowel disease, liver disease, and neurological disorders. Moreover, they have been shown to serve as effective carriers for drug delivery. Genetic engineering of these exosomes has also shown promise in enhancing their therapeutic potential. Overall, Lactobacillus-derived exosomes represent a promising area of research for the development of novel therapeutics for immunomodulation, gut health, and drug delivery.

KEYWORDS

Lactobacillus-derived exosomes, isolation methods, immunomodulation, intestinal microecological balance, genetic engineering

Introduction

Lactobacilli are a group of Gram-positive bacteria widely distributed both within and outside of the human body, which produce lactic acid by fermenting lactose and other carbohydrates (Bintsis, 2018; Ibrahim and Ouwehand, 2019). They have been extensively studied and applied as a crucial probiotic in the food industry, animal husbandry, and healthcare (Alayande et al., 2020; Ayivi et al., 2020). Their probiotic effects include promoting intestinal health, enhancing immunity, and regulating the balance of intestinal flora (Mitsuoka, 2000; Tsai et al., 2012; Deng et al., 2022). Moreover, exosomes secreted by lactic acid bacteria have gained increasing attention as a novel type of biological agent (González-Lozano et al., 2022).

Exosomes are small extracellular vesicles secreted by cells via the endocrine pathway, ranging from 20 to 400 nm in size, and containing a variety of bioactive substances such as proteins, nucleic acids, and metabolites (Yu et al., 2023). They are widely produced in various organisms such as bacteria, fungi, plants, and animals (Schuh et al., 2019; Zhou et al., 2022), and are involved in multiple biological processes, including cell signaling, pathogenic microorganism infection, and immune regulation (Wang et al., 2017; Li et al., 2019). As their importance is gradually recognized, their applications in medicine, agriculture, and other

fields are gaining attention. Currently, the study of exosomes has become one of the hotspots in the field of biology.

In recent years, the study of Lactobacillus-derived exosomes has attracted widespread attention, as they have been shown to possess various biological functions, such as antibacterial (Lee et al., 2021), immunomodulatory (Liu et al., 2021b), and intestinal protection (Choi et al., 2020; Tong et al., 2021). Recent studies have revealed that the protein, DNA, and RNA components in Lactobacillus-derived exosomes can exert a broad range of effects on the host through the transfer of commensal microorganisms in the intestine (Liu et al., 2021a). Additionally, the components and mechanisms of action of Lactobacillus-derived exosomes are gradually being revealed. For instance, Lactobacillus-derived exosomes can modulate the host immune system, improve the imbalance of intestinal flora, and inhibit the growth of harmful bacteria, thus having a wide range of applications in food, healthcare, and agriculture. In this paper, we will review the recent advances in the properties and functions of Lactobacilli exosomes, isolation and preparation methods, engineering modifications, and their applications.

Structure and function of Lactobacillus-derived exosomes

Structure

Similar to the structure of exosomes from other sources, Lactobacillus-derived exosomes are extracellular vesicles that are secreted by Lactobacillus and have a diameter between 20 and 400 nm, usually consist of one or more lipid bilayers, wrapped in a similar structure to the cell membrane (Yu et al., 2019; Gu et al., 2021). These exosomes contain a variety of bioactive components such as proteins, polysaccharides, and lipids. Lactobacillus exosome proteins are important components and consist of a variety of enzymes and structural proteins (Behzadi et al., 2017; Domínguez Rubio et al., 2017). These enzymes play a vital role in breaking down food and regulating flora in the intestine. Polysaccharides in exosomes are also essential components that promote the proliferation and differentiation of intestinal mucosal cells and enhance intestinal immunity (Huang et al., 2017; Sha et al., 2021). Nucleic acids in exosomes have important biological functions as RNA carriers that can transfer information and influence gene expression in the host (Munir et al., 2020; Askenase, 2021).

The complex composition and structure of Lactobacillus-derived exosomes give them diverse biological functions and wide-ranging application prospects. Current research on Lactobacillus-derived exosomes is still ongoing, and more discoveries and applications are expected to emerge in the future.

Immunomodulation

Exosomes released by lactic acid bacteria have gained considerable interest due to their potential immunomodulatory effects. In particular, exosomes from Lactobacillus species have been found to exert anti-inflammatory, antibacterial, antiviral, and immune-enhancing effects (Hsu et al., 2018; Lee et al., 2018; Kang et al., 2020). These bioactive molecules are involved in several mechanisms that modulate the host immune system (Figure 1).

Lactobacillus-derived exosomes are key in modulating immune responses, primarily by activating cells like macrophages, dendritic cells, T cells, and B cells (Leung et al., 2006; Chen et al., 2008; Kim et al., 2020). These exosomes contain proteins such as Fatty Acid Binding Protein 6 (FABP6), Epithelial Cell Adhesion Molecule (EPCAM), and C1q and Tumor Necrosis Factor (TNF) related 3 (C1QTNF3), and engage in Peroxisome Proliferator Activated Receptor (PPAR) [Integrin Linked Kinase (ILK)/FABP6] pathways, alongside various polysaccharide molecules (Tang et al., 2015). These components induce dendritic cells to produce pro-inflammatory cytokines, including TNF-α, Interleukin (IL)-6, IL-12, lymphotoxin α (LTA), C-C Motif Ligand 2 (CCL2), and C-X-C Motif Ligands 9 and 10 (CXCL9 and CXCL10) (Liu et al., 2021b). Moreover, polysaccharide molecules in the exosomes trigger signal transduction in immune cells, further promoting cytokine production via immune receptor binding. The impact of these exosomes on bone marrow-derived dendritic cells (BM-DC) varies, particularly in response to *Lactoplantibacillus plantarum* WCFS1. For example, exposure to the L900/2 strain increases IL-10 production, whereas L900/3 boosts IL-12p70 production. *L. plantarum* exopolysaccharide amplifies nitric oxide, IL-12p70, and RANTES (Regulated upon Activation, Normal T Cell Expressed and Presumably Secreted; CCL5) production, while reducing IL-10 secretion in serum, intestinal fluid, and dendritic cell supernatants (Górska et al., 2014). Furthermore, this exopolysaccharide upregulates Major Histocompatibility Complex (MHC) II and Cluster of Differentiation (CD) 86 expression on DC-surfaces and stimulates T cell proliferation *in vitro*, illustrating its profound effect on immune cell function and response (Tang et al., 2015).

Recent studies reveal that lncRNAs and lincRNAs, particularly in response to Lipopolysaccharides (LPS) stimulation, play a pivotal role in immune regulation. These include lnc-IL7R, which represses proinflammatory mediators by maintaining a repressive chromatin mark, and NeST Long noncoding (lnc)RNA, which activates transcription at the interferons (IFNs) -γ locus. The lincRNA-Cyclooxygenase-2 (Cox2), notably expressed in Lipopolysaccharides (LPS)-stimulated dendritic cells, modulates immune gene expression by forming complexes with nuclear RNA-binding proteins (Duval et al., 2017; Yang F. et al., 2022).

Certain Lactobacillus-derived exosomes have shown promising anti-tumor and anti-viral properties, potentially reducing the occurrence of tumors and viral infections. *Lactobacillus gasseri* and *Lactobacillus jensenii* have been identified as particularly effective in stimulating the production of IFN-γ by human mononuclear cells from peripheral blood (PBMCs) (Jounai et al., 2018; Tsuji et al., 2018; Nicolò et al., 2021).

In summary, exosomes from lactic acid bacteria have a wide range of immunomodulatory effects, enhancing intestinal immune responses and reducing intestinal inflammatory and allergic reactions. Future research should explore the mechanism of Lactobacillus-derived exosomes in immunomodulation and develop their application in the prevention and treatment of immune-related diseases.

Intestinal protection and microecological balance

Lactobacilli exosomes have emerged as a significant probiotic metabolite that plays a pivotal role in maintaining intestinal protection and microecological balance (Figure 1).

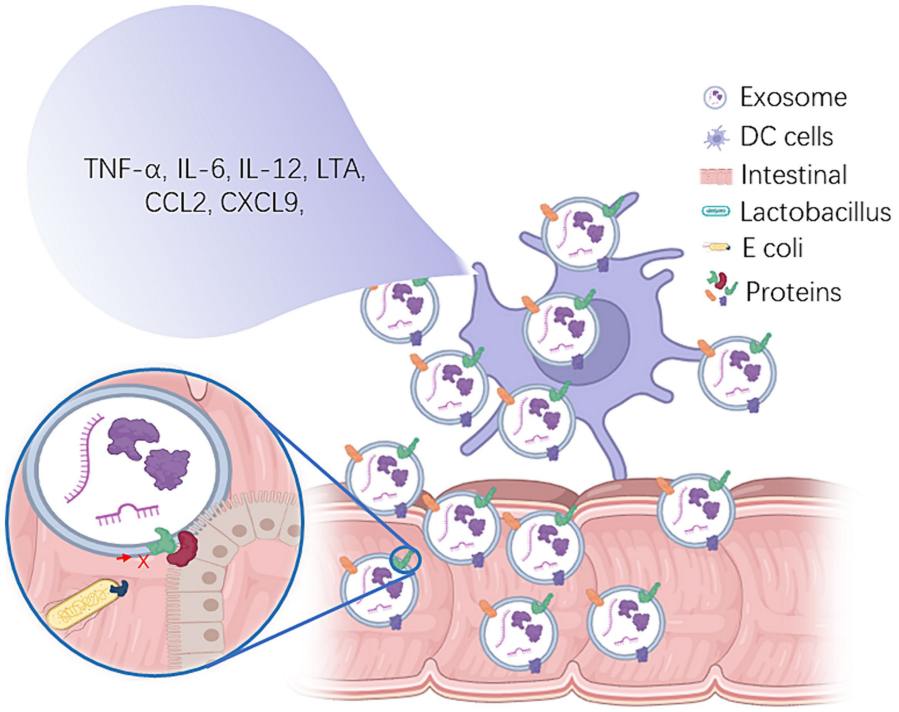

FIGURE 1
The immunomodulatory role of Lactobacillus-derived exosomes and their impact on intestinal health. Lactobacillus-derived exosomes play a pivotal role in modulating immune responses by containing proteins such as FABP6, EPCAM, and various polysaccharide molecules (Górska et al., 2014). These exosome components have the capacity to stimulate dendritic cells, resulting in the production of pro-inflammatory cytokines, including TNF-α, IL-6, IL-12, CCL2, and CXCL9 (Liu et al., 2021a,b), ultimately contributing to the potential stimulation of T cell proliferation *in vitro*. This underscores their profound influence on immune cell function and response, particularly within the context of intestinal immune regulation. Furthermore, proteins within Lactobacillus-derived exosomes exhibit a competitive binding capacity to the intestinal surface, thereby reducing the adhesion of harmful bacteria and mitigating the ensuing intestinal inflammatory response (Doron et al., 2005). Additionally, these exosomes encapsulate bioactive substances, such as extracellular enzymes, antibiotics, antimicrobials, antibiotic enzymes, iron carrier proteins, β-glucan, siRNA and polysaccharides, which collectively exert regulatory control over the intestinal microbiome (Uddin et al., 2020; Díaz-Garrido et al., 2021; Yang F. et al., 2022; Yang Q. et al., 2022; Yang Z. et al., 2022). This regulation impacts both the composition and abundance of intestinal flora, facilitating the enhancement of probiotic growth and metabolic activity within the intestinal environment, thus contributing to the maintenance of intestinal health.

Exosomes act through various mechanisms to maintain the intestinal microecological balance, regulate the intestinal microbial composition, and uphold the stability of the intestinal microenvironment. For instance, certain proteins in *Lacticaseibacillus rhamnosus* GG-derived exosomes can competitively bind to the intestinal surface, reducing the adhesion of harmful bacteria and ameliorating the intestinal inflammatory response (Doron et al., 2005). Additionally, a highly expressed sequence (sRNA71) was identified in Exosomes which were isolated from the culture supernatant of *L. plantarum* WCFS1 using ultracentrifugation. sRNA71 substantially reduced Tp53 expression in HEK293T cells and suppressed the gene expression through binding to the 3′UTR of Tp53 mRNA (Yu et al., 2022). These exosomes contain bioactive substances that regulate the intestinal microbiome, such as extracellular enzymes, antibiotics, antimicrobials, antibiotic enzymes, iron carrier proteins, β-glucan, siRNA and polysaccharides, which can impact the type and quantity of intestinal flora, improve the growth and metabolism of probiotics in the intestine, and maintain intestinal health (Uddin et al., 2020; Díaz-Garrido et al., 2021; Yang Z. et al., 2022). Lactobacilli exosomes can also protect the intestinal tract by regulating intestinal immune function. Studies have demonstrated that *Lacticaseibacillus rhamnosus* GG-derived exosomes can enhance the integrity of the intestinal mucosal barrier, regulate the activity of immune cells in the intestine, and improve the intestinal immune function and disease resistance (Tong et al., 2021). Additionally, specific components of *Lacticaseibacillus rhamnosus* GG-derived exosomes (such as proteins, polysaccharides, etc.) also can interact with intestinal epithelial cells and regulate their signal transduction pathways, thereby affecting the integrity of the intestinal mucosal barrier and the balance of the immune response (Tong et al., 2021).

Recent studies using C57BL/6J mice have shown that *Lactobacillus plantarum* Q7 extracellular vesicles (Q7-EVs) enhance intestinal mucosal barrier functions and reduce inflammation and allergic responses. Q7-EVs were effective in alleviating DSS-induced colitis symptoms, such as colon shortening, bleeding, and weight loss, and decreased histological damage. They downregulated proinflammatory cytokines (IL-6, IL-1β, IL-2, TNF-α) and corrected gut microbiota dysbiosis, increasing anti-inflammatory Bifidobacteria and Muribaculaceae while reducing Proteobacteria, demonstrating their potential in improving gut health maintenance (Hao et al., 2021).

Some studies have also shown that Lactobacillus-derived exosomes. Influence the regulation of gut microbial composition and metabolites, promoting the growth of probiotic bacteria and inhibiting the growth of harmful bacteria. For example, *Lacticaseibacillus rhamnosus* GG (LGG) derived EVs could potentially alleviate intestinal inflammation by diminishing the activation of the Toll-Like Receptor

(TLR4)- Nuclear Factor Kappa (NF-K) B1- Nucleotide-binding oligomerization domain (NLRP3) axis. The effectiveness of this treatment is evident in its ability to decrease pro-inflammatory cytokines such as TNF-α, IL-1β, IL-6, and IL-2. Furthermore, 16S rRNA sequencing reveals that LGG-EVs administration can alter the composition of gut microbiota in mice affected by colitis, subsequently influencing the microbiota's metabolic processes (Tong et al., 2021). This process helps to regulate the intestinal microbial composition and promote the balance of the immune system. Additionally, exosome components have specific immunomodulatory functions, with some proteins inducing the proliferation and differentiation of immune cells and nucleic acid molecules enhancing the function of the intestinal barrier by binding to Toll-like receptors in intestinal epithelial cells (Caputi and Giron, 2018).

On the other hand, Lactobacillus-derived exosomes can also regulate the intestinal immune system. Extracellular vesicles derived from *Latocseibacillus. paracasei* (LpEVs) were effective in diminishing the levels of pro-inflammatory cytokines such as IL-1α, IL-1β, IL-2, and TNFα, which were initially elevated due to LPS stimulation. These vesicles enhanced the levels of anti-inflammatory cytokines IL-10 and TGFβ. In HT29 cells, LpEVs mitigated LPS-induced inflammation and reduced the activation of inflammation-related proteins like COX-2, iNOS, and NFκB, as well as the production of nitric oxide (Choi et al., 2020). Moreover, the polysaccharides and lipids in *Lactiplantibacillus plantarum* BGAN8 -derived exosomes can regulate the inflammatory response of the intestinal immune system, ameliorate intestinal inflammation and autoimmune response, and thereby maintain intestinal immune homeostasis (Bajic et al., 2020).

Recent research has demonstrated that exosomes from *Limosiactobacillus reuteri* strains DSM 17938 and BG-R46 promote the proliferation and differentiation of T cells and stimulate peripheral blood mononuclear cells (PBMC) and intestinal macrophages to release inflammatory cytokines, notably IL-6 and IL-1β. Additionally, they exert a modulatory effect by inhibiting the secretion of IFN-γ and reducing the secretion of TNF-α, which are typically induced by *Staphylococcus aureus* (Pang et al., 2022).

In summary, significant advances have been made in the study of Lactobacilli exosomes' role in intestinal protection and flora homeostasis. Further research is warranted to explore the composition, structure, and function of Lactobacillus-derived exosomes and their mechanisms of interaction with intestinal microecological homeostasis. These findings hold great promise in the development of novel intestinal health products and therapeutic approaches.

Isolation and purification of Lactobacilli exosomes: methods and techniques

The isolation and purification of Lactobacillus-derived exosomes have become a subject of great interest to researchers due to their potential applications in various fields. Due to the similarities in characteristics between Lactobacillus-derived exosomes and exosomes from other sources, the methods for isolation and purification should also be similar. Over the years, several methods have been developed for the isolation and purification of these exosomes, including ultrafiltration, gel filtration, polyethylene glycol (PEG) precipitation, isoelectric focusing, affinity chromatography, calcium ion column chromatography, and counter-current chromatography.

Ultrafiltration is one of the most commonly used methods to isolate Lactobacillus-derived exosomes (Lee et al., 2018; Wang et al., 2021). This method involves screening exosomes from the culture medium, and the separation and enrichment of exosomes can be achieved by varying the pore size and pressure of the ultrafiltration membrane. However, this method may result in the loss of exosomes and protein contamination during the separation process, necessitating a subsequent purification step.

Centrifugation (Lei et al., 2021; Kim et al., 2022) is another frequently used method to isolate exosomes. It involves separating exosomes from other cellular components, such as bacteriophages and cell walls, by centrifuging the culture medium several times. Although this method is simpler than the ultrafiltration method, the separation efficiency is relatively low.

Precipitation is another effective method for isolating Lactobacillus-derived exosomes, typically achieved by adding salts or acidic precipitants. It enables the quick and efficient separation of exosomes but is prone to exosome loss and protein contamination problems.

Chromatography (Baranyai et al., 2015; Sidhom et al., 2020) is a highly accurate method of separation and purification, which includes gel filtration chromatography, ion exchange chromatography, reverse phase chromatography, and many other techniques. Reverse-phase high-performance liquid chromatography (RP-HPLC) is widely used for the purification of exosomes. This method can improve purity without losing exosome activity and can obtain high-purity exosomes in a single operation in a single pass.

Affinity chromatography (Burkova et al., 2018; Sedykh et al., 2022) is a molecular recognition-based separation method that involves affinity chromatography and immunoaffinity chromatography, among others. These techniques use the binding of specific compounds or antibodies to exosome molecules to isolate exosomes, enabling efficient separation and purification. However, they require high-cost molecular recognition materials and specialized operational skills and are therefore currently less frequently employed for the isolation of Lactobacillus-derived exosomes.

The aggregate method is commonly employed for exosome extraction from lactic acid bacteria, which leverages the interaction force between aggregates and polysaccharides or proteins to isolate exosomes. Aggregating agents such as PEG (Weng et al., 2016) or polyacrylamide (PAA) (Li et al., 2023b) can be used to separate exosomes. PEG6000 is typically employed due to its optimal separation efficiency, as molecular weight greater than 6,000 diminishes its effectiveness. Meanwhile, PAA is effective in precipitating microbial cell walls and intracellular material together with exosomes. The aggregate method is a cost-effective, easy-to-control, and scalable technique; however, contamination of the target material is a concern.

Recently, some novel techniques have been proposed by researchers for the isolation and purification of exosomes, such as magnetic-bead-affinity chromatography (MBAC) (Wu et al., 2021). MBAC enables the quick and efficient separation and purification of exosomes from complex samples by selecting antibodies that specifically bind to target exosomes.

Each of these methods has its advantages and limitations and can be selected based on the nature of the desired exosome and the research objectives. For instance, ultrafiltration and gel filtration are commonly employed to isolate exosomes with different molecular weights, while PEG precipitation is useful for the large-scale

preparation of exosomes. Isoelectric focusing is an effective method for purifying exosomes with electric charges, and affinity chromatography can be used to purify exosomes with specific activities by selecting appropriate affinity substrates.

Moreover, operational steps are often more intricate. Other factors that can affect the extraction efficiency include culture medium, culture conditions, and time. A medium rich in carbon and nitrogen sources and the addition of certain small molecules such as citric acid can improve exosome yield and isolation efficiency (Royo et al., 2016).

The selection of a method depends on the exosomes' size, morphology, composition, and intended use. In particular, ultrafiltration and molecular sieve filtration are commonly used techniques. The former allows for the screening of particles of desired size through different pore sizes, while the latter utilizes molecular sieve materials' effect to filter by molecular size. While these methods have been useful, more research is needed to explore exosomes' composition and biological functions.

Application of Lactobacillus-derived exosomes

Lactobacillus-derived exosomes have been investigated for their therapeutic effects on a range of diseases. For instance, they have been shown to have anti-inflammatory and immunomodulatory effects, making them attractive candidates for treating autoimmune and inflammatory diseases. Due to the potential presence of heterologous proteins in Lactobacillus-derived exosomes, oral administration of Lactobacillus-derived exosomes is an ideal delivery route. Studies have demonstrated the feasibility of using exosomes as a therapeutic strategy via oral administration to treat diseases. In a study on a mouse model of colitis, bovine colostrum-derived exosomes administrated orally were found to significantly alleviate colonic inflammation and promote tissue repair (Han et al., 2022; Li et al., 2023a). Furthermore, food-derived exosomes have been shown to improve gut microbiota dysbiosis and intestinal barrier function, which are associated with a range of diseases such as human irritable bowel syndrome and inflammatory bowel disease (Díez-Sainz et al., 2021a). These findings suggest that Lactobacillus-derived exosomes may have potential therapeutic applications in various disease settings.

Lactobacillus-derived exosomes have been shown to contain various functional molecules, such as proteins and RNA, which can influence the composition and function of the gut microbiota. For example, a recent study demonstrated that exosomes could modulate the gut microbiota of mice by promoting the growth of beneficial bacteria and inhibiting the growth of harmful bacteria, which could potentially improve gut health in humans (Díez-Sainz et al., 2021b). Furthermore, Lactobacillus-derived exosomes have been shown to regulate the gut-brain axis, which is a bidirectional communication system between the gut and the central nervous system and is involved in the regulation of a range of physiological functions such as mood and appetite in humans (Evrensel and Ceylan, 2015). These findings suggest that Lactobacillus-derived exosomes may be useful for modulating the gut microbiome and the gut-brain axis, which could have implications for a range of health conditions.

Despite the potential of Lactobacillus-derived exosomes, there are still some challenges that need to be addressed. For example, the isolation and purification of Lactobacillus-derived exosomes are not yet fully optimized, which could affect their yield and purity. Furthermore, the mechanisms of action of Lactobacillus-derived exosomes *in vivo* are not fully understood, and their long-term safety needs to be further investigated.

In conclusion, Lactobacillus-derived exosomes represent a promising area of research in the field of medicine, with potential applications in drug delivery, disease treatment, and gut microbiome modulation. The latest research findings have demonstrated their effectiveness in promoting tissue repair, modulating the gut microbiota, and regulating the gut-brain axis. While further research is needed to fully understand their potential applications and address remaining challenges, the progress in the field of Lactobacillus-derived exosomes has provided new insights and potential treatments for a range of diseases.

Engineering Lactobacilli exosomes for enhanced functionality

The engineering of Lactobacilli exosomes involves the construction of exosomes with specific functions using gene editing and transformation techniques. There are two main aspects of engineering Lactobacilli exosomes: modifying the bacteria to produce more or more effective exosomes, and genetically or chemically modifying the already isolated exosomes to give them new or improved functions. Researchers have employed recombinant genetic engineering techniques to insert exosome-related genes into the genome of cells to improve exosome production (Jafari et al., 2020). They have also optimized the culture conditions of lactic acid bacteria to enhance exosome production (Garcia et al., 2015). To modify exosomes, researchers have used gene editing techniques to implant specific peptide sequences on the surface of exosomes to give them specific recognition and binding ability (Ye et al., 2020). Chemical modification methods have also been employed to add molecules such as polysaccharides and peptides to enhance their biological activity (Luo et al., 2021; Yang Q. et al., 2022).

In addition, exosome engineering can be applied to the preparation of novel vaccines. For example, researchers integrated the human papillomavirus E7 protein gene into the DNA sequence of *L. lactis*, resulting in a better immune-protective effect in mouse experiments (Smalley Rumfield et al., 2020; Krishnan et al., 2022), which implies the potency of Lactobacilli exosomes as the vaccine carrier.

In conclusion, while the engineering study of Lactobacillus-derived exosomes is still in its early stages, it has enormous potential for various applications. Further research is needed to refine the feasibility and application prospects of this technology.

Conclusion and perspectives

Lactobacillus-derived exosomes, a novel type of biological drug, hold immense potential in the medical realm. They also modulate intestinal microflora, thereby maintaining gut health and boosting immunity (Figure 1). These exosomes, acting as natural carriers, can transport diverse drug molecules with excellent therapeutic benefits and mitigate adverse drug reactions. However, despite these advantages, lactobacillus exosome research

and application are still challenging. Firstly, the isolation and purification methods employed for these exosomes are not yet perfect and require optimization to enhance their yield and purity. Secondly, the intricate and heterogeneous structure and composition of Lactobacillus-derived exosomes necessitate a more comprehensive analysis of their structural and functional relationships to unravel their mechanism of action in living organisms. Furthermore, additional investigations are imperative to evaluate drug delivery mechanisms, *in vivo* distribution, metabolism, and long-term safety of Lactobacillus-derived exosomes. In conclusion, while lactobacillus exosome research offers a promising avenue for drug delivery, a significant number of basic and clinical studies are imperative to realize their potential in the pharmaceutical sector. Moreover, standardized production and quality control protocols for Lactobacillus-derived exosomes need to be strengthened to ensure their safe and efficacious application.

Author contributions

RL: Conceptualization, Formal analysis, Investigation, Writing – original draft, Writing – review & editing.

Funding

The author(s) declare financial support was received for the research, authorship, and/or publication of this article. The study is financially sponsored by Hebei Province Rural Revitalization Technology Innovation Special Project (No. 22322907D).

Conflict of interest

The author declares that the research was conducted in the absence of any commercial or financial relationships that could be construed as a potential conflict of interest.

Publisher's note

References

Alayande, K. A., Aiyegoro, O. A., and Ateba, C. N. (2020). Probiotics in animal husbandry: applicability and associated risk factors. *Sustain. For.* 12:1087. doi: 10.3390/su12031087

Askenase, P. W. (2021). Exosomes provide unappreciated carrier effects that assist transfers of their miRNAs to targeted cells; I. They are 'the elephant in the room'. *RNA Biol.* 18, 2038–2053. doi: 10.1080/15476286.2021.1885189

Ayivi, R. D., Gyawali, R., Krastanov, A., Aljaloud, S. O., Worku, M., Tahergorabi, R., et al. (2020). Lactic acid bacteria: food safety and human health applications. *Dairy* 1, 202–232. doi: 10.3390/dairy1030015

Bajic, S. S., Cañas, M.-A., Tolinacki, M., Badia, J., Sánchez, B., Golic, N., et al. (2020). Proteomic profile of extracellular vesicles released by *Lactiplantibacillus plantarum* BGAN8 and their internalization by non-polarized HT29 cell line. *Sci. Rep.* 10, 1–12. doi: 10.1038/s41598-020-78920-z

Baranyai, T., Herczeg, K., Onódi, Z., Voszka, I., Módos, K., Marton, N., et al. (2015). Isolation of exosomes from blood plasma: qualitative and quantitative comparison of ultracentrifugation and size exclusion chromatography methods. *PLoS One* 10:e0145686. doi: 10.1371/journal.pone.0145686

Behzadi, E., Hosseini, H. M., and Fooladi, A. A. I. (2017). The inhibitory impacts of *Lactobacillus rhamnosus* GG-derived extracellular vesicles on the growth of hepatic cancer cells. *Microb. Pathog.* 110, 1–6. doi: 10.1016/j.micpath.2017.06.016

Bintsis, T. (2018). Lactic acid bacteria as starter cultures: an update in their metabolism and genetics. *AIMS Microbiol.* 4, 665–684. doi: 10.3934/microbiol.2018.4.665

Burkova, E. E., Dmitrenok, P. S., Bulgakov, D. V., Vlassov, V. V., Ryabchikova, E. I., and Nevinsky, G. A. (2018). Exosomes from human placenta purified by affinity chromatography on sepharose bearing immobilized antibodies against CD81 tetraspanin contain many peptides and small proteins. *IUBMB Life* 70, 1144–1155. doi: 10.1002/iub.1928

Caputi, V., and Giron, M. C. (2018). Microbiome-gut-brain axis and toll-like receptors in Parkinson's disease. *Int. J. Mol. Sci.* 19:1689. doi: 10.3390/ijms19061689

Chen, D., Wu, X. Z., and Wen, Z. Y. (2008). Sulfated polysaccharides and immune response: promoter or inhibitor? *Panminerva Med.* 50, 177–183.

Choi, J. H., Moon, C. M., Shin, T.-S., Kim, E. K., McDowell, A., Jo, M.-K., et al. (2020). *Lactobacillus paracasei*-derived extracellular vesicles attenuate the intestinal inflammatory response by augmenting the endoplasmic reticulum stress pathway. *Exp. Mol. Med.* 52, 423–437. doi: 10.1038/s12276-019-0359-3

Deng, Z., Hou, K., Zhao, J., and Wang, H. (2022). The probiotic properties of lactic acid bacteria and their applications in animal husbandry. *Curr. Microbiol.* 79, 1–11. doi: 10.1007/s00284-021-02722-3

Díaz-Garrido, N., Badia, J., and Baldomà, L. (2021). Microbiota-derived extracellular vesicles in interkingdom communication in the gut. *J. Extracell. Vesicles* 10:e12161. doi: 10.1002/jev2.12161

Díez-Sainz, E., Lorente-Cebrián, S., Aranaz, P., Riezu-Boj, J. I., Martínez, J. A., and Milagro, F. I. (2021a). Potential mechanisms linking food-derived microRNAs, gut microbiota and intestinal barrier functions in the context of nutrition and human health. *Front. Nutr.* 8:586564. doi: 10.3389/fnut.2021.586564

Díez-Sainz, E., Milagro, F. I., Riezu-Boj, J. I., and Lorente-Cebrián, S. (2021b). Effects of gut microbiota–derived extracellular vesicles on obesity and diabetes and their potential modulation through diet. *J. Physiol. Biochem.* 78, 485–499. doi: 10.1007/s13105-021-00837-6

Domínguez Rubio, A. P., Martínez, J. H., Martínez Casillas, D. C., Coluccio Leskow, F., Piuri, M., and Pérez, O. E. (2017). *Lactobacillus casei* BL23 produces microvesicles carrying proteins that have been associated with its probiotic effect. *Front. Microbiol.* 8:1783. doi: 10.3389/fmicb.2017.01783

Doron, S., Snydman, D. R., and Gorbach, S. L. (2005). Lactobacillus GG: bacteriology and clinical applications. *Gastroenterol. Clin.* 34, 483–498. doi: 10.1016/j.gtc.2005.05.011

Duval, M., Cossart, P., and Lebreton, A. (2017). Mammalian microRNAs and long noncoding RNAs in the host-bacterial pathogen crosstalk. *Semin Cell Dev Biol.* 65, 11–19. doi: 10.1016/j.semcdb.2016.06.016

Evrensel, A., and Ceylan, M. E. (2015). The gut-brain axis: the missing link in depression. *Clin. Psychopharmacol. Neurosci.* 13, 239–244. doi: 10.9758/cpn.2015.13.3.239

Garcia, N. A., Ontoria-Oviedo, I., González-King, H., Diez-Juan, A., and Sepúlveda, P. (2015). Glucose starvation in cardiomyocytes enhances exosome secretion and promotes angiogenesis in endothelial cells. *PLoS One* 10:e0138849. doi: 10.1371/journal.pone.0138849

González-Lozano, E., García-García, J., Gálvez, J., Hidalgo-García, L., Rodríguez-Nogales, A., Rodríguez-Cabezas, M. E., et al. (2022). Novel horizons in Postbiotics: Lactobacillaceae extracellular vesicles and their applications in health and disease. *Nutrients* 14:5296. doi: 10.3390/nu14245296

Górska, S., Schwarzer, M., Jachymek, W., Srutkova, D., Brzozowska, E., Kozakova, H., et al. (2014). Distinct immunomodulation of bone marrow-derived dendritic cell responses to *Lactobacillus plantarum* WCFS1 by two different polysaccharides isolated from *Lactobacillus rhamnosus* LOCK 0900. *Appl. Environ. Microbiol.* 80, 6506–6516. doi: 10.1128/AEM.02104-14

Gu, Z., Li, F., Liu, Y., Jiang, M., Zhang, L., He, L., et al. (2021). Exosome-like nanoparticles from *Lactobacillus rhamnosus* GG protect against alcohol-associated liver disease through intestinal aryl hydrocarbon receptor in mice. *Hepatol. Commun.* 5, 846–864. doi: 10.1002/hep4.1679

Han, G., Cho, H., Kim, H., Jang, Y., Jang, H., Kim, E. S., et al. (2022). Bovine colostrum derived-exosomes prevent dextran sulfate sodium-induced intestinal colitis via suppression of inflammation and oxidative stress. *Biomater. Sci.* 10, 2076–2087. doi: 10.1039/D1BM01797G

Hao, H., Zhang, X., Tong, L., Liu, Q., Liang, X., Bu, Y., et al. (2021). Effect of extracellular vesicles derived from *Lactobacillus plantarum* Q7 on gut microbiota and ulcerative colitis in mice. *Front. Immunol.* 12:777147. doi: 10.3389/fimmu.2021.777147

Hsu, W.-H., Chen, K.-C., and Shen, T.-L. (2018). *Lactobacillus plantarum*-derived extracellular vesicles improved the quality and safety of tuna meat. *J. Extracell. Vesicles* 7:172.

Huang, X., Nie, S., and Xie, M. (2017). Interaction between gut immunity and polysaccharides. *Crit. Rev. Food Sci. Nutr.* 57, 2943–2955. doi: 10.1080/10408398.2015.1079165

Ibrahim, F., and Ouwehand, A. C. (2019). The genus Lactobacillus. *Lact. Acid Bact. Microbiol. Funct. Asp* 47:23. doi: 10.1201/9780429057465-4

Jafari, D., Malih, S., Eini, M., Jafari, R., Gholipourmalekabadi, M., Sadeghizadeh, M., et al. (2020). Improvement, scaling-up, and downstream analysis of exosome production. *Crit. Rev. Biotechnol.* 40, 1098–1112. doi: 10.1080/07388551.2020.1805406

Jounai, K., Sugimura, T., Morita, Y., Ohshio, K., and Fujiwara, D. (2018). Administration of *Lactococcus lactis* strain plasma induces maturation of plasmacytoid dendritic cells and protection from rotavirus infection in suckling mice. *Int. Immunopharmacol.* 56, 205–211. doi: 10.1016/j.intimp.2018.01.034

Kang, E. A., Choi, H.-I., Hong, S. W., Kang, S., Jegal, H.-Y., Choi, E. W., et al. (2020). Extracellular vesicles derived from kefir grain Lactobacillus ameliorate intestinal inflammation via regulation of proinflammatory pathway and tight junction integrity. *Biomedicines* 8:522. doi: 10.3390/biomedicines8110522

Kim, W., Lee, E. J., Bae, I.-H., Myoung, K., Kim, S. T., Park, P. J., et al. (2020). *Lactobacillus plantarum*-derived extracellular vesicles induce anti-inflammatory M2 macrophage polarization in vitro. *J. Extracell. Vesicles* 9:1793514. doi: 10.1080/20013078.2020.1793514

Kim, S.-H., Lee, J. H., Kim, E. H., Reaney, M. J., Shim, Y. Y., and Chung, M. J. (2022). Immunomodulatory activity of extracellular vesicles of kimchi-derived lactic acid Bacteria (*Leuconostoc mesenteroides*, *Latilactobacillus curvatus*, and *Lactiplantibacillus plantarum*). *Food Secur.* 11:313. doi: 10.3390/foods11030313

Krishnan, N., Kubiatowicz, L. J., Holay, M., Zhou, J., Fang, R. H., and Zhang, L. (2022). Bacterial membrane vesicles for vaccine applications. *Adv. Drug Deliv. Rev.* 185:114294. doi: 10.1016/j.addr.2022.114294

Lee, B.-H., Hsu, W.-H., and Shen, T.-L. (2018). Impact of pathogenic microbes and healthy microbiota by Lactobacillus-derived extracellular vesicles. *J. Extracell. Vesicles* 7:24.

Lee, B.-H., Wu, S.-C., Shen, T.-L., Hsu, Y.-Y., Chen, C.-H., and Hsu, W.-H. (2021). The applications of *Lactobacillus plantarum*-derived extracellular vesicles as a novel natural antibacterial agent for improving quality and safety in tuna fish. *Food Chem.* 340:128104. doi: 10.1016/j.foodchem.2020.128104

Lei, C., Teng, Y., He, L., Sayed, M., Mu, J., Xu, F., et al. (2021). Lemon exosome-like nanoparticles enhance stress survival of gut bacteria by RNase P-mediated specific tRNA decay. *Iscience* 24:102511. doi: 10.1016/j.isci.2021.102511

Leung, M. Y. K., Liu, C., Koon, J. C. M., and Fung, K. P. (2006). Polysaccharide biological response modifiers. *Immunol. Lett.* 105, 101–114. doi: 10.1016/j.imlet.2006.01.009

Li, T., Chen, X., Liu, Y., Hua, R., Qi, Q., and Feng, X. (2023a). Bovine milk derived exosomes affect gut microbiota of DSS-induced colitis mouse. *Indian J Microbiol.* 64, 100–109. doi: 10.1007/s12088-023-01131-3

Li, W., Li, J., Xie, Y., Tan, Y., Wang, H., Su, L., et al. (2023b). A facile method based on a superabsorbent polymer composite for concentration and separation of exosomes from cell culture media. *Polym. Chem.* 14, 542–546. doi: 10.1039/D2PY01377K

Li, Q., Wang, H., Peng, H., Huyan, T., and Cacalano, N. A. (2019). Exosomes: versatile nano mediators of immune regulation. *Cancers* 11:1557. doi: 10.3390/cancers11101557

Liu, H., Zhao, F., Zhang, K., Zhao, J., and Wang, Y. (2021a). Investigating the growth performance, meat quality, immune function and proteomic profiles of plasmal exosomes in *Lactobacillus plantarum*-treated broilers with immunological stress. *Food Funct.* 12, 11790–11807. doi: 10.1039/D1FO01936H

Liu, H., Zhao, F., Zhang, K., Zhao, J., and Wang, Y. (2021b). Investigating the immune function and proteomic profiles of Plasmal exosomes in Lactobacillus Plantarum-treated immunosuppressive broilers. *Semantic Scholar.* doi: 10.21203/rs.3.rs-612007/v1

Luo, M., Zhang, X., Wu, J., and Zhao, J. (2021). Modifications of polysaccharide-based biomaterials under structure-property relationship for biomedical applications. *Carbohydr. Polym.* 266:118097. doi: 10.1016/j.carbpol.2021.118097

Mitsuoka, T. (2000). Significance of dietary modulation of intestinal flora and intestinal environment. *Biosci. Microflora* 19, 15–25. doi: 10.12938/bifidus1996.19.15

Munir, J., Lee, M., and Ryu, S. (2020). Exosomes in food: health benefits and clinical relevance in diseases. *Adv. Nutr.* 11, 687–696. doi: 10.1093/advances/nmz123

Nicolò, S., Tanturli, M., Mattiuz, G., Antonelli, A., Baccani, I., Bonaiuto, C., et al. (2021). Vaginal lactobacilli and vaginal dysbiosis-associated bacteria differently affect cervical epithelial and immune homeostasis and anti-viral defenses. *Int. J. Mol. Sci.* 22:6487. doi: 10.3390/ijms22126487

Pang, Y., Lundberg, L. E., Forsberg, M. M., Ahl, D., Bysell, H., Pallin, A., et al. (2022). Extracellular membrane vesicles from *Limosilactobacillus reuteri* strengthen the intestinal epithelial integrity, modulate cytokine responses and antagonize activation of TRPV1. *Front. Microbiol.* 13:1032202. doi: 10.3389/fmicb.2022.1032202

Royo, F., Zuñiga-Garcia, P., Sanchez-Mosquera, P., Egia, A., Perez, A., Loizaga, A., et al. (2016). Different EV enrichment methods suitable for clinical settings yield different subpopulations of urinary extracellular vesicles from human samples. *J. Extracell. Vesicles* 5:29497. doi: 10.3402/jev.v5.29497

Schuh, C. M., Cuenca, J., Alcayaga-Miranda, F., and Khoury, M. (2019). Exosomes on the border of species and kingdom intercommunication. *Transl. Res.* 210, 80–98. doi: 10.1016/j.trsl.2019.03.008

Sedykh, S. E., Purvinsh, L. V., Burkova, E. E., Dmitrenok, P. S., Ryabchikova, E. I., and Nevinsky, G. A. (2022). Analysis of proteins and peptides of highly purified CD9+ and CD63+ horse Milk exosomes isolated by affinity chromatography. *Int. J. Mol. Sci.* 23:16106. doi: 10.3390/ijms232416106

Sha, Z., Shang, H., Miao, Y., Huang, J., Niu, X., Chen, R., et al. (2021). Polysaccharides from *Pinus massoniana* pollen improve intestinal mucosal immunity in chickens. *Poult. Sci.* 100, 507–516. doi: 10.1016/j.psj.2020.09.015

Sidhom, K., Obi, P. O., and Saleem, A. (2020). A review of exosomal isolation methods: is size exclusion chromatography the best option? *Int. J. Mol. Sci.* 21:6466. doi: 10.3390/ijms21186466

Smalley Rumfield, C., Roller, N., Pellom, S. T., Schlom, J., and Jochems, C. (2020). Therapeutic vaccines for HPV-associated malignancies. *ImmunoTargets Therapy* 9, 167–200. doi: 10.2147/ITT.S273327

Tang, Y., Dong, W., Wan, K., Zhang, L., Li, C., Zhang, L., et al. (2015). Exopolysaccharide produced by *Lactobacillus plantarum* induces maturation of dendritic cells in BALB/c mice. *PLoS One* 10:e0143743. doi: 10.1371/journal.pone.0143743

Tong, L., Zhang, X., Hao, H., Liu, Q., Zhou, Z., Liang, X., et al. (2021). *Lactobacillus rhamnosus* GG derived extracellular vesicles modulate gut microbiota and attenuate inflammatory in DSS-induced colitis mice. *Nutrients* 13:3319. doi: 10.3390/nu13103319

Tsai, Y.-T., Cheng, P.-C., and Pan, T.-M. (2012). The immunomodulatory effects of lactic acid bacteria for improving immune functions and benefits. *Appl. Microbiol. Biotechnol.* 96, 853–862. doi: 10.1007/s00253-012-4407-3

Tsuji, R., Komano, Y., Ohshio, K., Ishii, N., and Kanauchi, O. (2018). Long-term administration of pDC stimulative lactic acid bacteria, *Lactococcus lactis* strain plasma, prevents immune-senescence and decelerates individual senescence. *Exp. Gerontol.* 111, 10–16. doi: 10.1016/j.exger.2018.06.028

Uddin, M. J., Dawan, J., Jeon, G., Yu, T., He, X., and Ahn, J. (2020). The role of bacterial membrane vesicles in the dissemination of antibiotic resistance and as promising carriers for therapeutic agent delivery. *Microorganisms* 8:670. doi: 10.3390/microorganisms8050670

Wang, H., Lee, K.-S., and Kang, Y.-W. (2021). Skin barrier improvement effect of Exosomal Nanovesicles derived from lactic acid Bacteria. *J. Soc. Cosmetic Sci. Korea* 47, 171–178. doi: 10.15230/SCSK.2021.47.2.171

Wang, J., Sun, X., Zhao, J., Yang, Y., Cai, X., Xu, J., et al. (2017). Exosomes: a novel strategy for treatment and prevention of diseases. *Front. Pharmacol.* 8:300. doi: 10.3389/fphar.2017.00300

Weng, Y., Sui, Z., Shan, Y., Hu, Y., Chen, Y., Zhang, L., et al. (2016). Effective isolation of exosomes with polyethylene glycol from cell culture supernatant for in-depth proteome profiling. *Analyst* 141, 4640–4646. doi: 10.1039/C6AN00892E

Wu, S.-C., Kuo, P.-J., Rau, C.-S., Wu, Y.-C., Wu, C.-J., Lu, T.-H., et al. (2021). Subpopulations of exosomes purified via different exosomal markers carry different microRNA contents. *Int. J. Med. Sci.* 18, 1058–1066. doi: 10.7150/ijms.52768

Yang, F., Ao, X., Ding, L., Ye, L., Zhang, X., Yang, L., et al. (2022). Non-coding RNAs in Kawasaki disease: molecular mechanisms and clinical implications. *BioEssays* 44:e2100256. doi: 10.1002/bies.202100256

Yang, Z., Gao, Z., Yang, Z., Zhang, Y., Chen, H., Yang, X., et al. (2022). *Lactobacillus plantarum*-derived extracellular vesicles protect against ischemic brain injury via the microRNA-101a-3p/c-Fos/TGF-β axis. *Pharmacol. Res.* 182:106332. doi: 10.1016/j.phrs.2022.106332

Yang, Q., Peng, J., Xiao, H., Xu, X., and Qian, Z. (2022). Polysaccharide hydrogels: functionalization, construction and served as scaffold for tissue engineering. *Carbohydr. Polym.* 278:118952. doi: 10.1016/j.carbpol.2021.118952

Ye, Y., Zhang, X., Xie, F., Xu, B., Xie, P., Yang, T., et al. (2020). An engineered exosome for delivering sgRNA: Cas9 ribonucleoprotein complex and genome editing in recipient cells. *Biomater. Sci.* 8, 2966–2976. doi: 10.1039/D0BM00427H

Yu, Y., Lin, S., Chen, Z., Qin, B., He, Z., Cheng, M., et al. (2023). Bacteria-driven bio-therapy: from fundamental studies to clinical trials. *Nano Today* 48:101731. doi: 10.1016/j.nantod.2022.101731

Yu, S., Zhao, Z., Hao, P., Qiu, Y., Zhao, M., Zhou, G., et al. (2022). Biological functions and cross-kingdom host gene regulation of small RNAs in *Lactobacillus plantarum*-derived extracellular vesicles. *Front. Microbiol.* 13:944361. doi: 10.3389/fmicb.2022.944361

Yu, S., Zhao, Z., Xu, X., Li, M., and Li, P. (2019). Characterization of three different types of extracellular vesicles and their impact on bacterial growth. *Food Chem.* 272, 372–378. doi: 10.1016/j.foodchem.2018.08.059

Zhou, Q., Ma, K., Hu, H., Xing, X., Huang, X., and Gao, H. (2022). Extracellular vesicles: their functions in plant–pathogen interactions. *Mol. Plant Pathol.* 23, 760–771. doi: 10.1111/mpp.13170

frontiers | Frontiers in Microbiology

TYPE Original Research
PUBLISHED 13 May 2024
DOI 10.3389/fmicb.2024.1384027

OPEN ACCESS

EDITED BY
Monika Prakash Rai,
Motilal Nehru National Institute of Technology Allahabad, India

REVIEWED BY
Arun Karnwal,
Lovely Professional University, India
M. Sarvajith,
King Abdullah University of Science and Technology, Saudi Arabia

*CORRESPONDENCE
Haihua Ruan
ruanhaihua@tjcu.edu.cn

RECEIVED 08 February 2024
ACCEPTED 25 April 2024
PUBLISHED 13 May 2024

CITATION
Zhu K, Ruan H, Wu T, Zhang H, Han W and Shen Q (2024) Exploiting the roles of nitrogen sources for HEA increment in *Cordyceps cicadae*.
Front. Microbiol. 15:1384027.
doi: 10.3389/fmicb.2024.1384027

Exploiting the roles of nitrogen sources for HEA increment in *Cordyceps cicadae*

Kexin Zhu, Haihua Ruan*, Tao Wu, Hongyang Zhang, Wenying Han and Qiqing Shen

Tianjin Key Laboratory of Food Science and Biotechnology, College of Biotechnology and Food Science, Tianjin University of Commerce, Tianjin, China

Cordyceps cicadae, as a new food ingredient, is a valuable edible and medicinal fungi. However, its resources are severely depleted due to environmental limitations and excessive harvesting practices. N^6-(2-hydroxyethyl) adenosine (HEA), as an important product of *Cordyceps cicadae*, has the potential to be used in medical industry due to its diverse disease curing potential. However, the disclosure of HEA synthesis still severely limited its application until now. In this study, the kinetic curves for adenosine and HEA under shaker fermentation were explored. The kinetics of HEA and adenosine production exhibited a competitive pattern, implicating a possibility of sharing a same step during their synthesis. Due to HEA as a derivative of nitrogen metabolism, the effect of different nitrogen sources (peptone, yeast extract, ammonium sulfate, diammonium oxalate monohydrate, ammonium citrate dibasic, and ammonium citrate tribasic) on HEA production in *Cordyceps cicadae* strain AH 10-4 had been explored under different incubation conditions (shaker fermentation, stationary fermentation, and submerged fermentation). Our results indicated that the complex organic nitrogen sources were found to improve the accumulation of HEA content under shaker fermentation. In contrast, the optimal nitrogen source for the accumulation of HEA under stationary fermentation and submerged fermentation was ammonium citrate tribasic. But submerged fermentation obviously shortened the incubation time and had a comparable capacity of HEA accumulation by 2.578 mg/g compared with stationary fermentation of 2.535 mg/g, implicating a possibility of scaled-up production of HEA in industry by submerged fermentation. Based on the dramatic HEA production by ammonium sulfate as nitrogen resources between stationary and shaker fermentations, alanine, aspartate and glutamate as well as arginine metabolic pathway were related to the production of HEA by comparative transcriptome. Further investigation indicated that glutamic acid, which is an analog of Asp, showed an optimum production of HEA in comparison with other amino acids.

KEYWORDS

***Cordyceps cicadae*, source of nitrogen, nucleosides, N^6-(2-hydroxyethyl)-adenosine, transcriptome analysis**

1 Introduction

Cordyceps cicadae (*C. cicadae*), a high-quality *cordyceps* similar to *Cordyceps sinensis* and *Cordyceps militaris* (Cheng et al., 2012), is a fungi abundant with bioactive compounds such as nucleoside, ergosterol, cordycepic acid, and polysaccharide, etc. It is reported possessing remarkable clinical activities including anti-tumor (Yang and Zhang, 2016), immune

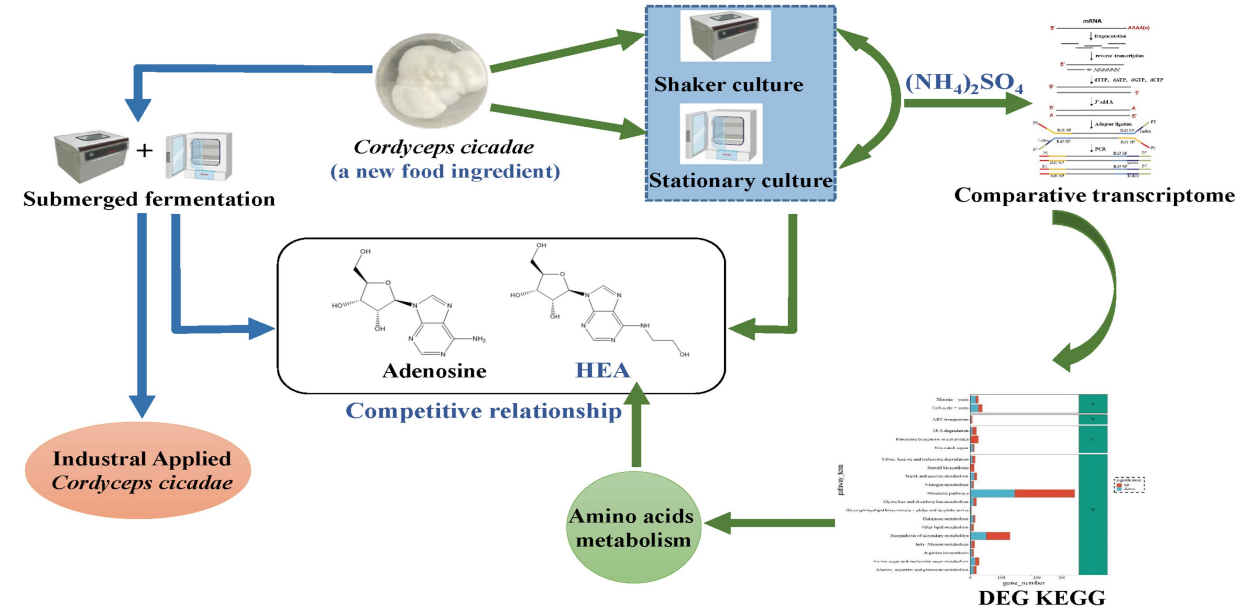

GRAPHICAL ABSTRACT

regulation (Zheng et al., 2022), and significant resistance to renal failure (Zhu et al., 2011) etc. *Cordyceps cicadae* has been used as an important herbal medicine for more than 1,600 years (Nxumalo et al., 2020). Particularly since 2021, artificially cultivated *C. cicadae* is approved as a new food ingredient (National Health Commission, 2020), expanding the application field of *C. cicadae* from traditional Chinese medicine to food, which indicates a promising future for its wide-ranging applications.

The majority of *Cordyceps cicadae* is obtained from the wild, particularly in Southeast Asia (Xie et al., 2023). Wild Cicada flowers require specific environments and parasitic hosts to grow, resulting in its rare resources (Zeng et al., 2021). Given its use as both medicine and food, the increasing demand for this valuable fungus has led to unsustainable harvesting practices (Liu et al., 2008). Therefore, mycelial fermentation to produce the bioactive compounds need to be investigated as an alternative substitute for wild *C. cicadae*. *Paecilomyces cicadae* (*P. cicadae*), reported as the anamorph stage of *C. cicadae*, is mainly used as the strain for artificial culture of *C. cicadae*, and this kind of cultivated *P. cicadae* has been shown controllable quality (Li et al., 2019). The artificial cultivation techniques of *C. cicadae* comprise liquid fermentation (Horng et al., 2021), solid fermentation (Lu et al., 2017; Shi et al., 2022), and artificial culture of alternative host insects (Liu et al., 2018).

Adenosine (Figure 1A) and N^6-(2-hydroxyethyl) adenosine (HEA) (Figure 1B), as purine nucleosides, are the major bioactive constituents of *Cordyceps*. As far as 1983, HEA was first isolated and purified from the fermentation broth of cultured *Cordyceps* (Furuya et al., 1983). Since then, adenosine and HEA have become important indicators for assessing the quality of *Cordyceps* products. A wild cicada flowers from Anji, Zhejiang city in China was isolated and purified in our laboratory (Huang et al., 2021), which was identified as a new strain of *C. cicadae* by phylogenetic tree with higher yield of adenosine and HEA as compared to previous studies (Chunyu et al., 2019; Qu et al., 2019).

N^6-(2-hydroxyethyl) adenosine (HEA) is an important bioactive substance with cancer cell inhibition (Xie et al., 2020; Chen et al., 2021; Fu et al., 2023), kidney protection (Wang et al., 2019; Deng et al., 2020), and anti-inflammatory effects (Lu et al., 2015). Therefore, it has attracted much attention for its potential application in the medical industry, especially in the field of cancer therapy. Currently, HEA has been obtained mainly by chemical synthesis (Qu et al., 2006) and liquid fermentation mycelium extraction (Qu et al., 2006). However, chemical synthesis of HEA involves multiple steps, low yields and expensive raw materials, hindering its synthesis on an industrial scale. The liquid fermentation process is easy to control and has become the main means of HEA production (Tsai et al., 2021). It is undoubted that the disclosure of HEA biosynthesis pathway will open up new ways for the wider application of HEA. Previously, a many of generalized Cordyceps species and the strains isolated from it had been characterized as the main HEA-producing species, such as *Cordyceps cicadae* (Zhang et al., 2018), *Cordyceps militaris* (Zhang et al., 2016), *Beauveria bassiana* (Liu et al., 2017), *Cordyceps pruinose* (Meng et al., 2015a, 2015b) *Isaria tenuipes* (Chang et al., 2019) etc. It was demonstrated that A diverse range of amino acids promoted the production of HEA in *Isaria tenuipes* E3, such as arginine, L-glutamic acid, and serine etc., among which arginine is reported as the most effective amino acid (Lei et al., 2013). Moreover, the supplementation of serine, alanine, histidine, and aspartic acid to the culture medium can promote the increase of mycelial HEA content. Three precursor substances, including hypoxanthine, adenine, and adenosine, which share similar chemical structure to HEA, can increase the content of HEA in the mycelium during fermentation (Lei et al., 2014). By comparing the chemical structures of adenosine and HEA, it is seen that HEA has an additional hydroxyethyl group at the N6 position of the purine ring of adenosine, meaning that the HEA is an analog of

10.3389/fmicb.2024.1384027

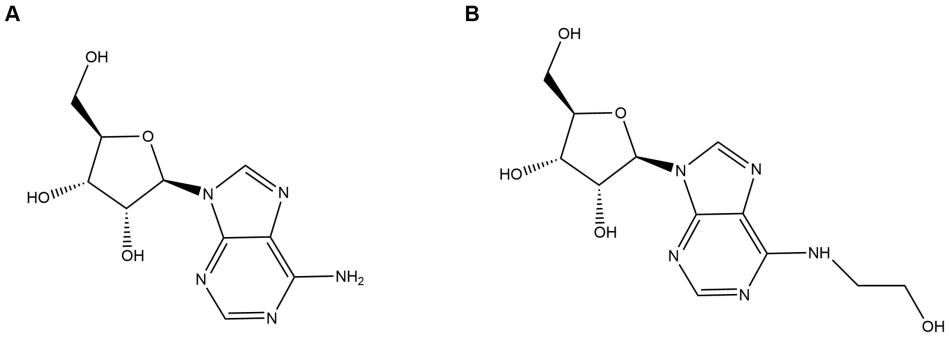

FIGURE 1
Structure diagrams of **(A)** adenosine and **(B)** N^6-(2-hydroxyethyl) adenosine.

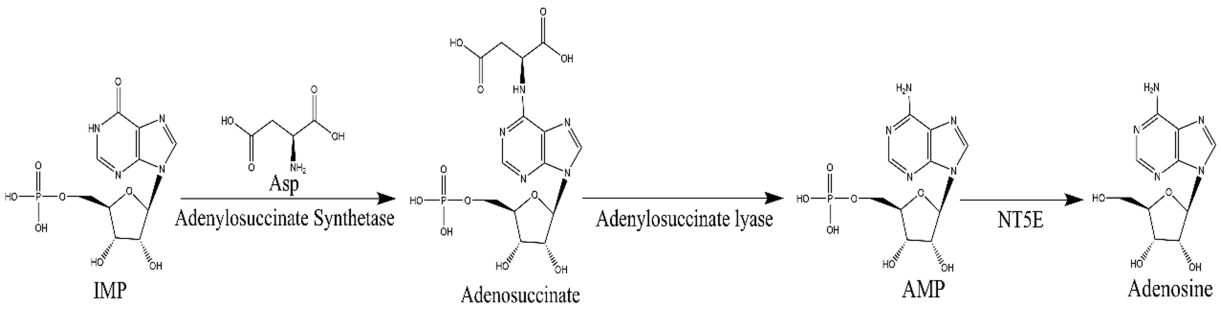

FIGURE 2
The biosynthetic pathway of adenosine: inosinate acid (IMP) and aspartic acid in the presence of adenylosuccinate synthetase to produce adenosuccinate, which in the further generates fumaric acid and AMP by adenylosuccinate lase, then AMP by 5′-nucleotidase (NT5E) to generate adenosine.

adenosine. Recently, the biosynthetic pathway of adenosine in *Cordyceps militaris* has been resolved as is shown in Figure 2. IMP and aspartic acid are converted into adenosuccinate under the catalysis of adenylosuccinate synthase, which is successively catalyzed by adenylosuccinate lyase (ADSL) and 5′-nucleotidase (NT5E) to produce adenosine. Given the structural similarity between HEA and adenosine, it is speculated that amino acids may be the substrates for HEA synthesis.

In recent years, based on the advances of multi-omics technologies, especially metabolomics and transcriptomics, has been reported in illuminating the biosynthesis of active substances, which has provided effective methods for uncovering the biosynthetic pathways of secondary metabolism and identifying candidate genes involved (Han et al., 2016). For example, a previous study on *C. kyushuensis Kob* identified the highly homologous cordycepin biosynthesis gene cluster ck1-ck4 by means of transcriptomic and proteomic analysis (Zhao et al., 2019). Recent studies have uncovered the inherited basis for the development of *C. cicadae*. However, comparative transcriptomic studies related to HEA biosynthesis have not been reported. In this study, due to HEA as a derivative of nitrogen metabolism, we attempted to investigate the effect of nitrogen sources and the means of fermentation on promoting the production of HEA and adenosine, which supplies the evidences for the enclosure of the biosynthetic pathways of HEA.

2 Materials and methods

2.1 Preparation of *Cordyceps cicadae* strain AH 10-4

The *C. cicadae* strain AH 10-4 with higher yield of HEA was used in this study, which was isolated and purified in our laboratory in the previous study (Huang et al., 2021). *Cordyceps cicadae* stain AH 10-4 was plated to PDA medium and incubated at 26°C for 7 days. Three 25 mm^2 PDA cultures were punched out by the inoculation spatula and then transferred to the seed medium. The seed culture was then grown in a 250-mL flask containing 100 mL of its medium (per liter: glucose 20 g, peptone 10 g, yeast extract 10 g, KH_2PO_4 2 g, $MgSO_4$ 0.5 g, $ZnSO_4$ 0.5 g, and pH natural) at 26°C and 140 rpm for 2 days (Huang et al., 2021).

2.2 Shaker fermentation

The *C. cicadae* stain AH 10-4 was cultivated in 250-mL flasks containing 100 mL medium using 5% inoculum (v/v) and then cultured at 26°C and 140 rpm for 10 days. The flask samples were harvested every day. The fermentation medium was referenced to the seed medium (increasing the concentration of glucose to 30 g/L).

N^6-(2-hydroxyethyl) adenosine, as an important nucleoside analog of fungi, was closely linked to nitrogen metabolism. In order to investigate the effects of compound and simple nitrogen sources on the production of adenosine and HEA, compound nitrogen sources (peptone, yeast extract) and simple nitrogen sources (ammonium sulfate, ammonium citrate dibasic, diammonium oxalate monohydrate, and ammonium citrate tribasic) were added to basal medium at 10 g/L supplementation, respectively, and incubated at 26°C and 140 rpm for 5 days. The composition of the basal medium was as following (per liter): glucose 30 g, KH_2PO_4 2 g, $MgSO_4$ 0.5 g, $ZnSO_4$ 0.5 g, and pH natural.

To investigate the impact of predictive amino acids on HEA production, 30 g/L glucose with 0.25 g/L amino acids were added to 67 g/L yeast nitrogen base w/o amino acids and then cultured at 26°C and 140 rpm for 7 days, the amount of each ingredient added in Table 1. The 15 amino acids are valine, leucine, isoleucine, proline, phenylalanine, tyrosine, tryptophan, threonine, cysteine, methionine, asparagine, glutamine, lysine, arginine, and histidine. The five forecast amino acids are alanine, serine, glutamic acid, aspartic acid and glycine.

2.3 Stationary fermentation

The *C. cicadae* stain AH 10–4 was cultivated in 250-mL flasks containing 100 mL medium using 5% inoculum (v /v). It was cultured at 26°C for 17 days by liquid static culture. In order to investigate the effect of amino acids on the production of HEA, amino acids (alanine, serine, aspartic acid, glycine as well as glutamic acid), were added at an addition of 5 g/L to the base medium (per liter: glucose 30 g, peptone 5 g, KH_2PO_4 2 g, $MgSO_4$ 0.5 g, $ZnSO_4$ 0.5 g, pH natural). The incubation was then incubated at 26°C for 17 days.

2.4 Submerged fermentation

Submerged fermentation was cultured with a 5% seed-cultured solution at 26°C, shaking at 140 rpm in the first 3 days and then static incubation for the latter 6 days. It was collected after 9 days incubation.

2.5 Extraction and quantitative analysis of adenosine and HEA

The fermentation broth of *C. cicadae* strain AH 10-4 was centrifuged at 4,500 rpm for 30 min to obtain mycelium, which was then oven-dried at 60°C to a constant weight. For the extraction of adenosine and HEA, the mycelium was ground into a powder that was sieved through a 60-mesh sieve. Then the powder was weighed and extracted by ultrasonic extraction with 20 fold of ultrapure water for 90 min with mixing at 10 min intervals. The extracts were centrifuged at 4,500 rpm for 30 min, and the supernatant was filtered through a Minisart R filter with a pore size of 0.22 μm for later use. The HPLC detection conditions for adenosine and HEA were consistent with the previous studies (Huang et al., 2021). The adenosine and HEA content in mycelium was measured in mg/g, with "g" representing the dry weight of the mycelium.

2.6 RNA extraction and transcriptomic sequencing

Total RNA was extracted from mycelium in shaker and stationary cultures (ammonium sulfate as nitrogen source) by the TRIzol method. The poly-T Oligo-attached magnet was used to enrich mRNA from the total RNA, which was subsequently fragmented in fragmentation buffer. And then a total amount of 1.5 μg mRNA was used to construct cDNA library for each sample by using Illumina's NEBNext® Ultra™ RNA Library Preparation Kit. 200–250 bp cDNA fragments were screened and purified using the AMPure XP system (Beckman Coulter, Beverly, United States). The quality of the libraries was then assessed on an Agilent Bioanalyzer 2100 system and sequenced (150 bp paired-end) on an Illumina Novaseq 6000 platform. A total of six libraries were constructed with three biological replicates per sample.

2.7 *De novo* assembly and annotation

The clean reads were obtained by removing reads with adapter, ploy-N, and low quality reads from the raw paired-end reads, which were then assembled using Trinity (Grabherr et al., 2011). To further explore the annotation function of the assembled and spliced transcripts, the assembled unigene was annotated against Nt, Nr,

TABLE 1 Additive ratio of each ingredient.

Glucose	Yeast nitrogen base w/o amino acids	Amino acid
3%	6.7%	15 + Ala
3%	6.7%	15 + Ser
3%	6.7%	15 + Glu
3%	6.7%	15 + Asp
3%	6.7%	15 + Gly
3%	6.7%	15 + Ala+Ser + Glu + Asp+Gly
3%	6.7%	15
3%	6.7%	Control

"15" represents 15 amino acids, including valine, leucine, isoleucine, proline, phenylalanine, tyrosine, tryptophan, threonine, cysteine, methionine, asparagine, glutamine, lysine, arginine, and histidine.

Swiss-Prot, GO, KOG, KEGG, and Pfam databases to obtain the annotation of the unigene.

2.8 Differential expression analysis and functional enrichment

The stationary and shaker fermentation mycelium was analyzed for differential expression using the DESeq R software package (Anders and Huber, 2010). The genes with a p value of less than 0.05 on an adjusted basis found by DESeq were then classified as differentially expressed genes. In addition, the mycelium from stationary and shaker fermentation cultures were analyzed for functional enrichment that was performed for GO and KEGG by using the GOsep R software package and KOBAS, respectively (Mao et al., 2005). The screening criteria for significantly enriched GO and KEGG by DEGS were Bonferroni corrected p values of less than or equal to 0.05.

2.9 Statistics

The data were reported as mean ± SD and analyzed using one-way ANOVA with Duncan's multiple rang test in SPSS software version 23.0 (IBM Corp., Armonk, NY, United States) to determine the significance of group differences. A p value less than 0.05 was considered statistically significant.

3 Results

3.1 Production of HEA in the *Cordyceps cicadae* strain AH 10-4 by shaker culture

A time course analysis was conducted to study the kinetics of HEA production in strain AH 10–4 grown in shaker culture for 10 days. Firstly, in terms of biomass, it was seen that the biomass of mycelium increased with incubation time from Day 1 to Day 8, reaching the highest level of 2.403 g/100 mL on Day 8, and then slightly decreased (Supplementary Table S1). As was shown in Figure 3, after the 2 days culture, the content of adenosine reached to the highest level of 5.836 ± 0.486 mg/g, and then decreased gradually until Day 5. Distinct from adenosine, the content of HEA gradually increased with the incubation time, reaching its highest level on the 5th day (2.257 mg/g), and then slightly decreased since the sixth day. Interestingly, the content of HEA obviously increased from Day 2 to Day 5, in which time the content of adenosine decreased gradually, showing a correlation between the increasing trend in HEA production and the decreasing trend in adenosine production. Therefore, we speculated that there was a connection between the synthesis pathways of HEA and adenosine.

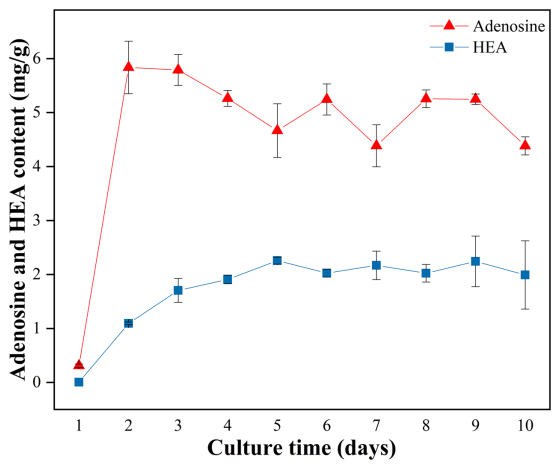

FIGURE 3
Production of adenosine and HEA within strain AH 10-4 mycelial during shaker culture. Values are shown as mean ± SD of triple determinations.

3.2 Effect of different nitrogen sources on the production of HEA by shaker culture

Due to the reason that adenosine and HEA belong to nucleosides produced by fungus, and nucleosides are known to be the derivatives of nitrogen metabolism. Given the advantages of the shaker culture, such as shorter fermentation time, it was chosen as the main method for obtaining mycelium. Thus, in order to investigate the effects of various nitrogen sources on the content of adenosine and HEA in mycelial, we measured the production of adenosine and HEA after 5 days of shaker culture, a time point that showed optimal of HEA production in Figure 3. As shown in Figure 4A, the HEA content was 0.047, 0.730, 0.284, and 0.547 mg/g mycelia dry weight by using ammonium sulfate, diammonium oxalate monohydrate, ammonium citrate dibasic, and ammonium citrate tribasic as nitrogen source, respectively. Among the ammonium salts, the use of diammonium oxalate monohydrate and ammonium citrate tribasic possessed more superior HEA content in mycelium, while the biomass of ammonium citrate tribasic was remarkably higher than that of diammonium oxalate monohydrate ($p < 0.05$) (Supplementary Table S2). Therefore, ammonium citrate tribasic was determined to be the optimum nitrogen source among the ammonium salts. Distinct from ammonium salts, the yields of HEA were 1.872 and 0.892 mg/g from yeast extract and peptone medium respectively, which were significantly superior to those from ammonium salts ($p < 0.05$). By comparison with ammonium salts, complex nitrogen sources (peptone, yeast extract) were more favorable for the accumulation of HEA production in mycelium during shaker fermentation, which might due to their enrichment in amino acids.

3.3 Effect of different nitrogen sources under stationary fermentation on the production of HEA

In contrast to shaker fermentation, it has been demonstrated that stationary culture has the advantages of low energy consumption, low requirements for production conditions and easy scale-up (Liao et al., 2021). Therefore, we probed the ability of various nitrogen sources to yield HEA and adenosine after 17 days of stationary culture. In terms of biomass, complex nitrogen sources (yeast extract, peptone)

10.3389/fmicb.2024.1384027

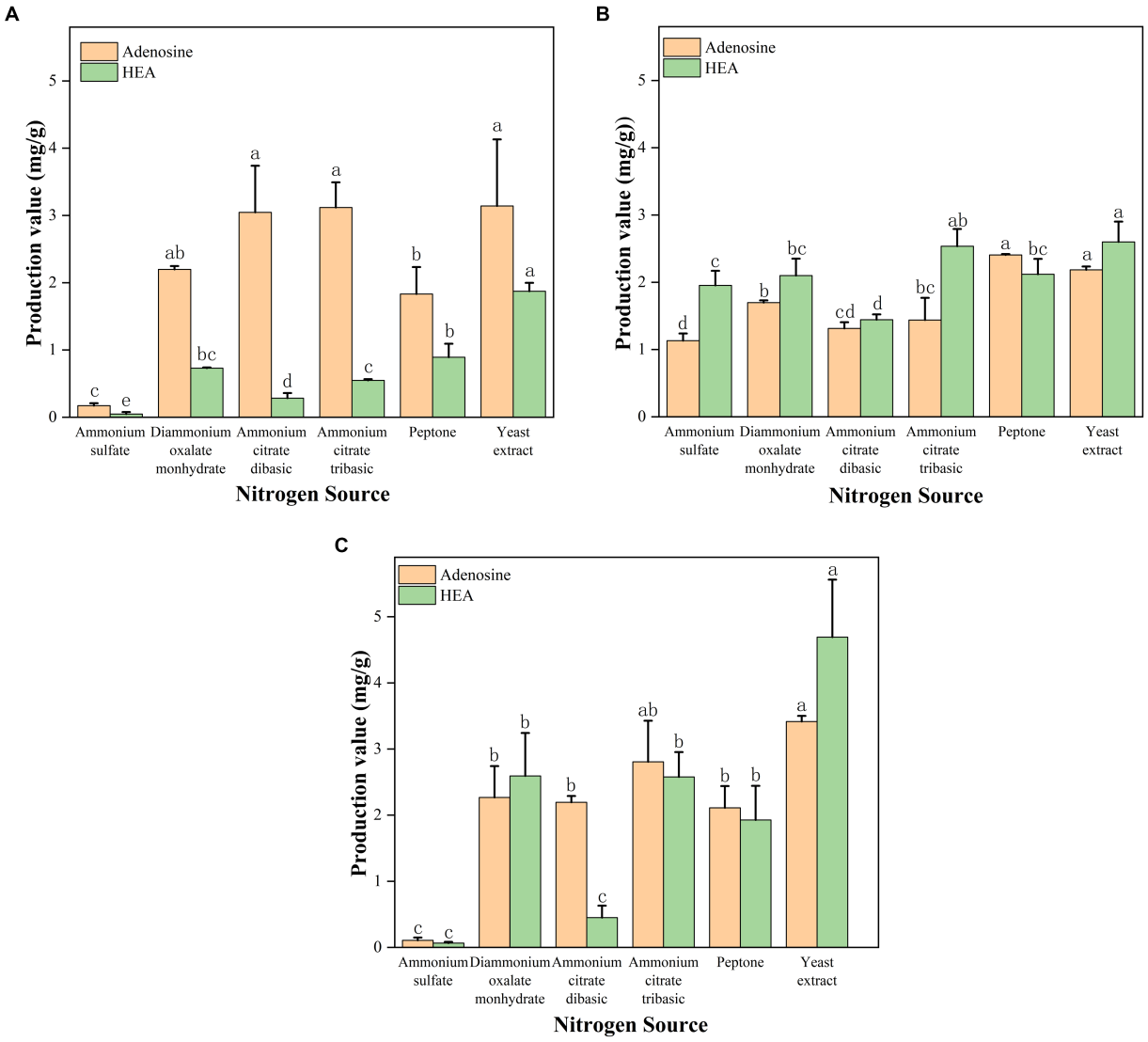

FIGURE 4
(A) Effect of shaker culture with different nitrogen source on the production of adenosine and HEA. **(B)** Effect of stationary culture with different nitrogen source on the production of adenosine and HEA. **(C)** Effect of submerged fermentation with different nitrogen source on the production of adenosine and HEA. Values are shown as mean ± SD of triple determinations. Different letters indicate significantly different values according to a one-way ANOVA with Duncan's multiple test ($p < 0.05$).

promoted the growth of *C. cicadae* strain AH 10-4 mycelium better than ammonium salt ($p < 0.05$) (Supplementary Table S3), including ammonium citrate tribasic, ammonium citrate dibasic, and diammonium oxalate monohydrate (Figure 4B). Interestingly, ammonium citrate tribasic, ammonium citrate dibasic, and diammonium oxalate monohydrate were better than ammonium sulfate in stimulating mycelial growth of *C. cicadae* ($p < 0.05$). Complex organic nitrogen sources (yeast extract, peptone) were found to favor adenosine accumulation in the mycelium. As for HEA production, yeast extract and ammonium citrate tribasic were the most effective nitrogen sources, with HEA yields of 2.599 and 2.535 mg/g, respectively. These were followed by diammonium oxalate monohydrate and peptone ($p < 0.05$). Notably, stationary fermentation caused an increase in the HEA content within mycelium, while the opposite was found for the biomass. Therefore, diammonium oxalate monohydrate and ammonium citrate tribasic can be considered viable alternatives to complex nitrogen source to obtain high HEA yield industrially through stationary fermentation.

3.4 Effect of different nitrogen sources on the production of HEA by submerged fermentation

Submerged fermentation, a novel approach combining shaker and stationary fermentation, was investigated in order to identify an optimal fermentation method and nitrogen source for industrial application. We also explored the ability of different nitrogen sources to produce HEA of *C. cicadae* strain AH 10-4 under submerged fermentation. The result of mycelial biomass was shown in Figure 4C. Yeast extract was most effective for the growth of *C. cicadae* mycelium, which was followed at more than 1 g/100 mL for

10.3389/fmicb.2024.1384027

TABLE 2 Overview of transcriptome sequencing and *de novo* assembly results.

Sample	Raw reads	Clean reads	Error rate	Q20	Q30	GC content
A_1	58,062,016	57,581,622	0.03%	97.58%	93.55%	56.12%
A_2	50,645,198	50,041,026	0.03%	97.68%	93.69%	55.80%
A_3	59,883,168	59,299,218	0.02%	97.94%	94.46%	55.53%
B_1	56,441,966	55,835,776	0.03%	97.70%	93.91%	55.73%
B_2	53,825,912	53,189,416	0.03%	97.68%	93.83%	55.60%
B_3	57,562,606	56,878,932	0.03%	97.68%	93.92%	55.94%

ammonium citrate, diammonium oxalate monohydrate and peptone as nitrogen source (Supplementary Table S4). Yeast extract as a nitrogen source yielded the highest levels of adenosine (3.416 mg/g) and HEA (4.691 mg/g) within *C. cicadae* strain AH 10–4 mycelium. The HEA concentration was 1.928, 0.065, 2.593, 0.450, and 2.578 mg/g mycelia dry weight by using peptone, ammonium sulfate, diammonium oxalate monohydrate, ammonium citrate dibasic, and ammonium citrate tribasic. The result indicated that diammonium oxalate monohydrate and ammonium citrate tribasic were comparable to peptone in enhancing HEA accumulation within the mycelium. Additionally, ammonium citrate tribasic and diammonium oxalate monohydrate were inexpensive and could be used as an alternative source of organic nitrogen. Notably, ammonium citrate tribasic had superior production of adenosine and HEA compared to diammonium oxalate monohydrate. Consequently, ammonium citrate tribasic was regarded as the optimal nitrogen source to produce higher HEA concentrations in *C. cicadae* strain AH 10-4 mycelium. Submerged fermentation increased the biomass and reduced incubation time than stationary fermentation. Importantly, this can be easily scaled-up in the fermentation industry.

3.5 Illumina sequencing and *de novo* assembly

In this study, we did transcriptomic analysis to compare mycelium under high-HEA-producing and low-HEA-producing conditions with the aim to find the different metabolic pathways related to HEA biosynthesis. Comparing HEA content in stationary (Figure 4B) and shaker cultured mycelium (Figure 4A), ammonium sulfate has a simple composition and a significant difference of HEA content, which was chosen a suitable nitrogen source for transcriptomics. Therefore, samples of mycelium cultured with ammonium sulfate as a nitrogen source in stationary (A1-3) and shaker (B1-3) cultures, including three biological replicates, were selected for transcriptomics. For the purpose of distinguishing transcriptomic features during HEA biosynthesis, RNA-seq libraries were performed by extracting total RNA from stationary and shaker fermentation mycelium, respectively. Then, the RNA-seq libraries were sequenced using Illumina Novaseq 6000. The raw reads obtained for the stationary culture and shaker fermentation samples ranged from 50,645,198 to 59,883,168, and raw reads were filtered to obtain clean reads ranging from 50,041,026 to 59,299,218 (Table 2). Among all six samples, the proportion of bases with quality value ≥20 was above 97.58% in Q20 and the proportion of bases with quality value ≥30 was above 93.55% in Q30 in all groups, which indicated that the sequencing results were satisfactory and could be used for subsequent analysis.

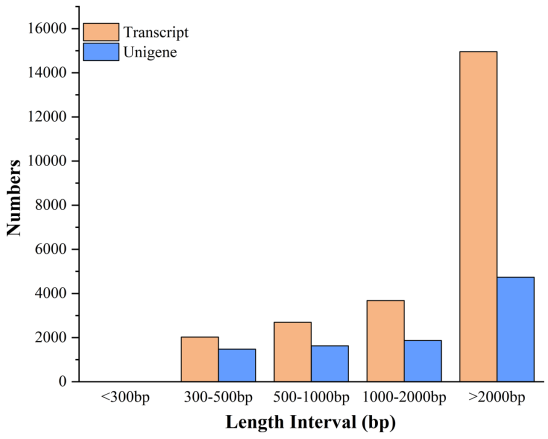

FIGURE 5
Length distribution of assembled transcripts and unigenes between stationary and shaker fermentation mycelium.

The clean reads were assembled into 9,713 unigenes and 23,356 transcripts using Trinity software (Trinity Technologies, CA, United States), with an average assembled single gene length of 2,721 bp (N50 = 4,483) (Supplementary Table S5). The 23,356 transcripts comprised 2,024 (8.67%) transcripts within the length range of 300–500 bp, 2,694 (11.53%) with 500–1,000 bp, 3,680 (15.76%) with 1,000–2,000 bp, and 14,958 (64.04%) with >2,000 bp. The 9,713 unigenes consist of 1,478 (15.22%) unigenes with length range of 300–500 bp, 1,627 (16.75%) with 500–1,000 bp, 1,872 (19.27%) with 1,000–2,000 bp, and 4,736(48.76%) with the length of more than 2,000 bp (Figure 5).

To annotate the gene functions of the stationary and shaker culture samples, the Nr, Nt, Pfam, KOG, Swiss-Prot, KEGG, and GO databases were used, which matched to 6,734, 6,393, 5,966, 2,171, 4,595, 1,443, and 4,636 unigenes, respectively, (Supplementary Table S6). The annotations of the unigenes sequences in the seven database species were shown in the Figure 6A, which indicated that the unigenes sequences were quite similar to the known proteins in the public databases. The 46.36% of the genes displayed an *E*-value of 0, indicating the reliability of these matches (Figure 6B). Regarding the identity distribution of the predicted proteins, the majority of hits (78.46%) in the NR database exhibited 80–100% identity with other fungi proteins, while only 0.03% of the sequences had 18–40% identity (Figure 6C). Furthermore, the distribution of species was also analyzed (Figure 6D), with the annotation results based on the NR library indicating that the genes of *C. cicadae* displayed the highest number of matches with the genes of *Cordyceps fumosorosea*.

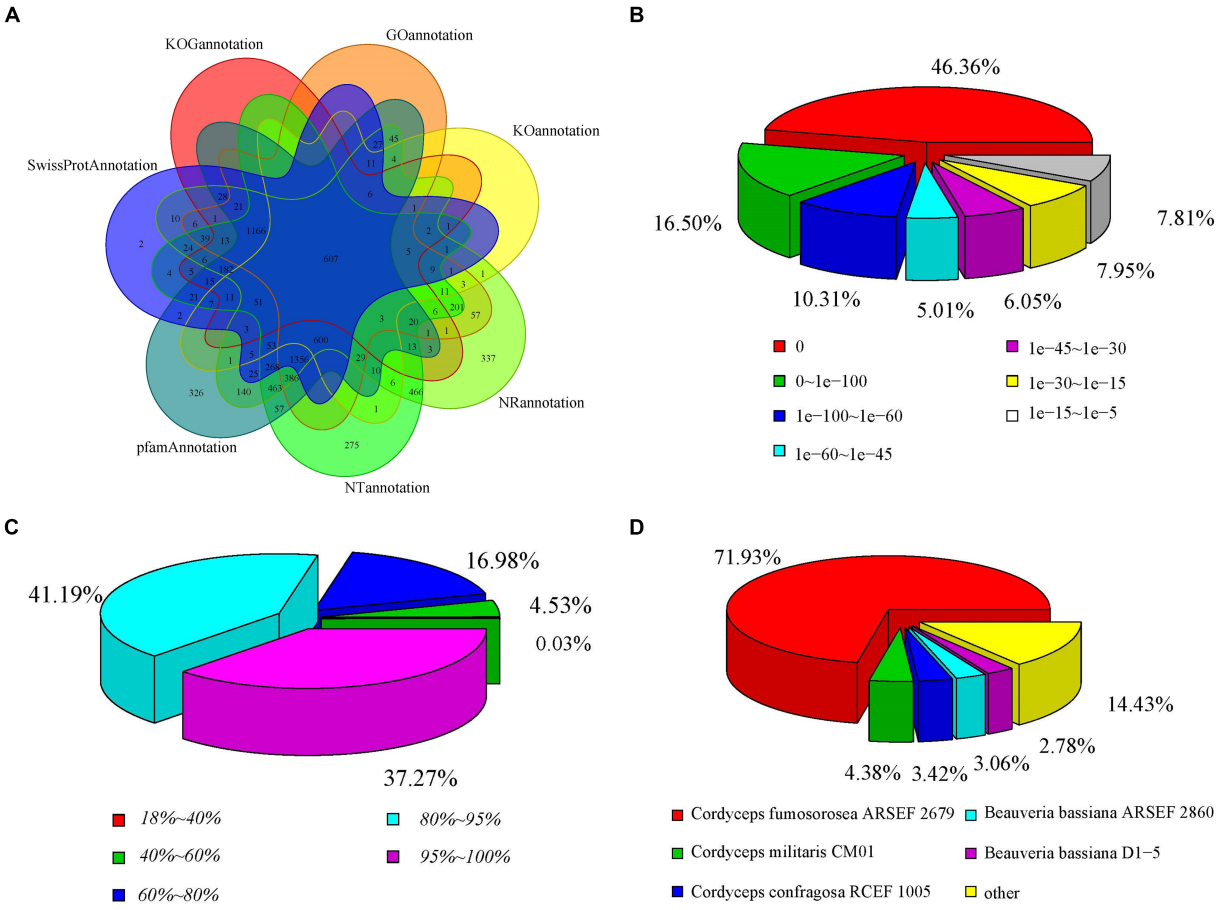

FIGURE 6
Distribution of the homology search against the NCBI database between stationary and shaker fermentation mycelium: **(A)** Venn diagram of the number of orthologous unigenes. **(B)** Distribution of *E*-value. **(C)** Similarity of expressed sequence tags against the NR database. **(D)** Distribution of annotated species.

3.6 DEGs between stationary and shaker fermentation mycelial libraries

Approximately 87–89% of the total reads were successfully mapped to the *C. cicadae* transcriptome (Supplementary Table S7), indicating a high mapping efficiency. We then examined the number of DEGs, with p value of less than or equal to 0.05 (Supplementary Figure S3A). A total of 4,121 DEGs were detected, with 2,038 upregulated and 2,083 downregulated genes (Supplementary Figure S3B). The Venn diagram analysis revealed that 6,499 genes were co-expressed genes (Supplementary Figure S4). These data indicated that the gene expression patterns remained consistent in mycelium cultured with ammonium sulfate as nitrogen source in stationary and shaker cultures.

3.7 Functional and GO annotations of DEGs

To explore the functions of the identified unigenes in the *C. cicadae* transcriptome analysis, GO enrichment analysis was performed. The successfully annotated unigenes were grouped according to GO categories, including biological processes (BP), cellular components (CC) as well as molecular functions (MF). It was found that 9,713 unigenes were classified into 49 functional groups. The most common of these groups were metabolic process (2,516 unigenes), cell (1,984 unigenes), and catalytic activity (2,342 unigenes) (Figure 7). This analysis provided insights into the diverse functions and activities of the identified unigenes in *C. cicadae*.

The DEGs identified between stationary and shaker fermentation were further used for GO enrichment analysis. It was found that the DEGs were mainly related to “RNA processing” (116), “ncRNA processing” (76), “nucleolus” (66), “ribosome biogenesis” (69), “preribosome” (40), “peptidase activity” (113), “peptidase activity, and acting on L-amino acid peptides” (93) (Figure 8). These up- and downregulated genes were crucial for the notable difference in HEA production between stationary and shaker-cultured mycelium. Thus, these DEGs provided potential targets for future functional studies aiming to elucidate the underlying mechanisms involved in HEA production.

3.8 Mapping and enrichment of KEGG pathways

To seek metabolic pathways related to HEA synthesis, we annotated all differentially expressed genes against the KEGG

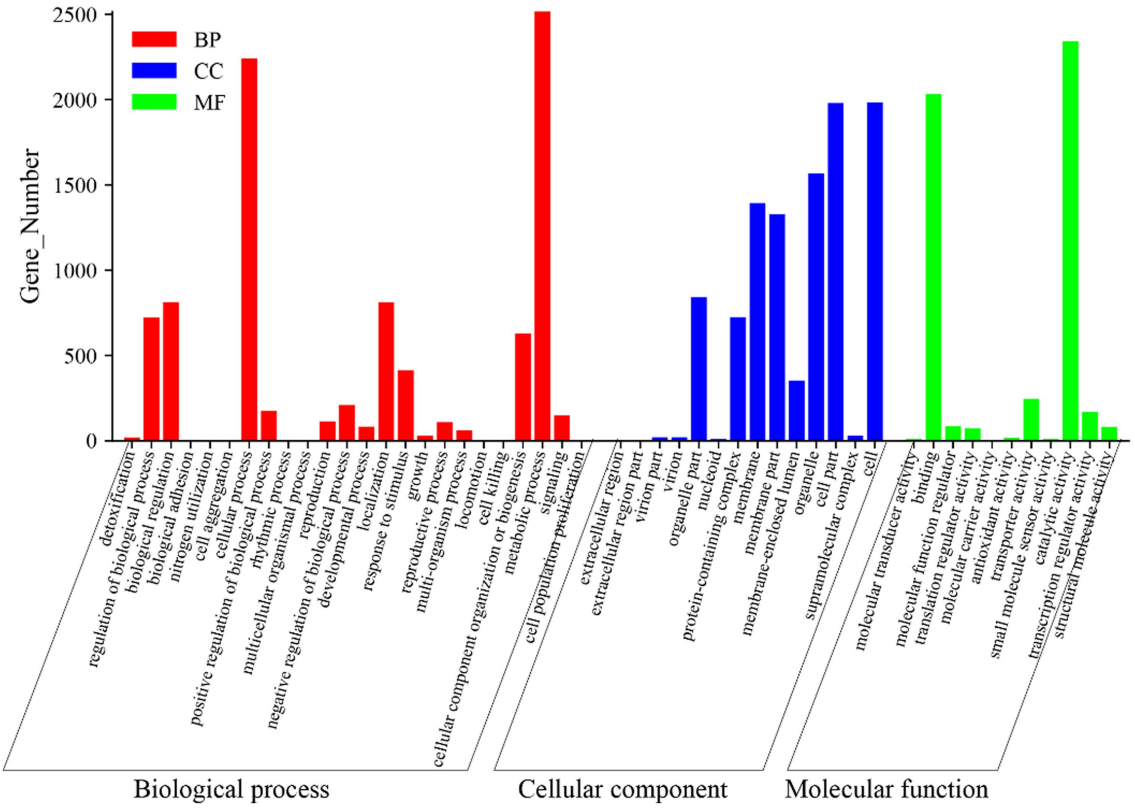

FIGURE 7
GO analysis between stationary and shaker fermentation mycelium. BP, Biological processes; CC, Cellular components; and MF, Molecular functions.

database. The DEGs of top 20 pathways were categorized into four branches: cellular processes, environmental information processing, information processing and metabolism. Among the top 20 pathways, the highest number of differential genes are shown in Figure 9. The largest group of the top 20 enriched pathways was responsible for metabolism, including "Alanine, aspartate and glutamate metabolism" (20), "Glyoxylate and dicarboxylate metabolism" (20), "Galactose metabolism" (14), "Nitrogen metabolism" (10), "Starch and sucrose metabolism" (21), "Amino sugar and nucleotide sugar metabolism" (28), 'beta-Alanine metabolism" (13), "Ether lipid metabolism" (10), "Biosynthesis of secondary metabolites" (130), "Glycosphingolipid biosynthesis—globo and isoglobo series" (4), "Valine, leucine and isoleucine degradation" (15), "Arginine biosynthesis" (10), "Steroid biosynthesis" (12), and "Metabolic pathways" (342). We speculated that HEA synthesis might be closely linked to pathways such as "alanine, aspartate and glutamate metabolism," "nitrogen metabolism" and "β-alanine metabolism." It was well known that amino acids provided the backbone of the purine metabolic pathway. However, the relationship of alanine, aspartate and glutamate metabolism to the synthesis of HEA needs to be further investigated. Furthermore, HEA is an adenosine derivative, so transcriptional studies of amino acid synthesis pathways and purine metabolic pathways of metabolism in combination with analyses of biosynthesis genes have the potential to dissect biosynthesis pathways of HEA.

3.9 Effect of amino acid type on HEA production

As shown in Figure 4A, the complex nitrogen source promoted the accumulation of HEA in mycelium during shaker fermentation. The complex nitrogen sources had a superior production of HEA since they were rich in amino acids. In addition, alanine, aspartate, and glutamate as well as arginine metabolic pathways were significantly different, which is consistent with our speculation that amino acids can be used as substrates for HEA synthesis (Figure 9). Due to HEA as a purine derivative, glutamic acid, glycine, serine, and aspartic acid are involved in purine metabolism. In addition, the former research has also indicated that alanine promotes HEA accumulation in mycelium (Lei et al., 2014). Therefore, we used yeast nitrogen base w/o amino acids supplemented with 15 amino acids as the basal medium, and then the five presumed amino acids were added, respectively, to explore their relationship with the HEA content. The result was as shown in Table 3, there was no statistically significant difference in the content of HEA between the group with the addition of the 15 amino acids and the control group, so we inferred that the 15 amino acids had no relevance to the biosynthesis of HEA (Table 3). However, the group supplemented with glutamate exhibited significantly higher HEA content compared to the other groups.

In addition, in order to further validate, we also added the presumed 5 amino acids (Gly, Glu, Ser, Asp, and Ala) to the peptone

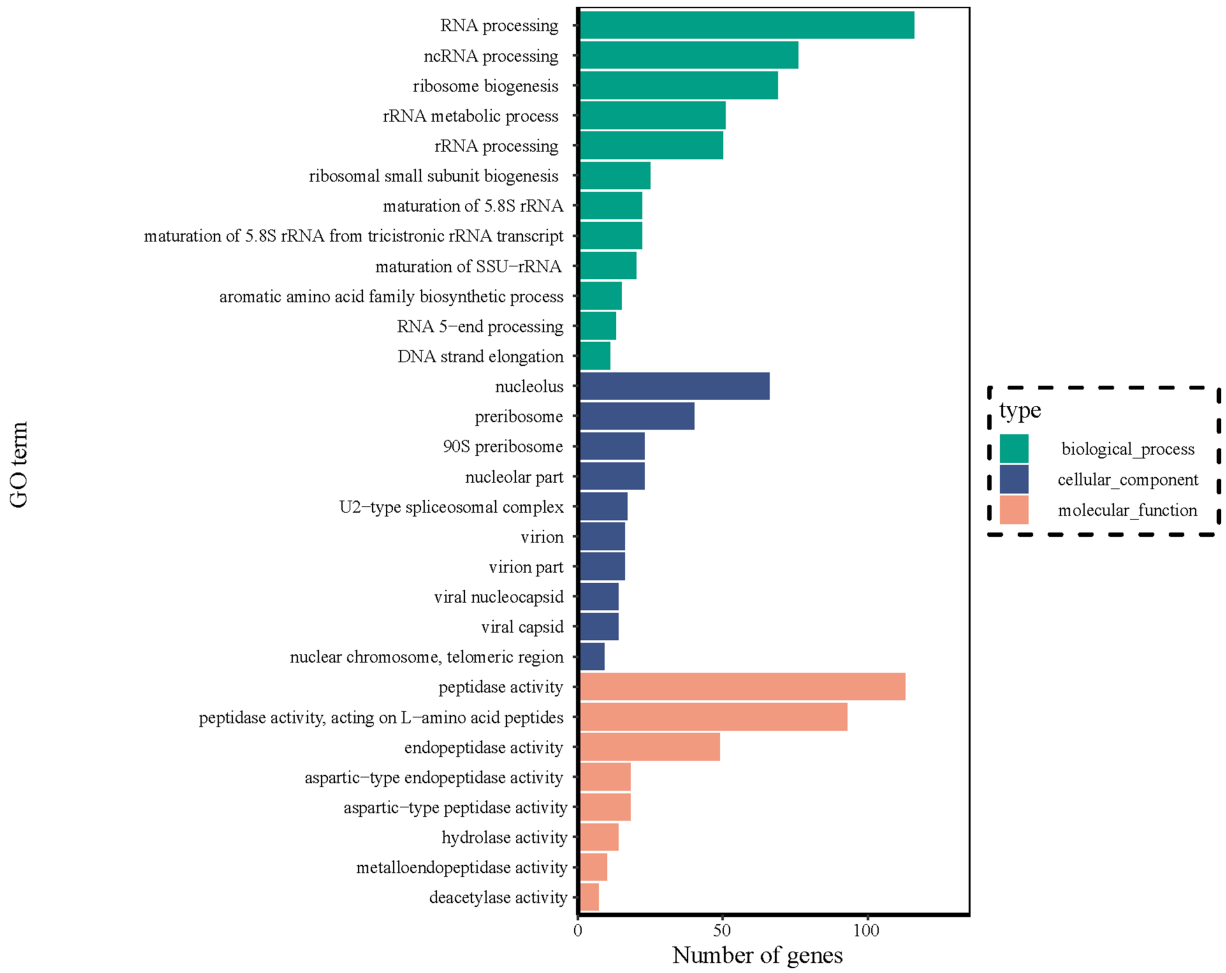

FIGURE 8
DEGs of transcripts in different GO categories between stationary and shaker fermentation mycelium. BP, Biological processes; CC, Cellular component; and MF, Molecular function.

medium and then HEA content was tested, respectively, after 17 days of stationary fermentation, respectively. Addition of amino acids (glutamate, glycine, serine, aspartate, and alanine) resulted in lower biomass compared to the control (Supplementary Table S8). As shown in Figure 10. When peptone was used as nitrogen source, the adenosine content of the strain AH 10-4 fermenting mycelium was 2.332 mg/g and HEA content was 1.422 mg/g. Interestingly, the addition of amino acids to based medium led to a decrease in HEA content. Hence, it was speculated that excess nitrogen source inhibited HEA synthesis after 17 days of fermentation. Among the peptone medium added with five amino acids, glutamate showed a significant effect on the HEA content in the fermenting mycelia of the strain AH 10-4, which is consistent with the results in Table 3.

4 Discussion

In this study, we comprehensively compared the effects of three fermentation methods on HEA production in the *C. cicadae* strain AH 10-4 mycelia. The results revealed that shaker fermentation resulted in high mycelial biomass but low HEA production. Conversely, stationary fermentation favored HEA concentration while exhibiting relatively low biomass even after long-term fermentation. Submerged fermentation, combining with the advantages of both, shortened the incubation time and simultaneously promoted the HEA accumulation. In conclusion, submerged fermentation was deemed more suitable for the industrial-scale HEA production than shaker and stationary fermentation in the *C. cicadae* strain AH 10-4 mycelia, which was consistent with the previous results (Shih et al., 2007). By dissecting the possible factors among these three kinds of fermentation on the perspective of HEA production, dissolved oxygen (DO) was identified as a major factor. To our knowledge, DO was an important indicator for secondary metabolites in the mycelium (Mao and Zhong, 2004; Suparmin et al., 2017), and HEA belonged to the secondary metabolites with special biological activity. Shaker fermentation, with higher DO levels, promoted mycelial growth but inhibited HEA synthesis. On the other hand, the thick mycelia formed by *C. cicadae* in stationary fermentation and submerged fermentation covered the medium surface and seemed to create a hypoxic condition in the medium, which aligned with previous research (Tang and Zhong, 2003). It has been demonstrated that *Cordyceps militaris* induced the production of cordycepin (a nucleoside analog with HEA) under hypoxic conditions (Suparmin et al., 2017), supporting our speculation that high DO inhibits the production of HEA. Transcriptomics results

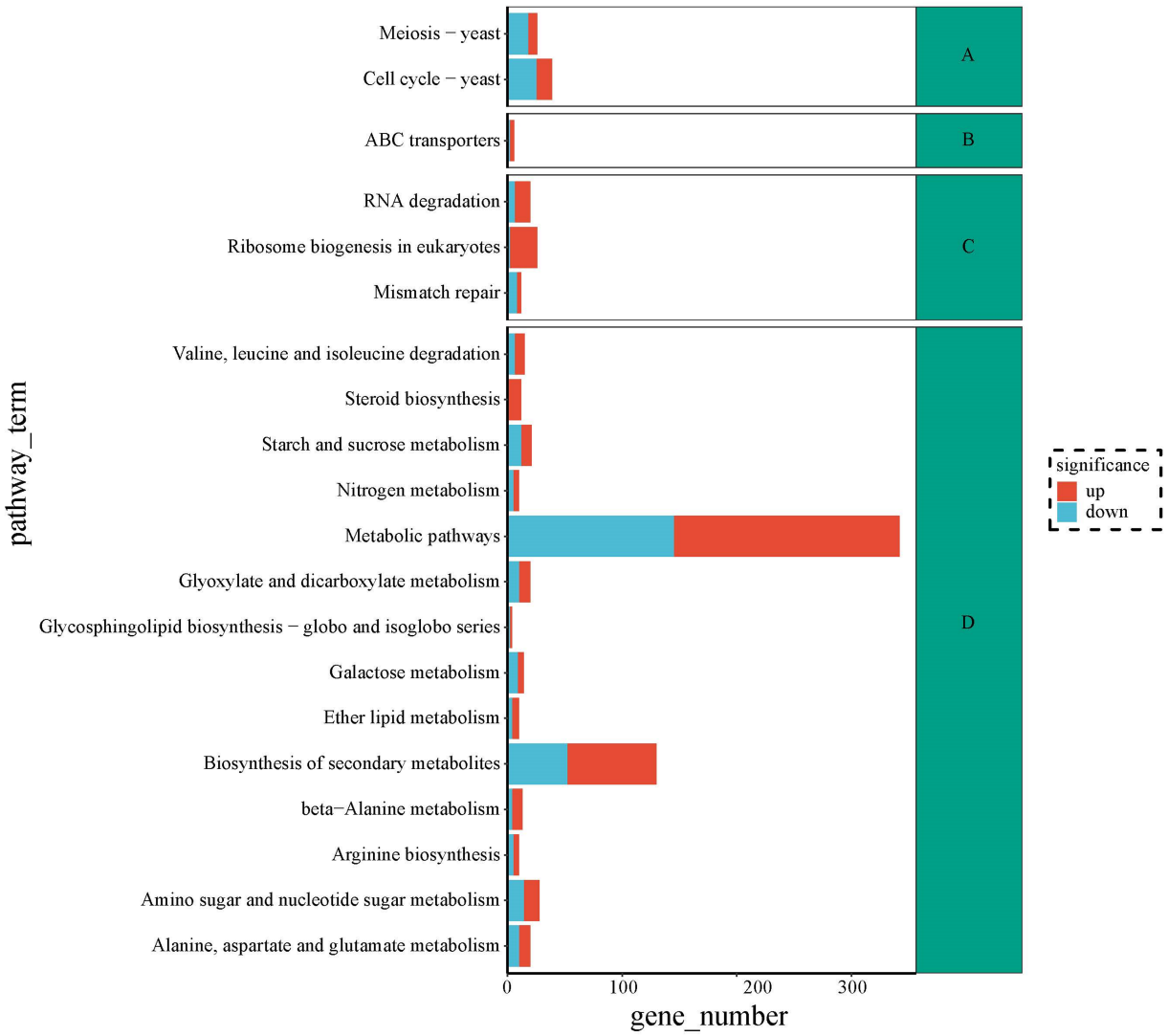

FIGURE 9
The top 20 metabolic pathways between stationary and shaker fermentation mycelium: **(A)** Cellular processes; **(B)** Environmental information processing; **(C)** Information processing; **(D)** Metabolism.

TABLE 3 **Effect of 20 amino acids on production HEA in mycelium.**

Amino acid types	HEA content(mg/g)
15 + Ala	0.020 ± 0.008b
15 + Ser	0.015 ± 0.003b
15 + Glu	0.078 ± 0.064a
15 + Asp	0.015 ± 0.000b
15 + Gly	0.012 ± 0.006b
15 + Ala+Ser + Glu + Asp+Gly	0.027 ± 0.007b
15	0.010 ± 0.000b
Control	——b

"15" represents 15 amino acids, including valine, leucine, isoleucine, proline, phenylalanine, tyrosine, tryptophan, threonine, cysteine, methionine, asparagine, glutamine, lysine, arginine, and histidine. Values are showed as mean ± SD of triple determinations. Different letters in the same column indicate significantly different values according to a one-way ANOVA with Duncan's multiple test ($p < 0.05$).

of mycelia from stationary and shaker fermentation with significant up-regulated genes were enriched to TCA and nitrogen metabolism pathways, which might be more favorable for the synthesis of HEA. Another study showed that upregulation of purine metabolism pathway and energy metabolism gene transcript levels promoted the synthesis of precursors, resulting in increased cordycepin content

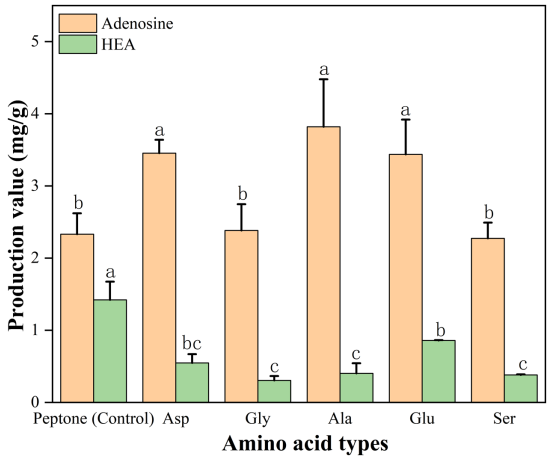

FIGURE 10
Effect of amino acid type on HEA production in mycelium. Values are showed as mean ± SD of triple determinations. Different letters indicate significantly different values according to a one-way ANOVA with Duncan's multiple test ($p < 0.05$).

(Long et al., 2023). It indicated that upregulation of energy metabolism genes favored nucleoside synthesis, which was consistent with our findings. Additionally, it has been observed that in some filamentous fungi, the expression of genes in the γ-aminobutyric acid (GABA) shunt pathway is upregulated during hypoxia (Suparmin et al., 2017), redirecting L-glutamate to the TCA cycle and promoting the accumulation of secondary metabolites (Hillmann et al., 2015). Moreover, stationary and submerged fermentations were found more favorable for HEA accumulation production in mycelium might be due to the slow growth of mycelium and glucose metabolism was mainly directed toward HEA synthesis (Zhao et al., 2020).

Fermentation time and cost were considered important limiting factors in the development of the fungal industry. In this study, submerged fermentation achieved a significant reduction in incubation time compared to stationary fermentation, decreasing from 17 days to 9 days, which resulted in a time–cost savings. In summary, submerged fermentation was a more favorable method to produce HEA industrially than shaker or stationary fermentation including three reasons. Firstly, submerged fermentation reduced the fermentation time than stationary fermentation, which resulted in a time–cost savings. Secondly, submerged fermentation needed a lower level of dissolved oxygen. Lower DO promoted the TCA cycle, for which the concentration of HEA in mycelium was favored. Thirdly, biomass was accumulated more in submerged fermentation than stationary fermentation. Biomass served as a crucial indicator of fungal fermentation, and a higher biomass supported the industrial expansion of cultivation.

Nitrogen sources were essential for the growth and nucleoside synthesis regulation of Cordyceps specie (Shih et al., 2007; Su et al., 2021). In our study, *C. cicadae* mycelium had a various preference for nitrogen sources during growth and HEA synthesis. Yeast extract or peptone was rich in nutrients required for growth, providing the necessary foundation for mycelial growth and cell division. Previous studies had shown that complex organic nitrogen sources, such as yeast extract and peptone showed more efficient growth (Kocharin and Wongsa, 2006; Sung et al., 2010, 2011). Interestingly, the ammonium citrate tribasic promoted HEA synthesis than peptone, with HEA production reaching 2.535 and 2.119 mg/g, respectively. The results of our study indicated that the addition of NH_4^+ had a direct promotion effect on HEA content. Consistent with previously research, the cordycepin-producing capacity of Cordyceps species can be significantly enhanced by ammonium supplementation (Mao et al., 2005; Leung and Wu, 2007). Furthermore, yeast extract had the most remarkable effect on HEA accumulation. Compared to peptone, yeast extract more effectively promoted HEA synthesis in the mycelium under any fermentation conditions, mainly due to its high utilization by *C. cicadae* for protein, nucleotide synthesis or other substances. As opposed to yeast extract, peptone mainly supported mycelial growth, and then synthesized its own nitrogenous substances. A previous study showed yeast extract was the optimal additional nitrogen source for increasing adenosine and HEA concentrations in PDB (Liang et al., 2014; Ke and Lee, 2019). Considering cost, ammonium citrate tribasic promoted HEA accumulation in the mycelium, following yeast extract with a HEA yield of 2.578 mg/g. Another study showed ammonium citrate tribasic as a major factor in nucleoside (cordycepin) synthesis, which was consistent with our results (Long et al., 2023). Overall, based on the accumulation of HEA using different nitrogen sources under three fermentation conditions, the use of ammonium citrate tribasic provided the possibility of industrialized production of HEA during submerged fermentation.

Furthermore, our research utilized comparative transcriptomics to explore the potential association between amino acids and HEA biosynthesis. By comparing mycelium with high and low HEA production, we identified significant differences in amino acid metabolic pathways, including β-alanine metabolism, arginine biosynthesis as well as alanine, aspartate, and glutamate metabolism, which indicated a robust relationship between amino acids and the biosynthesis of HEA. It was speculated that amino acids might be direct or indirect substrates for HEA synthesis. Previous studies showed that the content of glutamate was higher than other amino acids (Ji et al., 2023; Tang et al., 2023), which may be related to the involvement of glutamate in the synthesis of some critical substance in *C. cicadae*.

Our study showed that glutamate was closely linked to the biosynthetic pathway of HEA. Since HEA as a purine derivative, amino acid synthesis pathway and purine metabolism pathway transcriptional studies as well as gene analyses of HEA biosynthesis may be useful in exploring the biosynthesis pathway of HEA. Transcriptome analysis of *C. cicadae* strain AH 10-4 identified two ADSS sequences, with one showing a significant fold difference of 27.173. Previous research had demonstrated that ADSS was a key enzyme in the adenosine synthesis pathway (Xia et al., 2017). Considering the complexity of the HEA synthesis pathway, we believed that the correlation between ADSS and the HEA synthesis pathway needs to be further verified. The growth kinetics of *C. cicadae* indicated a correlation between adenosine and HEA biosynthesis pathways, which was consistent with previous studies (Liu et al., 2017). Based on this, we proposed the following hypotheses regarding the synthesis pathway of HEA. Firstly, there was a competition between adenosine and HEA synthesis, potentially due to shared precursor substances. Secondly, adenosine consistently exceeded the yield of HEA. This suggested that adenosine might serve as a precursor for HEA synthesis and that other regulatory factors

might limit the process of HEA synthesis. In addition, by analyzing the purine metabolic pathway, we observed that adenosine accumulation was converted to inosine by adenosine deaminase. Adenosine deaminase was a significantly up-regulated gene with a fold difference of 1.752. It was hypothesized that the link between adenosine and HEA may be regulated by adenosine deaminase.

In conclusion, the in-depth study of the production mechanism of HEA can provide guidance for future research and industrial application, which will further improve the yield and process efficiency of HEA, promoting the industrialized production and application of HEA.

5 Conclusion

In summary, the effect of different nitrogen sources on HEA production in *Cordyceps cicadae* strain AH 10-4 had been explored under different incubation conditions. The production kinetics of HEA and adenosine exhibited a competitive pattern, implicating a potential shared step in their synthesis. The use of ammonium citrate tribasic resulted in higher HEA content (2.578 mg/g mycelia dry weight) in the mycelium, which provided the possibility of scaled-up HEA production in the fermentation industry by submerged fermentation. Comparative *de novo* transcriptomic analysis of *C. cicadae* mycelium between stationary and shaker fermentation (with ammonium sulfate as nitrogen source) revealed amino acid metabolic pathways were significantly different. Glutamate may play a critical substrate for HEA synthesis, which has yet to be subsequently validated. Further studies are needed to elucidate the mechanism by which these amino acids contribute to HEA biosynthesis. Our results provide a foundation for further pharmaceutical and industrial applications of *C. cicadae*, as well as further exploration of the HEA biosynthesis pathway in *C. cicadae*. Future research can combine with genomics technology to explore the gene regulation mechanism, and further use genetic engineering technology to improve the yield and quality of HEA, which promotes the industrialized production and application of HEA.

Data availability statement

The datasets presented in this study can be found in NCBI SRA repository, accession number PRJNA1075488 (https://www.ncbi.nlm.nih.gov/sra/PRJNA1075488).

Author contributions

KZ: Formal analysis, Investigation, Methodology, Writing – original draft. HR: Formal analysis, Investigation, Methodology, Supervision, Writing – review & editing. TW: Formal analysis, Methodology, Investigation, Writing – original draft. HZ: Formal analysis, Writing – review & editing. WH: Investigation, Writing – original draft. QS: Investigation, Writing – original draft.

Funding

The author(s) declare that financial support was received for the research, authorship, and/or publication of this article. This work was supported by the General Program of National Natural Science Foundation of China (Grant no. 31870122), the Natural Science Foundation of Tianjin (Grant no. 18JCYBJC96000), the Youth Program of National Natural Science Foundation of China (Grant no. 21908168), Tianjin Research Innovation Project for Postgraduate Students (Grant no. 2022SKYZ080) the Tianjin "131" innovative talent team (Team no. 201927), and the Tianjin Education Commission Scientific Research Project (grant number 2022KJ004).

Conflict of interest

The authors declare that the research was conducted in the absence of any commercial or financial relationships that could be construed as a potential conflict of interest.

Publisher's note

Supplementary material

The Supplementary material for this article can be found online at: https://www.frontiersin.org/articles/10.3389/fmicb.2024.1384027/full#supplementary-material

References

Anders, S., and Huber, W. (2010). Differential expression analysis for sequence count data. *Genome Biol.* 11:R106. doi: 10.1186/gb-2010-11-10-r106

Chang, C., Qin, L., Yu, W., Li, F., Wu, X., Wang, Q., et al. (2019). Optimization of ultrasound extraction of n ^{6}-(2-hydroxyethyl)—adenosine from isaria tenuipes using response surface methodology. *Mycosystema* 38, 1559–1569. doi: 10.13346/j.mycosystema.190083

Chen, Y., Wu, Y., Li, S., Du, S., Hao, X., Zhang, J., et al. (2021). Large-scale isolation and antitumor mechanism evaluation of compounds from the traditional chinese medicine cordyceps militaris. *Eur. J. Med. Chem.* 212:113142. doi: 10.1016/j.ejmech.2020.113142

Cheng, J. W., Wang, Y. B., He, L., Qian, H., Fu, L. Z., and Li, H. B. (2012). Optimization of fermentation process for the production of intracellular polysaccharide from paecilomyces cicadae and the immuno-stimulating activity of intracellular polysaccharide. *World J. Microbiol. Biotechnol.* 28, 3293–3299. doi: 10.1007/s11274-012-1140-0

Chunyu, Y., Lu, Z., Luo, Z., Li, S., Li, H., Geng, Y., et al. (2019). Promotion of metabolite synthesis in isaria cicadae, a dominant species in the cicada flower microbiota, by cicada pupae. *J. Agric. Food Chem.* 67, 8476–8484. doi: 10.1021/acs.jafc.9b02705

Deng, J. S., Jiang, W. P., Chen, C. C., Lee, L. Y., Li, P. Y., Huang, W. C., et al. (2020). Cordyceps cicadae mycelia ameliorate cisplatin-induced acute kidney injury by suppressing the tlr4/nf-kappab/mapk and activating the ho-1/nrf2 and sirt-1/ampk pathways in mice. *Oxidative Med. Cell. Longev.* 2020:7912763. doi: 10.1155/2020/7912763

Fu, J., Song, B., Du, J., Liu, S., He, J., Xiao, T., et al. (2023). Impact of bsg/cd147 gene expression on diagnostic, prognostic and therapeutic strategies towards

malignant cancers and possible susceptibility to SARS-cov-2. *Mol. Biol. Rep.* 50, 2269–2281. doi: 10.1007/s11033-022-08231-1

Furuya, T., Hirotani, M., and Matsuzawa, M. (1983). N6-(2-hydroxyethyl) adenosine, a biologically active compound from cultured mycelia of cordyceps and isaria species. *Phytochemistry* 22, 2509–2512. doi: 10.1016/0031-9422(83)80150-2

Grabherr, M. G., Haas, B. J., Yassour, M., Levin, J. Z., Thompson, D. A., Amit, I., et al. (2011). Full-length transcriptome assembly from rna-seq data without a reference genome. *Nat. Biotechnol.* 29, 644–652. doi: 10.1038/nbt.1883

Han, R., Rai, A., Nakamura, M., Suzuki, H., Takahashi, H., Yamazaki, M., et al. (2016). De novo deep transcriptome analysis of medicinal plants for gene discovery in biosynthesis of plant natural products. *Methods Enzymol.* 576, 19–45. doi: 10.1016/bs.mie.2016.03.001

Hillmann, F., Shekhova, E., and Kniemeyer, O. (2015). Insights into the cellular responses to hypoxia in filamentous fungi. *Curr. Genet.* 61, 441–455. doi: 10.1007/s00294-015-0487-9

Horng, C., Yang, Y., Chen, C., Huang, Y., Chen, C., and Chen, F. (2021). Intraocular pressure-lowering effect of cordyceps cicadae mycelia extract in a glaucoma rat model. *Int. J. Med. Sci.* 18, 1007–1014. doi: 10.7150/ijms.47912

Huang, A., Wu, T., Wu, X., Zhang, B., Shen, Y., Wang, S., et al. (2021). Analysis of internal and external microorganism community of wild cicada flowers and identification of the predominant cordyceps cicadae fungus. *Front. Microbiol.* 12:752791. doi: 10.3389/fmicb.2021.752791

Ji, W., Wang, Y., Su, W., Liu, X., Ren, L., and Chen, K. (2023). Comparative analysis of nutritional value and active ingredients of two substrate from cordyceps. *Food Indus.* 44, 342–346,

Ke, B. J., and Lee, C. L. (2019). Using submerged fermentation to fast increase n6-(2-hydroxyethyl)—adenosine, adenosine and polysaccharide productions of cordyceps cicadae nttu 868. *AMB Express* 9:198. doi: 10.1186/s13568-019-0892-4

Kocharin, K., and Wongsa, P. (2006). Semi-defined medium for in vitro cultivation of the fastidious insect pathogenic fungus cordyceps unilateralis. *Mycopathologia* 161, 255–260. doi: 10.1007/s11046-005-0224-x

Lei, B., He, J., Li, S., Zeng, X., Kang, J., Wen, T., et al. (2013). Screening of culture medium constituents and additives for producing of n6-(2-hydroxyethyl)-adenosine by isaria tenuipes. *Acta Edulis Fungi.* 20, 46–51. doi: 10.16488/j.cnki.1005-9873.2013.02.014

Lei, B., Zeng, X., Li, S., Kang, J., He, J., and Wen, T. (2014). Screening of culture medium constituents and additives for producing n6-(2-hydroxyethyl)-adenosine by cordyceps pruinosa strain cp incubated statically. *Mycosystema* 33, 103–113. doi: 10.13346/j.mycosystema.120248

Leung, P. H., and Wu, J. Y. (2007). Effects of ammonium feeding on the production of bioactive metabolites (cordycepin and exopolysaccharides) in mycelial culture of a cordyceps sinensis fungus. *J. Appl. Microbiol.* 103, 1942–1949. doi: 10.1111/j.1365-2672.2007.03451.x

Li, L., Zhang, T., Li, C., Xie, L., Li, N., Hou, T., et al. (2019). Potential therapeutic effects of cordyceps cicadae and paecilomyces cicadae on adenine-induced chronic renal failure in rats and their phytochemical analysis. *Drug Des. Devel. Ther.* 13, 103–117. doi: 10.2147/DDDT.S180543

Liang, Z. C., Liang, C. H., and Wu, C. Y. (2014). Various grain substrates for the production of fruiting bodies and bioactive compounds of the medicinal caterpillar mushroom, cordyceps militaris (ascomycetes). *Int. J. Med. Mushrooms* 16, 569–578. doi: 10.1615/intjmedmushrooms.v16.i6.60

Liao, X., Meng, Z., He, F., and Wen, T. (2021). Effects of medium constituents on the n6-(2-hydroxyethyl)-adenosine production of cordyceps pruinosa by liquid static culture. *Molecular Plant Breeding*. 1–11. Available at: http://kns.cnki.net/kcms/detail/46.1068.S.20211227.0920.004.html

Liu, T., Liu, Z., Yao, X., Huang, Y., Qu, Q., Shi, X., et al. (2018). Identification of cordycepin biosynthesis-related genes through de novo transcriptome assembly and analysis in cordyceps cicadae. *R. Soc. Open Sci.* 5:181247. doi: 10.1098/rsos.181247

Liu, K., Wang, F., and Wang, W. (2017). Beauveria bassiana: a new n6-(2-hydroxyethyl)-adenosine–producing fungus. *Mycology* 8, 259–266. doi: 10.1080/21501203.2017.1375040

Liu, S., Wen, L., Xia, M., and Jiang, N. (2008). Determination of the active ingredient produced in the artificial cultivated cordyceps sobolifera. *J. Anhui Agric. Sci.* 2, 429–467.

Long, L., Liu, Z., Wang, Y., Lin, Q., Ding, S., Li, C., et al. (2023). High-level production of cordycepin by the xylose-utilising cordyceps militaris strain 147 in an optimised medium. *Bioresour. Technol.* 388:129742. doi: 10.1016/j.biortech.2023.129742

Lu, M. Y., Chen, C. C., Lee, L. Y., Lin, T. W., and Kuo, C. F. (2015). N (6)-(2-hydroxyethyl) adenosine in the medicinal mushroom cordyceps cicadae attenuates lipopolysaccharide-stimulated pro-inflammatory responses by suppressing tlr4-mediated nf-kappab signaling pathways. *J. Nat. Prod.* 78, 2452–2460. doi: 10.1021/acs.jnatprod.5b00573

Lu, Y., Luo, F., Cen, K., Xiao, G., Yin, Y., Li, C., et al. (2017). Omics data reveal the unusual asexual-fruiting nature and secondary metabolic potentials of the medicinal fungus cordyceps cicadae. *BMC Genomics* 18:668. doi: 10.1186/s12864-017-4060-4

Mao, X., Cai, T., Olyarchuk, J. G., and Wei, L. (2005). Automated genome annotation and pathway identification using the kegg orthology (ko) as a controlled vocabulary. *Bioinformatics* 21, 3787–3793. doi: 10.1093/bioinformatics/bti430

Mao, X. B., and Zhong, J. J. (2004). Hyperproduction of cordycepin by two-stage dissolved oxygen control in submerged cultivation of medicinal mushroom cordyceps militaris in bioreactors. *Biotechnol. Prog.* 20, 1408–1413. doi: 10.1021/bp049765r

Meng, Z., Kang, J., Wen, T., Lei, B., and Hyde, K. D. (2015a). Cordycepin and n6-(2-hydroxyethyl) -adenosine from cordyceps pruinosa and their interaction with human serum albumin. *PLoS One* 10:e0121669. doi: 10.1371/journal.pone.0121669

Meng, Z., Wen, T., Kang, J., Lei, B., and Hyde, K. D. (2015b). Characterization of a new cordyceps pruinosa isolate producing cordycepin and n^6-(2-hydroxyethyl)-adenosine. *Chiang Mai J. Sci.* 43, 449–455. doi: 10.1590/S1517-83822012000200004

National Health Commission. (2020). Announcement on 15 "three new foods" including cicada flower fruiting entities (artificial cultivation). Available at: https://zwfw.nhc.gov.cn/kzx/tzgg/xspylsp_225/202101/t20210108_1688.html (Accessed January 7, 2021).

Nxumalo, W., Elateeq, A. A., and Sun, Y. (2020). Can cordyceps cicadae be used as an alternative to cordyceps militaris and cordyceps sinensis?—a review. *J. Ethnopharmacol.* 257:112879. doi: 10.1016/j.jep.2020.112879

Qu, G., Geng, W., Hui, S., Guang, Z., Zhang, F., and Xue, (2006). Microwave-assisted green and efficient synthesis of n 6-(2-hydroxyethyl) adenosine and its analogues. *Chin. Chem. Lett.* 17.

Qu, Q. S., Yang, F., Zhao, C. Y., and Shi, X. Y. (2019). Analysis of the bacteria community in wild cordyceps cicadae and its influence on the production of hea and nucleosides in cordyceps cicadae. *J. Appl. Microbiol.* 127, 1759–1767. doi: 10.1111/jam.14432

Shi, C., Song, W., Gao, J., Yan, S., Guo, C., and Zhang, T. (2022). Enhanced production of cordycepic acid from cordyceps cicadae isolated from a wild environment. *Braz. J. Microbiol.* 53, 673–688. doi: 10.1007/s42770-022-00687-4

Shih, I., Tsai, K., and Hsieh, C. (2007). Effects of culture conditions on the mycelial growth and bioactive metabolite production in submerged culture of cordyceps militaris. *Biochem. Eng. J.* 33, 193–201. doi: 10.1016/j.bej.2006.10.019

Su, Q., Zhang, Z., Liu, X., and Wang, F. (2021). The transcriptome analysis on urea response mechanism in the process of ergosterol synthesis by cordyceps cicadae. *Sci. Rep.* 11:10927. doi: 10.1038/s41598-021-90377-2

Sung, G. H., Shrestha, B., Han, S. K., and Sung, J. M. (2011). Cultural characteristics of ophiocordyceps heteropoda collected from Korea. *Mycobiology* 39, 1–6. doi: 10.4489/MYCO.2011.39.1.001

Sung, G. H., Shrestha, B., and Sung, J. M. (2010). Characteristics of metacordyceps yongmunensis, a new species from Korea. *Mycobiology* 38, 171–175. doi: 10.4489/MYCO.2010.38.3.171

Suparmin, A., Kato, T., Dohra, H., and Park, E. Y. (2017). Insight into cordycepin biosynthesis of cordyceps militaris: comparison between a liquid surface culture and a submerged culture through transcriptomic analysis. *PLoS One* 12:e0187052. doi: 10.1371/journal.pone.0187052

Tang, C., Li, X., Wang, T., Wang, J., Xiao, M., He, M., et al. (2023). Characterization of metabolite landscape distinguishes medicinal fungus cordyceps sinensis and other cordyceps by uhplc-q exactive hf-x untargeted metabolomics. *Molecules* 28:7745. doi: 10.3390/molecules28237745

Tang, Y. J., and Zhong, J. J. (2003). Scale-up of a liquid static culture process for hyperproduction of ganoderic acid by the medicinal mushroom ganoderma lucidum. *Biotechnol. Prog.* 19, 1842–1846. doi: 10.1021/bp0341592

Tsai, Y. S., Hsu, J. H., Lin, D. P., Chang, H. H., Chang, W. J., Chen, Y. L., et al. (2021). Safety assessment of hea-enriched cordyceps cicadae mycelium: a randomized clinical trial. *J. Am. Coll. Nutr.* 40, 127–132. doi: 10.1080/07315724.2020.1743211

Wang, X., Qin, A., Xiao, F., Olatunji, O. J., Zhang, S., Pan, D., et al. (2019). N (6) -(2-hydroxyethyl)-adenosine from cordyceps cicadae protects against diabetic kidney disease via alleviation of oxidative stress and inflammation. *J. Food Biochem.* 43:e12727. doi: 10.1111/jfbc.12727

Xia, Y., Luo, F., Shang, Y., Chen, P., Lu, Y., and Wang, C. (2017). Fungal cordycepin biosynthesis is coupled with the production of the safeguard molecule pentostatin. *Cell Chem. Biol.* 24, 1479–1489.e4. doi: 10.1016/j.chembiol.2017.09.001

Xie, X., Guo, H., Liu, J., Wang, J., Li, H., and Deng, Z. (2023). Edible and medicinal progress of cryptotympana atrata (fabricius) in China. *Nutrients* 15:4266. doi: 10.3390/nu15194266

Xie, H., Li, X., Yang, W., Yu, L., Jiang, X., Chen, Y., et al. (2020). N6-(2-hydroxyethyl)-adenosine induces apoptosis via er stress and autophagy of gastric carcinoma cells in vitro and in vivo. *Int. J. Mol. Sci.* 21:5815. doi: 10.3390/ijms21165815

Yang, S., and Zhang, H. (2016). Optimization of the fermentation process of cordyceps sobolifera se-ceps and its anti-tumor activity in vivo. *J. Biol. Eng.* 10:8. doi: 10.1186/s13036-016-0029-0

Zeng, Z., Mou, D., Luo, L., Zhong, W., Duan, L., and Zou, X. (2021). Different cultivation environments affect the yield, bacterial community and metabolites of cordyceps cicadae. *Front. Microbiol.* 12:669785. doi: 10.3389/fmicb.2021.669785

Zhang, X., Hu, Q., and Weng, Q. (2018). Secondary metabolites (sms) of isaria cicadae and isaria tenuipes. *RSC Adv.* 9, 172–184. doi: 10.1039/c8ra09039d

Zhang, Z., Tudi, T., Liu, Y., Zhou, S., Feng, N., Yang, Y., et al. (2016). Preparative isolation of cordycepin, n(6)-(2-hydroxyethyl)-adenosine and adenosine from cordyceps militaris by macroporous resin and purification by recycling high-speed counter-current chromatography. *J. Chromatogr. B* 1033-1034, 218–225. doi: 10.1016/j.jchromb.2016.08.025

Zhao, X., Li, Q., Liu, W., Guan, H., Li, C., Wang, J., et al. (2020). Advances in biosynthesis of cordycepin from cordyceps militaris. *Chin. J. Biotechnol.* 36, 1293–1304. doi: 10.13345/j.cjb.190500

Zhao, X., Zhang, G., Li, C., and Ling, J. (2019). Cordycepin and pentostatin biosynthesis gene identified through transcriptome and proteomics analysis of cordyceps kyushuensis kob. *Microbiol. Res.* 218, 12–21. doi: 10.1016/j.micres.2018.09.005

Zheng, Y., Li, S., Li, C., Shao, Y., and Chen, A. (2022). Polysaccharides from spores of cordyceps cicadae protect against cyclophosphamide-induced immunosuppression and oxidative stress in mice. *Food Secur.* 11:515. doi: 10.3390/foods11040515

Zhu, R., Chen, Y., and Deng, Y. (2011). Cordyceps cicadae extracts ameliorate renal malfunction in a remnant kidney model. *J. Zhejiang Univ. Sci. B* 12, 1024–1033. doi: 10.1631/jzus.B1100034

Frontiers in Microbiology

Explores the habitable world and the potential of microbial life

The largest and most cited microbiology journal which advances our understanding of the role microbes play in addressing global challenges such as healthcare, food security, and climate change.

Discover the latest Research Topics

See more →

Frontiers

Avenue du Tribunal-Fédéral 34
1005 Lausanne, Switzerland
frontiersin.org

Contact us

+41 (0)21 510 17 00
frontiersin.org/about/contact